Springer Series in Materials Science 271

Vitaly Yu. Topolov
Christopher R. Bowen · Paolo Bisegna

Piezo-Active Composites

Microgeometry–Sensitivity Relations

Springer

Springer Series in Materials Science

Volume 271

The Springer Series in Materials Science covers the complete spectrum of materials physics, including fundamental principles, physical properties, materials theory and design. Recognizing the increasing importance of materials science in future device technologies, the book titles in this series reflect the state-of-the-art in understanding and controlling the structure and properties of all important classes of materials.

More information about this series at http://www.springer.com/series/856

Vitaly Yu. Topolov · Christopher R. Bowen
Paolo Bisegna

Piezo-Active Composites

Microgeometry–Sensitivity Relations

With 61 Figures

Springer

Vitaly Yu. Topolov
Department of Physics
Southern Federal University
Rostov-on-Don, Russia

Christopher R. Bowen
Department of Mechanical Engineering
University of Bath
Bath, Somerset, UK

Paolo Bisegna
Department of Civil Engineering
and Computer Science
University of Rome Tor Vergata
Rome, Italy

ISSN 0933-033X ISSN 2196-2812 (electronic)
Springer Series in Materials Science
ISBN 978-3-319-93927-8 ISBN 978-3-319-93928-5 (eBook)
https://doi.org/10.1007/978-3-319-93928-5

Library of Congress Control Number: 2018945075

Printed on acid-free paper

This Springer imprint is published by the registered company Springer International Publishing AG
part of Springer Nature
The registered company address is: Gewerbestrasse 11, 6330 Cham, Switzerland

To our colleagues, friends and loved ones

Preface

... functional composites make use of a number of underlying ideas including connectivity patterns leading to field and force concentration; the use of periodicity and scale in resonant structures; the symmetry of composite structures and its influence on physical properties; polychromatic percolation and coupled conduction paths; varistor action and other interfacial effects; sum, combination, and product properties; coupled phase transformation phenomena; and the important role that porosity and inner composites play in composite materials.

R. E. Newnham

We have a paradox in the method of science. The research man may often think and work like an artist, but he has to talk like a bookkeeper, in terms of facts, figures, and logical sequences of thought.

H. D. Smyth

Composites based on ferroelectrics are heterogeneous materials that contain two or more components and are characterised by ferroelectric, piezoelectric, pyroelectric and other important properties. These materials have been manufactured and developed since the late 1970s, and their properties are the focus of attention by specialists in physics of active dielectrics, mechanics of heterogeneous media, piezoelectric materials science, etc. The composites in the poled state exhibit a remarkable ability to convert mechanical energy into electric energy and vice versa as a result of the electromechanical coupling and piezoelectric effect. Due to various adaptive characteristics and possibilities to vary and tailor their properties under the application of external electric and/or mechanical fields, these composites are often regarded as an important group of smart materials [1, 2]. The studies on their properties and other characteristics require a multidisciplinary effort of specialists and are impossible without a good physics-mathematical basis and understanding of the classical *composition–structure–properties* relations.

The aim of the present monograph is to describe and discuss the relations between the microgeometry and piezoelectric sensitivity of composites based on either ferroelectric ceramics or single crystals. In this monograph, we develop the

materials science concepts on the *composition–structure–properties* relations in the piezo-active composites and the analytical approach [1, 2] to show different "faces" of the piezoelectric sensitivity. Links between the microgeometry and piezoelectric properties of the composites are, as a rule, intricate [1–5], however one can reveal and describe the main factors and microgeometric features that influence the piezoelectric sensitivity at specific connectivity patterns. Despite a large number of the connectivity patterns [1, 2] related to the two- and three-component composites, one can mention a few composite types (2–2, 1–3, 0–3, and 3–3) that have been under intensive study in the last decades. Some advantages of the piezoelectric sensitivity are first discussed in the context of the piezoelectric coefficients of four types (d_{ij}^*, e_{ij}^*, g_{ij}^*, and h_{ij}^*). As is known, these parameters are used to fully describe links between mechanical and electric fields in piezoelectric media [6]. In keeping with modern trends in materials science and engineering, numerous examples of the piezoelectric sensitivity are analysed and compared, and these examples are also of value for potential piezotechnical (sensors, actuators and transducers), energy-harvesting, hydroacoustic and other applications. The novelty of the present monograph consists in the first systematisation of many authors' results on the piezoelectric sensitivity and microgeometric features of modern composites based ferroelectrics, and links between the microgeometry and piezoelectric sensitivity for a series of two- and three-component composites form the mainstream of this scientific work. Hereby, we remember the following phrase: "Science answers the question why, and art the question why not" (Sol Le Witt).

Answering the question why in the present monograph, we fill a gap in the description of the piezoelectric performance of modern anisotropic composites characterised by various microgeometric and symmetry features. This new work represents an international edition written by three specialists working in adjacent areas of science and engineering, in the areas where the piezo-active composites are of academic interest and importance for applications.

The monograph has been written on the basis of the authors' research results obtained at the Southern Federal University (Russia), University of Bath (UK) and University of Rome Tor Vergata (Italy). The academic style of presentation of the research results and the discussion about these results indicate that the present monograph would be useful to engineers, postgraduate students, researchers and lecturers, i.e. to many specialists working in the field of heterogeneous ferroelectric, piezoelectric and related materials, studying and improving their effective properties for specific applications and so on. The present monograph will be of benefit to all specialists looking to understand the important links between the microgeometric and sensitivity characteristics of the modern piezo-active composites. Some chapters and sections of the monograph may be a basis for a university course devoted to composites based on ferroelectrics, their properties and potential applications.

Based on our knowledge, experience and research results, we hope that the twenty-first century termed *The Century of New Materials and Technologies* will lead to the fruitful development of new scientific directions in the field of advanced composite materials.

Rostov-on-Don, Russia — Prof. Dr. Vitaly Yu. Topolov
Bath, UK — Prof. Dr. Christopher R. Bowen
Rome, Italy — Prof. Dr. Paolo Bisegna

References

1. Topolov VYu, Bowen CR (2009) Electromechanical properties in composites based on ferroelectrics. Springer, London
2. Topolov VYu, Bisegna P, Bowen CR (2014) Piezo-active composites: Orientation effects and anisotropy factors. Springer, Berlin, Heidelberg
3. Khoroshun LP, Maslov BP, Leshchenko PV (1989) Prediction of effective properties of piezo-active composite materials. Naukova Dumka, Kiev (in Russian)
4. Sokolkin YuV, Pan'kov AA (2003) Electroelasticity of piezo-composites with irregular structures. Fizmatlit, Moscow (in Russian)
5. Bowen CR, Topolov VYu, Kim HA (2016) Modern piezoelectric energy-harvesting materials. Springer International Publishing Switzerland
6. Ikeda T (1990) Fundamentals of piezoelectricity. Oxford University Press, Oxford, New York, Toronto

Acknowledgements

The authors are grateful to Prof. Dr. A. V. Turik, Prof. Dr. A. E. Panich, Prof. Dr. V. G. Gavrilyachenko, Prof. Dr. V. P. Sakhnenko, Prof. Dr. I. A. Parinov, Prof. Dr. A. A. Panich, Prof. Dr. A. A. Nesterov, Dr. V. V. Eremkin, Dr. V. G. Smotrakov, Dr. V. K. Dolya, Dr. S. E. Filippov, and Ms. A. N. Isaeva (Southern Federal University, Russia), Prof. Dr. A. Miles (University of Bath, UK), Prof. Dr. F. Maceri (University of Rome Tor Vergata, Italy), Prof. Dr. O. Kraft and Prof. Dr. M. Kamlah (Karlsruhe Institute of Technology, Germany), Prof. Dr. M. Lethiecq and Prof. Dr. F. Levassort (University of Tours, France), Prof. Dr. S.-H. Chang (National Kaohsiung Marine University, Taiwan, Republic of China), Prof. Dr. W. Cao (The Pennsylvania State University, USA), Prof. Dr. A. Safari and Dr. E. K. Akdogan (Rutgers—The State University of New Jersey, USA), Prof. Dr. A. S. Sidorkin (Voronezh State University, Russia), Prof. Dr. L. N. Korotkov and Prof. Dr. S. A. Gridnev (Voronezh State Technical University, Russia) and Dr. A. V. Krivoruchko (Don State Technical University, Russia) for their interest in the research problems and for their interesting research results that have been taken into account at writing the present monograph. The authors emphasise the vast geographic area wherein the piezo-active and related composites are studied, developed and manufactured. The author Prof. Dr. C. R. Bowen would also like to thank his past supervisors including Prof. Dr. B. Derby (University of Manchester, UK), Prof. Dr. N. Claussen (Technical University of Hamburg-Harburg, Germany) and Prof. Dr. R. Stevens (University of Bath, UK, who passed away in 2015 and is greatly thanked for support and missed).

The authors express much thanks to Prof. Dr. C. Ascheron and Mrs. E. Sauer (Springer-Verlag, Heidelberg, Germany) for their effective and timely cooperation in the field of editing and producing this monograph. The authors sincerely thank Mrs. C. A. Rothwell and Mrs. M. Biles (University of Bath, UK) for the technical help. Copyright permissions obtained from Springer (www.springer.com), Elsevier (www.elsevier.com), IOP Publishing (www.iop.org), AIP (www.aip.org), Taylor & Francis (www.informaworld.com) and Royal Society of Chemistry (www.rsc.org) are acknowledged with due attention and gratitude.

Financial support that promoted the fruitful research collaboration and writing this book is acknowledged with many thanks. Hereupon gratefully and proudly the authors mention the timely and effective support from the EPSRC (UK), National Physical Laboratory, QinetiQ (UK), Great Western Research (GWR, UK), University of Bath (UK), University of Rome Tor Vergata (Italy), and Southern Federal University (Russia). The author Prof. Dr. C. R. Bowen gratefully acknowledges support of ERC Advanced Fellowship (Project "NEMESIS", Grant Agreement No. 320963).

Research has been carried out at the financial support from the Ministry of Education and Science of the Russian Federation within the framework of the complex project "Working out and creation of a high-technological production of a mobile hydroacoustic complex to highlight a situation in various areas of the World ocean on the basis of modern piezoelectric means of the new generation" (contract No. 03.G25.31.0276, May 29th, 2017) by using the equipment of the Centre of Collective Use "High Technologies" at the Southern Federal University. Hereby the author Prof. Dr. V. Yu. Topolov acknowledges support with thanks.

Rostov-on-Don, Russia — Vitaly Yu. Topolov
Bath, UK — Christopher R. Bowen
Rome, Italy — Paolo Bisegna

Contents

1 The Piezoelectric Medium and Piezoelectric Sensitivity 1
1.1 Piezoelectric Effect and Electromechanical Coupling 2
1.2 Piezoelectric Coefficients and Sensitivity 7
1.3 Figures of Merit and Sensitivity 12
1.4 Effective Electromechanical Properties in Heterogeneous Piezoelectric Materials 13
1.4.1 Polydomain Ferroelectric Single Crystals 14
1.4.2 Domain-Engineered Relaxor-Ferroelectric Single Crystals 17
1.4.3 Poled Ferroelectric Ceramics 20
1.4.4 Piezo-Active Composites 26
1.5 Conclusion 28
References 29

2 Effective Piezoelectric Coefficients d_{ij}^{*}: From Microgeometry to Anisotropy 35
2.1 2–2-Type Composites 36
2.1.1 2–2 Ceramic/Polymer Composites 36
2.1.2 2–2 Single Crystal/Polymer Composites 43
2.1.3 2–0–2 Single Crystal/Ceramic/Polymer Composites 50
2.2 1–3-Type Composites 55
2.2.1 1–3 Ceramic/Polymer Composites 56
2.2.2 1–3 Single Crystal/Polymer Composites 62
2.2.3 1–2–2 Composites Based on Single Crystals 64
2.2.4 1–3–0 Composites Based on Single Crystals 66
2.2.5 1–0–3 Composites Based on Single Crystals 70
2.3 1–1-Type Composites 76
2.3.1 1–1 Ceramic/Polymer Composites 77
2.3.2 1–1–0 Ceramic/Porous Polymer Composites 78

2.4 0–3-Type Composites . . . 81
2.5 3–β Composites . . . 85
2.6 Electromechanical Coupling Factors and Their Relations to d_{ij}^* . . . 89
2.7 Hydrostatic Piezoelectric Response and Its Relation to d_{ij}^* . . . 91
2.8 Conclusion . . . 93
References . . . 95

3 Microgeometry of Composites and Their Piezoelectric Coefficients g_{ij}^* . . . 99
3.1 2–2-Type Composites . . . 100
3.2 1–3-Type Composites . . . 106
3.3 1–1-Type Composites . . . 111
3.4 0–3-Type Composites . . . 111
3.5 3–β Composites . . . 120
3.6 Piezoelectric Sensitivity, Figures of Merit and Anisotropy . . . 122
3.7 Hydrostatic Piezoelectric Sensitivity and Figures of Merit . . . 126
3.8 Conclusion . . . 130
References . . . 131

4 Piezoelectric Coefficients e_{ij}^* and d_{ij}^*: Combination of Properties at Specific Microgeometry . . . 135
4.1 2–2-Type Composites . . . 136
4.2 1–3-Type Composites . . . 142
4.3 0–3-Type Composites . . . 147
4.4 Conclusion . . . 150
References . . . 151

5 Piezoelectric Coefficients h_{ij}^*: New Opportunities to Improve Sensitivity . . . 153
5.1 2–2-Type Composites . . . 154
5.2 1–3-Type Composites . . . 156
5.3 0–3-Type Composites . . . 159
5.4 Conclusion . . . 160
References . . . 161

6 Improving Piezoelectric Sensitivity . . . 163
6.1 Piezoelectric Coefficients and Ways to Improve Piezoelectric Sensitivity of Modern Composites . . . 163
References . . . 169

Appendix A: List of Abbreviations . . . 171

Appendix B: Electromechanical Constants of Components . . . 173

Index . . . 177

About the Authors

Vitaly Yu. Topolov was born in Rostov-on-Don, Russia (former USSR) on 8 November 1961. He earned the qualification "Physicist. Educator" (honours degree) in 1984 along with the degrees "Candidate of Sciences (Physics and Mathematics)" and "Doctor of Sciences (Physics and Mathematics)" in 1987 and 2000, respectively, all from the Rostov State University, Russia. From 1987 to 1991, he worked as a research scientist of the Institute of Physics at the Rostov State University. From 1991 to 2000, he worked as a Senior Lecturer (1991–1992) and an Associate Professor (1992–2000) of the Department of Physics at the Rostov State University. Since 2000, he has been a Professor of the same Department. Since December 2006, after reforming the Rostov State University, he is a Professor of the Department of Physics at the Southern Federal University (Rostov-on-Don, Russia).

Dr. V. Yu. Topolov was also a visiting scientist at the Moscow State University, Russia (former USSR, 1989), University of Saarland, Germany (1994–1995), Aachen University of Technology—RWTH Aachen, Germany (1998), Karlsruhe Research Center, Germany (2002 and 2003–2004), University of Bath, UK (2006, 2007, 2012, 2013, 2014, 2015, and 2016), and University of Rome Tor Vergata, Italy (2008). His research interests include heterogeneous ferroelectrics, smart materials, domain and heterophase structures, as well as electromechanical effects in ferroelectrics and related materials. He earned the special award from the International Science Foundation (1993) and the Soros Associate Professor title and awards from the International Soros Science-Educational Program and the Open Society Institute (1997, 1998, 2000, and 2001). He presented the best poster at the International Symposium on Ferroelectric Domains (China, 2000), the best oral report at the International Conference on Relaxation Phenomena in Solids (Russia, 2010), the best training aids in the Department of Physics, Southern Federal University (Russia, 2006 and 2011) and the best research works in the Department of High Technologies, Southern Federal University (Russia, 2008 and 2011). He is an author of five monographs published at *Springer* (London, UK, 2009; Berlin, Heidelberg, Germany, 2012; Berlin, Heidelberg, Germany, 2014; Cham, Switzerland, 2016 and 2018), two edited monographs published at *Springer*

(Cham, Heidelberg, New York, Switzerland, Germany, USA, 2014 and 2016), one edited monograph published at *Nova Science Publishers* (New York, USA, 2016), five chapters in monographs published at *Nova Science Publishers* (New York, USA, 2010–2013) and over 430 scientific papers, reviews, conference proceedings and abstracts. Dr. V. Yu. Topolov has been included in the list of Active Russian Scientists.

Honorary co-worker of Higher Professional Education of the Russian Federation (Ministry of Education and Science of the Russian Federation, Moscow, Russia, 2009). Member of the International Biographical Centre Top 100 Educators (Cambridge, UK, 2010) and Top 100 Scientists (Cambridge, UK, 2012). Biographical data by Dr. V. Yu. Topolov have been published in "Dictionary of International Biography" (*IBC*, Cambridge, UK), "2000 Outstanding Intellectuals of the twenty-first Century" (*IBC*, Cambridge, UK) and "Who's Who in the World" (*Marquis*, New Providence, USA).

Christopher R. Bowen was born on 18 January 1968 and grew up in Beddau, South Wales (UK). He earned a B.Sc. (First Class) in Materials Science at the School of Materials, University of Bath, UK in 1990 and worked on his DPhil thesis in ceramic manufacture under the supervision of Prof. Brian Derby in the Department of Materials, University of Oxford, UK in 1990–1993 (Ph.D. awarded in 1994). During 1993–1994, he worked as a Researcher in the Advanced Ceramics Group at the Technical University of Hamburg-Harburg (TUHH), Germany under the supervision of Prof. Nils Claussen. From 1994 to 1996, he was research fellow at the School of Materials, University of Leeds, UK working with Prof. Ron Stevens. From 1996 to 1998, he was a Senior Scientist at the Defence Evaluation and Research Agency (DERA), Functional Materials Group, UK working on ferroelectric ceramics and composites. He joined the University of Bath, UK in August 1998, and now he is a Professor at the same University.

The research interests of Dr. C. R. Bowen are concerned with modern functional materials, including ferroelectric ceramics and piezo-active composites for modern sensors and actuators, as well as with manufacturing and characterisation of these materials. Continuing interest includes the use of piezoelectric materials combined with structural composites, such as bistable laminates, for energy harvesting and shape changing applications. Additional interest is concerned with pyroelectric materials, their performance and use in energy-harvesting applications. Dr. C. R. Bowen earned the Thornton and Hazelwood prizes for academic work (1986–1990), Institute of Materials National Lecture Competition award (1993), SET award (2002), and John Willis award for excellence in research and teaching (2003). Dr. C. R. Bowen has published three monographs and over 250 scientific papers, conference proceedings and abstracts. He has been awarded an ERC Advanced Fellowship in Novel Energy Materials, Engineering Science and Integrated Systems (NEMESIS, Grant Agreement No. 320963).

Paolo Bisegna was born on 13 June 1968 in Italy. He earned a MSc (First Class) in Engineering at the University of Naples "Federico II", Naples, Italy in 1991, and a M.Sc. (First Class) in Mathematics at the University of Rome Tor Vergata, Rome, Italy in 1994, where he earned a M.D. (First Class) at the School of Medicine in 2006. From 1992 to 1994, he worked as a Research Assistant for the Italian National Research Council. From 1994 to 2000, he worked as an Assistant Professor at the Department of Civil Engineering, University of Rome Tor Vergata. Since 2001, he has been a Professor of Mechanics at the same Department. Since 2012, after reforming the University of Rome Tor Vergata, he has been a Professor at the Department of Civil Engineering and Computer Science. In 2000, he has been visiting scholar at the Department of Mathematics, Northwestern University, Evanston, IL, USA. During 2001–2008, he has been yearly visiting scholar at the Department of Mathematics, Vanderbilt University, Nashville, TN, USA. Since 2011, he has been Program Director of the Biomedical Engineering Program, University of Rome Tor Vergata, and Director of the Structural Engineering Doctoral Program, University of Rome Tor Vergata (Italy).

He is a Member of the Editorial Board of *Annals of Solid and Structural Mechanics* (Springer). He served as a Reviewer for over 30 international journals. His research interests are concerned with smart materials, piezoelectric composites, ferroelectric ceramics and composites for modern sensors and actuators. Additional research interest includes computational mechanics, mechanics of materials and biomedical engineering. He has published one monograph (Springer, Berlin, Heidelberg, Germany, 2014), approximately 180 journal papers, chapters in monographs and articles in conference proceedings. His research activity is funded by national and international institutions, including the Italian Ministry of Education, Universities and Research and 7th Framework Programme, SME-2011 (DIMID, Grant Agreement No. 286692).

Chapter 1
The Piezoelectric Medium and Piezoelectric Sensitivity

Abstract The piezoelectric effect and related electromechanical properties are described, and examples of modern piezoelectric materials and their sensitivity are considered. Full sets of electromechanical constants of various piezoelectric materials are given for comparison. Examples of electromechanical coupling factors and figures of merit are also considered to show links between the piezoelectric sensitivity and these parameters. Among materials exhibiting the important piezoelectric properties, of interest are domain-engineered relaxor-ferroelectric single crystals, poled ferroelectric ceramics and piezo-active composites based on ferroelectrics. The importance of the piezoelectric sensitivity in piezotechnical applications is briefly discussed.

Piezoelectricity as a phenomenon discovered in 1880 is of great interest from a number of viewpoints. From the physical viewpoint, mechanical fields generate electric fields, and vice versa: for example, an electric polarisation of a piezoelectric material can be the result of either a mechanical stress or strain. In this context a piezoelectric property of a dielectric serves as a linkage between the fields that are described by tensors of different ranks, namely, by the first-rank (electric field or electric displacement) and second-rank tensors (mechanical stress or strain). From the crystallographic viewpoint, there are symmetry restrictions that do not enable observation of the piezoelectric effect in all of dielectric single crystals (SCs). From the materials-science viewpoint, no universal approach was put forward for a number of decades to describe the features of piezoelectricity in a variety of dielectrics, such as SCs, ceramics, textures, thin films, and composites. Moreover, piezoelectricity is often observed in dielectric materials that exhibit other important properties. Among them, first of all one can highlight their electrostrictive, pyroelectric and ferroelectric properties. Such a complex range of the physical properties, their interconnections in dielectric materials and intricate linkages between electric, mechanical and thermal fields are of an independent interest for applications such as pyroelectric sensors, piezoelectric sensors, actuators, transformers, accelerometers, strain gauges, electromechanical frequency filters, acoustic antennae, ultrasonic imaging systems, etc.

V. Y. Topolov et al., *Piezo-Active Composites*, Springer Series in Materials Science 271, https://doi.org/10.1007/978-3-319-93928-5_1

In this chapter we highlight some characteristics of the piezoelectric medium to demonstrate the important role of its piezoelectric sensitivity (PS). We add that parameters concerned with the PS are of interest to both academia and industry, and improving the parameters of modern piezoelectric materials is to be based on knowledge from physics, mechanics, crystallography and materials science.

1.1 Piezoelectric Effect and Electromechanical Coupling

The direct piezoelectric effect was discovered by brothers P. Curie and J. Curie during the experimental study of the behaviour of quartz SC under mechanical loads (1880). An electric response of the quartz sample consists in its polarisation (appearance of surface charges at the SC faces), and the direction of the polarisation vector $\boldsymbol{P}$ changes on switching the external mechanical stress σ. The polarisation P of the sample is proportional to the stress σ, and the stress field applied to the sample is regarded as a homogeneous field. In 1881 the converse piezoelectric effect was described by P. Curie and J. Curie. In the converse piezoelectric effect an external electric field $\boldsymbol{E}$ applied to the material leads to a mechanical response: in this case a stress σ or a strain ξ in the material is achieved [1, 2]. The application of a homogeneous electric field generates a homogeneous mechanical field in the sample, and a proportionality between the components of the electric and mechanical fields can be measured experimentally. Undoubtedly the converse piezoelectric effect is similar to electrostriction that is the strain ξ of a dielectric under an external electric field $\boldsymbol{E}$. However, for electrostriction the strain ξ is proportional to E^2, and no symmetry restrictions are needed [1] to observe such an effect. In contrast to the electrostriction, the piezoelectric effect follows a linear relationship between electric and mechanical components and originates from the displacement of ions of an acentric unit cell under an electric field [1–4]. The linear relationship that is valid at the specific symmetry restrictions [1, 4, 5] for piezoelectric SCs, textures, ceramics, and composites enables one to explain the change in the sign of the piezoelectric effect when the direction of the external field $\boldsymbol{E}$ is switched. In piezo-passive dielectrics the switching of the $\boldsymbol{E}$ direction does not lead to the change of the sign of the strain ξ because of the electrostrictive character of the strain $\xi \sim E^2$. In piezoelectrics, as a rule, the electrostrictive strain is small in comparison to the piezoelectric strain $\xi \sim E$.

The piezoelectric medium is of specific interest due to the potential for an electromechanical coupling and piezoelectric properties concerned with non-trivial links between electric and mechanical fields, especially in anisotropic and heterogeneous materials. The piezoelectric effect in poled ferroelectric ceramics (FCs) [2–4, 6, 7] and composites based on ferroelectrics [8, 9] is complex in comparison to the piezoelectric effect in quartz [1] or single-domain ferroelectric SCs [4, 10] because of the impact of microstructure, domain and heterophase structures, orientations, intrinsic and extrinsic contributions, mutual arrangement of components and orientation effects [11–13].

A description of the piezoelectric effect in SCs is often carried out in terms of thermodynamic functions, such as Helmholtz free energy, Gibbs free energy, elastic Gibbs energy, and electric Gibbs energy [1–4]. Each of these functions has at least three arguments that characterise the mechanical, electric and thermal states of the SC. The first argument can be either mechanical stress σ_{kl} or mechanical strain ξ_{jr} (components of the second-rank tensors), the second argument can be either electric field $\boldsymbol{E}$ or electric displacement $\boldsymbol{D}$ (components of the first-rank tensors), and the third argument can be either temperature T or entropy S (components of the zeroth-rank tensors). In some cases additional arguments, such as an external magnetic field $\boldsymbol{H}$ or magnetic induction $\boldsymbol{B}$ [8] are taken into consideration.

Based on the thermodynamic functions and relations between the arguments of the mechanical, electric and thermal states [1, 2], we describe the linked 'response—actions' in the piezoelectric medium as follows:

$$\sigma_{kl} = c^{E}_{kljr}\xi_{jr} - e_{ikl}E_i + \beta_{kl}\Delta T \tag{1.1}$$

$$D_i = e_{ikl}\xi_{kl} + \varepsilon^{\xi}_{if}E_f + p_i\Delta T \tag{1.2}$$

$$\Delta S = \beta_{jr}\xi_{jr} + p_iE_i + (\rho/T_0)c\Delta T \tag{1.3}$$

In (1.1)–(1.3) the constants are the elastic moduli at electric field E = const (c^{E}_{kljr}, fourth-rank tensor), piezoelectric coefficients (e_{ikl}, third-rank tensor), coefficients of thermal stress (β_{kl}, second-rank tensor), dielectric permittivities at mechanical strain ξ = const (ε^{ξ}_{if}, second-rank tensor), pyroelectric coefficients (p_i, first-rank tensor), density (ρ, zeroth-rank tensor), and specific heat (c, zeroth-rank tensor). Summing over the repeated subscripts in (1.1)–(1.3) is to be performed from 1 to 3. The increments ΔT and ΔS in (1.1)–(1.3) denote differences $T - T_0$ and $S - S_0$, respectively, where T_0 is the initial temperature, and S_0 is the initial entropy of the SC. It should be noted that the linear relations from (1.1) to (1.3) hold at relatively weak external fields [1–3]. For example, as follows from experimental data [1, 3, 4, 6, 14, 15], the linear dependence $\sigma_{kl}(\xi_{jr})$ from (1.1) obeys Hooke's law in an anisotropic medium at small (less than 1%) strains ξ_{jr}, and the linear dependence $D_i(E_f)$ from (1.2) is valid at relatively low levels of electric field E_f applied to a dielectric SC. For acentric dielectric SC, a low level of electric field is one, in which the E_f value is much smaller than the electric breakdown field. Ferroelectric single-domain SCs are piezo-active [1, 4, 6, 10] due to the acentric crystal structure and spontaneous polarisation axis. For these SCs, the requirements concerning the linear dependences $\sigma_{kl}(\xi_{jr})$ and $D_i(E_f)$ are also valid, however the E_f range becomes narrower than that in the acentric linear dielectric SCs. It is well known that in the presence of a low electric field E, the polarisation P of a ferroelectric SC linearly depends on E [1, 6] so that domain-wall displacements are reversible and no nuclei of reoriented domains [10] are formed. To follow the linear dependence $D_i(E_f)$, the electric field E applied to the ferroelectric SC is to be several times lower than the coercive field E_c [1, 6].

Using (1.1)–(1.3), one can determine a set of isothermal constants (at T = const) that describe a performance of a piezoelectric SC. A set of adiabatic constants (at S = const) can also be derived using thermodynamic functions and a combination of three arguments including ΔS (for example, ξ_{jr}, E_i and ΔS). Usually the difference between the related isothermal and adiabatic constants of the piezoelectric SCs is approximately 1% or less [1, 8]. In this case the effect of thermal fields on the elastic and electric responses of the piezoelectric SCs is often neglected [1, 4], and the description of the piezoelectric effect is carried out in terms of (1.1) and (1.2) at $\Delta T = 0$, i.e., under isothermal conditions.

Equations (1.1) and (1.2) at $\Delta T = 0$ can be given in the matrix form [1, 2] as follows:

$$\sigma_p = c_{pq}^{E} \xi_q - e_{fp} E_f \tag{1.4}$$

$$D_k = e_{kl} \xi_l + \varepsilon_{kr}^{\xi} E_r \tag{1.5}$$

Writing (1.4) and (1.5), we used the conventional transition from two subscripts to one subscript in accordance with the well-known Vogt's rule [1–4, 8, 15]. Equations (1.4) and (1.5) represent the first pair of piezoelectric equations that links two variables, namely, mechanical strain ξ and electric field E. In (1.5) $P_k = e_{kl}\xi_l$ is the piezoelectric polarisation caused by the external mechanical strain at the direct piezoelectric effect. The converse piezoelectric effect is described by the stress $-e_{fp}E_f$ in (1.4), and the sequence of subscripts (fp, f) at the converse piezoelectric effect differs from the sequence (kl, l) at the direct effect.

As follows from the thermodynamic treatment of the interrelations between the electric and elastic fields [1, 2] in piezoelectric SCs, the converse and direct piezoelectric effects can also be described by the three following pairs of equations:

$$\xi_p = s_{pq}^{E} \sigma_q + d_{fp} E_f \tag{1.6}$$

$$D_k = d_{kl} \sigma_l + \varepsilon_{kr}^{\sigma} E_r \tag{1.7}$$

in variables of mechanical stress σ and electric field E,

$$\xi_p = s_{pq}^{D} \sigma_q + g_{fp} D_f \tag{1.8}$$

$$E_k = -g_{kl} \sigma_l + \beta_{kr}^{\sigma} D_r \tag{1.9}$$

in variables of mechanical stress σ and electric displacement D, and

$$\sigma_p = c_{pq}^{D} \xi_q - h_{fp} D_f \tag{1.10}$$

$$E_k = -h_{kl} \xi_l + \beta_{kr}^{\xi} D_r \tag{1.11}$$

in variables of mechanical strain ξ and electric displacement D. Superscripts σ and D denote measurement conditions at $\sigma = \text{const}$ and $D = \text{const}$, respectively. Dielectric impermittivities β_{kr}^{σ} (at $\sigma = \text{const}$) from (1.9) and β_{kr}^{ξ} (at $\xi = \text{const}$) (1.11) are found using relations [1, 2] $\beta_{kr}^{\sigma}\varepsilon_{rv}^{\sigma} = \delta_{kv}$ and $\beta_{kr}^{\xi}\varepsilon_{rv}^{\xi} = \delta_{kv}$. Elastic moduli c_{pq}^{E} (or c_{pq}^{D}) and elastic compliances s_{pq}^{E} (or s_{pq}^{D}) are linked by formulae [1, 2] $c_{pq}^{E}s_{qr}^{E} = \delta_{pr}$ and $c_{pq}^{D}s_{qr}^{D} = \delta_{pr}$, where δ_{kv} is the Kronecker symbol.

It should be added that (1.4)–(1.11) illustrate the electromechanical coupling in the piezoelectric medium. This coupling stems from the link between the electric and mechanical fields [i.e., items in the left and right parts of (1.4)–(1.11)], and this link is maintained due to the appropriate piezoelectric coefficient that depends on the SC symmetry, temperature etc. The full set of elastic, piezoelectric and dielectric constants from (1.4)–(1.11) is also termed '*electromechanical constants*'. We list the full sets of the electromechanical constants of the piezoelectric medium as follows:

(i) c_{pq}^{E}, e_{fp} and ε_{kr}^{ξ},
(ii) s_{pq}^{E}, d_{fp} and $\varepsilon_{kr}^{\sigma}$,
(iii) s_{pq}^{D}, g_{fp} and β_{kr}^{σ}, and
(iv) c_{pq}^{D}, h_{fp} and β_{kr}^{ξ}.

In accordance with work [4], d_{fp} and g_{fp} are termed '*piezoelectric coefficients*', and e_{fp} and h_{fp} are termed '*piezoelectric moduli*'. In work [1] d_{fp} is termed '*piezoelectric modulus*', and e_{fp}, g_{fp} and h_{fp} are termed '*piezoelectric coefficients*'. In work [7] the terms '*piezoelectric coefficients*' and '*piezoelectric moduli*' are related to d_{fp}, and e_{fp}, g_{fp} and h_{fp} are termed '*piezoelectric coefficients*'. Sometimes d_{kl} and g_{kl} are termed '*piezoelectric strain coefficients*' because of their link to the piezoelectric strain [see the second item in the right part of (1.6) or (1.8)], and e_{kl} and h_{kl} are also termed '*piezoelectric stress coefficients*' because of their link to the stress caused by the converse piezoelectric effect [see the second item in the right part of (1.4) or (1.10)]. In work [9, 13, 16] the term '*piezoelectric coefficient*' is used to denote d_{fp}, e_{fp}, g_{fp}, and h_{fp}.

By knowing the electromechanical properties (or the full set of electromechanical constants) of a piezoelectric, it is possible to evaluate the effectiveness of the conversion of electric energy into mechanical energy and vice versa. This effectiveness is one of the main characteristics of a piezoelectric element [1–4] as a transducer device, sensor or actuator. The effectiveness of the energy conversion in the piezoelectric medium is characterised by an electromechanical coupling factor (ECF) [3, 4, 6, 15]

$$k = w_{piezo}/\sqrt{w_{el}w_{mech}} \tag{1.12}$$

The ECF is also termed 'the electromechanical coupling coefficient' [1]. In (1.12) the volume densities of piezoelectric (or mutual) energy $w_{piezo} = \sigma_i\ d_{mi}\ E_m/2$,

electric energy $w_{el} = E_l \varepsilon^{\sigma}_{lr} E_r/2$, and mechanical energy $w_{mech} = \sigma_p s^E_{pq} \sigma_q/2$ are used to describe the electromechanical coupling.

The k^2 value calculated from (1.12) characterises [1–4, 7, 15] the ratio of stored mechanical energy to electric energy input (when a portion of electric energy is applied to the piezoelectric material) or a ratio of stored electric energy to mechanical energy input (when a portion of mechanical energy is applied to the piezoelectric material). The k^2 value is used to estimate a measure of the magnitude of the piezoelectric transducer bandwidth [2]. The absolute ECF value depends [2, 3, 15] on the oscillation mode, shape of the piezoelectric element, measurement methodology, and the electromechanical properties. As follows from numerous literature data, two kinds of ECFs are distinguished in piezoelectrics. The first kind is the static ECF determined from equations of the state of the piezoelectric medium. The second kind is the dynamic (or effective) ECF related to the individual piezoelectric element [2, 7, 15].

As an example, a poled FC element with a remanent polarisation vector $\boldsymbol{P_r} \parallel OX_3$ [$(X_1X_2X_3)$ is the rectangular co-ordinate system] is characterised [1–4, 7, 15] by ∞mm symmetry. The piezoelectric effect in the poled FC sample can be described in terms of (1.6) and (1.7) where three independent piezoelectric coefficients, namely, d_{31}, d_{33} and d_{15} are involved. They are linked to the ECFs as follows:

$$k_{33} = d_{33}/(\varepsilon^{\sigma}_{33} s^E_{33})^{1/2} \tag{1.13}$$

(ECF at the longitudinal oscillation mode, or longitudinal ECF),

$$k_{31} = d_{31}/(\varepsilon^{\sigma}_{33} s^E_{11})^{1/2} \tag{1.14}$$

(ECF at the transverse oscillation mode) and

$$k_{15} = d_{15}/(\varepsilon^{\sigma}_{11} s^E_{55})^{1/2} \tag{1.15}$$

(ECF at the shear oscillation mode). Since an equality $s^E_{55} = s^E_{44}$ holds [2–5] in the poled FC, (1.15) is often represented as $k_{15} = d_{15}/(\varepsilon^{\sigma}_{11} s^E_{44})^{1/2}$.

Equations (1.13)–(1.15) are written in the general form [1, 2, 7, 15] as

$$k_{ij} = d_{ij}/(\varepsilon^{\sigma}_{ii} s^E_{jj})^{1/2} \tag{1.16}$$

The piezoelectric coefficient d_{ij} in (1.16) plays a key role in determining the electromechanical coupling in the piezoelectric element, and therefore, strongly influences the energy conversion therein.

Along with the ECFs from (1.13)–(1.15), the following ECFs are often measured on poled FC and piezo-active composite samples with ∞mm symmetry [2–4, 6, 7, 9, 13–15]:

$$k_t = e_{33}/(c_{33}^D \varepsilon_{33}^\xi)^{1/2} \tag{1.17}$$

(ECF at the thickness oscillation mode, or thickness ECF),

$$k_p = k_{31}[2/(1-\sigma_E)]^{1/2} \tag{1.18}$$

(ECF at the planar oscillation mode, or planar ECF) and

$$k_h = d_h/(\varepsilon_{33}^\sigma s_h^E)^{1/2} \tag{1.19}$$

(ECF at hydrostatic loading, or hydrostatic ECF). In (1.18) σ_E is the Poisson's ratio at electric field E = const, and in (1.19) d_h and s_h^E are the hydrostatic piezoelectric coefficient and hydrostatic elastic compliance at E = const, respectively. As seen from (1.16)–(1.19), irrespective of the oscillation mode, the ECF is related to a set of piezoelectric, dielectric and elastic constants. Data on the ECFs from (1.13)–(1.19) can be analysed for the selection of piezoelectric materials for active elements of electromechanical transducers, hydrophones, sensors, actuators, and piezoelectric energy harvesters [3, 4, 6, 7, 9, 13, 15, 16].

1.2 Piezoelectric Coefficients and Sensitivity

Equations (1.4)–(1.11) contain four types of piezoelectric coefficients, namely e_{kl}, d_{kl}, g_{kl}, and h_{kl}. In each pair of (1.4)–(1.11), there is a term corresponding to the direct piezoelectric effect and a term corresponding to the converse piezoelectric effect. Each piezoelectric coefficient is a component of the third-rank tensor that links the electric and mechanical fields. It should be noted that (1.4)–(1.11) are written in the matrix form, and each piezoelectric coefficient has two subscripts. Links between the piezoelectric coefficients d_{kl}, e_{kl}, g_{kl}, and h_{kl} can be derived from the thermodynamic description of the piezoelectric effect [1, 2, 4] and are represented as follows:

$$d_{fp} = \varepsilon_{fk}^\sigma g_{kp} = e_{fq} s_{qp}^E \tag{1.20}$$

$$e_{fp} = \varepsilon_{fk}^\xi h_{kp} = d_{fq} c_{qp}^E \tag{1.21}$$

$$g_{fp} = \beta_{fk}^\sigma d_{kp} = h_{fq} s_{qp}^D \tag{1.22}$$

$$h_{fp} = \beta_{fk}^\xi e_{kp} = g_{fq} c_{qp}^D \tag{1.23}$$

The piezoelectric coefficients d_{kl}, e_{kl}, g_{kl}, and h_{kl} influence the dielectric and elastic properties measured at different conditions:

$$\varepsilon_{kr}^{\sigma} - \varepsilon_{kr}^{\xi} = d_{kf} e_{rf} \tag{1.24}$$

$$\beta_{kr}^{\xi} - \beta_{kr}^{\sigma} = g_{kf} e_{rf} \tag{1.25}$$

$$c_{pq}^{D} - c_{pq}^{E} = e_{fp} h_{fq} \tag{1.26}$$

$$s_{pq}^{D} - s_{pq}^{E} = d_{fp} g_{fq} \tag{1.27}$$

Equations (1.24) and (1.25) suggest that the differences between the dielectric properties measured at the constant stress and constant strain are caused by the piezoelectric effect. As follows from (1.26) and (1.27), the differences between the elastic properties measured at the constant electric displacement and constant electric field are also due to the piezoelectric effect. Based on the full set of electromechanical constants from one of the pairs of (1.4)–(1.11), it is possible to determine the three other sets of electromechanical constants of the same piezoelectric. For this evaluation, we should take into consideration symmetry of the piezoelectric and relations (1.20)–(1.23).

The symmetry classes that obey the conditions for the piezoelectric effect [1, 2, 4, 5] in dielectric SCs are non-centrosymmetrical and listed as follows:

(i) 1 (triclinic system),
(ii) 2 and *m* (monoclinic system),
(iii) 222 and *mm*2 (orthorhombic system),
(iv) 3, 32 and 3*m* (trigonal or rhombohedral system),
(v) 4, 422, 4*mm*, $\overline{4}$, and $\overline{4}2m$ (tetragonal system),
(vi) 6, 622, 6*mm*, $\overline{6}$, and $\overline{6}m2$ (hexagonal system), and
(vii) 23 and $\overline{4}3m$ (cubic system).

For the non-centrosymmetrical 432 class from the cubic system, every piezoelectric coefficient equals zero because of features of symmetry [1, 4]. Among the aforementioned non-centrosymmetrical classes, 1, 2, 3, 4, 6, *m*, *mm*2, 3*m*, 4*mm* and 6*mm* (i.e., 10 symmetry classes) are related to polar dielectric SCs [1, 4] that exhibit both the piezoelectric and pyroelectric properties. Ferroelectric properties can be detected among pyroelectrics from one of the 10 symmetry classes [1, 4–6].

The Curie groups that satisfy conditions for the piezoelectric texture [1, 2, 4, 8, 15] are ∞, ∞mm and $\infty/2$. The number of independent piezoelectric coefficients strongly depends on features of symmetry. For instance, in the 1 symmetry class, the $\|d\|$ matrix comprises the largest number of independent constants, i.e., d_{11}, d_{12}, …, d_{16}, d_{21}, d_{22}, …, d_{26}, d_{31}, d_{32}, …, and d_{36}, or 18 piezoelectric coefficients. These piezoelectric coefficients are written in the matrix form [1, 2, 4] as follows:

$$\|d\| = \begin{pmatrix} d_{11} & d_{12} & d_{13} & d_{14} & d_{15} & d_{16} \\ d_{21} & d_{22} & d_{23} & d_{24} & d_{25} & d_{26} \\ d_{31} & d_{32} & d_{33} & d_{34} & d_{35} & d_{36} \end{pmatrix} \tag{1.28}$$

The $\|d\|$ matrix related to the $mm2$ symmetry class is written as

$$\|d\| = \begin{pmatrix} 0 & 0 & 0 & 0 & d_{15} & 0 \\ 0 & 0 & 0 & d_{24} & 0 & 0 \\ d_{31} & d_{32} & d_{33} & 0 & 0 & 0 \end{pmatrix} \tag{1.29}$$

As seen from (1.29), there are five independent piezoelectric coefficients d_{ij}. The piezoelectric coefficients in the $4mm$ and $6mm$ symmetry classes and ∞mm Curie group are represented as follows:

$$\|d\| = \begin{pmatrix} 0 & 0 & 0 & 0 & d_{15} & 0 \\ 0 & 0 & 0 & d_{15} & 0 & 0 \\ d_{31} & d_{31} & d_{33} & 0 & 0 & 0 \end{pmatrix} \tag{1.30}$$

In the $\|d\|$ matrix from (1.30) there are three independent piezoelectric coefficients d_{ij}. The minimal number of the independent piezoelectric coefficients d_{ij} is one, and it is observed in the following symmetry classes: 422, 622, $\overline{6}m2$, 23, and $\overline{4}3m$ [1, 2, 4].

For the overwhelming majority of the symmetry classes, the $\|e\|$, $\|g\|$ and $\|h\|$ matrices have the form that coincides with that of the $\|d\|$ matrix. However there are five symmetry classes in which the form of the $\|e\|$ and $\|h\|$ matrices differs from the form of the $\|d\|$ and $\|g\|$ matrices. According to work [1, 2], these symmetry classes are 3, 32, $3m$, $\overline{6}$, and $\overline{6}m2$.

Conditions for measuring the piezoelectric coefficients are associated with the electric and mechanical variables from (1.4) to (1.11). At the direct piezoelectric effect, the piezoelectric coefficients are measured [1] using the following relations for the electric polarisation P_k and field E_k:

$$P_k = d_{kl}\sigma_l \tag{1.31}$$

(for d_{kl}),

$$E_k = -g_{kl}\sigma_l \tag{1.32}$$

(for g_{kl}),

$$E_k = -h_{kl}\xi_l \tag{1.33}$$

(for h_{kl}), and

$$P_k = e_{kl}\xi_l \tag{1.34}$$

(for e_{kl}). It should be added that the piezoelectric polarisation is $P_k = D_k$ at $E_k = 0$, and the value of P_k is determined from a surface density of electric charges on the

sample face [1]. At the converse piezoelectric effect, the following relations are taken into account when measuring the piezoelectric coefficients:

$$\xi_p = d_{fp} E_f \tag{1.35}$$

(for d_{fp}),

$$\xi_p = g_{fp} D_f \tag{1.36}$$

(for g_{fp}),

$$\sigma_p = -h_{fp} D_f \tag{1.37}$$

(for h_{fp}), and

$$\sigma_p = -e_{fp} E_f \tag{1.38}$$

(for e_{fp}). Equations (1.31)–(1.38) suggest that it is relatively easy to find e_{kl} and h_{kl} as constants of the direct piezoelectric effect and d_{kl} as a constant of the converse piezoelectric effect [1].

The piezoelectric coefficients from (1.31)–(1.38) characterise the PS of a material to an external field (electric or mechanical), or more exactly, to specific components of the field that acts on a piezoelectric element made of this material. For the direct piezoelectric effect, the PS originates from the reaction of the piezoelectric element to an external field, either from a mechanical stress or strain. We assume that this field is homogeneous, and its frequency is much less than a resonance frequency of a piezoelectric element [15].

In Fig. 1.1 we show a schematic of a piezoelectric element in the form of the rectangular parallelepiped. The piezoelectric element can 'feel' the external mechanical field in different ways, and a reaction of the field can be registered in different ways. According to (1.31) and (1.32), the piezoelectric coefficients d_{kl} and g_{kl} are introduced to show the PS with respect to the stress field (components σ_1, σ_2, …, and σ_6) applied to the piezoelectric element. In fact, the PS reflects an ability of the piezoelectric element to convert a mechanical stress (or force) into an electric field (or voltage). The PS in terms of d_{kl} links the surface charge density on the piezoelectric element and the mechanical stress, and PS in terms of g_{kl} links the

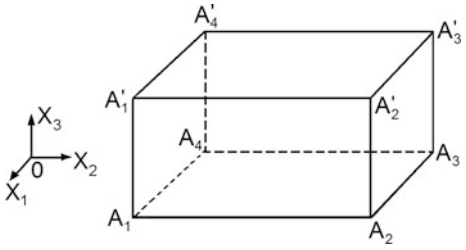

Fig. 1.1 Schematic of the piezoelectric element. ($X_1X_2X_3$) is the rectangular co-ordinate system

electric field and mechanical stress at the direct piezoelectric effect [1, 2]. Taking into account the longitudinal, transverse and shear piezoelectric effects, we distinguish the longitudinal PS, transverse PS and shear PS, respectively. A more careful analysis of links between the mechanical fields and electric responses enables us to distinguish the following four types of the piezoelectric coefficients X_{kl} from (1.31)–(1.34), where $X = d$, e, g, or h:

(i) X_{11}, X_{22} and X_{33} (related to the longitudinal PS),
(ii) X_{12}, X_{13}, X_{21}, X_{23}, X_{31}, and X_{32} (related to the transverse PS),
(iii) X_{15}, X_{16}, X_{24}, X_{26}, and X_{34}, X_{35} (related to the thickness shear PS), and
(iv) X_{14}, X_{25}, X_{36} (related to the face shear PS).

The piezoelectric coefficients from the group (iii) are concerned with the electric response (e.g., polarisation P_k) that is caused by a mechanical field (e.g., stress σ_{kl}), and one of the subscripts of σ_{kl} would be equal to that of $\boldsymbol{P}(P_1, P_2, P_3)$. In other words, the piezoelectric polarisation vector $\boldsymbol{P}$ is parallel to the face subjected by the shear stress. In contrast to this, the piezoelectric coefficients from the group (iv) are concerned with different subscripts in P_j and σ_{kl}: this means that the $\boldsymbol{P}$ vector is perpendicular to the face subjected by the shear stress. Oscillation modes associated with the shear stress (or strain) are often termed [17] '*thickness shear modes*' and '*face shear modes*'.

As seen from (1.33) and (1.34), the piezoelectric coefficients h_{kl} and e_{kl} are concerned with the strain field applied to the piezoelectric element at the direct piezoelectric effect. This kind of mechanical loading is less acceptable at the characterisation of the piezoelectric element because of a relatively narrow range of strains that can be applied to the piezoelectric element to follow the Hooke's law (as a rule, the order-of-magnitude of strains in dielectrics [1] is 10^{-3} or less). Under the external strain field with components ξ_1, ξ_2, …, and ξ_6, the surface charge density on the piezoelectric element (PS in terms of e_{kl}) or the electric field between the surfaces of the piezoelectric element (PS in terms of h_{kl}) can be detected. It should be added that PS of various materials is often associated with either g_{kl} [9, 18–21] or d_{kl} [22, 23]. This may be explained by the relatively simple link between the external action (mechanical stress or a force applied to the piezoelectric element) and the response (electric field or charge). At the converse piezoelectric effect, according to (1.36), the piezoelectric coefficients g_{kl} link the external electric displacement D_f and the mechanical strain ξ_p as a response of the piezoelectric element. In this case its PS can be determined by using D_f, however an experimental implementation of a simultaneous measurement of D_f and ξ_p with a due accuracy becomes an independent difficult task [1]. The piezoelectric coefficients d_{kl} can be measured at the converse piezoelectric effect [1] by taking into account the relation (1.35) between the strain of the sample ξ_p and the applied electric field E_f.

The piezoelectric coefficients e_{kl}, d_{kl}, g_{kl}, and h_{kl} can be used as an aid in the selection of piezoelectric materials for various applications [3, 4, 7, 15, 16, 20, 24]. For an actuator application [3], materials with a high strain per unit applied electric field (i.e., with large values of $|d_{kl}|$) would be preferable. For pressure sensors and

listening devices [1, 4, 15], the electric field generated per unit mechanical stress and therefore large values of $|g_{kl}|$ are of importance. The piezoelectric coefficients d_{kl} and g_{kl} are readily available in the literature on piezoelectric materials (see, for instance, [2–4, 6, 7, 13, 15, 16, 20], and Sect. 1.4), and as a rule, many authors pay significant attention to improve these constants and to make the materials more effective for specific piezotechnical applications.

1.3 Figures of Merit and Sensitivity

In a piezoelectric element reacting to the direct piezoelectric effect, a portion of mechanical energy is converted into electric energy [1, 2], and the effectiveness of the conversion of energy is described in terms of (1.13)–(1.19). A voltage V induced between the surfaces of the piezoelectric element (Fig. 1.1) under a mechanical load is related to the electric field [see (1.32)] and given by

$$V = g_{ij} F t / \Sigma \tag{1.39}$$

In (1.39) g_{ij} is the piezoelectric coefficient, F is the applied force, t is the thickness of the piezoelectric element, and Σ is the area of the surface on which the force acts. An output electric power that develops due to the piezoelectric effect in the electric condenser is expressed by

$$N_{out} = \left(CV^2/2\right) f \tag{1.40}$$

In (1.40) C is the electric capacitance of the piezoelectric element, and f is the frequency of the vibration caused by the force F. We assume that electrodes applied to the piezoelectric element are parallel to the (X_1OX_2) plane (Fig. 1.1), and the thickness of the piezoelectric element is $t = |A_1A_1'|$. Its capacitance C is proportional to the dielectric permittivity $\varepsilon_{33}^{\sigma}$ measured along the OX_3 axis, i.e., on the direction that is perpendicular to the (X_1OX_2) plane. The frequency f is chosen in a low-frequency range, so that f is much less than the resonance frequency of the piezoelectric element.When the force F acts along the OX_3 axis (as is conventional, for instance, for poled FCs [1–4, 7, 15]) on the area $\Sigma = |A_1A_2| \cdot |A_2A_3|$, the output electric power of the piezoelectric element (Fig. 1.1) is $N_{out} \sim CV^2 \sim \varepsilon_{33}^{\sigma}(g_{33})^2 \sim d_{33}g_{33}$. Based on this relation, the squared figure of merit [16, 25, 26]

$$(Q_{33})^2 = d_{33}g_{33} \tag{1.41}$$

is introduced. $(Q_{33})^2$ from (1.41) is concerned with the longitudinal piezoelectric effect and oscillation 33 mode (longitudinal mode). Based on (1.39) and (1.41), we represent electric energy generated at the applied force F as

$W_{gen} = (Q_{33})^2 F^2 t/(2lw)$, where $l = |A_1A_2|$ is the length of the piezoelectric element, and $w = |A_2A_3|$ is its width (Fig. 1.1).

Along with $(Q_{33})^2$ which is related to the longitudinal piezoelectric effect, we introduce squared figures of merit [16, 26]

$$(Q_{31})^2 = d_{31}g_{31} \quad \text{and} \quad (Q_{32})^2 = d_{32}g_{32} \tag{1.42}$$

which are related to the transverse piezoelectric effect and oscillation 31 and 32 modes (transverse modes), respectively, and

$$(Q_h)^2 = d_h g_h \tag{1.43}$$

that is a hydrostatic analog [9, 27, 28] of the squared figure of merit $(Q_{33})^2$ from (1.41). The hydrostatic squared figure of merit (1.43) characterises the sensing and actuating capability of a hydrophone [27]. The PS of a hydrophone depends on the voltage generated due to the hydrostatic pressure, and g_h is a measure of this PS. The hydrostatic piezoelectric coefficient d_h is directly used as a measure of PS at the transmitter function of the hydrophone [27, 28]. Formulae of the aforementioned hydrostatic parameters related to piezo-active composites are given in Sect. 2.1.1.

The squared figures of merit (1.42)–(1.43) are often used to characterise the sensor signal-to-noise ratio of the piezoelectric material and its PS at specific oscillation modes [9, 16, 29]. A piezoelectric element with a large value of $(Q_{3j})^2$ from (1.41) or (1.42) will generate a large value of electric power W_{gen} caused by an external mechanical stress. An electrical damping can additionally influence the piezoelectric performance and to take into account dielectric losses ($\tan\delta$) in a low-frequency region, one can represent the squared figure of merit in an off-resonance region [26] as $(Q_{31})^2 = d_{31}g_{31}/\tan\delta$ (for a 31 oscillation mode), $(Q_{32})^2 = d_{32}g_{32}/\tan\delta$ (for a 32 oscillation mode) or $(Q_{33})^2 = d_{33}g_{33}/\tan\delta$ (for a 33 oscillation mode).

1.4 Effective Electromechanical Properties in Heterogeneous Piezoelectric Materials

Numerous experimental data [1, 3, 4, 6, 7, 10, 15, 30–33] show that many ferroelectric materials exhibit good piezoelectric properties and relatively strong electromechanical coupling. Among ferroelectrics of interest it is worth noting compounds with the general chemical formula ABO_3 and the perovskite-type structure. After discovering the ferroelectric and piezoelectric properties in $BaTiO_3$, $PbTiO_3$, $KNbO_3$ in the 1940s [1, 32] and after the detailed study of various solid solutions based on the perovskite-type ferroelectrics in the 1950–90s [6, 7, 15, 30], the merit of these materials has been obvious. In piezotechnical applications, ferroelectrics and related materials are often used as heterogeneous materials with

predictable electromechanical properties [3, 6–9, 34]. The heterogeneous character of these materials is demonstrated at different levels including ferroelectric polydomain SCs [6, 10, 11, 32], ferroelectric polycrystalline media (FCs) [3, 4, 6, 7, 15, 30, 32–34] and composites based on either a ferroelectric SC or FC [8, 9, 13, 16, 34]. Each kind of heterogeneity influences the electromechanical properties that may be regarded as effective [7–9, 11, 34] or averaged on a large macroscopic volume of a sample. In Sect. 1.4 we show examples of the piezoelectric performance of heterogeneous ferroelectric materials.

1.4.1 Polydomain Ferroelectric Single Crystals

The first example of the electromechanical properties is related to the polydomain $BaTiO_3$ SC. At room temperature the ferroelectric phase is characterised by the 4*mm* symmetry, and the full sets of electromechanical constants of the single-domain $BaTiO_3$ SCs are known from experimental studies [10, 31]. However below the Curie point T_C, as a rule, the ferroelectric SC is split into domains, and the electromechanical properties of polydomain samples are to be taken into account. In the 4*mm* phase of $BaTiO_3$ there are 180° and 90° domain types, and their features have been studied by using different methods (see, for instance, monographs [6, 10, 32]). The 90° domain structure plays an important role in forming the piezoelectric properties.

We assume that the SC sample is split into the 90° domains with the conventional 'head-to-tail' arrangement [11], and these domains are regularly distributed over the SC sample. In the rectangular co-ordinate system $(X_1X_2X_3)$, spontaneous polarisation vectors of the 90° domains are $\boldsymbol{P}_s^{(1)}(-P;\ 0;\ P)$ and $\boldsymbol{P}_s^{(2)}(P;\ 0;\ P)$. The planar 90° domain walls that separate the domains are parallel to the (X_1OX_2) plane, i.e., parallel to the crystallographic plane of the {110}-type. The average spontaneous polarisation vector of the polydomain SC is $\boldsymbol{P}_s \uparrow\uparrow OX_3$ at equal volume fractions of the domain types. The co-ordinate axes OX_1, OX_2 and OX_3 are parallel to the main crystallographic axes X, Y and Z, respectively. Such a polydomain $BaTiO_3$ SC is described by a *mm*2 symmetry, and the piezoelectric coefficients of this SC are represented in the matrix form as shown in (1.29). The full set of electromechanical constants of the polydomain SC (Table 1.1) was calculated [11] for a case of the motionless 90° domain walls. A contribution from the domain-wall displacements in the electromechanical properties of the $BaTiO_3$ SC split into the 90° domains was evaluated in work [12].

We add for comparison that the piezoelectric coefficients d_{ij} of the single-domain $BaTiO_3$ SC are described by the matrix (1.30), and the experimental values $d_{31} = -38$ pC/N, $d_{33} = 110$ pC/N and $d_{15} = 407$ pC/N are known, for instance, from monograph [10]. The specific arrangement of the 90° domains and the large shear piezoelectric activity in the single-domain state (i.e., $d_{15} \gg |d_{31}|$) lead to an increase of the longitudinal piezoelectric activity of the polydomain $BaTiO_3$ SC

Table 1.1 Elastic compliances s_{ab}^{E} (in 10^{-12} Pa^{-1}), piezoelectric coefficients d_{ij} (in pC/N) and dielectric permittivities $\varepsilon_{pp}^{\sigma}$ [7, 11] of the polydomain $BaTiO_3$ SC (*mm*2 symmetry) at room temperature

s_{11}^{E}	7.92
s_{12}^{E}	−3.80
s_{13}^{E}	−1.28
s_{22}^{E}	8.05
s_{23}^{E}	−3.80
s_{33}^{E}	7.92
s_{44}^{E}	11.9
s_{55}^{E}	30.2
s_{66}^{E}	13.6
d_{31}	−189
d_{32}	−24.5
d_{33}	225
d_{15}	126
d_{24}	269
$\varepsilon_{11}^{\sigma}/\varepsilon_0$	265
$\varepsilon_{22}^{\sigma}/\varepsilon_0$	2680
$\varepsilon_{33}^{\sigma}/\varepsilon_0$	2130

(see d_{33} from Table 1.1). We mention that quartz, the first piezoelectric SC on which the new physical phenomenon has been discovered in 1880, is characterised by 32 symmetry and by relatively small piezoelectric coefficients d_{11} = 2.30 pC/N and d_{14} = −0.693 pC/N at room temperature [31]. The $\|d\|$ matrix of the quartz SC [1, 2, 31] has the form shown in (1.28) and comprises five non-zero elements as follows: d_{11}, $d_{12} = -d_{11}$, d_{14}, $d_{25} = -d_{14}$, and $d_{26} = -2d_{11}$.

In the two last decades, a number of attempts have been made to obtain and study ferroelectric SCs with domain-engineered structures [35–39]. Such domain structures (see schematics in Fig. 1.2) can be formed in an electric field [35–38] applied along a specific crystallographic direction of the SC sample. Among the

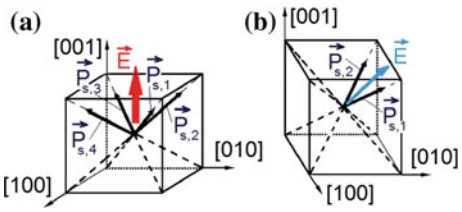

Fig. 1.2 Schematics of non-180° domains in the [001]-poled **a** and [011]-poled **b** domain-engineered SCs with the perovskite-type structure. $\boldsymbol{P}_{s,1}$, $\boldsymbol{P}_{s,2}$, $\boldsymbol{P}_{s,3}$, and $\boldsymbol{P}_{s,4}$ are spontaneous polarisation vectors of several domain types, $\boldsymbol{E}$ is the poling direction, and [100], [010] and [001] are perovskite unit-cell directions (reprinted from Bowen et al. [40], with permission from the Royal Society of Chemistry)

Table 1.2 Elastic compliances s_{ab}^{E} (in 10^{-12} Pa^{-1}), piezoelectric coefficients d_{ij} (in pC/N) and dielectric permittivities $\varepsilon_{pp}^{\sigma}$ of domain-engineered [001]-poled $KNbO_3$-based SCs (4*mm* symmetry) at room temperature

	KNN-T[a] [41]	KNN-TL[b] [42]	KNNTL:Mn[c] [43]
s_{11}^{E}	11.9	17.2	33.4
s_{12}^{E}	−4.30	−5.11	−7.36
s_{13}^{E}	−5.60	−10.7	−25.8
s_{33}^{E}	15.5	27.0	57.7
s_{44}^{E}	12.0	15.4	12.8
s_{66}^{E}	10.7	13.9	13.5
d_{31}	−77.0	−163	−260
d_{33}	162	354	545
d_{15}	45.0	171	66
$\varepsilon_{11}^{\sigma}/\varepsilon_0$	291	1100	400
$\varepsilon_{33}^{\sigma}/\varepsilon_0$	267	790	650

[a] $(K_{0.562}Na_{0.438})(Nb_{0.768}Ta_{0.232})O_3$ SC
[b] $Li_x(K_{0.501}Na_{0.499})_{1-x}](Nb_{0.660}Ta_{0.340})O_3$
[c] $[Li_x(K_{1-y}Na_y)_{1-x}](Nb_{1-z}Ta_z)O_3$:Mn, where $x = 0.06$, $y = 0.1$–0.3, $z = 0.07$–0.17, and the level of Mn doping is 0.25 mol%

perovskite-type domain-engineered SCs that are of interest due to their remarkable electromechanical properties [40], first of all we mention relaxor-ferroelectric solid solutions of $(1 - x)Pb(B_1, B_2)O_3$–$xPbTiO_3$ (see Sect. 1.4.2) and lead-free solid solutions based on $KNbO_3$ [41–43]. Examples of the full sets of electromechanical constants of the $KNbO_3$-based domain-engineered SCs poled along [001] of the perovskite unit cell are given in Table 1.2. The domain arrangement obtained in the ferroelectric rhombohedral (3*m* symmetry) phase at the poling field $\boldsymbol{E} \parallel [001]$ is shown in Fig. 1.2a. Data from Table 1.2 suggest that increasing the elastic compliance (mainly s_{11}^{E} and s_{33}^{E} of the SC) leads to an increase of the piezoelectric coefficients d_{3j}. We add that the single-domain $KNbO_3$ SC at room temperature is characterised by *mm*2 symmetry [see the matrix of d_{ij} in (1.29)], and its electromechanical constants have been measured by different authors [44, 45]. According to experimental data [44], the piezoelectric coefficients of the single-domain $KNbO_3$ SC are $d_{31} = 11$, $d_{32} = -19$, $d_{33} = 20$, $d_{15} = 22$, and $d_{24} = 17.5$ (in pC/N). The full set of optimised constants related to the (YXt)-45° of the single-domain $KNbO_3$ SC [45] comprises $d_{31} = 12.73$, $d_{32} = -31.96$, $d_{33} = 28.95$, $d_{15} = 25.10$, and $d_{24} = 79.19$ (in pC/N). The domain-engineered SCs with compositions chosen near the morphotropic phase boundary exhibit improved piezoelectric properties (Table 1.2) in comparison to the $KNbO_3$ SC [44] due to the domain-orientation effect [46] and possible displacements of interphase boundaries in external electric or mechanical fields.

1.4.2 Domain-Engineered Relaxor-Ferroelectric Single Crystals

Many perovskite-type relaxor-ferroelectric solid solutions studied in the last 20–30 years [35, 47–51] exhibit outstanding electromechanical properties and related parameters. Widespread representatives of relaxor-ferroelectric SCs with high piezoelectric performance are described by one of the following general formulae: $(1 - x)Pb(B_1, B_2)O_3$–$xPbTiO_3$ or $(1 - x - y)Pb(B_1, B_2)O_3$–$xPb(B_1', B_2')O_3$–$yPbTiO_3$. Hereby $Pb(B_1, B_2)O_3$ and $Pb(B_1', B_2')O_3$ are complex perovskites that are regarded as disordered dielectric compounds where B_1 (or B_1') = Mg, Zn, Ni, Fe, Sc, Yb, and In (low-valence metals), and B_2 (or B_2') = Nb, Ta and W (high-valence metals) [48, 51]. A combination of metal ions with low and high valences results in the properties that distinguish $Pb(B_1, B_2)O_3$ from 'normal' (ordered or regular) perovskite-type ferroelectrics such as $PbTiO_3$, $BaTiO_3$ or $KNbO_3$. The complex perovskites $Pb(B_1, B_2)O_3$ exhibit a broad and frequency-dispersive dielectric maxima and contain polar nanoregions (with ferroelectric or antiferroelectric ordering) in a non-polar phase over a wide temperature range. These materials are often termed '*relaxors*' or '*ferroelectric relaxors*' [32, 47, 50] because of the relaxation dielectric polarisation.

The perovskite-type solid solutions of $(1 - x)Pb(B_1, B_2)O_3$–$xPbTiO_3$ combine the physical properties of the relaxor-type and 'normal' (or regular) ferroelectric components, and, as a rule, excellent electromechanical properties are observed near the morphotropic phase boundary [47–51]. To achieve a high piezoelectric activity in SC samples, the relaxor-ferroelectric solid solutions are often engineered by compositional adjustment with a corresponding decrease in Curie temperature T_C of the paraelectric-to-ferroelectric phase transition [47, 48, 51], and domain-engineered structures are formed in the electric field [35, 48].

The domain-engineered SCs of $(1 - x)Pb(Mg_{1/3}Nb_{2/3})O_3$–$xPbTiO_3$ (PMN–xPT) and $(1 - x)Pb(Zn_{1/3}Nb_{2/3})O_3$–$yPbTiO_3$ (PZN–yPT) have been the focus of many experimental and theoretical studies, see for instance, [39, 48, 51, 52]. Of particular interest are compositions in the vicinity of the morphotropic phase boundary [47, 51], with intricate domain/heterophase states [52–54]. From numerous experimental results, the non-180° domain structures engineered in the electric field [36, 47, 48, 51, 55], intermediate ferroelectric phases and related heterophase structures [48, 50, 54, 56], and domain-orientation processes [57–59] lead to excellent electromechanical properties. Due to these and other phenomena, the domain-engineered PMN–xPT and PZN–yPT SCs poled along the certain crystallographic directions (often along [001], [011] or [111] of the perovskite unit cell, see examples of the crystallographic directions in Fig. 1.2) are characterised by very large piezoelectric coefficients $d_{ij} \sim 10^3$ pC/N and ECFs [60–66]. Undoubtedly, these parameters are of value for piezoelectric trandsucer, sensor, actuator, and energy-harvesting applications [16, 17, 47, 48, 51, 58]. Other relaxor-ferroelectric solid solutions that are of interest for applications include $(1 - x - y)Pb(In_{1/2}Nb_{1/2})O_3$–$yPb(Mg_{1/3}Nb_{2/3})O_3$–$xPbTiO_3$ [$(1 - x - y)$PIN–yPMN–xPT], $(1 - x - y)Pb(Yb_{1/2}Nb_{1/2})$

O_3–yPb($Mg_{1/3}Nb_{2/3}$)O_3–$x$$PbTiO_3$ [(1 − x − y)PYN–yPMN–xPT], and lead-free (1 − x)($Na_{1/2}Bi_{1/2}$)TiO_3–$x$$BaTiO_3$ (NBT–xBT).

The full sets of electromechanical constants of a number of relaxor-ferroelectric SCs poled along [001] are given in Table 1.3. The non-180° domains in these SCs are arranged as shown in Fig. 1.2a. We add for comparison that, at room temperature, the single-domain $PbTiO_3$ SC is characterised by the 4*mm* symmetry and piezoelectric coefficients [10] d_{31} = –26 pC/N, d_{33} = 160 pC/N and d_{15} = 56 pC/N. The absolute values of piezoelectric coefficients $|d_{3j}| \sim 10^3$ pC/N in the domain-engineered PMN–xPT and PZN–yPT SCs (Table 1.3) are larger than the values of $|d_{3j}|$ of conventional FC materials based on Pb($Zr_{1-x}Ti_x$)O_3 (see Sect. 1.4.3). Moreover, the piezoelectric coefficient d_{33} in the [001]-poled heterophase PZN–0.08PT SC can reach approximately 12,000 pC/N [56] due to the electric-field-induced phase transition and the presence of the ferroelectric intermediate monoclinic phase.

Important interconnections between the structure and properties in the PMN–xPT and PZN–yPT SCs have been discussed in work [49, 50, 57–59]. The high piezoelectric activity in these SCs is associated with a polarisation rotation under an electric field $\boldsymbol{E}$. The polarisation rotation between the single-domain states in the ferroelectric 4*mm* and 3*m* phases [57, 59] can be implemented in different ways that form intermediate monoclinic phases [49] and complex heterophase states [54, 56].

The formation of other types of non-180° domain structures in the relaxor-ferroelectric SCs leads to changes in their electromechanical properties. Data in Table 1.4 are related to the domain-engineered SCs, but with *mm*2 symmetry [62, 65, 67–69] that is achieved at electric poling along [011] of the perovskite unit cell. On poling the SC sample along [011], two domain types (Fig. 1.2b) are formed in the ferroelectric 3*m* phase. As a consequence, we observe significant changes in the piezoelectric coefficients d_{ij} in comparison to those from Table 1.3. For example, we observe a violation of the condition $|d_{31}| = |d_{32}| < d_{33}$ that is typical of the [001]-poled SCs (see Table 1.3). The piezoelectric effect in the [011]-poled SCs is characterised by the relation $|d_{32}| > d_{33} > d_{31}$ (see Table 1.4). For the [011]-poled SCs, the inequality $d_{15} \gg d_{24}$ is also valid. The change in the poling direction of the relaxor-ferroelectric SC also gives rise to changes in its piezoelectric anisotropy.

It should be added that in some cases the full sets of electromechanical constants measured on relaxor-ferroelectric SC samples are inconsistent in terms of the piezoelectric coefficients d_{ij}, e_{fp}, g_{ij}, and h_{ij}. Some examples of the inconsistency and violation of relations (1.20)–(1.27) were discussed in work [70, 71].

The relaxor-ferroelectric SCs are often used as active elements of piezoelectric energy harvesters [72–75] and as piezoelectric components of advanced composites [9, 13, 16, 17, 76, 77] that are suitable for many piezotechnical applications due to the large piezoelectric coefficients d_{3j}, ECFs k_{3j} and other parameters.

Table 1.3 Elastic compliances s_{ab}^{E} (in 10^{-12} Pa^{-1}), piezoelectric coefficients d_{ij} (in pC/N) and dielectric permittivities $\varepsilon_{pp}^{\sigma}$ of domain-engineered [001]-poled relaxor-ferroelectric SCs (4*mm* symmetry) at room temperature

SC	s_{11}^{E}	s_{12}^{E}	s_{13}^{E}	s_{33}^{E}	s_{44}^{E}	s_{66}^{E}	$\boldsymbol{d_{31}}$	$\boldsymbol{d_{33}}$	$\boldsymbol{d_{15}}$	$\varepsilon_{11}^{\sigma}/\ \varepsilon_0$	$\varepsilon_{33}^{\sigma}/\ \varepsilon_0$
PMN–0.33PT [60]	69.0	−11.1	−55.7	119.6	14.5	15.2	−1330	2820	146	1600	8200
PMN–0.30PT [61]	52.0	−18.9	−31.1	67.7	14.0	15.2	−921	1981	190	3600	7800
PMN–0.28PT [62]	44.57	−28.91	−13.91	34.38	15.22	16.34	−569	1182	122	1672	5479
PZN–0.045PT [63]	82.0	−28.5	−51.0	108	15.6	15.9	−970	2000	140	3100	5200
PZN–0.07PT [64]	85.9	−14.1	−69.0	142	15.9	14.1	−1204	2455	176	3000	5622
PZN–0.08PT [64]	87.0	−13.1	−70.0	141	15.8	15.4	−1455	2890	158	2900	7700
0.26PIN–0.42PMN–0.32PT:Mn[a] [65]	45.4	−15.9	−28.1	62.4	15.4	27.8	−609	1341	133	1326	3811
0.27PIN–0.40PMN–0.33PT [66]	75.5	−38.3	−35.8	77.8	14.5	16.1	−1337	2742	232	10,081	7244
NBT–0.05BT [103]	12.2	−3.4	−8.2	27.7	13.4	12.9	−113	360	162	1099	1021

[a] Level of doping Mn is from 1 to 5 mol%

Table 1.4 Elastic compliances s_{ab}^{E} (in 10^{-12} Pa^{-1}), piezoelectric coefficients d_{ij} (in pC/N) and dielectric permittivities $\varepsilon_{pp}^{\sigma}$ of domain-engineered [011]-poled relaxor-ferroelectric SCs (*mm*2 symmetry) at room temperature

	PMN–0.28PT [62]	PMN–0.29PT [67]	PZN–0.07PT [68]	PZN–0.09PT [69]	0.26PIN–0.42PMN–0.32PT:Mn,[a] composition A [65]	0.26PIN–0.42PMN–0.32PT:Mn,[a] composition B [65]
s_{11}^{E}	13.40	18.0	67.52	73.07	18.0	23.5
s_{12}^{E}	−21.18	−31.1	−60.16	−63.98	−28.0	−39.0
s_{13}^{E}	−12.67	8.4	3.355	4.256	13.1	20.6
s_{22}^{E}	54.36	11.2	102.0	125.6	68.1	90.4
s_{23}^{E}	−39.59	−61.9	−54.47	−68.04	−39.4	−56.4
s_{33}^{E}	28.02	49.6	62.02	67.49	30.9	43.8
s_{44}^{E}	15.22	14.9	15.45	15.12	15.5	16.2
s_{55}^{E}	147.06	69.4	291.5	299.3	116	189
s_{66}^{E}	22.47	13.0	14.08	16.54	20.0	21.1
d_{15}	2162	1188	1823	2012	2030	2986
d_{24}	160	167	50	118.7	125	160
d_{31}	447	610	478	476.0	455	608
d_{32}	−1150	−1883	−1460	−1705	−1200	−1508
d_{33}	860	1030	1150	1237	810	1053
$\varepsilon_{11}^{\sigma}/\varepsilon_0$	4235	3564	8240	8740	4916	6274
$\varepsilon_{22}^{\sigma}/\varepsilon_0$	1081	1127	1865	2075	1084	1499
$\varepsilon_{33}^{\sigma}/\varepsilon_0$	3873	4033	3180	3202	3213	3523

[a]Level of doping Mn is from 1 to 5 mol% [65]

1.4.3 Poled Ferroelectric Ceramics

Compositions of perovskite-type ferroelectric solid solutions [6, 7, 30, 32] can be varied in a wide range to improve specific properties of active dielectric materials. Among them the poled FCs are most widespread, and this is mainly concerned with the important electromechanical properties [3, 4, 6, 7]. Attempts to classify the FCs have been made by many researchers [7, 78, 79]. From the classification scheme [78] and by considering the widespread FCs based on $Pb(Zr_{1-x}Ti_x)O_3$ [6, 7, 15, 30, 32–34], it is possible to identify materials which are stable with regard to electric and mechanical loads, materials with high dielectric permittivity $\varepsilon_{33}^{\sigma}$, materials having high PS with respect to mechanical stress fields (large absolute values of piezoelectric coefficients g_{fp}), materials with the large piezoelectric anisotropy, materials with high stability with regard to resonance frequency, materials with low dielectric permittivity $\varepsilon_{33}^{\sigma}$, and high-temperature materials (materials with high T_C). From the classification method proposed by Gorish et al. [7], the FCs based on $Pb(Zr_{1-x}Ti_x)O_3$ are divided into four groups that are related to molar concentrations x as follows: $0 \le x \le 0.1$, $0.1 \le x \le 0.4$, $0.4 \le x \le 0.6$, and $0.6 \le x \le 1$.

Table 1.5 Elastic compliances s_{pq}^{E} (in 10^{-12} Pa^{-1}), piezoelectric coefficients d_{ij} (in pC/N) and dielectric permittivities $\varepsilon_{kk}^{\sigma}$ of poled perovskite-type FCs at room temperature [16][a]

FC	s_{11}^{E}	s_{12}^{E}	s_{13}^{E}	s_{33}^{E}	s_{44}^{E}	d_{31}	d_{33}	d_{15}	$\varepsilon_{11}^{\sigma}/\varepsilon_0$	$\varepsilon_{33}^{\sigma}/\varepsilon_0$
$BaTiO_3$ (I)	8.55	−2.61	−2.85	8.93	23.3	−79	191	270	1623	1900
$BaTiO_3$ (II)	9.1	−2.7	−2.9	9.5	22.8	−78	190	260	1450	1700
ZTS-19	15.1	−5.76	−5.41	17.0	41.7	−126	307	442	1350	1500
PZT-4	12.3	−4.03	−5.35	15.6	39.1	−124	291	496	1440	1280
PZT-5	16.3	−5.67	−7.17	18.7	47.4	−170	373	583	1730	1700
PZT-5H	10.8	−3.28	−3.41	11.6	28.3	−128	315	482	2640	2490
PZT-7A	10.7	−3.22	−4.62	13.9	39.5	−60.2	151	364	843	427
PZ 27	16.9	−6.32	−8.56	22.5	43.9	−174	419	515	1800	1770
PZ 34	7.71	−1.54	−3.99	13.0	17.0	−3.92	59.1	39.2	191	196
PCR-1, hp[b]	12.5	−4.4	−5.8	15.9	38.8	−95	220	420	1130	650
PCR-7, hp	17.2	−7.2	−6.7	17.3	42.4	−280	610	760	2970	3500
PCR-7M, hp	17.5	−6.7	−7.9	19.6	43.8	−350	760	880	3990	5000
PCR-8, hp	12.5	−4.6	−5.2	15.6	35.3	−130	290	410	1380	1400
PCR-8, ct	13.3	−4.8	−4.4	14.5	39.5	−125	280	458	1320	1300
PCR-13, ct	10.4	−3.7	−2.1	11.3	28.5	−65	140	200	870	780
PCR-21, hp	11.8	−4.5	−3.9	12.6	40.8	−109	250	370	1400	1350
PCR-63, hp	9.8	−3.5	−2.7	9.8	24.1	−60	140	166	960	1170
PCR-73, hp	17.9	−6.8	−9.6	23.5	43.7	−380	860	980	4750	6000
$Pb(Zr_{0.54}Ti_{0.46})O_3$	11.6	−3.33	−4.97	14.8	45.0	−60.2	152	440	990	450
$Pb(Zr_{0.52}Ti_{0.48})O_3$	13.8	−4.07	−5.80	17.1	48.2	−93.5	223	494	1180	730
$(Pb_{0.94}Sr_{0.06})^{\cdot}$ $^{\cdot}(Ti_{0.47}Zr_{0.53})O_3$	12.3	−4.05	−5.31	15.5	39.0	−123	289	496	1475	1300
Modified $PbTiO_3$ (I)	7.50	−1.51	−1.10	8.00	17.9	−4.40	51.0	53.0	228	177
Modified $PbTiO_3$ (II)	7.7	−1.7	−1.2	8.2	19	−6.8	56	68	240	190
Modified $PbTiO_3$ (III)	7.51	−1.5	−1.1	8.0	18	−5.0	53	54	230	180
$(Pb_{0.9625}La_{0.025})^{\cdot}$ $^{\cdot}(Ti_{0.99}Mn_{0.01})O_3$	7.20	−1.42	−1.73	7.62	15.8	−4.15	47.2	53.0	223	168
$(Pb_{0.85}Nd_{0.10})^{\cdot}$ $^{\cdot}(Ti_{0.99}Mn_{0.01})O_3$	6.84	−1.50	−1.83	7.27	16.4	−5.42	56.8	79.5	313	252
$(Pb_{0.855}Nd_{0.11})^{\cdot}$ $^{\cdot}(Ti_{0.94}Mn_{0.02}In_{0.04})O_3$	6.77	−1.55	−1.79	7.29	16.0	−6.40	57.9	86.4	318	248
PMN–0.35PT	13.2	−3.96	−6.05	14.7	33.4	−133	270	936	4610	3270

[a]Based on experimental data [6, 8, 15, 30, 78, 80, 81, 85, 97, 104–106] on poled FCs

[b]FC samples of the PCR type have been manufactured using either the conventional technology (ct) or hot pressing (hp). PCR is the abbreviation for the group 'piezoelectric ceramics from Rostov-on-Don' (Russia) [78]

Each group of the FCs exhibits properties that are useful for specific piezotechnical and transducer applications.

Examples of the full sets of electromechanical constants of poled FCs with the perovskite-type structure are given in Table 1.5. It should be noted that the FC material poled along the OX_3 axis is characterised by the ∞mm symmetry [1, 2, 4], and the matrix of the piezoelectric coefficients d_{ij} is given in (1.30). The elastic

compliance s_{66} of the poled FC obeys the condition [1, 2, 4, 7, 15] $s_{66} = 2(s_{11}^E - s_{12}^E)$.

Absolute values of the piezoelectric coefficients d_{3j} of the FCs are smaller (and sometimes considerably smaller) than $|d_{3j}|$ of many domain-engineered relaxor-ferroelectric SCs (see Tables 1.3 and 1.4). This feature can be associated with the granular microstructure of the FC sample, with internal mechanical stress fields in each grain and the restricted possibilities of domain reorientations within the material.

Based on formulae (1.20)–(1.27) and experimental data from Table 1.5, we evaluate the piezoelectric coefficients e_{ij}, g_{ij} and h_{ij} of the FCs (Table 1.6). It is seen that the studied materials can be divided into the following groups: FCs with $e_{33} > 0$ and $e_{31} < 0$ and FCs with $e_{3j} > 0$. For all the FCs listed in Tables 1.5 and 1.6, inequalities $d_{33} > 0$, $d_{31} < 0$, $g_{33} > 0$, and $g_{31} < 0$ are valid irrespective of sgne_{3j}. Moreover, the piezoelectric coefficients d_{3j} of the FCs with positive e_{3j} satisfy the condition for a large piezoelectric anisotropy

$$d_{33}/|d_{31}| \gg 1 \tag{1.44}$$

that is equivalent to the condition

$$g_{33}/|g_{31}| \gg 1 \tag{1.45}$$

due to the relation (1.20) and ∞mm symmetry. The elastic anisotropy of these FCs also influences the signs and anisotropy of the piezoelectric coefficients e_{3j} and h_{3j}. Such a performance is typical of the poled $PbTiO_3$-type FCs [80, 81]. The physical reasons that lead to the large piezoelectric anisotropy in these FCs are discussed in work [82–84]. The condition

$$e_{33}/|e_{31}| \gg 1 \tag{1.46}$$

holds for the modified $PbTiO_3$ FCs simultaneously with the conditions (1.44) and (1.45), see Tables 1.5 and 1.6. The condition (1.46) is equivalent to the condition

$$h_{33}/|h_{31}| \gg 1 \tag{1.47}$$

due to the relation (1.21) and ∞mm symmetry of the poled FC. It should be also noted that the FCs with $e_{3j} > 0$ are characterised by largest values of h_{33} listed in Table 1.6. It is seen, for instance, that the piezoelectric coefficient h_{33} of modified $PbTiO_3$ (compositions I–III) is about three times larger than h_{33} of the widespread PZT-5H FC and about twice larger than h_{33} of the PZT-4 FC. Such an unexpected advantage of the FCs with $e_{3j} > 0$ over the PZT-type FCs is accounted for by moderate dielectric permittivities ε_{kk}^{ξ} of the FCs [80, 85] with $e_{3j} > 0$. For these FCs, the ε_{kk}^{ξ} values are almost order-of-magnitude smaller than ε_{kk}^{ξ} of the PZT-type FCs and promote larger values of h_{33} in accordance with the relation (1.21) even at moderate values of the piezoelectric coefficient e_{33} (see Table 1.6).

Table 1.6 Piezoelectric coefficients e_{ij} (in C/m^2), g_{ij} (in mV m/N) and h_{ij} (in 10^8 V/m) of poled perovskite-type FCs at room temperature[a]

FC	e_{31}	e_{33}	e_{15}	g_{31}	g_{33}	g_{15}	h_{31}	h_{33}	h_{15}
FCs with $e_{33} > 0$ and $e_{31} < 0$									
$BaTiO_3$ (I)	−4.38	18.6	11.6	−4.70	11.4	18.8	−3.48	14.8	10.3
$BaTiO_3$ (II)	−4.32	17.4	11.4	−5.18	12.6	20.3	−3.90	15.7	11.6
ZTS-19	−4.80	15.0	10.6	−9.49	23.1	37.0	−6.43	20.1	14.6
PZT-4	−5.26	15.0	12.7	−10.9	25.7	38.9	−9.32	26.7	19.7
PZT-5	−5.26	15.9	12.3	−11.3	24.2	38.1	−7.18	21.7	15.1
PZT-5H	−6.42	23.4	17.0	−5.81	14.3	27.6	−4.93	17.9	11.2
PZT-7A	−2.27	9.35	9.22	−15.9	49.0	48.8	−10.8	44.7	22.4
PZ 27	−3.59	15.9	11.7	−11.1	26.7	32.3	−4.63	20.5	11.9
PCR-1, hp[b]	−3.81	11.1	10.8	−16.5	38.2	42.0	−14.7	42.6	19.8
PCR-7, hp	−9.10	28.2	17.9	−9.04	19.7	28.9	−10.5	37.5	14.2
PCR-7M, hp	−9.85	30.8	20.1	−7.91	17.2	24.9	−7.08	28.1	11.4
PCR-8, hp	−7.52	13.6	11.6	−10.5	23.4	33.6	−11.6	20.9	15.6
PCR-8, ct	−6.87	15.1	11.6	−10.9	24.2	39.2	−12.4	27.3	18.2
PCR-13, ct	−6.59	9.94	7.02	−9.42	20.3	26.0	−14.1	21.4	11.1
PCR-21, hp	−6.47	15.8	9.07	−9.12	20.9	29.9	−9.84	24.1	10.0
PCR-63, hp	−4.45	11.8	6.89	−5.79	13.5	19.5	−5.45	14.5	9.37
PCR-73, hp	−8.81	29.4	22.4	−7.16	16.2	23.3	−4.17	13.9	11.2
$Pb(Zr_{0.54}Ti_{0.46})O_3$	−1.86	9.02	9.78	−15.1	38.2	50.2	−7.78	37.8	21.9
$Pb(Zr_{0.52}Ti_{0.48})O_3$	−3.08	11.0	10.2	−14.5	34.5	47.3	−8.95	31.8	19.1
$(Pb_{0.94}Sr_{0.06})(Ti_{0.47}Zr_{0.53})O_3$	−5.20	15.1	12.7	−10.7	25.1	38.0	−8.87	25.7	18.9
PMN–0.35PT	−5.14	14.1	28.0	−4.60	9.33	22.9	−2.16	5.95	19.2

(continued)

Table 1.6 (continued)

FC	e_{31}	e_{33}	e_{15}	g_{31}	g_{33}	g_{15}	h_{31}	h_{33}	h_{15}
FCs with $e_{3j} > 0$									
PZ 34	3.82	6.89	2.31	−2.26	34.1	23.2	28.2	50.8	14.4
Modified $PbTiO_3$ (I)	0.459	6.50	2.96	−2.81	32.6	26.3	3.71	52.5	15.9
Modified $PbTiO_3$ (II)	0.247	6.90	3.58	−4.04	33.3	32.0	1.90	53.2	19.0
Modified $PbTiO_3$ (III)	0.401	6.74	3.00	−3.14	33.3	26.5	3.23	54.4	16.0
$(Pb_{0.9625}La_{0.025})(Ti_{0.99}Mn_{0.01})O_3$	1.31	6.79	3.35	−2.79	31.7	26.9	11.2	57.7	18.7
$(Pb_{0.85}Nd_{0.10})(Ti_{0.99}.Mn_{0.01})O_3$	2.01	8.82	4.85	−2.43	25.5	28.7	11.5	50.4	20.3
$(Pb_{0.855}Nd_{0.11})(Ti_{0.94}Mn_{0.02}In_{0.04})O_3$	1.80	8.83	5.40	−2.92	26.4	30.7	10.6	51.7	23.0

[a]Based on data from Table 1.5

Analysing the longitudinal piezoelectric effect in the FCs [2, 6–9], one can state that their piezoelectric coefficients d_{33} and g_{33} vary in wider ranges than e_{33} and h_{33}. However a piezoelectric polarisation $\boldsymbol{P}(0; 0; P_3)$ of the poled FC element shown in Fig. 1.1 can be achieved under a mechanical stress σ_3 or at a strain ξ_3:

$$P_3 = d_{33}\sigma_3 = e_{33}\xi_3 \tag{1.48}$$

In (1.48) it is assumed that a homogeneous mechanical field is applied to the piezoelectric element. As a rule, the mechanical stress σ_3 remains relatively small (i.e., satisfying the Hooke's law) in a wide range. At the same time, a range of permissible strain ξ_3 values that obey the Hooke's law is relatively narrow due to the elastic properties of the piezoelectric medium. This distinction influences the ranges wherein the piezoelectric coefficients d_{33} and e_{33} of the FCs can be found. A similar variation of d_{33} and e_{33} can be detected in ferroelectric and relaxor-ferroelectric SCs.

In Fig. 1.3 we show examples of the piezoelectric polarisation $\boldsymbol{P}$ caused by homogeneous mechanical stresses in a poled FC sample. The matrix of the piezoelectric coefficients $\|d\|$ from (1.30) means that conditions $d_{31} = d_{32} \neq d_{33}$ and $d_{15} = d_{24}$ hold for the FC sample poled along the OX_3 axis (Fig. 1.3a). In Fig. 1.3a various components of the mechanical stress tensor σ_{tu} are shown. To follow (1.31) where the mechanical stress σ_l is given in the one-index form, we remind that the components σ_{tu} are expressed [1, 2] in terms of σ_l as follows: $\sigma_{11} = \sigma_1$, $\sigma_{22} = \sigma_2$, $\sigma_{33} = \sigma_3$, $\sigma_{12} = \sigma_{21} = \sigma_6$, $\sigma_{13} = \sigma_{31} = \sigma_5$, and $\sigma_{23} = \sigma_{32} = \sigma_4$. The piezoelectric

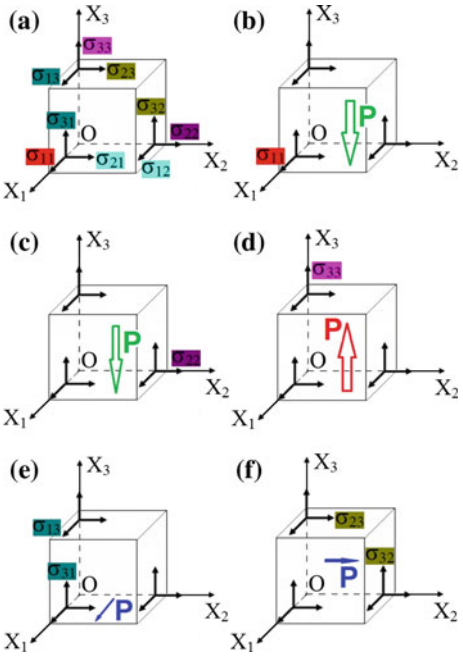

Fig. 1.3 Schematics of mechanical stress components σ_{tu} applied to a poled FC sample (**a**) and the piezoelectric polarisation $\boldsymbol{P}$ (**b**–**f**) caused by specific components of σ_{tu} in the same sample. The orientation of the $\boldsymbol{P}$ vector means that conditions $d_{31} < 0$ (**b**) $d_{32} < 0$ (**c**) $d_{33} > 0$ (**d**) $d_{15} > 0$ (**e**), and $d_{24} > 0$ (**f**) hold at $\sigma_{tu} > 0$

polarisation $\boldsymbol{P}$ of the sample can be thereafter detected on electric charges at the sample faces that are perpendicular to the $\boldsymbol{P}$ arrow in Fig. 1.3b–f. It is obvious that the PS of the FC sample is linked with the non-zero elements of $\|d\|$: the larger absolute value of d_{ij} would lead to a larger PS at the constant mechanical stress.

The PS can be also analysed in terms of the piezoelectric coefficients e_{ij}. At the direct piezoelectric effect, they link the piezoelectric polarisation $\boldsymbol{P}$ of the sample and the mechanical strain ξ_{tu} applied to the sample [1, 2]. Equation (1.34) describes the aforementioned link, however the mechanical strain ξ_l is represented in the one-index form. We note that the tensor components ξ_{tu} are expressed [1, 2] in terms of ξ_l as follows: $\xi_{11} = \xi_1$, $\xi_{22} = \xi_2$, $\xi_{33} = \xi_3$, $\xi_{12} = \xi_{21} = \xi_6/2$, $\xi_{13} = \xi_{31} = \xi_5/2$, and $\xi_{23} = \xi_{32} = \xi_4/2$. In the piezoelectric sample loaded by an external mechanical strain ξ_{tu} = const, the larger PS is achieved in a case of the larger absolute value of the piezoelectric coefficient e_{ij}.

The similar analysis of the PS characteristic of poled FCs at the direct piezoelectric effect can be carried out in terms of the piezoelectric coefficients g_{ij} or h_{ij} [see (1.32) and (1.33)].

Among the modern FC materials with high PS, we mention a nanostructured $(K_{0.5}Na_{0.5})NbO_3$:Mn FC. According to work [86], for this FC, d_{33} = 340 pC/N, g_{33} = 220 mV.m/N, T_C = 673 K, and the valid condition (1.44) are stated. Such a performance enables us to regard this lead-free nanostructure FC as a good counterpart to many FCs from Tables 1.5 and 1.6 and a promising candidate for sensor applications with high PS.

1.4.4 Piezo-Active Composites

Composites are heterogeneous systems that consist of two or more components. These components differ in chemical composition and physical properties and are separated by distinct interfaces [8]. Each composite material is characterised by the following features [8, 9]:

(i) the typical size of the separate structural elements are small in comparison with the whole composite sample (i.e., there is an element of micro-inhomogeneity) and
(ii) the typical sizes of the structural elements are greater than the size of their individual atoms or molecules so that each component of the composite sample is regarded as a continuous medium. As a result, to describe the composite effective properties, it is possible to apply appropriate physical laws and equations suitable for continuous media.

Piezo-active composites (often termed '*piezo-composites*') are heterogeneous materials that contain at least one piezoelectric component. The piezo-active composites form the vast and important group of modern smart materials. This group is of interest due to the large number of components that may be involved in

the design of the composites [6–9, 13, 16, 20, 21, 27]. The piezo-active composites are also of interest due to the ability to vary and tailor the microgeometry, effective physical properties, their anisotropy, and hydrostatic and other parameters across a wide range. The piezo-active composites based on ferroelectrics form the final (and very important) link in hierarchy-of-properties chains [7, 9, 83, 84] of 'single-domain ferroelectric SC → polydomain ferroelectric SC → FC → composite' and 'single-domain ferroelectric SC → polydomain ferroelectric SC → heterophase ferroelectric SC → composite'.

Since the 1980s, FC materials have been of interest as main piezoelectric components of composites [3, 6–8, 14, 28, 87]. However since the 2000s, relaxor-ferroelectric SCs with the large piezoelectric coefficients d_{3j} (see Sect. 1.4.2) are also used as components of modern composites [9, 13, 16, 17, 76, 77]. The second component of the composite are often chosen among polymers that can be piezoelectric [9, 87, 88], piezo-passive [9, 76, 77, 89], monolithic, auxetic, or porous [9, 13, 16, 20, 21, 90], In the last decade construction materials such as cement and clay are also of interest to manufacture novel piezo-active composites (see, for instance, [91, 92]). In some papers a porous piezoelectric medium based on FC is interpreted as a composite [9, 16, 93, 94] with a specific mictogeometry. There are also FC samples with oriented pores therein [95].

The well-known classification of the two-component composites with planar interfaces was first put forward by Newnham et al. [87]. This classification is concerned with the so-called *connectivity* of each component. Connectivity is regarded as one of the main characteristics of the microstructure and expressed by the numbers of dimensions (or co-ordinate axes) in which each component is continuously distributed between limiting surfaces of the composite sample. The distribution of a self-connected state of a component can take place along zero, one, two, or three co-ordinate axes, i.e., connectivity $\alpha = 0, 1, 2$, or 3 for component 1 and connectivity $\beta = 0, 1, 2$, or 3 for component 2. The connectivity of a two-component composite is written [9, 87] as α–β where the connectivity of the piezoelectric or most piezo-active component takes the first position (α). In the case of $\alpha \leq \beta$, the n-component composites are described by $(n + 3)!/(3!\, n!)$ connectivities [87], and for instance, the number of connectivities is 10 for $n = 2$. It is also possible to introduce 10 alternative connectivities, namely, α–β at $\alpha \geq \beta$ and $n = 2$.

The concept of connectivity [87, 96] is fundamental in developing an understanding of the electromechanical interaction between components within the piezo-active composites, in the study of the distribution of internal electric and mechanical fields and in the interpretation of experimental or calculated data related to composites with a specific connectivity. The connectivity of the piezo-active composites is a crucial factor in influencing the piezoelectric response and electromechanical coupling of these materials [9, 13, 16, 87, 96].

The entire complex of the α–β connectivity patterns, their evolution and interconnections between them in the two-component composites with a system of planar interfaces were analysed in work [96]. To describe the evolution and determine the effective electromechanical properties in the α–β composite with planar interfaces, a group of so-called *junction* connectivity patterns (1–1, 1–3, 2–2,

and 3–1) was introduced. Knowledge of the evolution of the connectivity patterns enables the analysis of the α–β composites and their effective electromechanical properties [9, 96].

The problem of predicting the effective physical properties is of interest to many specialists undertaking theoretical and experimental studies of these heterogeneous materials. A formulation of the related problem on the effective electromechanical properties in a piezo-active composite is given in work [8]. If the averaged components of the electric field $\langle E_f \rangle$ and the mechanical strain $\langle \xi_q \rangle$ in a macroscopic region of the composite sample are independent of co-ordinates x_j (j = 1, 2 and 3), then (1.4) and (1.5) can be written for the piezo-active composite in the following form:

$$\langle \sigma_p \rangle = c_{pq}^{*E} \langle \xi_q \rangle - e_{fp}^{*} \langle E_f \rangle \tag{1.49}$$

$$\langle D_k \rangle = e_{kl}^{*} \langle \xi_l \rangle + \varepsilon_{kr}^{*\xi} \langle E_r \rangle \tag{1.50}$$

In (1.49) and (1.50) elastic moduli c_{pq}^{*E}, piezoelectric coefficients e_{fp}^{*} and dielectric permittivities $\varepsilon_{kr}^{*\xi}$ constitute the full set of effective electromechanical constants of the piezo-active composite. Hereafter we use the asterisk (*) to denote the effective properties and parameters of the composite. The effective properties from (1.49) and (1.50) are found [8, 9] by taking into account equations of electric and mechanical equilibrium and boundary conditions at the surface of the macroscopic region in the heterogeneous medium. The determination of the effective electromechanical properties is concerned with an averaging of a series of vector and tensor components of the electric and mechanical fields, for example, ξ_q, E_f, σ_p, and D_k. This averaging procedure is performed on volume fractions of components, for which the full sets of electromechanical constants (for instance, $c_{pq}^{(n),E}$, $e_{fp}^{(n)}$ and $\varepsilon_{kr}^{(n),\xi}$) are known, and n = 1, 2, …, can be used to denote the nth component in the composite.

In the present monograph we apply a number of methods to predict, interpret and compare the PS and related parameters of the composites with specific connectivity patterns. The main methods to be used are the matrix method, effective field method (EFM) and finite element method (FEM) [9, 13, 16, 24, 34, 40, 92, 94, 97–102].

1.5 Conclusion

This chapter has been devoted to the introduction and description of the electromechanical properties and PS of the piezoelectric medium. By taking into account formulae (1.31)–(1.34) for the direct piezoelectric effect and (1.35)–(1.38) for the converse piezoelectric effect, one can consider four types of the piezoelectric coefficients (d_{kl}, e_{kl}, g_{kl}, and h_{kl}) that characterise PS of materials in different ways

(longitudinal, transverse, thickness shear, or face shear PS). To the best of our knowledge, no systematic study of the kinds of PS in various materials has been carried out before writing the present monograph.

As follows from numerous literature data, the most important piezoelectric materials have been poled FCs, domain-engineered relaxor-ferroelectric SCs and piezo-active composites with at least one of the aforementioned components. The use of highly-effective relaxor-ferroelectric SCs with compositions near the morphotropic phase boundary is of significant interest due to their electromechanical properties. The excellent electromechanical properties of the relaxor-ferroelectric PMN–xPT and PZN–yPT SCs (Tables 1.3 and 1.4) in the domain-engineered/heterophase states are achieved due to the large piezoelectric coefficients d_{ij}, elastic compliances s_{ab}^{E} and ECFs k_{ij}. It is shown that changes in the poling direction of these SCs lead to changes in their PS, ECFs and anisotropy of the piezoelectric properties.

The electromechanical properties of the poled FCs (Tables 1.5 and 1.6) depend on microstructure, composition, poling conditions and technological factors such as a range of sintering temperatures, and temperature-pressure parameters, etc. The lower piezoelectric activity of the poled FCs in comparison to the domain-engineered PMN–xPT and PZN–yPT SCs leads to smaller values of $|d_{ij}|$. In some piezotechnical applications the poled FCs with large values of $|g_{ij}|$ and $|h_{ij}|$ as well as with the large piezoelectric anisotropy [see conditions (1.44)–(1.47)] are preferable.

The electromechanical properties of the polydomain and domain-engineered SCs, poled FCs and piezo-active composites are regarded as *effective properties* of heterogeneous materials in accordance with features of their microstructure, domain structure, arrangement of components, and connectivity. The piezo-active composites based on ferroelectrics are the final link in the hierarchy-of-properties chains, and this feature is to be taken into account when PS can be varied in wide ranges due to a range of factors (physical, chemical, microgeometric, technological, etc.). The variety of the effective electromechanical properties and related parameters of the piezo-active composites open up new possibilities for piezotechnical applications of these materials.

References

1. Zheludev IS (1971) Physics of crystalline dielectrics. Vol 2: Electrical properties. Plenum, New York
2. Ikeda T (1990) Fundamentals of piezoelectricity. Oxford University Press, Oxford, New York, Toronto
3. Uchino K (1997) Piezoelectric actuators and ultrasonic motors. Kluwer, Boston, Dordrecht, London
4. Tichý J, Erhart J, Kittinger E, Přívratská J (2010) Fundamentals of piezoelectric sensorics. Mechanical, dielectric, and thermodynamical properties of piezoelectric materials. Springer, Berlin, Heidelberg

5. Kholkin AL, Pertsev NA, Goltsev AV (2008) Piezoelectricity and crystal symmetry. In: Safari A, Akdoğan EK (eds) Piezoelectric and acoustic materials for transducer applications. Springer, New York, pp 17–38
6. Xu Y (1991) Ferroelectric materials and their applications. North-Holland, Amsterdam, London, New York, Toronto
7. Gorish AV, Dudkevich VP, Kupriyanov MF, Panich AE, Turik AV (1999) Piezoelectric device-making. Vol 1: Physics of ferroelectric ceramics. Radiotekhnika, Moscow (in Russian)
8. Khoroshun LP, Maslov BP, Leshchenko PV (1989) Prediction of effective properties of piezo-active composite materials. Naukova Dumka, Kiev (in Russian)
9. Topolov VYu, Bowen CR (2009) Electromechanical properties in composites based on ferroelectrics. Springer, London
10. Fesenko EG, Gavrilyachenko VG, Semenchev AF (1990) Domain structure of multiaxial ferroelectric crystals. Rostov University Press, Rostov-on-Don (in Russian)
11. Turik AV (1970) Elastic, piezoelectric, and dielectric properties of single crystals of $BaTiO_3$ with a laminar domain structure. Sov Phys Solid State 12:688–693
12. Aleshin VI (1990) Domain-orientation contribution into constants of ferroelectric polydomain single crystal. Zh Tekh Fiz 60:179–183 (in Russian)
13. Topolov VYu, Bisegna P, Bowen CR (2014) Piezo-active composites. Orientation effects and anisotropy factors. Springer, Berlin, Heidelberg
14. Newnham RE (2005) Properties of materials. Anisotropy, symmetry, structure. Oxford University Press, New York
15. Berlincourt DA, Cerran DR, Jaffe H (1964) Piezoelectric and piezomagnetic materials and their function in transducers. In: Mason W (ed) Physical acoustics. Principles and methods. Vol 1: Methods and devices. Part A. Academic Press, New York, London, pp 169–270
16. Bowen CR, Topolov VYu, Kim HA (2016) Modern piezoelectric energy-harvesting materials. Springer, Switzerland
17. Zhang S, Li F, Jiang X, Kim J, Luo J, Geng X (2015) Advantages and challenges of relaxor-$PbTiO_3$ ferroelectric crystals for electroacoustic transducers—a review. Prog Mater Sci 68:1–66
18. Petrov VM (1987) Effect of intensification of piezoelectric sensitivity of textures at the converse piezoelectric effect. Zh Tekh Fiz 57:2273–2275 (in Russian)
19. Hillenbrand J, Sessler GM (2004) High-sensitivity piezoelectric microphones based on stacked cellular polymer films (L). J Acoust Soc Am 116:3267–3270
20. Bowen CR, Topolov VYu (2003) Piezoelectric sensitivity of $PbTiO_3$-based ceramic/polymer composites with 0–3 and 3–3 connectivity. Acta Mater 51:4965–4976
21. Topolov VYu, Panich AE (2009) Problem of piezoelectric sensitivity of 1–3-type composites based on ferroelectric ceramics. Ferroelectrics 392:107–119
22. Sirohi J, Chopra E (2000) Fundamental understanding of piezoelectric strain sensors. J Intell Mater Syst Struct 11:246–257
23. Payo I, Hale JM (2011) Sensitivity analysis of piezoelectric paint sensors made up of PZT ceramic powder and water-based acrylic polymer. Sens Actuators A Phys 168:77–89
24. Glushanin SV, Topolov VYu, Krivoruchko AV (2006) Features of piezoelectric properties of 0–3 $PbTiO_3$-type ceramic/polymer composites. Mater Chem Phys 97:357–364
25. Uchino K, Ishii T (2010) Energy flow analysis in piezoelectric energy harvesting systems. Ferroelectrics 400:305–320
26. Priya S (2010) Criterion for material selection in design of bulk piezoelectric energy harvesters. IEEE Trans Ultrason Ferroelectr Freq Control 57:2610–2612
27. Iyer S, Venkatesh TA (2014) Electromechanical response of (3–0, 3–1) particulate, fibrous, and porous piezoelectric composites with anisotropic constituents: A model based on the homogenization method. Int J Solids Struct 51:1221–1234
28. Sherman CH, Butler JL (2007) Transducers and arrays for underwater sound. Springer, New York

29. Grekov AA, Kramarov SO, Kuprienko AA (1989) Effective properties of a transversely isotropic piezoelectric composite with cylindrical inclusions. Mech Compos Mater 25:54–61
30. Jaffe B, Cook WR, Jaffe H (1971) Piezoelectric ceramics. Academic Press, London, New York
31. Blistanov AA, Bondarenko VS, Perelomova NV, Strizhevskaya FN, Chkalova VV, Shaskol'skaya MP (1982) Acoustic crystals. Handbook. Nauka, Moscow (in Russian)
32. Smolensky GA, Bokov VA, Isupov VA, Krainik NN, Pasynkov RE, Sokolov AI, Yushin NK (1985) Physics of ferroelectric phenomena. Nauka, Leningrad (in Russian)
33. Golovnin VA, Kaplunov IA, Malyshkina OV, Ped'ko BB, Movchikova AA (2013) Physical principles, methods of study and applications of piezomaterials. Tekhnosfera, Moscow (in Russian)
34. Luchaninov AG (2002) Piezoelectric effect in non-polar heterogeneous ferroelectric materials. Volgograd State Academy of Architecture and Construction, Volgograd (in Russian)
35. Wada S, Park S-E, Cross LE, Shrout TR (1999) Engineered domain configuration in rhombohedral PZN-PT single crystals and their ferroelectric related properties. Ferroelectrics 221:147–155
36. Wada S, Suzuki S, Noma T, Suzuki T, Osada M, Kakihana M, Park S-E, Cross LE, Shrout TR (1999) Enhanced piezoelectric property of barium titanate single crystals with engineered domain configurations. Jpn J Appl Phys Part 1 38:5505–5511
37. Wada S, Muraishi T, Yokoh K, Kakemoto H, Tsurumi T (2007) Preparation of barium titanate crystals with engineered domain configurations by using a new poling method with both an electric field and a uniaxial stress field and their piezoelectric properties. J Korean Phys Soc 51:874–877
38. Nakamura K, Tokiwa T, Kawamura Y (2002) Domain structures in $KNbO_3$ crystals and their piezoelectric properties. J Appl Phys 91:9272–9276
39. Erhart J (2011) Domain engineered piezoelectric resonators. In: Pardo L, Ricoto J (eds) Multifunctional polycrystalline ferroelectric materials. Springer, Dordrecht, Heidelberg, New York, London, pp 651–680
40. Bowen CR, Topolov VYu, Isaeva AN, Bisegna P (2016) Advanced composites based on relaxor-ferroelectric single crystals: from electromechanical coupling to energy-harvesting applications. CrystEngComm 18:5986–6001
41. Zheng LM, Huo XQ, Wang R, Wang JJ, Jiang WH, Cao WW (2013) Large size lead-free (Na, K)(Nb, Ta)O_3 piezoelectric single crystal: growth and full tensor properties. CrystEngComm 15:7718–7722
42. Huo X, Zheng L, Zhang R, Wang R, Wang J, Sang S, Wang Y, Yang B, Cao W (2014) High quality lead-free (Li, Ta) modified (K, Na)NbO_3 single crystal and its complete set of elastic, dielectric and piezoelectric coefficients with macroscopic 4*mm* symmetry. CrystEngComm 16:9828–9833
43. Huo X, Zhang R, Zheng L, Zhang S, Wang R, Wang J, Sang S, Yang B, Cao W (2015) (K, Na, Li)(Nb, Ta)O_3:Mn lead-free single crystal with high piezoelectric properties. J Am Ceram Soc 98:1829–1835
44. Wiesendanger E (1974) Dielectric, mechanical and optical properties of orthorhombic $KNbO_3$. Ferroelectrics 6:263–281
45. Rouffaud R, Marchet P, Hladky-Hennion A-C, Bantignies C, Pham-Thi M, Levassort F (2014) Complete electroelastic set for the (YXt)-45° cut of a $KNbO_3$ single crystal. J Appl Phys 116:194106
46. Topolov VYu (2003) Domain wall displacements and piezoelectric activity of $KNbO_3$ single crystals. J Phys: Condens Matter 15:561–565
47. Park S-E, Shrout TR (1997) Ultrahigh strain and piezoelectric behavior in relaxor based ferroelectric single crystals. J Appl Phys 82:1804–1811
48. Cross LE (2008) Relaxor ferroelectrics. In: Heywang W, Lubitz K, Wersing W (eds) Piezoelectricity. Evolution and future of a technology. Springer, Berlin, Heidelberg, pp 131–156

49. Noheda B (2002) Structure and high-piezoelectricity in lead oxide solid solutions. Curr Opin Solid State Mater Sci 6:27–34
50. Noheda B, Cox DE (2006) Bridging phases at the morphotropic boundaries of lead oxide solid solutions. Phase Transitions 70:5–20
51. Park S-E, Hackenberger W (2002) High performance single crystal piezoelectrics: applications and issues. Curr Opin Solid State Mater Sci 6:11–18
52. Ye Z-G (2002) Crystal chemistry and domain structure of relaxor piezocrystals. Curr Opin Solid State Mater Sci 6:35–44
53. Topolov VYu, Ye Z-G (2001) Elastic matching of morphotropic phases in polydomain $(1 - x)Pb(Zn_{1/3}Nb_{2/3})O_3$–$xPbTiO_3$ single crystals. Ferroelectrics 253:71–78
54. Topolov VYu (2012) Heterogeneous ferroelectric solid solutions. Phases and domain states. Springer, Berlin, Heidelberg
55. Dammak H, Renault A-É, Gaucher P, Thi MP, Calvarin G (2003) Origin of the giant piezoelectric properties in the [001] domain engineered relaxor single crystals. Jpn J Appl Phys Part 1 42:6477–6482
56. Topolov VYu, Turik AV (2002) An intermediate monoclinic phase and electromechanical interactions in $xPbTiO_3$–$(1 - x)Pb(Zn_{1/3}Nb_{2/3})O_3$ crystals. Phys Solid State 44:1355–1362
57. Fu H, Cohen RE (2000) Polarization rotation mechanism for ultrahigh electromechanical response in single-crystal piezoelectrics. Nature 403:281–283
58. Davis M (2007) Picturing the elephant: giant piezoelectric activity and the monoclinic phases of relaxor-ferroelectric single crystals. J Electroceram 19:23–45
59. Noheda B, Cox DE, Shirane G, Park S-E, Cross LE, Zhong Z (2001) Polarization rotation via a monoclinic phase in the piezoelectric $92\%PbZn_{1/3}Nb_{2/3}O_3$–$8\%PbTiO_3$. Phys Rev Lett 86:3891–3894
60. Zhang R, Jiang B, Cao W (2001) Elastic, piezoelectric, and dielectric properties of multidomain $0.67Pb(Mg_{1/3}Nb_{2/3})O_3$–$0.33PbTiO_3$ single crystals. J Appl Phys 90:3471–3475
61. Zhang R, Jiang W, Jiang B, Cao W (2002) Elastic, dielectric and piezoelectric coefficients of domain engineered $0.70Pb(Mg_{1/3}Nb_{2/3})O_3$–$0.30PbTiO_3$ single crystal. In: Cohen RE (ed) Fundamental physics of ferroelectrics. American Institute of Physics, Melville, pp 188–197
62. Liu G, Jiang W, Zhu J, Cao W (2011) Electromechanical properties and anisotropy of single- and multi-domain $0.72Pb(Mg_{1/3}Nb_{2/3})O_3$–$0.28PbTiO_3$ single crystals. Appl Phys Lett 99:162901
63. Yin J, Jiang B, Cao W (2000) Elastic, piezoelectric, and dielectric properties of $0.955Pb(Zn_{1/3}Nb_{2/3})O_3$–$0.045PbTiO_3$ single crystals. IEEE Trans Ultrason Ferroelectr Freq Control 47:285–291
64. Zhang R, Jiang B, Cao W, Amin A (2002) Complete set of material constants of $0.93Pb(Zn_{1/3}Nb_{2/3})O_3$–$0.07PbTiO_3$ domain engineered single crystal. J Mater Sci Lett 21:1877–1879
65. Huo X, Zhang S, Liu G, Zhang R, Luo J, Sahul R, Cao W, Shrout TR (2013) Complete set of elastic, dielectric, and piezoelectric constants of [011]C poled rhombohedral $Pb(In_{0.5}Nb_{0.5})O_3$–$Pb(Mg_{1/3}Nb_{2/3})O_3$–$PbTiO_3$:Mn single crystals. J Appl Phys 113:074106
66. Liu X, Zhang S, Luo J, Shrout TR, Cao W (2009) Complete set of material constants of $Pb(In_{1/2}Nb_{1/2})O_3$–$Pb(Mg_{1/3}Nb_{2/3})O_3$–$PbTiO_3$ single crystal with morphotropic phase boundary composition. J Appl Phys 106:074112
67. Wang F, Luo L, Zhou D (2007) Complete set of elastic, dielectric, and piezoelectric constants of orthorhombic $0.71Pb(Mg_{1/3}Nb_{2/3})O_3$–$0.29PbTiO_3$ single crystal. Appl Phys Lett 90:212903
68. Zhang R, Jiang B, Jiang W, Cao W (2006) Complete set of elastic, dielectric, and piezoelectric coefficents of $0.93Pb(Zn_{1/3}Nb_{2/3})O_3$–$0.33PbTiO_3$ single crystal poled along [011]. Appl Phys Lett 89:242908
69. He C, Jing W, Wang F, Zhu K, Qiu J (2011) Full tensorial elastic, piezoelectric, and dielectric properties characterization of [011]-poled PZN-9%PT single crystal. IEEE Trans Ultrason Ferroelectr Freq Control 58:1127–1130

70. Topolov VYu (2010) Comment on "Complete sets of elastic, dielectric, and piezoelectric properties of flux-grown [011]-poled $Pb(Mg_{1/3}Nb_{2/3})O_3$–(28–32)% $PbTiO_3$ single crystals" [Appl. Phys. Lett. 92, 142906 (2008)]. Appl Phys Lett 96:196101
71. Topolov VYu, Bowen CR (2011) Inconsistencies of the complete sets of electromechanical constants of relaxor-ferroelectric single crystals. J Appl Phys 109:094107
72. Hong YK, Moon KS (2005) Single crystal piezoelectric transducers to harvest vibration energy. Proc SPIE Optomechatronic Actuators Manipulation 6048:60480E
73. Sun C, Qin L, Li F, Wang Q-M (2009) Piezoelectric energy harvesting using single crystal $Pb(Mg_{1/3}Nb_{2/3})O_3$–$x PbTiO_3$ (PMN–PT) device. J Intell Mater Syst Struct 20:559–568
74. Moon SE, LeeSQ Lee S-K, Lee Y-G, Yang YS, Park K-H, Kim J (2009) Sustainable vibration energy harvesting based on Zr-doped PMN–PT piezoelectric single crystal cantilevers. ETRI J 31:688–694
75. Song HJ, Choi YT, Wang G, Wereley NM (2009) Energy harvesting utilizing single crystal PMN–PT material and application to a self-powered accelerometer. J Mech Des 131:091008
76. Ren K, Liu Y, Geng X, Hofmann HF, Zhang QM (2006) Single crystal PMN–PT/epoxy 1–3 composite for energy-harvesting application. IEEE Trans Ultrason Ferroelectr Freq Control 53:631–638
77. Ritter T, Geng X, Shung KK, Lopath PD, Park S-E, Shrout TR (2000) Single crystal PZN/PT-polymer composites for ultrasound transducer applications. IEEE Trans Ultrason Ferroelectr Freq Control 47:792–800
78. Dantsiger AY, Razumovskaya ON, Reznitchenko LA, Grineva LD, Devlikanova RU, Dudkina SI, Gavrilyatchenko SV, Dergunova NV, Klevtsov AN (1994) Highly effective piezoceramic materials (handbook). Kniga, Rostov-on-Don (in Russian)
79. Haertling G (1999) Ferroelectric ceramics: history and technology. J Am Ceram Soc 82:797–818
80. Nagatsuma K, Ito Y, Jyomura S, Takeuchi H, Ashida S (1985) Elastic properties of modified $PbTiO_3$ ceramics with zero temperature coefficients. In: Taylor GW (ed) Ferroelectricity and related phenomena. Vol 4: piezoelectricity. Gordon and Breach Science Publishers, New York, London, Paris, Montreux, Tokyo, pp 167–176
81. Levassort F, Thi MP, Hemery H, Marechal P, Tran-Huu-Hue L-P, Lethiecq M (2006) Piezoelectric textured ceramics: effective properties and application to ultrasonic transducers. Ultrasonics 44(Suppl 1):e621–e626
82. Topolov VYu, Bondarenko EI, Turik AV, Chernobabov AI (1993) The effect of domain structure on electromechanical properties of $PbTiO_3$-based ferroelectrics. Ferroelectrics 140:175–181
83. Topolov VYu, Turik AV, Chernobabov AI (1994) On the mechanism of high piezoelectric anisotropy in lead titanate-based ferroelectrics. Crystallogr Rep 39:805–809
84. Turik AV, Topolov VYu (1997) Ferroelectric ceramics with a large piezoelectric anisotropy. J Phys D Appl Phys 30:1541–1549
85. Ikegami S, Ueda I, Nagata T (1971) Electromechanical properties of $PbTiO_3$ ceramics containing La and Mn. J Acoust Soc Am 50:1060–1066
86. Gusakova LG, Poguibko VM, Spiridonov NA, Ishchuk VM, Kisel' NG (2012) Lead-free nanostructure piezoceramic material based on (K, Na)NbO_3. Nanosyst Nanomater Nanotechnol 10:303–312 (in Russian)
87. Newnham RE, Skinner DP, Cross LE (1978) Connectivity and piezoelectric-pyroelectric composites. Mater Res Bull 13:525–536
88. Chan HLW, Ng PKL, Choy CL (1999) Effect of poling procedure on the properties of lead zirconate titanate/vinylidene fluoride-trifluoroethylene composites. Appl Phys Lett 74:3029–3031
89. Borzov PA, Vorontsov AA, Topolov VYu, Brill OE (2016) Piezoelectric performance and features of microgeometry of novel composites based on ferroelectric ZTS-19 ceramics. In: Parinov IA, Chang S-H, Topolov VYu (eds) Proceedings of the 2015 International Conference on Physics, Mechanics of New Materials and Their Applications, devoted to the

100th Anniversary of the Southern Federal University. Nova Science Publishers, New York, pp 115–122
90. Topolov VYu, Bowen CR (2015) High-performance 1–3-type lead-free piezo-composites with auxetic polyethylene matrices. Mater Lett 142:265–268
91. Chaipanich A (2007) Dielectric and piezoelectric properties of PZT-silica fume cement composites. Curr Appl Phys 7:532–536
92. Filippov SE, Vorontsov AA, Topolov VYu, Brill OE, Bisegna P, Panich AE (2014) Features of the piezoelectric effect in a novel PZT-type ceramic/clay composite. Ferroelectr Lett Sect 41:82–88
93. Topolov VYu, Glushanin SV, Bowen CR (2005) Piezoelectric response of porous ceramic and composite materials based on Pb(Zr, Ti)O_3: experiment and modelling. Adv Appl Ceram 104:300–305
94. Topolov VYu, Bowen CR, Bisegna P, Filippov SE (2013) The piezoelectric performance and anisotropy factors of modern three-component composites. In: Parinov IA (ed) Nano- and piezoelectric technologies, materials and devices. Nova Science Publishers, New York, pp 51–78
95. Lopatin SS, Lupeiko TG, Nesterov AA (1989) Properties of lead zirconate titanate ceramic with oriented pores. Izv Akad Nauk SSSR Neorg Mater 24:1229–1230 (in Russian)
96. Topolov VYu, Glushanin SV (2002) Evolution of connectivity patterns and links between interfaces and piezoelectric properties of two-component composites. J Phys D Appl Phys 35:2008–2014
97. Levassort F, Lethiecq M, Millar C, Pourcelot L (1998) Modeling of highly loaded 0–3 piezoelectric composites using a matrix method. IEEE Trans Ultrason Ferroelectr Freq Control 45:1497–1505
98. Levin VM, Rakovskaja MI, Kreher WS (1999) The effective thermoelectroelastic properties of microinhomogeneous materials. Int J Solids Struct 36:2683–2705
99. Topolov VYu, Bisegna P (2010) Anisotropic piezoelectric properties of 1–3 ceramic/polymer composites comprising rods with elliptic cross section. J Electroceram 25:26–37
100. Topolov VYu, Bisegna P, Bowen CR (2011) Analysis of the piezoelectric performance of modern 0–3-type composites based on relaxor-ferroelectric single crystals. Ferroelectrics 413:176–191
101. Topolov VYu, Bowen CR, Bisegna P, Krivoruchko AV (2015) New orientation effect in piezo-active 1–3-type composites. Mater Chem Phys 151:187–195
102. Topolov VYu, Bowen CR, Bisegna P (2015) New aspect-ratio effect in three-component composites for piezoelectric sensor, hydrophone and energy-harvesting applications. Sens Actuators A Phys 229:94–103
103. Zheng L, Yi X, Zhang XC, Jiang W, Yang B (2013) Complete set of material constants of $0.95(Na_{0.5}Bi_{0.5})TiO_3$–$0.05BaTiO_3$ lead-free piezoelectric single crystal and the delineation of extrinsic contributions. Appl Phys Lett 103:122905
104. Bechmann R (1956) Elastic, piezoelectric, and dielectric constants of polarized barium titanate ceramics and some applications of the piezoelectric equations. J Acoust Soc Am 28:347–350
105. Huang JH, Kuo W-S (1996) Micromechanics determination of the effective properties of piezoelectric composites containing spatially oriented short fibers. Acta Mater 44:4889–4898
106. Dunn ML, Taya M (1993) Electromechanical properties of porous piezoelectric ceramics. J Am Ceram Soc 76:1697–1706

Chapter 2
Effective Piezoelectric Coefficients d_{ij}^*: From Microgeometry to Anisotropy

Abstract Piezoelectric coefficients d_{ij} are most widespread to describe the piezoelectric effect, electromechanical properties and other related parameters. The effective piezoelectric coefficients d_{ij}^* and their links to sensitivity are discussed for piezo-active composites with various connectivity patterns. Examples of the piezoelectric sensitivity of the 2–2-type, 1–3-type, 1–1-type, 0–3-type, and 3–β composites based on ferroelectics are considered. The role of the microgeometry in forming the piezoelectric sensitivity and anisotropy of the piezoelectric coefficients d_{3j}^* is analysed. Ways to improve the piezoelectric sensitivity in terms of d_{ij}^* are discussed in connection with potential piezotechnical applications.

Among the four types of the piezoelectric coefficients that are used to describe the piezoelectric effect, electromechanical properties and other related parameters [1–5] in a piezoelectric medium, the piezoelectric coefficients d_{ij} from (1.6) to (1.7) play an important role. In the historical sense, these piezoelectric coefficients enabled the study of the direct and converse piezoelectric effects within a relatively short time range in the 1880s and demonstrate important relations between the electric and elastic responses of dielectrics under the application of external fields [1, 2]. Examples of the sensor or actuator performance and energy-harvesting characteristics of piezoelectric devices [4–8] have been studied taking into account the piezoelectric coefficients d_{ij}. They play a vital role in the study of the performance of poled FEs by piezoresponse force microscopy [9], in forming the figures of merit of hydrophones [4, 10] and related hydroacoustic devices. Based on knowledge of the d_{ij} values, one can find implicit links between the piezoelectric performance and electromechanical coupling of the piezoelectric medium, for example, see (1.16), as well as important interrelations between the four types of its piezoelectric coefficients [see, for instance, (1.20)–(1.23)] in terms of the electromechanical properties. In piezo-active composites, these coefficients are regarded as ‘effective’ properties [8, 10–12] and depend on the properties of components, orientations of their main crystallographic axes, the connectivity and microgeometry of the composite, poling conditions, technological factors, etc. [12–14].

V. Y. Topolov et al., *Piezo-Active Composites*, Springer Series
in Materials Science 271, https://doi.org/10.1007/978-3-319-93928-5_2

In this chapter we discuss examples of the effective piezoelectric coefficients d_{ij}^* and their links to the PS of piezo-active composites. We also highlight examples of the anisotropy of the piezoelectric coefficients d_{ij}^* in specific composites and their advantages over poled FCs, especially highlighting the PS along specific directions of energy conversion.

2.1 2–2-Type Composites

2.1.1 2–2 Ceramic/Polymer Composites

Since the 1970s, two-component composites consisting of FC and polymer components have been studied and manufactured for various applications [4, 8, 10, 15, 16]. Usually a FC/polymer composite is formed by combining the high piezoelectric performance of a poled FC component with the beneficial mechanical properties of a polymer component [4, 15–18]. By correctly combining the properties of the FC and polymer components and tailoring the microgeometric features, the composite can achieve specific advantages [10, 14–18] over the FC component.

The 2–2 FC/polymer composite system is widespread [10, 15–18] due to its simple laminar microgeometry and electromechanical properties. We remind the reader that the '2' index in the connectivity formula '2–2' means that the first (or second) component of this composite is distributed continuously along two co-ordinate axes [15], and the component with the higher piezoelectric activity is assumed on the first position in the formula. We will consider the 2–2 composite as a system of layers of two components, and these layers are distributed regularly along one of the co-ordinate axes. The poling direction of each FC layer and the composite sample as a whole can be chosen to be either perpendicular (Fig. 2.1) or parallel (Fig. 2.2) to the system of interfaces that separate the FC and polymer layers. In some specific cases it is possible that the poling direction of the ferroelectric polymer component can differ from the poling direction of the FC component, but in the majority of cases, the polymer is inactive and is considered as a piezo-passive component [10–12, 17, 18]. Taking into account the mutual orientation of the poling axis and interfaces, specialists often term the 2–2 composites [10, 15] 'series-connected' (Fig. 2.1) or 'parallel-connected' (Fig. 2.2).

There are many methods suitable for manufacturing the 2–2 FC/polymer composites; see, for example, work [10, 17, 18]. Rapid prototyping methods (or solid freeform fabrication) [17–19] are effective for the manufacture of fine-scale 2–2 and other FC-based composites using computer-aided design. These methods are also suitable to manufacture 2–2 composites with a volume-fraction gradient, with curved FC skeletons and with a specific orientation of the layers with respect to the poling direction [17, 18].

The simplicity of the 2–2 structure, as shown in Figs. 2.1 and 2.2, and the possibility of varying and tailoring the volume fractions of the components in a

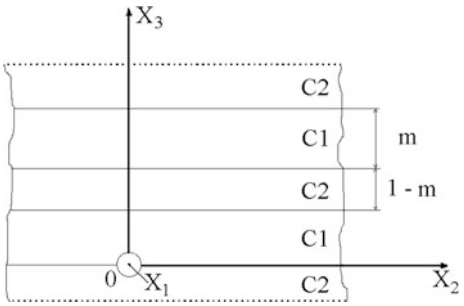

Fig. 2.1 Schematic of the 2–2 series-connected composite. m and $1 - m$ are volume fractions of components C1 and C2, respectively. $(X_1X_2X_3)$ is the rectangular co-ordinate system. In a case of the FC/polymer composite, it is assumed that OX_3 is the poling axis (reprinted from monograph by Topolov and Bowen [10], with permission from Springer)

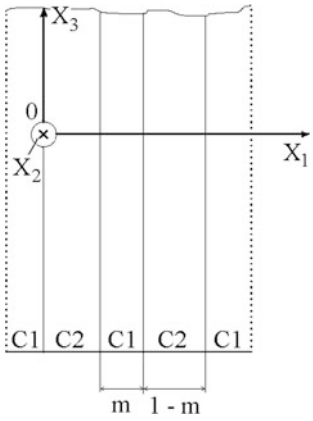

Fig. 2.2 Schematic of the 2–2 parallel-connected composite. m and $1 - m$ are volume fractions of components C1 and C2, respectively. $(X_1X_2X_3)$ is the rectangular co-ordinate system. In a case of the FC/polymer composite, it is assumed that OX_3 is the poling axis (reprinted from monograph by Topolov and Bowen [10], with permission from Springer)

wide range [10, 11, 17, 18] enable the manufacture and design of materials with extreme values of a variety of effective parameters concerned with the piezoelectric effect. For example, in the case of 2–2 series-connected FC/polymer composites based on PZT-type FCs, the non-monotonic volume-fraction dependence of the thickness ECF $k_t^* = e_{33}^* / \left(c_{33}^{*D} \varepsilon_{33}^{*\xi} \right)^{1/2}$ [see (1.17) in the similar form for a piezoelectric medium], piezoelectric coefficient e_{31}^* and dielectric permittivity $\varepsilon_{11}^{*\sigma}$ in the stress-free condition exhibit maxima [10, 11, 20], where e_{3j}^* is the piezoelectric coefficient, c_{33}^{*D} is elastic modulus measured at electric displacement D = const and $\varepsilon_{33}^{*\xi}$ is dielectric permittivity measured at mechanical strain ξ = const. The

piezoelectric coefficient e_{31}^* can pass through a value of zero and reach max $e_{31}^* > 0$ [11] even at negative values of the piezoelectric coefficient $e_{31}^{(n)}$ of the FC and polymer components. In the parallel-connected composites, the thickness ECF k_t^*, and hydrostatic (or hydrophone) piezoelectric coefficients

$$d_h^* = d_{33}^* + d_{32}^* + d_{31}^* \quad \text{and} \quad g_h^* = g_{33}^* + g_{32}^* + g_{31}^*, \tag{2.1}$$

and squared hydrostatic figure of merit

$$(Q_h^*)^2 = d_h^* g_h^* \tag{2.2}$$

pass through maxima [10, 21].

To predict the effective electromechanical properties and related parameters of the 2–2 composite, we assume that its layers have a large length in the OX_1 and OX_2 directions (Fig. 2.1) or in the OX_2 and OX_3 directions (Fig. 2.2). The interfaces separating these layers are considered planar, with perfect bonding between the adjacent layers.

To determine the effective electromechanical properties of the 2–2 composite, we apply the matrix method [10, 22]. The electromechanical constants of the nth component of the composite are given by the 9 × 9 matrix

$$\left\| C^{(n)} \right\| = \begin{pmatrix} ||s^{(n),E}|| & ||d^{(n)}||^t \\ ||d^{(n)}|| & ||\varepsilon^{(n),\sigma}|| \end{pmatrix} \tag{2.3}$$

In (2.3) $\|s^{(n),E}\|$ is the 6 × 6 matrix of elastic compliances, $\|d^{(n)}\|$ is the 6 × 3 matrix of piezoelectric coefficients and $\|\varepsilon^{(n),\sigma}\|$ is the 3 × 3 matrix of dielectric permittivities of the first component (n = 1) and second component (n = 2), and the superscript t denotes the transposition. In this method, the aforementioned matrices of properties belong to the components that can be from any symmetry class, and below we give formulae for this general case. A matrix $\|C^*\|$ of the effective electromechanical properties of the 2–2 composite is represented as [10, 22]

$$||C^*|| = \left[\left|\left|C^{(1)}\right|\right| \cdot ||M|| m + \left|\left|C^{(2)}\right|\right| (1-m) \right] [||M|| m + ||I|| (1-m)]^{-1} \tag{2.4}$$

The structure of the $\|C^*\|$ matrix from (2.4) is similar to $\|C^{(n)}\|$ from (2.3). The effective electromechanical properties of the composite are determined from (2.4) in a long-wave approximation [10, 21, 22]. This means that any wavelength from an external field is much longer than the thickness of separate layers (C1 or C2, see Figs. 2.1 and 2.1) in the composite system. In (2.4) $\|M\|$ is the matrix related to the boundary conditions at interfaces x_i = const (i = 3 for the series-connected composite, see Fig. 2.1, or i = 1 for the parallel-connected composite, see Fig. 2.1), and $\|I\|$ is the identity matrix. We remind the reader that in (2.4) we deal with the 9 × 9 matrices only.

In a 2–2 composite with a parallel connection of layers (see Fig. 2.2), the boundary conditions at x_1 = const imply a continuity of components of mechanical stress σ_{11}, σ_{12} and σ_{13}, mechanical strain ξ_{22}, ξ_{23} and ξ_{33}, electric displacement D_1, and electric field E_2 and E_3. We then represent $\|M\|$ for interfaces x_1 = const as

$$||M|| = ||p_1||^{-1}||p_2||, \tag{2.5}$$

where the matrix

$$||p_n|| = \begin{pmatrix} 1 & 0 & 0 & 0 & 0 & 0 & 0 & 0 & 0 \\ s_{12}^{(n),E} & s_{22}^{(n),E} & s_{23}^{(n),E} & s_{24}^{(n),E} & s_{25}^{(n),E} & s_{26}^{(n),E} & d_{12}^{(n)} & d_{22}^{(n)} & d_{32}^{(n)} \\ s_{13}^{(n),E} & s_{23}^{(n),E} & s_{33}^{(n),E} & s_{34}^{(n),E} & s_{35}^{(n),E} & s_{36}^{(n),E} & d_{13}^{(n)} & d_{23}^{(n)} & d_{33}^{(n)} \\ s_{14}^{(n),E} & s_{24}^{(n),E} & s_{34}^{(n),E} & s_{44}^{(n),E} & s_{45}^{(n),E} & s_{46}^{(n),E} & d_{14}^{(n)} & d_{24}^{(n)} & d_{34}^{(n)} \\ 0 & 0 & 0 & 0 & 1 & 0 & 0 & 0 & 0 \\ 0 & 0 & 0 & 0 & 0 & 1 & 0 & 0 & 0 \\ d_{11}^{(n)} & d_{12}^{(n)} & d_{13}^{(n)} & d_{14}^{(n)} & d_{15}^{(n)} & d_{16}^{(n)} & \varepsilon_{11}^{(n),\sigma} & \varepsilon_{12}^{(n),\sigma} & \varepsilon_{13}^{(n),\sigma} \\ 0 & 0 & 0 & 0 & 0 & 0 & 0 & 1 & 0 \\ 0 & 0 & 0 & 0 & 0 & 0 & 0 & 0 & 1 \end{pmatrix} \tag{2.6}$$

is written in terms of the electromechanical constants of the components, and n = 1 and 2. For the series-connected 2–2 composite, we write $\|p_n\|$ that has a form similar to that in (2.6), but is concerned with the boundary conditions at x_3 = const (Fig. 2.1). We now use $\|p_n\|$ to find $\|M\|$ from (2.5) and then to calculate the full set of electromechanical constants of the composite at m = const in accordance with (2.4).

Taking the matrix elements $C^*_{ab}(m)$ from (2.4), we analyse the effective piezoelectric coefficients $d^*_{ij}(m)$ of the 2–2 FC/polymer composite, where the volume fraction of the FC component m can be varied from 0 to 1. Here we consider examples of the piezoelectric performance of the composites whereby the polymer component is piezo-passive. The polymer components that are of interest for our analysis are shown in Table 2.1. We consider the polymer components with different stiffness characteristics, but of specific interest is so-called *auxetic*

Table 2.1 Elastic compliances s_{ab} (in 10^{-12} Pa^{-1}) and dielectric permittivity ε_{pp} of piezo-passive polymers at room temperature

Polymers	s_{11}	s_{12}	$\varepsilon_{pp}/\varepsilon_0$
Araldite [22]	216	−78	4.0
Polyurethane [23]	405	−151	3.5
Elastomer [24]	3300	−1480	5.0
Polyethylene (high-density) [8, 12, 25]	1540	−517	2.3
Auxetic polyethylene [8, 12, 25]	5260	4360	2.3

polyethylene (PE) with a negative Poisson's ratio [25]. In contrast to the remaining polymers from Table 2.1, this auxetic component is characterised by elastic compliances $s_{1b} > 0$, and such an elastic behaviour distinctively influences the piezoelectric properties of the composite. Hereby we neglect a specific microgeometry of auxetic PE [25] and regard a 2–2–γ FC/auxetic polymer composite as a material with 2–2 connectivity.

The studied 2–2 FC/polymer composites are characterised by ∞mm symmetry for a series connection (Fig. 2.1) or $mm2$ for a parallel connection (Fig. 2.2). This means that the matrix of the effective piezoelectric coefficients $\|d^{*}\|$ of the composite has the form of $\|d\|$ from (1.30) (series connection) or from (1.29) (parallel connection).

Typical examples of the piezoelectric performance of the 2–2 FC/polymer composites are shown in Figs. 2.3 and 2.4. In Fig. 2.3 the volume-fraction dependences $d_{ij}^{*}(m)$ are shown for the PCR-7M-based composite, where the PCR-7M FC is characterised by the high piezoelectric activity (as shown by data in Table 1.5). In Fig. 2.4 we show the volume-fraction dependences $d_{ij}^{*}(m)$ that are related to the composite based on the modified $PbTiO_3$ FC. It can be seen from Table 1.5 that the modified $PbTiO_3$ FC materials have a moderate piezoelectric

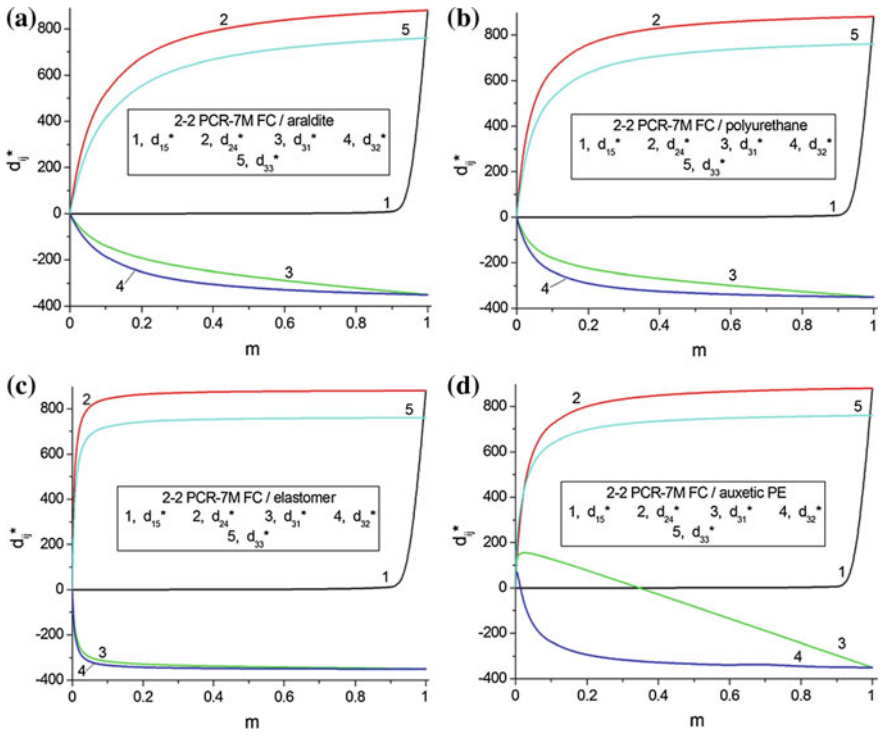

Fig. 2.3 Volume-fraction dependences of piezoelectric coefficients d_{ij}^{*} (in pC/N) of 2–2 parallel-connected PCR-7M FC/polymer composites

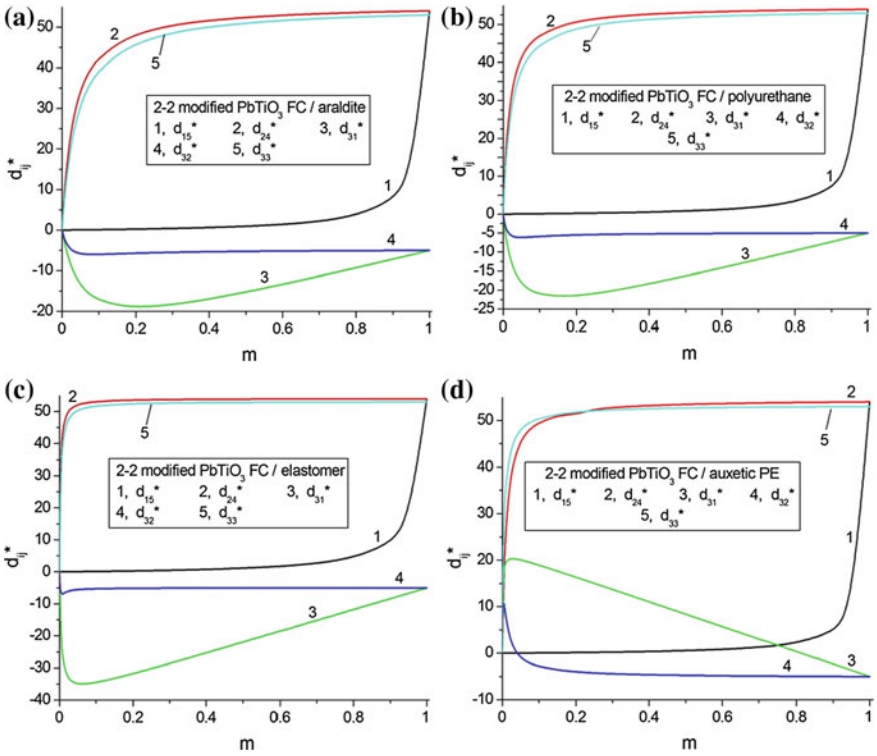

Fig. 2.4 Volume-fraction dependences of piezoelectric coefficients d_{ij}^* (in pC/N) of 2–2 parallel-connected modified $PbTiO_3$ (III) FC/polymer composites

activity (e.g., their piezoelectric coefficient d_{33} is approximately 15 times smaller than the piezoelectric coefficient d_{33} of PCR-7M), but it exhibits a large piezoelectric anisotropy, i.e., condition (1.44) holds. The graphs in Figs. 2.3 and 2.4 suggest that a change from araldite to polyurethane in the piezo-passive polymer layers of the composite does not lead to appreciable changes in the volume-fraction dependences $d_{ij}^*(m)$ (cf. Fig. 2.3a, b, as well as Fig. 2.4a, b). A change from polyurethane to elastomer in the polymer layers does however lead to distinct changes in $d_{ij}^*(m)$ (cf. Figure 2.3b, c, as well as Fig. 2.4b, c). The more remarkable changes are observed if we replace the elastomer layers with an auxetic PE, as shown in see Figs. 2.3d and 2.4d. The aforementioned changes in $d_{ij}^*(m)$ are a result of the role of the elastic properties of the polymer component. On lowering its stiffness, we achieve more rapid increase in $d_{24}^*(m)$ and $d_{33}^*(m)$, as shown by curves 2 and 5 in any graph of Figs. 2.3 and 2.4, which is a result of the piezoelectric response becoming more pronounced along the co-ordinate axes OX_2 and OX_3. As seen from Fig. 2.2, both the components are distributed continuously along these axes. In contrast to $d_{24}^*(m)$, the related shear piezoelectric coefficient $d_{15}^*(m)$ remains small in a wide m range as shown by curve 1 in any graph of Figs. 2.3 and 2.4, and

such behaviour can be accounted for by the strong influence of the interfaces x_1 = const in Fig. 2.2 on the shear piezoelectric effect. In fact, these interfaces suppress the piezoelectric polarisation along OX_1 in the presence of piezo-passive polymer layers. Changes in $d_{31}^{*}(m)$ as shown by curve 3 in any graph of Figs. 2.3 and 2.4 are concerned with the role of the interfaces x_1 = const and elastic properties of the FC and polymer components. Interrelations between their elastic compliances $s_{ab}^{(n)}$ lead to a non-monotonic volume-fraction dependence $d_{31}^{*}(m)$ (see curve 3 in Figs. 2.3d and 2.4), and in the $PbTiO_3$-based composite the elastic anisotropy of the FC component plays an important role in a wide m range.

The series-connected composites are characterised by relatively small values of $d_{3j}^{*}(m)$ at volume fractions $0 < m < 0.9$ due to the poor orientation of the layers (Fig. 2.1) with respect to the poling direction. Under an external electric field $\boldsymbol{E}\|OX_3$ a considerable depolarisation field appears in the FC layers that provide only a small contribution to the piezoelectric response of the composite along OX_3. In Table 2.2 we show examples of the volume-fraction dependences $d_{ij}^{*}(m)$ of the PCR-7M-based composite. It is clear that the lower piezoelectric activity of the modified $PbTiO_3$ FC leads to smaller values of $|d_{3j}^{*}(m)|$ in a wide m range. For instance, d_{33}^{*} = 1 pC/N at m = 0.433, and d_{31}^{*} = –1 pC/N at m = 0.910 in the 2–2 modified $PbTiO_3$ (III) FC/araldite composite with series-connected layers. In contrast to $d_{3j}^{*}(m)$, the $d_{15}^{*}(m)$ dependence follows a uniform increase with increasing m (see 4th and 7th columns in Table 2.2), and changes of the polymer component only lead to minor changes in $d_{15}^{*}(m)$. Hereby we observe the considerable shear PS, especially at $m > 0.3$. This is a result of the orientation of the interfaces (Fig. 2.1) that do not impede the shear piezoelectric effect in the series-connected composite. The auxetic polymer component strongly influences the piezoelectric coefficient

Table 2.2 Piezoelectric coefficients d_{ij}^{*} (in pC/N) of 2–2 series-connected PCR-7M-based composites

m	d_{31}^{*}	d_{33}^{*}	d_{15}^{*}	d_{31}^{*}	d_{33}^{*}	d_{15}^{*}
	PCR-7M FC/araldite			PCR-7M FC/auxetic PE		
0	0	0	0	0	0	0
0.01	–0.0593	0.0701	16.3	–0.155	–0.136	17.0
0.02	–0.0996	0.120	32.2	–0.160	–0.135	33.7
0.05	–0.171	0.211	78.6	–0.168	–0.127	82.1
0.10	–0.232	0.297	151	–0.178	–0.107	157
0.20	–0.304	0.419	280	–0.201	–0.0589	289
0.30	–0.367	0.544	391	–0.230	0.00337	401
0.50	–0.539	0.904	573	–0.322	0.203	583
0.70	–0.917	1.72	716	–0.536	0.669	723
0.90	–2.77	5.74	832	–1.60	2.99	834
0.95	–5.51	11.7	857	–3.19	6.44	858
0.99	–25.9	56.1	876	–15.4	33.0	877

$d_{33}^{*}(m)$ at volume fractions $m < 0.3$ (6th column in Table 2.2). We observe the non-monotonic behaviour of $d_{33}^{*}(m)$ at $m \ll 1$ due to the negative Poisson's ratio of auxetic PE. At $m > 0.3$ the role of the FC component becomes more active, and $d_{33}^{*}(m)$ resembles the behaviour of that in the parallel-connected composites; see, for instance, curve 5 in Fig. 2.3 or Fig. 2.4.

In general, the studied series-connected FC-based composites are characterised by the piezoelectric coefficients d_{ij}^{*} that obey the condition

$$d_{15}^{*} = d_{24}^{*} \gg \left| d_{3j}^{*} \right| \tag{2.7}$$

at $0.01 \leq m \leq 0.99$, where $j = 1$ and 3. The parallel-connected FC-based composites demonstrate different examples of the piezoelectric performance and anisotropy (Figs. 2.3 and 2.4) which depend on the properties of both the FC and polymer components. The electromechanical properties of the FC component play a dominant role at large volume fractions ($m > 0.5$), while the properties of the polymer component strongly influences the PS and anisotropy of d_{ij}^{*} in the composite, as a rule, at $m < 0.3$.

2.1.2 2–2 Single Crystal/Polymer Composites

Interest in the piezoelectric performance of modern SC/polymer composites [10, 12, 26–28] stems from the outstanding electromechanical properties of the relaxor-ferroelectric SC component [29–36]. To the best of our knowledge, full sets of electromechanical constants have been measured on samples of only perovskite-type relaxor-ferroelectric SCs along one of the following poling directions: [001], [011] or [111] in the perovskite unit cell. Examples of the electromechanical properties of the poled PMN–xPT SCs are shown in Tables 1.3, 1.4 and 2.3, and examples of the domain arrangement in the poled state are shown in Fig. 1.2. We note that PMN–0.28PT has been the first relaxor-ferroelectric SC, for which self-consistent and full sets of electromechanical constants were measured [33] on the [001]-, [011]- and [111]-poled samples. In the single-domain state at room temperature, the PMN–0.28PT SC is characterised by $3m$ symmetry with a spontaneous polarisation vector $\boldsymbol{P}_s \| [111]$. The domain-engineered SC poled along [001] exhibits $4mm$ symmetry and has an average spontaneous polarisation vector $\boldsymbol{P}_s \| [001]$. Poling along the perovskite unit-cell [011] axis leads to the domain-engineered state [32] with $mm2$ symmetry and an average spontaneous polarisation vector $\boldsymbol{P}_s \| [011]$. Data from Tables 1.3, 1.4 and 2.3 suggest that these SCs poled along the aforementioned crystallographic directions demonstrate high piezoelectric activity resulting in large absolute values of specific piezoelectric coefficients d_{ij}. Due to this piezoelectric performance and various symmetry features, the 2–2 SC/polymer composite poled along the specific direction becomes an

Table 2.3 Elastic compliances s_{ab}^E (in 10^{-12} Pa^{-1}), piezoelectric coefficients d_{ij} (in pC/N) and dielectric permittivity ε_{pp}^σ of [111]-poled single-domain PMN–xPT SCs ($3m$ symmetry) at room temperature

Electromechanical constants	Single-domain PMN–0.28PT SC [32]	Single-domain PMN–0.33PT SC [30]
s_{11}^E	8.78	62.16
s_{12}^E	−4.90	−53.85
s_{13}^E	−0.93	−5.58
s_{14}^E	16.87	−166.24
s_{33}^E	6.32	13.34
s_{44}^E	138.69	510.98
s_{66}^E	27.4	232.02
d_{15}	2382	4100
d_{22}	−312	1340
d_{31}	−43	–90
d_{33}	97	190
$\varepsilon_{11}^\sigma/\varepsilon_0$	4983	3950
$\varepsilon_{33}^\sigma/\varepsilon_0$	593	640

attractive composite material where different variants of the PS and anisotropy of d_{ij}^* can be observed. Such a composite is also of independent interest due to a variety of shear oscillation modes [36] that do not appear in conventional FC samples because of their ∞mm symmetry.

It is assumed that the 2–2 SC/polymer composite is characterised by a regular distribution of alternating SC and polymer layers in the OX_1 direction (Fig. 2.2), and the layers are continuous in the OX_2 and OX_3 directions. In Fig. 2.2 now C1 refers to SC, and C2 refers to polymer. The effective electromechanical properties of the 2–2 SC/polymer composite are determined by means of the matrix method, as described in Sect. 2.1.1. In Sect. 2.1.2 we analyse examples of the volume-fraction dependences of the piezoelectric coefficients $d_{ij}^*(m)$ (Figs. 2.5, 2.6 and 2.7) at specific orientations of the main crystallographic axes in the SC component. Among the polymer components of interest in Table 2.1, we consider araldite as a relatively stiff polymer with a positive Poisson's ratio and an auxetic PE as a very soft polymer with a negative Poisson's ratio.

The arrangement of curves in graphs of Fig. 2.5 for the SC based composites differs from the arrangement shown in Fig. 2.3 for the PCR-7M-based composite with the high piezoelectric activity. The smaller values of $d_{15}^*(m)$ and $d_{24}^*(m)$ (curves 1 and 2 in Fig. 2.5) are related to the PMN–xSC-based composites: their SC components poled along [001] are characterised by piezoelectric coefficients d_{15} (Table 1.3) that are smaller than d_{15} of the PCR-7M FC (Table 1.5). Comparing Fig. 2.5a–c leads to an increase in $|d_{3j}^*|$ due to larger values of $|d_{3j}|$ in the PMN–0.33PT SC in comparison to the PMN–0.28PT. The PMN–0.33PT is located almost at the morphotropic phase boundary and exhibits high piezoelectric activity and

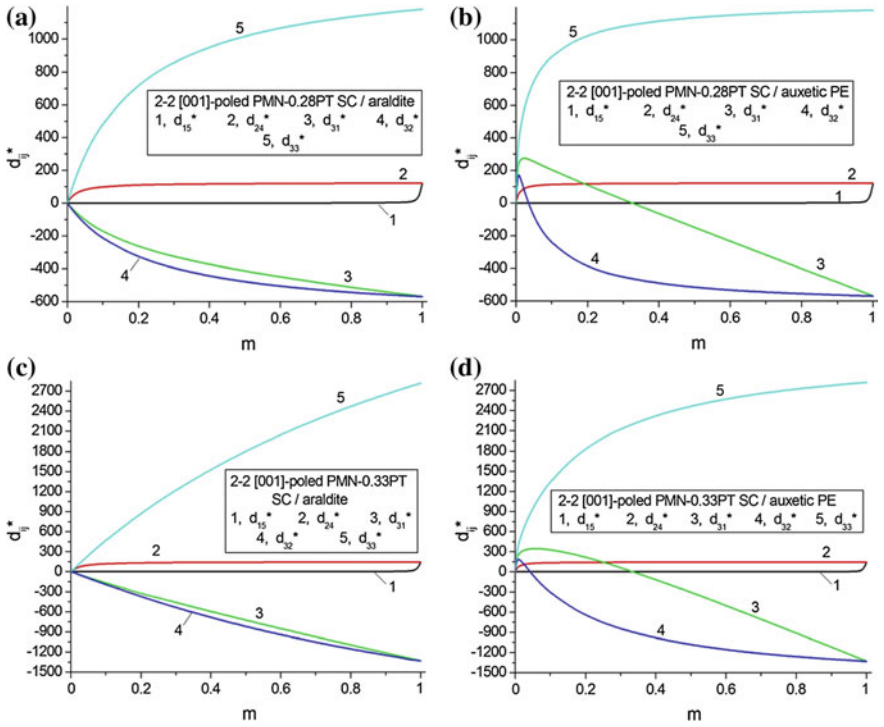

Fig. 2.5 Volume-fraction dependences of piezoelectric coefficients d_{ij}^{*} (in pC/N) of 2–2 parallel-connected [001]-poled PMN–xPT SC/polymer composites: $x = 0.28$ (**a** and **b**) and $x = 0.33$ (**c** and **d**)

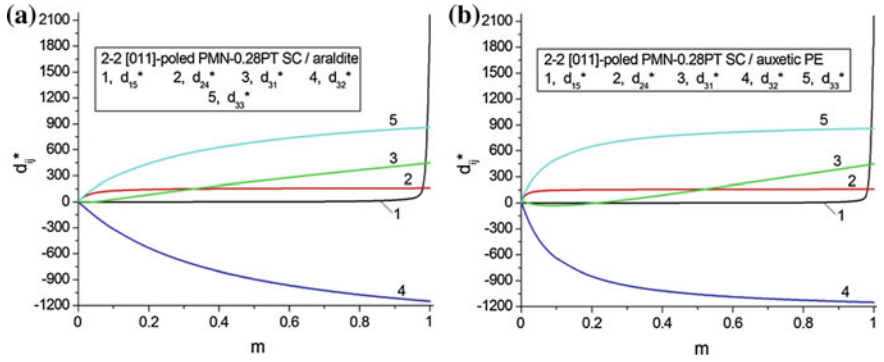

Fig. 2.6 Volume-fraction dependences of piezoelectric coefficients d_{ij}^{*} (in pC/N) of 2–2 parallel-connected [011]-poled PMN–0.28PT SC/polymer composites

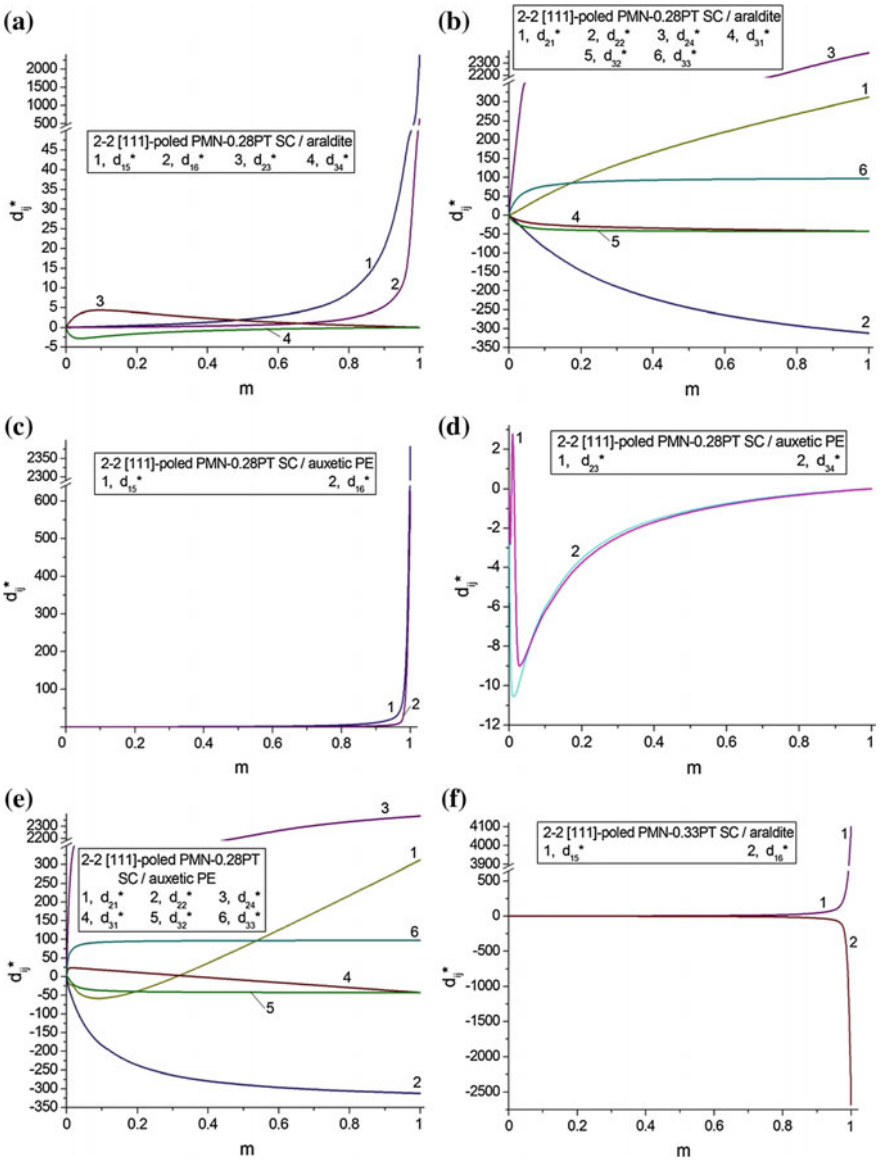

Fig. 2.7 Volume-fraction dependences of piezoelectric coefficients d_{ij}^* (in pC/N) of 2–2 parallel-connected [111]-poled PMN–xPT SC/polymer composites: $x = 0.28$ (**a**–**e**) and $x = 0.33$ (**f**–**k**)

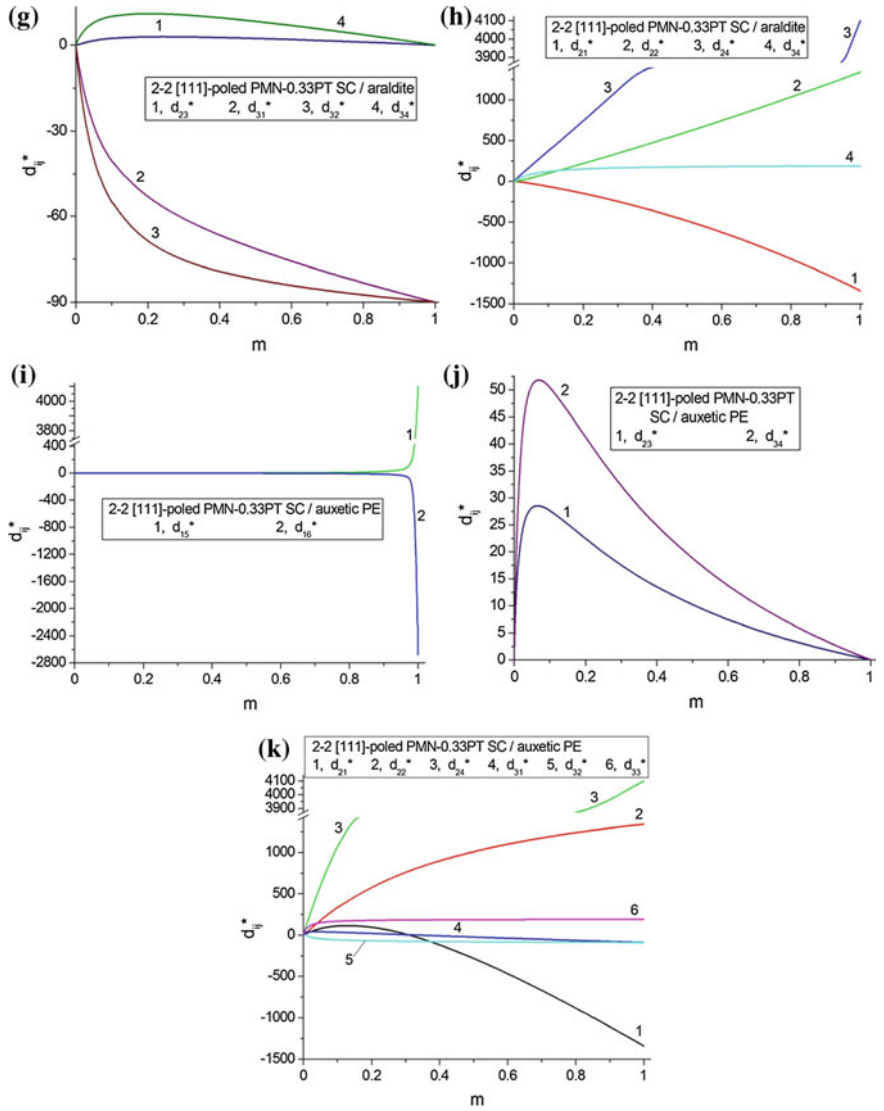

Fig. 2.7 (continued)

strong electromechanical coupling [29, 30, 36]. The auxetic polymer mainly influences the piezoelectric coefficients $d_{31}^*(m)$ and $d_{32}^*(m)$ at $m < 0.1$ (see curves 3 and 4 in Fig. 2.5b, d) irrespective of the molar concentration x in the SC component. The non-monotonic behaviour of $d_{31}^*(m)$ and $d_{32}^*(m)$ is observed at $0 < m < 0.03$, when the positive elastic compliance s_{12} of auxetic PE actively influence the transverse piezoelectric response.

In general one can state that the studied 2–2 composites based on the [001]-poled SCs are of interest due to the large values of $|d_{3j}^*|$ (Fig. 2.5) in a wide volume-fraction range.

In a case of the 2–2 composite based on the [011]-poled SC, we see minor changes in the $d_{ij}^*(m)$ dependences (Fig. 2.6) on changing the polymer component. There is the only non-monotonic $d_{31}^*(m)$ dependence in the PMN–0.28PT SC/auxetic PE composite, see curve 3 in Fig. 2.6b. This can be accounted for by the influence of the auxetic polymer component on the piezoelectric response as a result of the interfaces x_1 = const (Fig. 2.2). The piezoelectric coefficient $d_{15}^*(m)$ rapidly increases at $0.9 < m < 1$, see curve 1 in Fig. 2.6. Such a shear piezoelectric response represents an example of a '*sleeping* PS' and is strongly affected by the aforementioned interfaces x_1 = const. Due to the presence of these interfaces, the piezoelectric coefficient d_{15}^* of the composite can be considerable at very large volume fractions m of the SC component with high piezoelectric activity, and in a wide m range we observe a validity of the condition

$$d_{15}^* \ll d_{24}^* \tag{2.8}$$

(see curves 1 and 2 in Fig. 2.6). Moreover, the derivative dd_{15}^* / dm is small in the wide m range and increases at $m > 0.9$. The composite based on the [011]-poled SC is also characterised by the relation

$$d_{31}^* < d_{33}^* < \left|d_{32}^*\right| \tag{2.9}$$

as shown by curves 3–5 in Fig. 2.6. The inequality (2.9) correlates with values of the piezoelectric coefficients d_{3j} of the SC component (see Table 1.4).

The 2–2 composite based on the [111]-poled SC represents an example of the PS that depends on both the components and their volume fractions. Our analysis of the piezoelectric coefficients d_{ij}^* enables us to conclude that such a composite is described by m symmetry, and the corresponding matrix of d_{ij}^* in a case of the interfaces x_1 = const (Fig. 2.2) is given by

$$||d^*|| = \begin{pmatrix} 0 & 0 & 0 & 0 & d_{15}^* & d_{16}^* \\ d_{21}^* & d_{22}^* & d_{23}^* & d_{24}^* & 0 & 0 \\ d_{31}^* & d_{32}^* & d_{33}^* & d_{34}^* & 0 & 0 \end{pmatrix}. \tag{2.10}$$

Non-monotonic dependences of the piezoelectric coefficients $d_{ij}^*(m)$ are observed in Fig. 2.7 that are often concerned with the interfaces x_1 = const and elastic properties of the polymer component. The specific non-monotonic dependence is observed in a case when the piezoelectric coefficient $d_{ij} = 0$ for both the SC and polymer components, however $d_{ij}^* \neq 0$ is allowed for the m symmetry class, see Fig. 2.7d, j. In this situation we see relatively small deviations of d_{ij}^* from zero values at $m = 0$ and 1.

The very large values of the piezoelectric coefficient d_{15} of the [111]-poled SC (see Table 2.3) should promote large values of d_{15}^*, however the interfaces x_1 = const in the composite impede its shear piezoelectric response, and we again observe the 'sleeping PS' in the wide volume-fraction range, as shown by curve 1 in Fig. 2.7a, c, f, i. The similar 'sleeping PS' is also typical of the piezoelectric coefficient d_{16}^*, see curve 2 in Fig. 2.7a, c, f, i. In contrast to d_{15}^*, the piezoelectric coefficient d_{24}^* exhibits large values in a wide volume-fraction range irrespective of the SC and polymer component (see curve 3 in Fig. 2.7b, e, h, k), and the related shear PS may be of interest for piezoelectric sensor and actuator applications.

The large piezoelectric coefficient d_{22} of the [111]-poled PMN–0.33PT SC (see Table 2.3) leads to large values of d_{22}^* of the composite in a wide m range as shown by curve 2 in Fig. 2.7h, k, We remind the reader that the piezoelectric coefficient d_{22}^* characterises the longitudinal PS where the OX_2 axis is parallel to the interfaces x_1 = const (Fig. 2.2). In comparison to d_{22}^*, the piezoelectric coefficient d_{33}^* remains relatively small, see curve 6 in Fig. 2.7b, e, k. In the [111]-poled PMN–0.33PT SC the piezoelectric coefficient d_{33} is smaller than d_{22} by about seven times (Table 2.3), and this circumstance leads to a less favourable PS due to the piezoelectric coefficient d_{22}^* of the composite irrespective of its polymer component. Undoubtedly, the example of the pronounced longitudinal PS concerned with d_{22}^* in the PMN–0.33PT-based composite is important for sensor and actuator applications.

The [111]-poled PMN–xPT SC/auxetic PE composite is of specific interest due to the large anisotropy of the piezoelectric coefficients d_{2j}^* and changes in sgn d_{21}^*. Traditionally the poled $PbTiO_3$-type FCs and related composites exhibit a large anisotropy of d_{3j}^*: see, for instance, Table 1.5, (1.44) and work [10, 12, 37]. In the [111]-poled PMN–xPT SCs, as seen from Table 2.3, the largest longitudinal piezoelectric coefficient is d_{22}, but not d_{33}. As a consequence, the condition $d_{22}^* > d_{33}^*$ holds for the composite in a wide volume-fraction range; compare curves 2 and 6 in Fig. 2.7e or Fig. 2.7k. In the presence of auxetic polymer layer s, the effective redistribution of internal mechanical and electric fields takes place, so that conditions

$$\left| d_{22}^* / d_{2f}^* \right| \geq 5 \tag{2.11}$$

and

$$d_{21}^*(m_d) = 0 \tag{2.12}$$

can be valid. For the PMN–0.28PT-based composite, the condition (2.11) is valid at $0.178 < m < 0.449$, and $m_d = 0.312$. At $m = m_d$ the [111]-poled PMN–0.28PT SC/auxetic PE composite is characterised by the piezoelectric coefficients $d_{22}^* = -267$ pC/N and $d_{23}^* = -2.18$ pC/N, i.e., the longitudinal PS along OX_2 is dominating. For the PMN–0.33PT-based composite, the condition (2.11) is valid at $0.180 < m < 0.447$, $m_d = 0.312$, and values of $d_{22}^* = 779$ pC/N and $d_{23}^* = 17.0$ pC/N

are achieved at $m = m_d$. The piezoelectric performance at the valid condition (2.12) suggests that the studied composites have obvious advantages over the highly anisotropic $PbTiO_3$-type FCs [37] first and foremost due to the large d_{22}^{*} values. It should be added in connection with (2.11) that, in contrast to the conventional poled FCs [3, 4], electrodes on the 2–2 composite sample (Fig. 2.2) are perpendicular to the OX_2 axis. The validity of (2.11) and (2.12) opens up new possibilities of piezotechnical applications for the studied 2–2 composites. These applications can be concerned with the longitudinal oscillation modes, transducer, sensor, and other related functions of the studied piezo-active composites.

2.1.3 2–0–2 Single Crystal/Ceramic/Polymer Composites

In work [38] samples of a 2–2-type PZT FC/heterogeneous polymer composite were prepared by the adding of inorganic particles (for instance, graphite, silicon or strontium ferrite in the powder form) to each polymer layer. This use of the additives led to an improvement in specific effective parameters of the composite that is described by 2–0–2 connectivity. For instance, in the parallel-connected PZT-based composite containing strontium ferrite in the polymer layers, larger values of the ECF k_t^{*} at the thickness oscillation mode are achieved [38]. An improvement of the piezoelectric response and related parameters of the 2–2-type composites can be achieved by employing a system of 0–3 FC/polymer layers in addition to the main piezo-active component. The influence of FC inclusions in the 0–3 layer on the performance of the 2–2-type composites based on relaxor-ferroelectric SCs have been recently studied [39, 40].

Now it is assumed that the 2–0–2 composite consists of a system of parallel-connected layers of two types (Fig. 2.8), and these layers are arranged regularly along the OX_1 axis. The Type I layer is represented by a domain-engineered SC with a spontaneous polarisation $\boldsymbol{P}_s^{(1)}$ and volume fraction m. The Type II layer is regarded as a 0–3 FC/polymer composite, and the volume fraction of such layers in the composite sample is $1 - m$. The shape of each FC inclusion (see inset in Fig. 2.8) obeys the equation

$$(x_1/a_1)^2 + (x_2/a_2)^2 + (x_3/a_3)^2 = 1 \tag{2.13}$$

relative to the axes of the co-ordinate system $(X_1X_2X_3)$. In (2.13) a_1, $a_2 = a_1$ and a_3 are semi-axes of the inclusion. Its aspect ratio is $\rho_i = a_1/a_3$, and subscript 'i' denotes the inclusion. Linear sizes of each FC inclusion are much smaller than the thickness of each layer as measured along OX_1 (see Fig. 2.8). The FC inclusions in the Type II layer occupy sites of a simple tetragonal lattice with unit-cell vectors parallel to the OX_j axes. In Sect. 2.1.3 we consider the piezoelectric performance of the 2–0–2 composite that is based on either the [001]-poled SC or [011]-poled SC. Domain types in these SCs are schematically shown in Fig. 1.2.

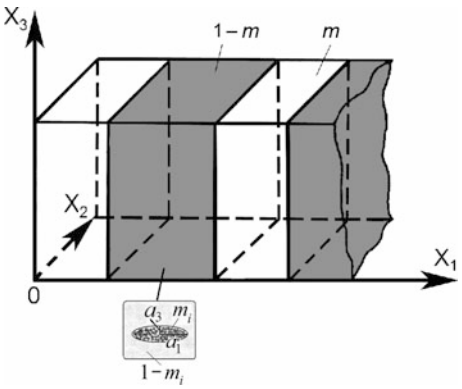

Fig. 2.8 Schematic of the 2–0–2 SC/FC/polymer composite. ($X_1X_2X_3$) is a rectangular co-ordinate system, m and $1 - m$ are volume fractions of the SC and FC/polymer layers, respectively, m_i is the volume fraction of isolated FC inclusions in the polymer medium, a_1 and a_3 are semi-axes of each inclusion (reprinted from paper by Topolov et al. [39], with permission from Taylor and Francis)

We evaluate the effective electromechanical properties of the 2–0–2 composite as follows [39]. At the first stage, the effective properties of the 0–3 FC/polymer composite in the Type II layer are determined using EFM [10] that takes into consideration an interaction between the FC inclusions. The effective electromechanical properties of the 0–3 composite are represented in the form of the 9×9 matrix as follows:

$$\left|\left|C^{(0-3)}\right|\right| = \begin{pmatrix} \left\|c^{(0-3),E}\right\| & \left\|e^{(0-3)}\right\|^t \\ \left\|e^{(0-3)}\right\| & -\left\|\varepsilon^{(0-3),\xi}\right\| \end{pmatrix}. \tag{2.14}$$

In (2.14) the superscript t denotes the transposition of the matrix. Elements of the $\|C^{(0-3)}\|$ matrix from (2.14) are found using the formula [10]

$$\begin{aligned} \left\|C^{(0-3)}\right\| = \left\|C^{(p)}\right\| + m_i\left(\left\|C^{(FC)}\right\| - \left\|C^{(p)}\right\|\right) \\ \left[\|I\| + (1-m_i)\|S\|\left\|C^{(p)}\right\|^{-1}\left(\left\|C^{(FC)}\right\| - \left\|C^{(p)}\right\|\right)\right]^{-1}. \end{aligned} \tag{2.15}$$

In (2.15), $\|C^{(FC)}\|$ and $\|C^{(p)}\|$ are matrices of the electromechanical properties of FC and polymer, respectively, $\|I\|$ is the identity matrix, and $\|S\|$ is the matrix that contains the Eshelby tensor components [41] and depends on elements of $\|C^{(p)}\|$ and the aspect ratio ρ_i. $\|C^{(FC)}\|$ and $\|C^{(p)}\|$ from (2.15) have the form shown in (2.14).

At the second stage, the effective properties of the 2–0–2 composite are evaluated using the matrix method (see Sect. 2.1.1). Hereby we use $\|C^{(0-3)}\|$ from (2.15) as the $\|C^{(2)}\|$ matrix that describes the properties of the Type II layer, and the $\|C^{(1)}\|$ matrix that characterises the properties of SC in the Type I layer. The effective electromechanical properties of the 2–0–2 composite are described by the $\|C^*\|$

matrix from (2.4). These properties are functions of the volume fraction of the SC component m, volume fraction of the FC inclusions m_i in the Type II layer and aspect ratio of these inclusions ρ_i.

Of particular interest is the combination of the soft polymer component and stiff modified $PbTiO_3$ FC in the Type II layer [39]. Differences in the elastic properties

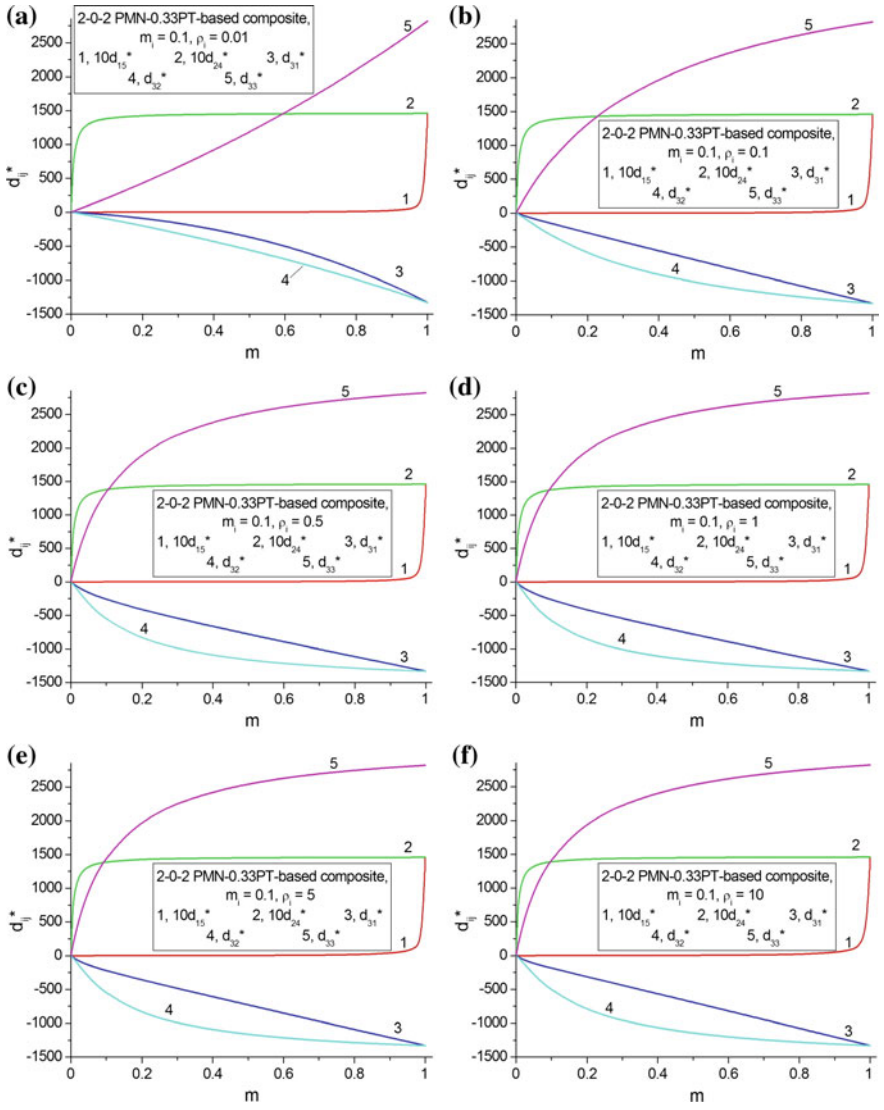

Fig. 2.9 Volume-fraction dependences of piezoelectric coefficients d_{ij}^* (in pC/N) of the 2–0–2 [001]-poled PMN–0.33PT SC/modified $PbTiO_3$ (I) FC/PE composite. The schematic of the composite is shown in Fig. 2.8

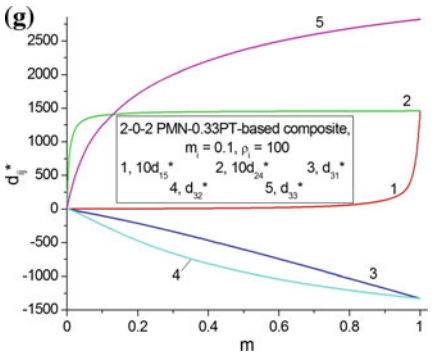

Fig. 2.9 (continued)

of the layers allow control of the dependence of the piezoelectric properties of the composite on the elastic properties and their anisotropy in the Type II layer. It is clear that changes in the elastic properties in the Type II layer are a result of changes in the volume fraction m_i and aspect ratio ρ_i of the FC inclusions therein. As follows from our evaluations, the Type II layer exhibits a low piezoelectric activity [39] compared to the SC component due to the presence of isolated FC inclusions at $0 < m_i \leq 0.3$ and $0.01 \leq \rho_i \leq 100$. The absolute values of the piezoelectric coefficients of the 0–3 modified $PbTiO_3$ FC/polymer composite are $|d_{3j}^{(0-3)}| < 10$ pC/N [39, 40], even under ideal electric poling conditions. We therefore neglect the lower piezoelectric properties of the Type II layer in the 2–0–2 composite and now consider only the piezo-active SC component, i.e., the [001]-poled domain-engineered SC (see the orientation of domains in Fig. 1.2a). Examples of the volume-fraction (m) dependence of the piezoelectric coefficients d_{ij}^* of the 2–0–2 composites are graphically represented in Figs. 2.9 and 2.10. In Figs. 2.9 and 2.10 we show the graphs for a case of a relatively small volume fraction of FC inclusions ($m_i = 0.1$) and vary their aspect ratio ρ_i in a wide range, i.e., $0.01 \leq \rho_i \leq 100$. The values of $0 < \rho_i < 1$ are related to prolate FC inclusions, and the values of $\rho_i > 1$ are related to oblate FC inclusions.

Graphs in Figs. 2.9 and 2.10 suggest that the Type II layers with the FC inclusions influence the piezoelectric properties of the studied composites in a variety of ways. The mutual arrangement of curves 1 and 2 in Figs. 2.9 and 2.10 undergo very minor changes at $0.01 \leq \rho_i \leq 100$, and this means that the shear piezoelectric effect is almost non-sensitive to changes in the microgeometry and elastic anisotropy in the Type II layer. This effect is less important in comparison to the longitudinal and transverse effects in the composite based on the [001]-poled PMN–0.33PT SC. Changes in the mutual arrangement of curves 3–5 in Figs. 2.9 and 2.10 are a result of the influence of the elastic anisotropy of the Type II layer on the piezoelectric effect (either longitudinal or transverse), and such an influence becomes more pronounced as the FC inclusions become either highly prolate or highly oblate.

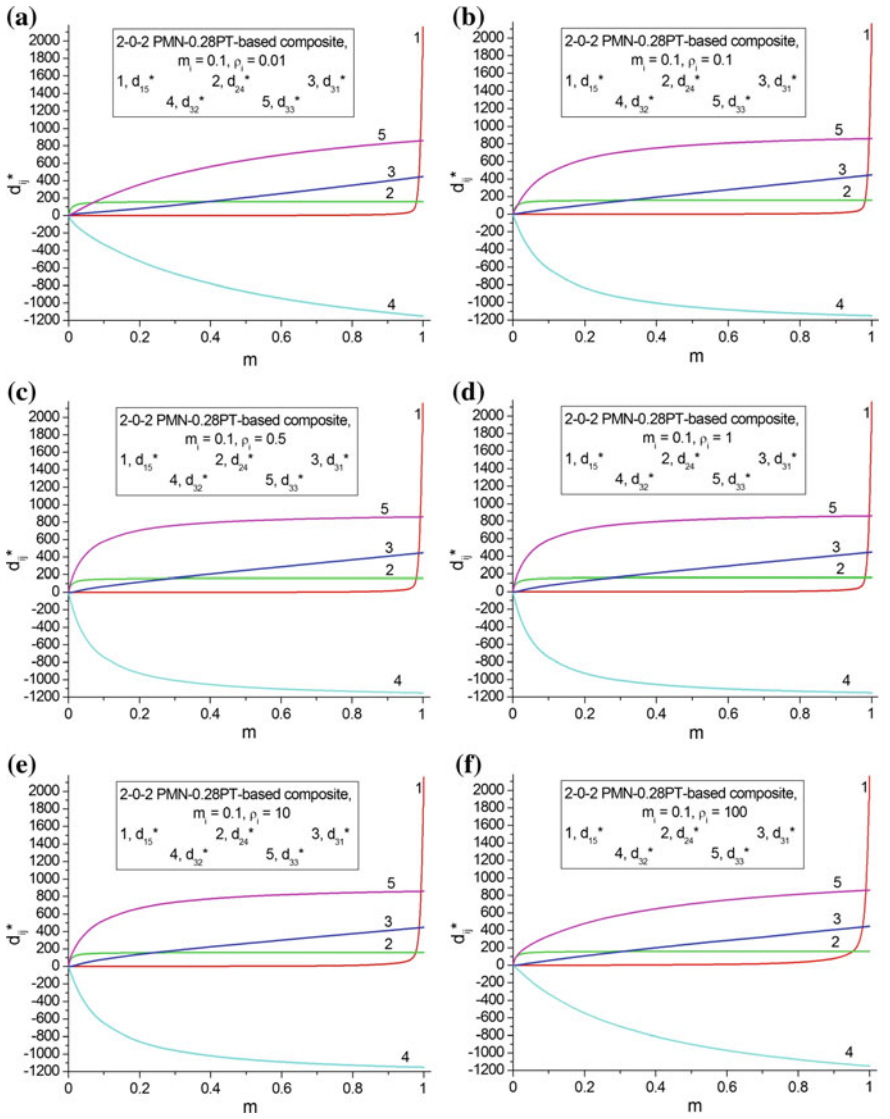

Fig. 2.10 Volume-fraction dependences of piezoelectric coefficients d_{ij}^* (in pC/N) of the 2–0–2 [011]-poled PMN–0.28PT SC/modified $PbTiO_3$ (I) FC/PE composite. The schematic of the composite is shown in Fig. 2.8

The main feature of the piezoelectric performance of the composite based on the [011]-poled PMN–0.28PT SC consists in the 'sleeping PS' concerned with the largest piezoelectric coefficient d_{15} of the SC component. The very small piezoelectric coefficient d_{15}^* in a wide m range, see curve 1 in Fig. 2.10, is due to the suppressing influence of the interfaces $x_1 = \text{const}$ (Fig. 2.8) on the shear

piezoelectric effect. The [011] poling direction leads to large values of $|d_{32}|$ of the SC component (see 2nd column in Table 1.4) and $|d_{32}^*|$ of the composite as a whole (see curve 4 in Fig. 2.10). The PMN–0.28PT-based composite is also of interest due to the relatively large values of d_{33}^*, see curve 5 in Fig. 2.10. It is obvious that the interfaces x_1 = const do not strongly influence the longitudinal piezoelectric effect in such a composite. The FC inclusions in the Type II layer influence the anisotropy of the piezoelectric coefficients d_{3j}^* to a restricted extent: there are no large changes in the mutual arrangement of curves 3–5 in Fig. 2.10 with changes of the aspect ratio ρ_i.

In our study on the 2–0–2 composites, we have used components with contrasting properties: for instance, the relaxor-ferroelectric SC with a strong shear piezoelectric effect, non-poled FC and piezo-passive polymer. The piezoelectric activity of the SC layer and the active role of the elastic subsystem in the 0–3 FC/polymer layer lead to large piezoelectric coefficients in specific ranges of the volume fraction of SC m. Such a performance of the studied 2–0–2 SC/FC/polymer composites is important for piezoelectric actuator, transducer and energy-harvesting applications concerned with specific oscillation modes.

2.2 1–3-Type Composites

In the 1–3 composite sample, a component with a higher piezoelectric activity is self-connected in one dimension, often along the poling axis, and a component with a lower piezoelectric activity, or a piezo-passive component, is self-connected in three dimensions. In fact, the 1–3 composite represents a system of long rods (component termed 'C1' in Fig. 2.11) aligned in a large matrix (component termed 'C2' in Fig. 2.11). The rods can be made of FC or ferroelectric SC, and the matrix of the composite can be made of polymer, cement, glass, etc. [4, 8, 10, 12, 17–20, 24]. The 1–3 FC/polymer composites are widespread [4, 8, 10–12, 16–18, 24, 42] for a few reasons. Among them we mention an ease of poling, available methods to manufacture high-quality composite samples and a variety of advantages for the 1–3 composite over poled monolithic FCs.

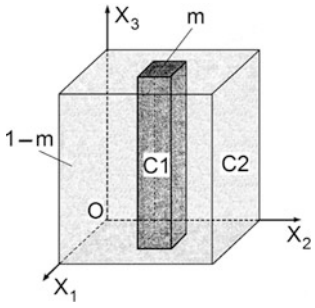

Fig. 2.11 Schematic of the 1–3 composite. m and $1 - m$ are volume fractions of components C1 and C2, respectively. $(X_1X_2X_3)$ is the rectangular co-ordinate system

The combination of the relatively low dielectric permittivity and high piezoelectric activity at small volume fractions of FC (often less than 10%) results in a significant PS associated with large values of the piezoelectric coefficient g_{33}^* of the 1–3 FC/polymer composite [10, 15, 16, 23, 24, 42]. On increasing the volume fraction of FC, the high PS of the composite is achieved due to the large piezoelectric coefficient d_{33}^* that becomes approximately equal to $d_{33}^{(1)}$ of the FC component even at its moderate volume fractions [24, 38]. Changes in the configuration of the cross section of the FC rod (C1 in Fig. 2.11) by the horizontal plane can lead to changes in the anisotropy of the piezoelectric properties of the 1–3 composite [12, 43]. Moreover, large values of its ECFs k_{33}^* and k_t^* are observed in wide volume-fraction ranges [10, 44]. These and other important parameters of the composite have stimulated intensive research into the development and manufacture of a variety of 1–3 composites in the last decades. Since the 2000s, the 1–3 relaxor-ferroelectric SC/polymer composites [8, 10, 12, 26, 27] have been advanced piezoelectric materials due to their high effective parameters and outstanding electromechanical properties of the SC components; see, for instance, Tables 1.3 and 1.4.

The piezo-active 1–3 composites are also of interest due to the non-monotonic dependence of their parameters on the volume fraction of the main piezoelectric component in rods. Among the parameters exhibiting the non-monotonic behaviour, one can mention the piezoelectric coefficients d_{3j}^*, e_{33}^*, g_{3j}^*, and h_{33}^* [10, 27, 42–44], hydrostatic piezoelectric coefficients d_h^* and g_h^* [4, 10, 24, 42, 43], thickness ECF k_t^* [10, 26, 42, 44], hydrostatic ECF k_h^* [8, 12, 23], and squared hydrostatic figure of merit $(Q_h^*)^2$ [10, 24, 44]. Of independent interest are the orientation effects [12, 45, 46] and aspect-ratio effects [47, 48] which enable us to improve some effective parameters of the 1–3-type composites based on relaxor-ferroelectric SCs. The main methods that can be applied to predict the effective electromechanical properties and related parameters of the 1–3-type composites are the matrix method, EFM and FEM [10, 22, 24, 43–48].

In Sect. 2.2 we analyse relations between the composite microgeometry and PS of various composites that are based on either FCs or ferroelectric SCs. Some modifications of the matrix and related examples of the PS will be discussed in the context of improving the performance of the composites for specific piezotechnical applications.

2.2.1 1–3 Ceramic/Polymer Composites

Since the 1980s, the 1–3 FC/polymer composite is of great interest as a heterogeneous material that combines the high PS, large figures of merit, ECFs, and other parameters [10, 11, 15, 24]. In Sect. 2.2.1 we show examples of the PS concerned with the piezoelectric coefficients d_{ij}^* of a few FC-based composites. Among the FC components of interest, as earlier, we choose the PCR-7M FC with large values of

$|d_{ij}|$ and the modified $PbTiO_3$ FC with a large anisotropy of d_{3j} (see data in Table 1.5). The polymer components that can form the matrices in the 1–3 composites are listed in Table 2.1. When using auxetic PE as a matrix component, we do not specify the connectivity pattern in the microporous polymer matrix [25] of the related composite (it should then be described by the formula 1–3–γ). In our study this composite is described by 1–3 connectivity.

It is assumed that the long FC rods (component termed 'C1' in Fig. 2.11) are arranged periodically in the large polymer matrix (component termed 'C2' in Fig. 2.11). Centres of symmetry of the bases of the FC rods form a square lattice in the (X_1OX_2) plane of the rectangular co-ordinate system $(X_1X_2X_3)$ shown in Fig. 2.11. The remanent polarisation vector of the FC rod is $\boldsymbol{P}_r^{(1)} \uparrow\uparrow OX_3$. The full set of electromechanical constants of the 1–3 composite with the square cross section rods is evaluated by means of either the matrix method [10, 22] or FEM [12, 43] via the COMSOL package [49]. The boundary conditions involve components of electric and mechanical fields at the rod—matrix interface. In FEM the rectangular representative unit cell, containing the FC rod that is adjusted to yield the appropriate volume fraction m of the FC component (Fig. 2.11), is discretised using triangular elements. The unknown displacement field is interpolated using second-order Lagrange shape functions, leading to a problem with approximately 120,000–200,000 degrees of freedom. Periodicity is enforced at the boundary of the rectangular representative unit cell of the composite. After solving the equilibrium problem, the effective elastic moduli $c_{ab}^{*E}(m)$, piezoelectric coefficients $e_{ij}^{*}(m)$ and dielectric permittivities $\varepsilon_{pq}^{*\xi}(m)$ of the composite are computed by means of averaging the resulting local stress and electric-displacement fields over the representative unit cell. The volume fraction m of FC can be varied from 0 to 1 due to the planar microgeometry of this composite, see Fig. 2.11. The matrix of its effective piezoelectric coefficients d_{ij}^{*} has the form similar to that shown in (1.30).

Examples of the volume-fraction dependences of d_{ij}^{*} are shown in Figs. 2.12 and 2.13. We observe the non-monotonic $d_{31}^{*}(m)$ dependence: see, for instance, curve 2 in Figs. 2.12d and 2.13. In the PCR-7M-based composite, d_{31}^{*} passes through a maximum point (see curve 2 in Fig. 2.12d) at small volume fractions m. A similar behaviour was observed for the related 2–2 composite, see curve 3 in Fig. 2.3d. Such a character of the $d_{31}^{*}(m)$ dependence is accounted for by the influence of the interface x_1 = const (both in the 2–2 and 1–3 composites) and by the active role of the auxetic polymer matrix. The condition $d_{31}^{*}(m) \approx 0$ holds at $m \approx 0.3$ (see curve 2 in Fig. 2.12d), and a large piezoelectric anisotropy is achieved, i.e., condition (1.44) holds for d_{3j}^{*} of the composite. Irrespective of the polymer component, the piezoelectric coefficient d_{15}^{*} exhibits minor changes at $m < 0.95$ (curve 1 in Fig. 2.12), and we observe the 'sleeping PS' due to the weak shear effect suppressed by the FC—polymer interfaces in the composite structure (Fig. 2.11). We remind the reader that the similar examples of the 'sleeping PS' concerned with d_{15}^{*} and planar interfaces were shown in Sect. 2.1.

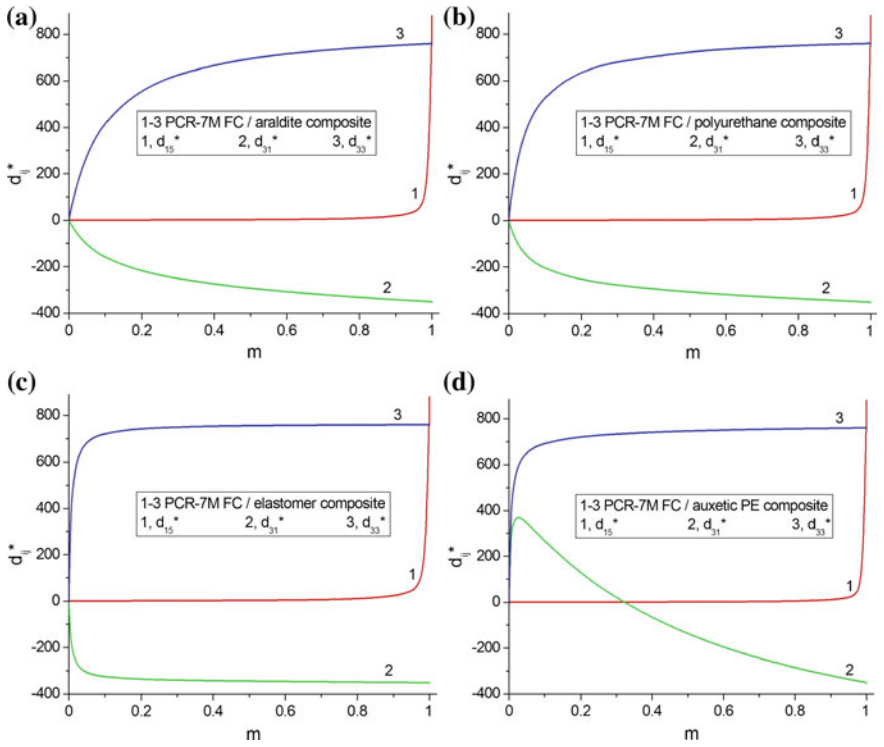

Fig. 2.12 Volume-fraction dependences of piezoelectric coefficients d_{ij}^* (in pC/N) of 1–3 PCR-7 M FC/polymer composites with square cross section rods. The schematic of the composite is shown in Fig. 2.11

In contrast to d_{15}^*, the piezoelectric coefficient d_{33}^* of the 1–3 composite is characterised by a rapid increase (see curve 3 in Fig. 2.12), and softening the polymer component promotes the larger values of d_{33}^*. This is due to the system of FC rods that are poled and distributed continuously along the OX_3 axis (see C1 in Fig. 2.11).

The 1–3 composite based on the modified $PbTiO_3$ FC demonstrates trends in the behaviour of $d_{15}^*(m)$ (curve 1 in Fig. 2.13) and $d_{33}^*(m)$ (curve 3 in Fig. 2.13) as shown in Fig. 2.12 for the PCR-7M-based composite. The non-monotonic $d_{31}^*(m)$ dependence (see curve 2 in Fig. 2.13a–c) at relatively small volume fractions m and in the presence of the polymer matrix with a positive Poisson's ratio is similar to that observed in the related 2–2 composite (see curve 3 in Fig. 2.4a–c). It is also seen that min $d_{31}^*(m)$ shifts towards the volume fraction $m = 0$ (see curve 2 in Fig. 2.13a–c) on softening the polymer matrix in the 1–3 composite or the polymer layers in 2–2 composites (see curve 3 in Fig. 2.4a–c). In both composite types, the interfaces x_1 = const play a key role in forming the lateral piezoelectric effect and strongly influence the $d_{31}^*(m)$ dependence, however the $|d_{31}^*|$ value remains fairly

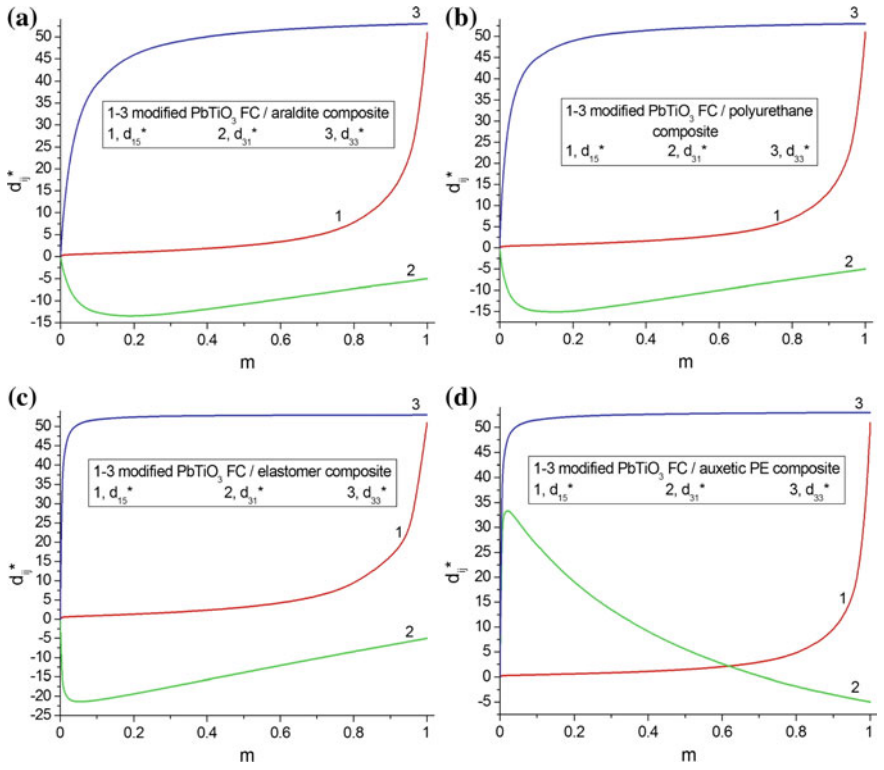

Fig. 2.13 Volume-fraction dependences of piezoelectric coefficients d_{ij}^* (in pC/N) of 1–3 modified $PbTiO_3$ (III) FC/polymer composites with square cross section rods. The schematic of the composite is shown in Fig. 2.11

small in comparison to $|d_{31}^*|$ of the aforementioned PCR-7M-based composite. It is striking that the auxetic polymer matrix leads to an increase in $d_{31}^*(m)$ in the modified $PbTiO_3$ FC/auxetic PE composite by approximately 6.5 times in comparison to $|d_{31}|$ of FC. As follows from our analysis, max $d_{31}^*(m)$ appears at a volume fraction $m \ll 1$ (see curve 2 in Fig. 2.13d) due to the active influence of elastic properties of the auxetic polymer component on the piezoelectric performance of the composite.

The 1–3 FC-based composites are also studied to show the role of the pillar effect in forming the effective properties and their anisotropy [12, 43]. The pillar effect in the 1–3 composite mainly means the influence of the cross section of the piezoelectric rod on the performance of the composite. In Sect. 2.2.1 we discuss a performance of a 1–3 FC/polymer composite with elliptical cross sections of rods (Fig. 2.14) in the (X_1OX_2) plane that is perpendicular to the poling axis OX_3. This 1–3 composite has a cellular structure and a regular distribution of FC rods in the large polymer matrix.

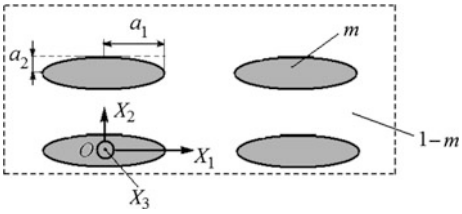

Fig. 2.14 Cross section of the 1–3 FC/polymer composite by the X_1OX_2 plane. ($X_1X_2X_3$) is the rectangular co-ordinate system, a_1 and a_2 are semi-axes of the ellipse, m is the volume fraction of FC, and $1 - m$ is the volume fraction of polymer (reprinted from paper by Topolov and Bisegna [43], with permission from Springer)

Cross sections of the FC rods by the (X_1OX_2) plane of the rectangular co-ordinate system ($X_1X_2X_3$) (Fig. 2.14) are described by the equation

$$(x_1/a_1)^2 + (x_2/a_2)^2 = 1 \tag{2.16}$$

relative to the axes of the rectangular co-ordinate system ($X_1X_2X_3$). Semi-axes of the ellipse a_f ($f = 1$ and 2) from (2.16) are constant in the whole composite sample. Centres of symmetry of these ellipses are arranged periodically on the OX_1 and OX_2 directions. The remanent polarisation vector of each FC rod is $\boldsymbol{P}_r^{(1)} \uparrow\uparrow OX_3$. It is assumed that the FC rods are aligned along the OX_3 axis (like the C1 rods in Fig. 2.11), and the height of each rod obeys the condition $h \gg a_f$.

The effective electromechanical properties of the 1–3 composite with elliptical cross sections of its rods are determined in the long-wave approximation [8, 12, 43] within the framework of the FEM via the COMSOL package. The rectangular representative unit cell, containing the FC rod in the form of an elliptical cylinder with semi-axes a_f adjusted to yield the appropriate volume fraction m of the FC component (Fig. 2.14), is discretised using triangular elements. The unknown displacement field is interpolated using second-order Lagrange shape functions, leading to a problem with approximately 120,000–200,000 degrees of freedom. The number of the degrees of freedom depends on the ratio of semi-axes $\eta = a_2/a_1$. Periodicity is enforced at the boundary of the rectangular representative unit cell of the composite. After solving the equilibrium problem, the effective elastic moduli $c_{ab}^{*E}(m, \eta)$, piezoelectric coefficients $e_{ij}^*(m, \eta)$ and dielectric permittivities $\varepsilon_{pq}^{*\zeta}(m, \eta)$ of the composite are computed by means of averaging the resulting local stress and electric-displacement fields over the representative unit cell. We add that the volume fraction m and the ratio of semi-axes η are varied [43] in ranges $0 < \eta \leq 1$ and $0 < m < \pi/4$, respectively. The limiting case of $\eta = 0$ corresponds to a 2–2 parallel-connected composite, and the limiting case of $\eta = 1$ is relevant to a circular rod cross section and the 1–3 connectivity pattern. The limiting case of the volume fraction $m = \pi/4$ is related to a system of the rods touching each other.

As follows from our analysis, the matrix of the piezoelectric coefficients d_{ij}^* of the 1–3 FC/polymer composite at $0 < \eta < 1$ has the form shown in (1.29), and at

$\eta = 1$ the matrix of d_{ij}^* is similar to that in (1.30). In a wide volume-fraction range, the shear piezoelectric coefficients d_{15}^* and d_{24}^* obey conditions

$$d_{15}^* \ll \left|d_{3j}^*\right| \quad \text{and} \quad d_{24}^* \ll \left|d_{3j}^*\right| \quad \text{at } m = \text{const}, \tag{2.17}$$

where $j = 1$, 2 and 3. We observed a similar 'sleeping PS' as a result of the very weak shear piezoelectric effect in the 1–3 PCR-7M-based composites with circular cylindrical rods, see curves 1 in graphs of Fig. 2.12. Changes in the piezoelectric coefficients $d_{3j}^*(m, \eta)$ at $0 \leq m \leq 0.7$ and $0.01 \leq \eta \leq 1$ are graphically represented in Fig. 2.15. Trends in changes of d_{3j}^* are similar to that shown in Fig. 2.12d: the configuration of curve 2 therein resembles the configuration of curves built for d_{31}^* (Fig. 2.15a) or d_{32}^* (Fig. 2.15b) at η = const, and the configuration of curve 3 in Fig. 2.12d is similar to the configuration of curves built for d_{33}^* (Fig. 2.15c) at η = const. The auxetic polymer component with a negative Poisson's ratio strongly

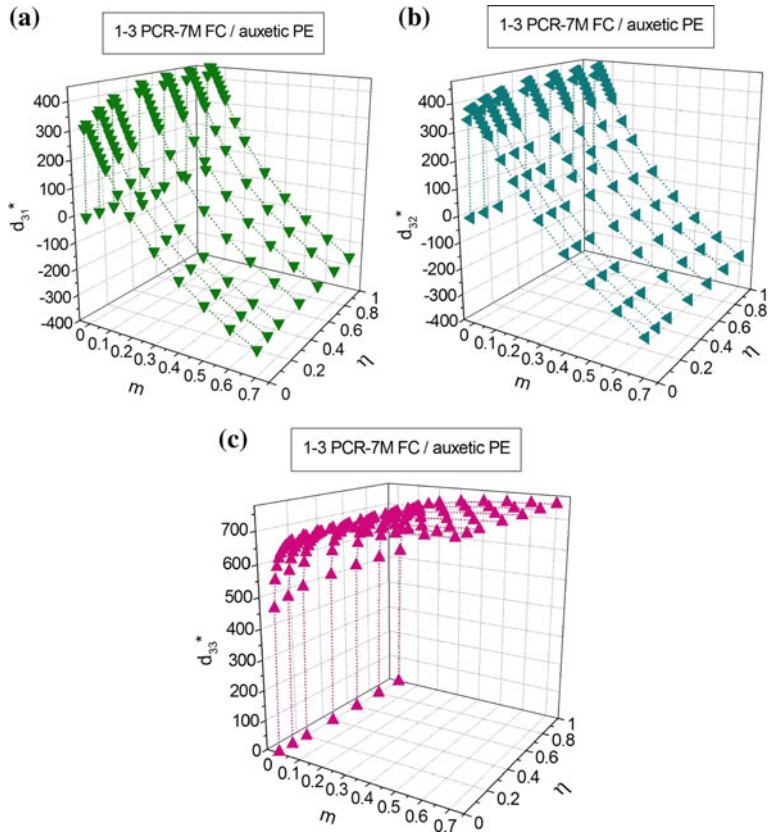

Fig. 2.15 Piezoelectric coefficients d_{3j}^* (in pC/N) of the 1–3 PCR-7M FC/auxetic PE composite with elliptical cross section rods

influences the lateral piezoelectric effect in the composite (Fig. 2.15a, b) at volume fractions $m \ll 1$. Due to the presence of the auxetic PE matrix, changes in sgn d_{31}^* and sgn d_{32}^* are observed, and this is also typical of the volume fractions $m \ll 1$, see Fig. 2.15a, b. Changes in the η value lead to the equality $d_{31}^* \approx d_{32}^*$ that holds in the wide m range. The range $0.2 < m < 0.4$ is of interest due to the large anisotropy of d_{3j}^*: we see that at increasing the volume fraction m, the condition $d_{31}^* = 0$ holds at $m = m_1$ and the condition $d_{32}^* = 0$ holds at $m = m_2 > m_1$. For the studied the 1–3 PCR-7M FC/auxetic PE composite, the difference $m_2 - m_1$ does not exceed 0.15 in the wide η range.

Figure 2.15c suggests that the longitudinal piezoelectric effect in the studied composite undergoes minor changes at varying η. Changes of the piezoelectric coefficient d_{33}^* at η = const are similar to those in the 1–3 composites wherein the polymer matrix is characterised by a positive Poisson's ratio (see, for instance, curve 3 in Fig. 2.13a–c), and the configuration of the cross section of the rod has a little influence on the $d_{33}^*(m)$ dependence. It should be added that the $d_{33}^*(m)$ dependence is similar to that related to the parallel-connected 2–2 FC/polymer composites (see curve 5 in Fig. 2.3a–c or Fig. 2.4a–c). This is accounted for by the continuous distribution of the FC component (i.e., rods in the 1–3 composite or layers in the 2–2 composite) along the OX_3 axis, see C1 in Figs. 2.2 and 2.11.

2.2.2 1–3 Single Crystal/Polymer Composites

Piezo-active 1–3 composites based on SCs of the perovskite-type relaxor-based solid solutions, e.g. PMN–xPT and PZN–xPT, are intensively studied as high-performance materials [8, 10, 12, 44, 50] and suitable [26, 27] for piezoelectric transducer and energy-harvesting applications. The main reason for the high piezoelectric performance of these composites is the outstanding electromechanical properties of the domain-engineered PMN–xPT and PZN–xPT SCs with compositions near the morphotropic phase boundary; see, for instance, the full sets of electromechanical constants of these SCs in Tables 1.3 and 1.4.

A modification of the 1–3 composite structure shown in Fig. 2.11 becomes an important factor [8, 9, 50] that influences the effective parameters and potential applications for advanced piezo-active composites. The relative simplicity of the 1–3 composite structure and possibilities for modification (such as reinforcing the polymer matrix with a third component, formation of a porous polymer matrix, etc. [9, 11]) open up possibilities to improve the PS of the 1–3-type composites.

The first example of the PS is concerned with the 1–3 composite based on the domain-engineered PMN–0.33PT SC, see graphs of d_{ij}^* in Fig. 2.16. The effective electromechanical properties of the 1–3 composite are determined by means of the matrix method, see (2.4) and work [10, 22]. It is seen that replacing the polymer component does not lead to appreciable changes of d_{15}^* (see curve 1 in Fig. 2.16). A transition from a hard polymer (araldite) to a soft polymer (elastomer) leads to a

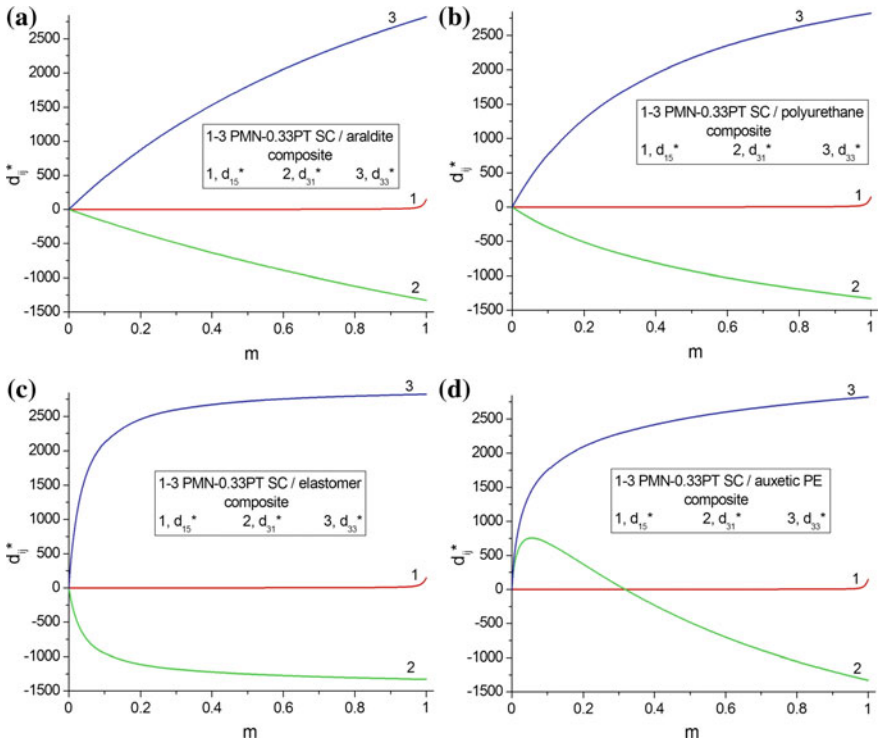

Fig. 2.16 Volume-fraction dependences of piezoelectric coefficients d_{ij}^* (in pC/N) of 1–3 [001]-poled PMN–0.33PT SC/polymer composites with square cross section rods. The schematic of the composite is shown in Fig. 2.11

more intensive increase of $|d_{3j}^*|$ at the volume fraction of SC in the range $0 < m < 0.2$ (see curves 2 and 3 in Fig. 2.16c), and the saturation of $|d_{3j}^*|$ is observed at $m > 0.6$. The auxetic polymer component strongly influences d_{31}^*, especially at $0 < m < 0.2$ (see curve 2 in Fig. 2.16d), and this effect concerned with the negative Poisson's ratio is similar to that in the 2–2 SC/auxetic PE composite (see curve 3 in Fig. 2.5b, d).

In the second example we consider a 1–3 composite based on the domain-engineered KNNTL:Mn SC. The volume-fraction dependences of d_{3j}^* of this lead-free composite (Fig. 2.17) are similar to those shown in Fig. 2.16. However a larger difference between elastic compliances of the KNNTL:Mn SC and polymer components enables us to observe the saturation of $|d_{3j}^*|$ even at $m > 0.2$ (Fig. 2.17c). The smaller values of the piezoelectric coefficients $|d_{3j}|$ of the KNNTL:Mn SC (Table 1.2) in comparison to $|d_{3j}|$ of the PMN–0.33PT SC (Table 1.3) lead to a lower PS of the lead-free composite in comparison to that based on the PMN–0.33PT SC. Nevertheless, the KNNTL:Mn-based composite may be of interest due to $d_{33}^* \approx 500$ pC/N (see curve 3 in Fig. 2.17) and $d_{31}^* = 0$

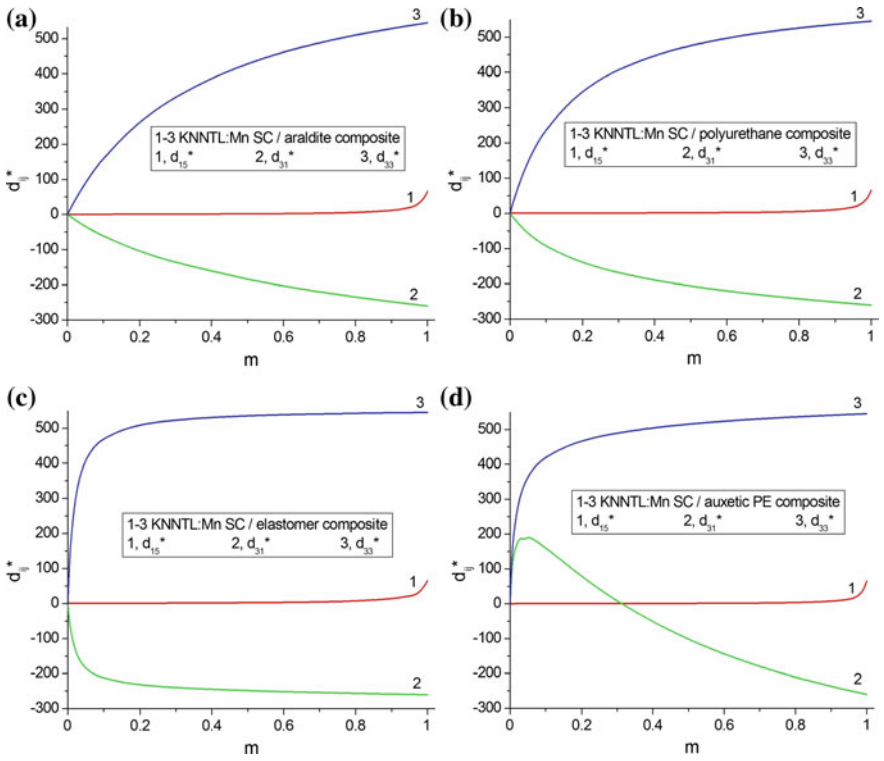

Fig. 2.17 Volume-fraction dependences of piezoelectric coefficients d_{ij}^* (in pC/N) of 1–3 [001]-poled KNNTL:Mn SC/polymer composites with square cross section rods. The schematic of the composite is shown in Fig. 2.11

(see curve 2 in Fig. 2.17d). The combination of these piezoelectric coefficients leads to the longitudinal PS that is approximately 8–9 times higher than in the highly anisotropic modified $PbTiO_3$ FCs [37] whose piezoelectric coefficients d_{3j} are known from Table 1.5. It should be noted that the value of $d_{33}^* \approx 500$ pC/N is also larger than d_{33} of many poled FCs based on Pb(Zr, Ti)O_3, see Table 1.5.

2.2.3 1–2–2 Composites Based on Single Crystals

The three-component 1–3-type composite structures consisting of FC rods and polymer layers were first studied in work [51, 52]. The piezoelectric performance of the three-component composite based on the [001]-poled PMN–0.33PT SC was first discussed in work [53]. Topolov et al. first studied a 1–3-type SC-based composite [53] wherein the matrix was laminar and comprised of two piezo-passive polymer components. Due to such a matrix, an effect of the elastic properties of the

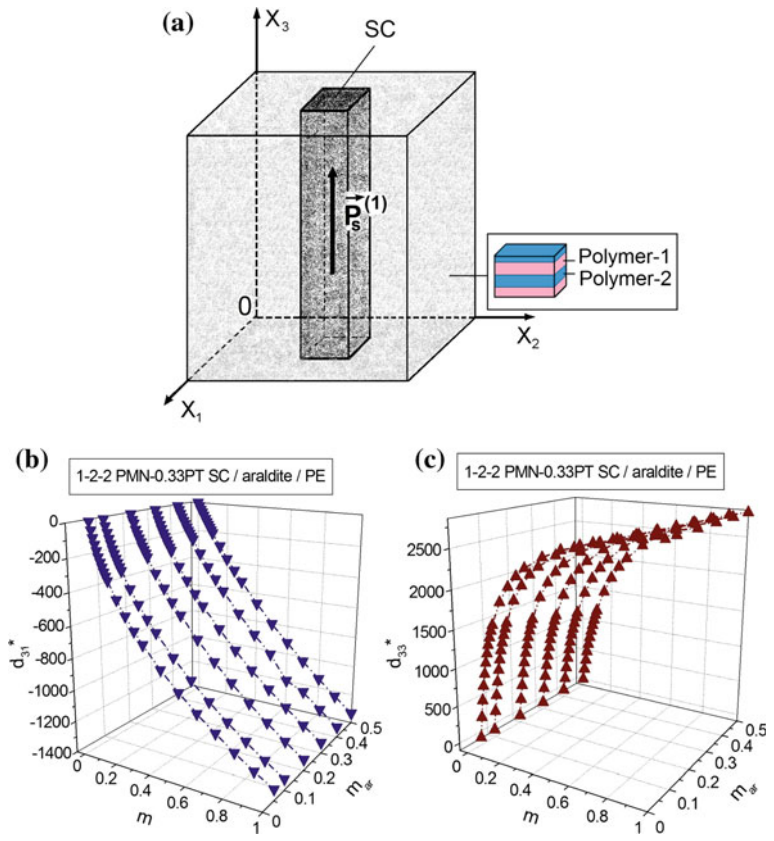

Fig. 2.18 Schematic of the 1–2–2 SC/polymer-1/polymer-2 composite (**a**) and volume-fraction dependences of piezoelectric coefficients d_{3j}^* (**b** and **c**, in pC/N) of the 1–2–2 [001]-poled PMN–0.33PT SC/araldite/monolithic PE composite with square cross section rods. In schematic a, $\boldsymbol{P}_s^{(1)}$ is the spontaneous polarisation vector of the SC component. In graphs **b** and **c**, m is the volume fraction of the SC component in the composite sample, and m_{ar} is the volume fraction of araldite in the laminar matrix

laminar polymer matrix on the performance and hydrostatic parameters of the composite based on the PMN–0.33PT SC was described in work [53].

We assume that the long SC rods are regularly distributed in the laminar matrix surrounding them (Fig. 2.18a), and a square arrangement of the rods is observed in the (X_1OX_2) plane. The main crystallographic axes of each SC rod are oriented as follows: X$\|OX_1$, Y$\|OX_2$ and Z$\|OX_3$. The layers of the two polymers are regularly distributed along the OX_3 axis (see inset in Fig. 2.18a) that is the poling axis of the composite. The composite system is described by 1–2–2 connectivity. For this composite, we first evaluate the electromechanical properties of the laminar polymer matrix (2–2 connectivity, matrix method) and then the properties of the system "Rods—laminar matrix" (1–3 connectivity, either by the matrix method or FEM).

Results based on the matrix method are shown in Fig. 2.18b, c. A difference between values of d_{3j}^{*} calculated by the matrix method and FEM does not exceed 2% in a wide m range.

The volume fraction of araldite m_{ar} in the laminar matrix influences an increase of $|d_{3j}^{*}|$ and PS of the composite with increasing m. At larger volume fractions m_{ar}, this increase becomes less intensive at $m \ll 1$. One of the main reasons for such a behaviour is related to a decrease of the elastic compliance $s_{33}^{(2)}$ of the laminar matrix on increasing m_{ar}, and this decrease strongly influences the piezoelectric effect, especially along the OX_3 axis. As is known from work [50], the combination of the polymer layers with the larger difference between their elastic constants influences the lateral piezoelectric effect in the 1–2–2 composite to a larger degree. Hereby the role of the laminar matrix is similar to the role of the system of the highly oblate pores in the porous polymer matrix [50], see Sect. 2.2.4. The aforementioned features of the PS and anisotropy of d_{3j}^{*} are to be taken into consideration at the prediction of the piezoelectric performance of the 1–3-type composites and important for some piezotechnical applications.

2.2.4 1–3–0 Composites Based on Single Crystals

The next example of the modification of the 1–3 composite structure is related to systems with 1–3–0 connectivity. This particular connectivity was studied in work [54, 55], however in [54, 55] no detailed study on the piezoelectric coefficients d_{ij}^{*} was carried out. In Sect. 2.2.4 we consider the behaviour of d_{ij}^{*} and related PS of the 1–3–0 composites based on SCs.

It is assumed that the composite shown in Fig. 2.19 contains a system of SC rods in a porous polymer matrix. The SC rods are in the form of rectangular parallelepipeds and continuous along the OX_3 axis. The SC rods have a square base and characterised by a regular square arrangement in the (X_1OX_2) plane. The main crystallographic axes X, Y, and Z of each SC rod are parallel to the following co-ordinate axes shown in Fig. 2.19: X$\|OX_1$, Y$\|OX_2$ and Z$\|OX_3$. Each SC rod is characterised by a spontaneous polarisation vector $\boldsymbol{P}_s^{(\mathbf{1})} \uparrow\uparrow OX_3$, and the OX_3 axis is the poling direction of the composite sample as a whole. The polymer matrix contains a system of spheroidal air pores that are described by the equation

$$\left(x_1/a_{1,p}\right)^2 + \left(x_2/a_{2,p}\right)^2 + \left(x_3/a_{3,p}\right)^2 = 1 \tag{2.18}$$

relative to the axes of the rectangular co-ordinate system $(X_1X_2X_3)$, and semi-axes of the spheroid from (2.18) are $a_{1,p}$, $a_{2,p} = a_{1,p}$ and $a_{3,p}$. The porous matrix is characterised by 3–0 connectivity. The air pores are regularly distributed in the polymer matrix and occupy the sites of a simple tetragonal lattice with unit-cell vectors parallel to the OX_k axes. The shape of each pore is characterised by the

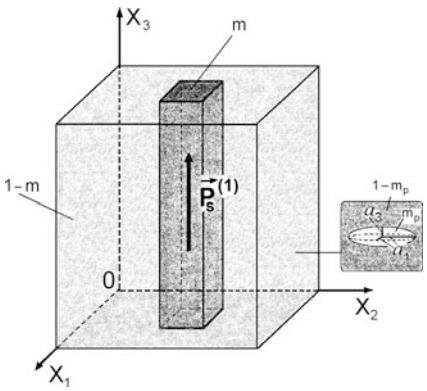

Fig. 2.19 Schematic of the 1–3–0 SC/porous polymer composite. m and $1 - m$ are volume fractions of the SC and porous polymer, respectively, m_p is the volume fraction of air in the porous polymer matrix. $\boldsymbol{P}_s^{(1)}$ is the spontaneous polarisation vector of the SC component. In the inset, a spheroidal pore with semi-axes a_f is shown schematically (reprinted from Topolov et al. [55], with permission from Elsevier)

aspect ratio $\rho_p = a_{1,p}/a_{3,p}$ that is assumed to be fixed over the composite sample. The radius or the largest semi-axis of each pore is considered to be much less than the length of the side of the square that is the intersection of the SC rod with the (X_1OX_2) plane shown in Fig. 2.19.

The effective electromechanical properties of the 1–3–0 composite shown in Fig. 2.19 are evaluated in two stages [54, 55]. During the first stage, the effective properties of the polymer matrix with spheroidal pores are determined as a function of the volume fraction of the pores (or porosity of the polymer matrix) m_p and the aspect ratio ρ_p. The corresponding calculation is based on Eshelby's concept of spheroidal inclusions in heterogeneous solids [41, 56]. The effective properties of the porous polymer medium with 3–0 connectivity are represented in the matrix form [55, 56] as follows:

$$\left|\left|C^{(3-0)}\right|\right| = \left|\left|C^{(2)}\right|\right| \left[||I|| - m_p\left(||I|| - \left(1 - m_p\right)||S||\right)^{-1}\right] \tag{2.19}$$

In (2.19) $\|C^{(2)}\|$ is the 9×9 matrix of the electromechanical properties of the polymer component, $\|I\|$ is 9×9 identity matrix, and $\|S\|$ is the 9×9 matrix that comprises components of the electroelastic Eshelby tensor [41]. The elements of $\|S\|$ depend on the aspect ratio ρ_p of the pore and on the properties of polymer. The effective properties of porous polymer are represented by

$$\left\|C^{(2)}\right\| = \begin{pmatrix} \left\|c^{(2),E}\right\| & \left\|e^{(2)}\right\|^t \\ \left\|e^{(2)}\right\| & -\left\|\varepsilon^{(2),\xi}\right\| \end{pmatrix}, \tag{2.20}$$

where $\|c^{(2),E}\|$ is the 6 × 6 matrix of elastic moduli measured at electric field E = const, $\|e^{(2)}\|$ is the 3 × 6 matrix of piezoelectric coefficients, $\|\varepsilon^{(2),\xi}\|$ is the 3 × 3 matrix of dielectric permittivities at mechanical strain ξ = const, and superscript 't' refers to the transposed matrix. The $\|C^{(3-0)}\|$ matrix from (2.19) has the structure similar to that of $\|C^{(2)}\|$ from (2.20) and $\|C^{(0-3)}\|$ from (2.14).

During the second stage of evaluations, the effective electromechanical properties of the 1–0–3 composite are calculated using either the matrix method [10, 12] or FEM [55]. Some results of calculations by means of these methods were compared in work [55]. The electromechanical properties of the 1–3–0 composite depend on the volume fractions m, m_p and aspect ratio ρ_p and are regarded as properties which are homogenised in the long-wave approximation. This means that the wavelength of an external acoustic field is much longer than the size of the SC rod in the composite sample [55].

The volume-fraction (m) dependence of the piezoelectric coefficients d_{ij}^* of the 1–0–3 composite (Fig. 2.20) shows that the main changes in the wide m range are related to d_{3j}^* (j = 1 and 3) while d_{15}^* remains small and almost constant at $0 < m < 0.9$. Thus, we observe the 'sleeping PS' at $d_{15}^* \ll d_{15}^{(1)}$ and $d\, d_{15}^*/dm \to 0$. Similar trends are observed in the 1–3 composites (see Figs. 2.12a–c, 2.16a–c and 2.17a–c) where the main piezoelectric component is characterised by a relatively small anisotropy of its piezoelectric coefficients $d_{3j}^{(1)}$ and by signs of the piezoelectric coefficients $e_{3j}^{(1)}$ [10, 12] as follows:

$$\operatorname{sgn} e_{33}^{(1)} = -\operatorname{sgn} e_{31}^{(1)} > 0. \tag{2.21}$$

A comparison of the graphs shown in Fig. 2.20 enables us to conclude that the piezoelectric coefficients d_{3j}^* at m = const undergo small changes due to the presence of both prolate ($0 < \rho_p < 1$) and spherical ($\rho_p = 1$) pores in the matrix. Distinct changes in the d_{3j}^* curves, especially at j = 3, are observed in the presence of the highly oblate pores ($\rho_p \gg 1$), see Fig. 2.20g–i. This is due to the relatively large elastic compliance $s_{33}^{(2)}$ of the porous matrix and to the considerable difference between $s_{33}^{(2)}$ and $s_{11}^{(2)}$. An increase of the porosity m_p in the matrix at ρ_p = const also leads to an increase of $s_{33}^{(2)}$, and this increase leads to a higher PS for the composite structure along the OX_3 axis. It should be added that the porous structure of the matrix in this composite system enables one to vary its piezoelectric anisotropy, but only to a restricted degree. This is a result of the presence of a SC component with a small anisotropy of its piezoelectric coefficients $d_{3j}^{(1)}$, see, for instance, data on the PMN–0.33PT SC in Table 1.3. The porous polymer matrix in the 1–3–0 composite plays an important role in forming a large anisotropy of the ECFs, and relevant examples are discussed in work [55].

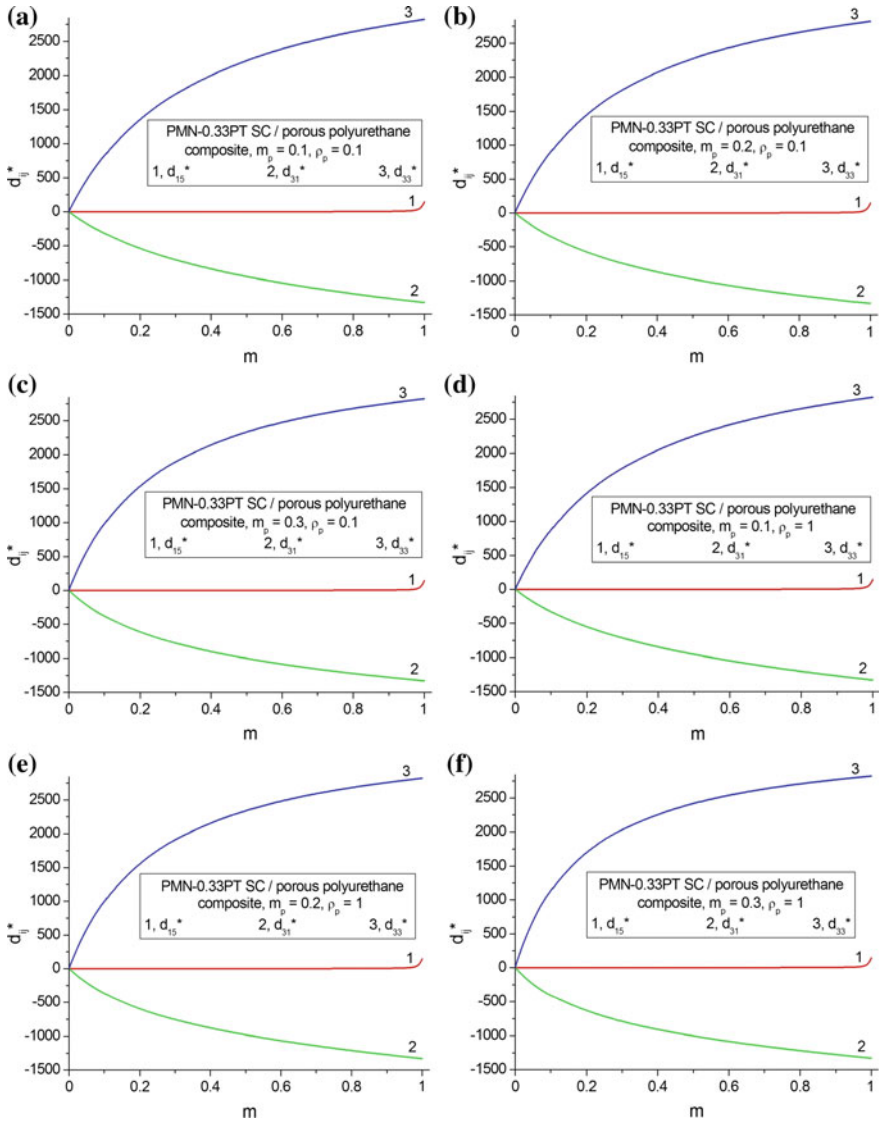

Fig. 2.20 Volume-fraction dependences of piezoelectric coefficients d_{ij}^{*} (in pC/N) of the 1–3–0 [001]-poled PMN–0.33PT SC/porous polyurethane composite with square cross section rods. The schematic of the composite is shown in Fig. 2.19

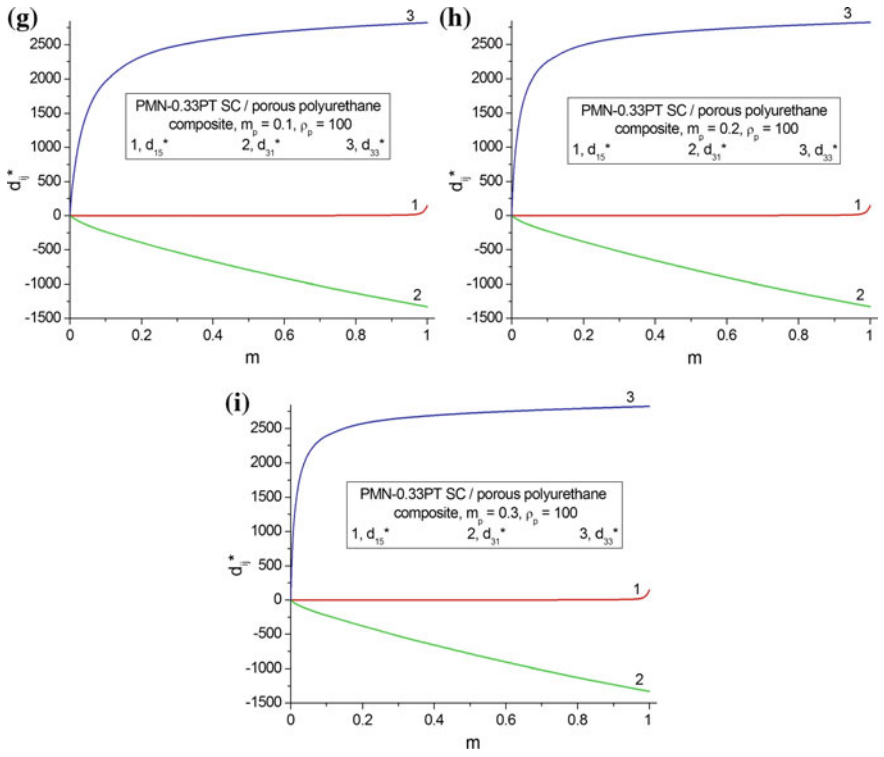

Fig. 2.20 (continued)

2.2.5 1–0–3 Composites Based on Single Crystals

The next important example of the modification of the 1–3 composite structure is concerned with the use of a 0–3 composite matrix. It is assumed that a 1–0–3 composite consists of a system of SC rods embedded in a FC/polymer matrix (Fig. 2.21). The structure of the 1–0–3 composite is similar to that shown in Fig. 2.19, however the isolated FC inclusions are regularly located in the matrix instead of the pores. The shape of each FC inclusion in the polymer matrix (see the inset in Fig. 2.19) obeys (2.13) relative to the axes of the rectangular co-ordinate system ($X_1X_2X_3$), where a_1, $a_2 = a_1$ and a_3 are the semi-axes of the FC inclusion, and $\rho_i = a_1/a_3$ is its aspect ratio. The FC inclusions occupy sites of a simple tetragonal lattice with unit-cell vectors parallel to the OX_k axes. We remind the reader that the similar 0–3 composite structure was considered in the Type II layers of the 2–0–2 SC/FC/polymer composite, see Sect. 2.1.3.

The effective electromechanical properties of the 1–0–3 composite shown in Fig. 2.21 are determined in two stages that are similar to those described in Sect. 2.2.4. However during the first stage, the effective properties of the 0–3 FC/polymer composite are evaluated within the framework of the EFM [46–48] that

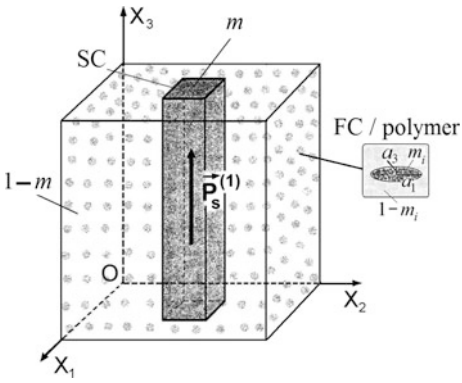

Fig. 2.21 Schematic of the 1–0–3 SC/FC/polymer composite. m and $1 - m$ are volume fractions of the SC and the FC/polymer matrix, respectively, m_i is the volume fraction of FC in the matrix, and $P_s^{(1)}$ is the spontaneous polarisation vector of the SC component. In the inset, a spheroidal FC inclusion with semi-axes a_f is shown schematically

takes into account an interaction between the FC inclusions in the polymer medium. We characterise the effective properties of the 0–3 composite by a 9×9 matrix [10]

$$\begin{aligned}\left\|C^{(0-3)}\right\| = \left\|C^{(p)}\right\| + m_i\left(\left\|C^{(FC)}\right\| - \left\|C^{(p)}\right\|\right) \\ \left[\|I\| + (1-m_i)\|S\|\left\|C^{(p)}\right\|^{-1}\left(\left\|C^{(FC)}\right\| - \left\|C^{(p)}\right\|\right)\right]^{-1}.\end{aligned} \tag{2.22}$$

$\|C^{(FC)}\|$ and $\|C^{(p)}\|$ from (2.22) characterise the properties of the FC and polymer components, respectively, and the structure of $\|C^{(0-3)}\|$, $\|C^{(FC)}\|$ and $\|C^{(p)}\|$ is similar to that of $\|C^{(2)}\|$ from (2.20). In (2.22) $\|I\|$ is the identity matrix, and $\|S\|$ is the matrix that comprises components of the electroelastic Eshelby tensor [41]. The second stage leads to the averaging of properties by means of either the matrix method or FEM [46–48]. As a result of the averaging, the effective electromechanical properties of the 1–0–3 composite are represented as functions of the volume fractions m and m_i and aspect ratio ρ_i.

By analogy with the 2–0–2 composite described in Sect. 2.1.3, we choose components with contrasting properties as follows: the [001]-poled PMN–0.33PT SC (main component, rods), modified $PbTiO_3$ FC (main component in the 0–3 matrix) and PE. Our evaluations of the properties of the 0–3 FC/polymer matrix suggest that it exhibits a low piezoelectric activity due to the presence of isolated inclusions at volume fractions of FC $0 < m_i \leq 0.3$ and aspect ratios $0.01 \leq \rho_i \leq 100$. Despite the assumption that the level of poling of the 0–3 matrix is ideal, the absolute values of its piezoelectric coefficients are relatively low whereby $|d_{3j}^{(0-3)}| < 10$ pC/N [47, 48], i.e., two orders-of-magnitude less than $|d_{3j}^{(1)}|$ of the PMN–0.33PT SC and related SCs listed in Table 1.3. Hereafter we neglect the piezoelectric activity of the 0–3 matrix in comparison to the piezoelectric activity of the SC rod and consider the FC inclusions

in the unpoled state. It is important to underline that any potential incomplete poling of the 0–3 matrix in the studied 1–0–3 composite is thereby avoided.

Graphs in Fig. 2.22 show that the FC inclusions in the polymer matrix can influence the PS of the composite even at the relatively small volume fraction

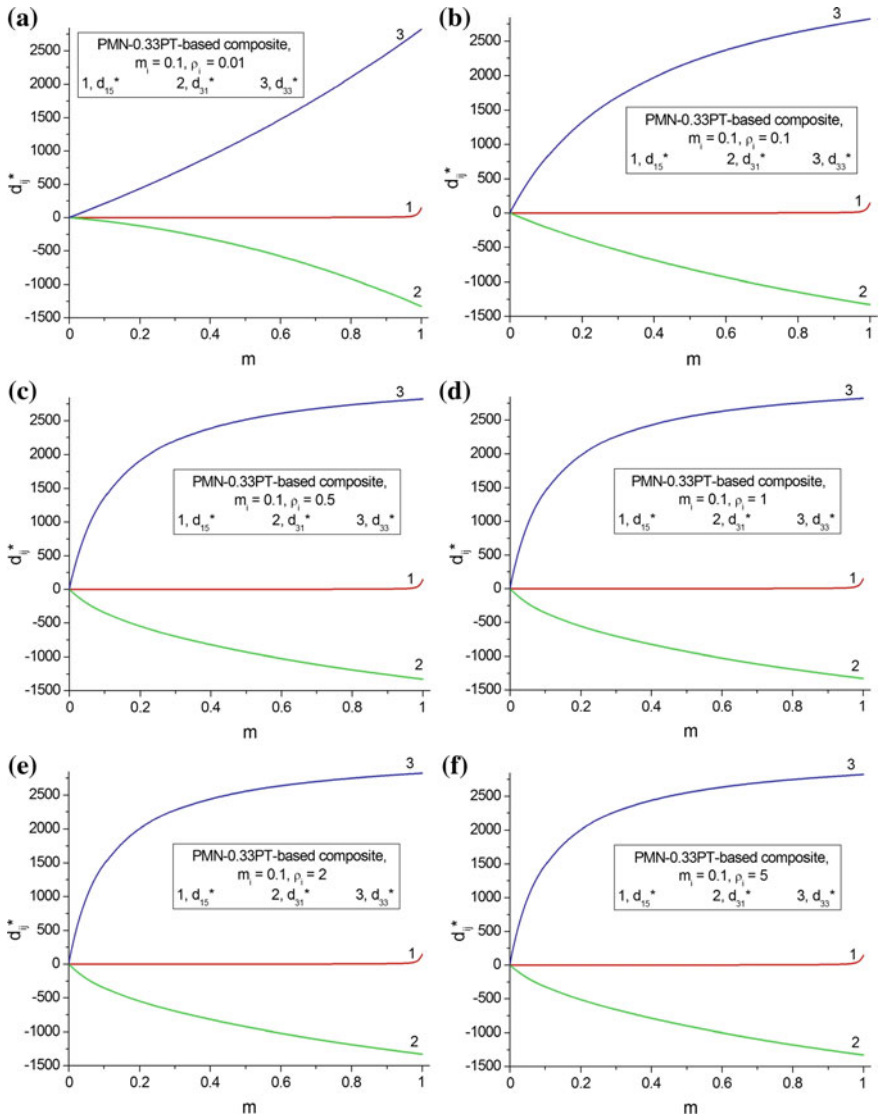

Fig. 2.22 Volume-fraction dependences of piezoelectric coefficients d_{ij}^* (in pC/N) of the 1–0–3 [001]-poled PMN–0.33PT SC/modified $PbTiO_3$ (I) FC/monolithic PE composite with square cross section rods at the volume fraction of FC $m_i = 0.1$. The schematic of the composite is shown in Fig. 2.21

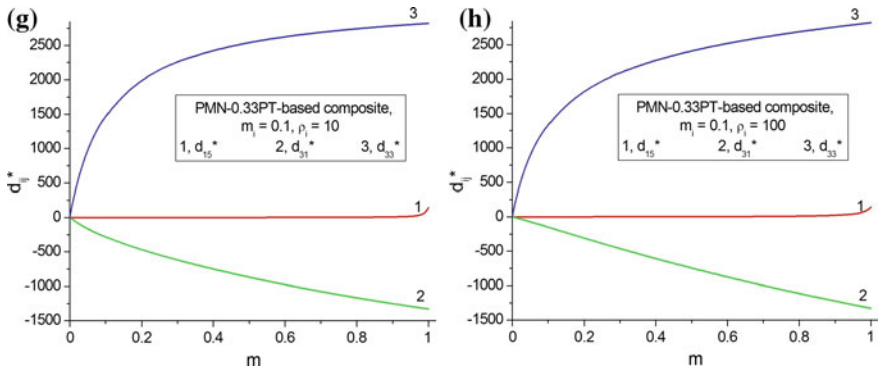

Fig. 2.22 (continued)

Table 2.4 Ratios of elastic compliances $s_{11}^{(0-3)}/s_{uv}^{(0-3)}$ of the 0–3 modified $PbTiO_3$ (I) FC/monolithic PE composite with non-poled aligned spheroidal inclusions (EFM calculations)

ρ_i	m_i	$s_{11}^{(0-3)}/s_{12}^{(0-3)}$	$s_{11}^{(0-3)}/s_{13}^{(0-3)}$	$s_{11}^{(0-3)}/s_{33}^{(0-3)}$
0.01	0.10	−3.95	−69.78	13.5
0.1	0.10	−4.22	−13.2	2.77
1	0.10	−4.86	−4.86	1.00
10	0.10	−5.14	−4.49	0.597
100	0.10	−5.65	−4.54	0.176
100	0.15	−5.67	−4.41	0.126
100	0.20	−5.68	−4.28	0.0998
100	0.25	−5.68	−4.18	0.0831
100	0.30	−5.67	−4.09	0.0709

$m_i = 0.1$. We see changes in the piezoelectric coefficients d_{3j}^* (see curves 2 and 3 in Fig. 2.22), while the piezoelectric coefficient d_{15}^* undergoes minor changes and remains small at $0 < m < 0.9$ (see curve 1 in Fig. 2.22). Such distinctions in the behaviour of the piezoelectric coefficients are observed due to the 1–3-type composite structure (Fig. 2.21) and were earlier mentioned for the 1–3 and 1–0–3 composites (see Sects. 2.2.1, 2.2.2 and 2.2.4). The changes in the piezoelectric coefficients d_{3j}^* are concerned with the changes in the aspect ratio of the FC inclusions, and the latter changes strongly influence the elastic anisotropy of the 0–3 matrix (Table 2.4). Data in Table 2.4 show that the $s_{11}^{(0-3)}/s_{uv}^{(0-3)}$ ratios undergo large changes during a transition of the FC inclusion in the 0–3 matrix from a prolate ($0 < \rho_i < 1$) to oblate ($\rho_i > 1$) shape.

An increase of the volume fraction of FC m_i leads to changes in the $s_{11}^{(0-3)}/s_{uv}^{(0-3)}$ ratios, but to a lesser degree. We show an example of such changes at $\rho_i = 100$ in Table 2.4. Figure 2.22 suggests that the piezoelectric anisotropy of the 1–0–3 composite can be varied at a relatively small anisotropy of the piezoelectric coefficients $d_{3j}^{(1)}$ of the PMN–0.33PT SC. A similar behaviour of d_{ij}^* and variations of the

piezoelectric anisotropy are observed (Fig. 2.23) when the PMN–0.33PT SC in the composite is replaced with the KNNTL:Mn SC, a component with a lower piezoelectric activity. This is due to the anisotropy of the elastic properties of the 0–3 FC/polymer matrix (Table 2.4). We remind the reader that, as with the

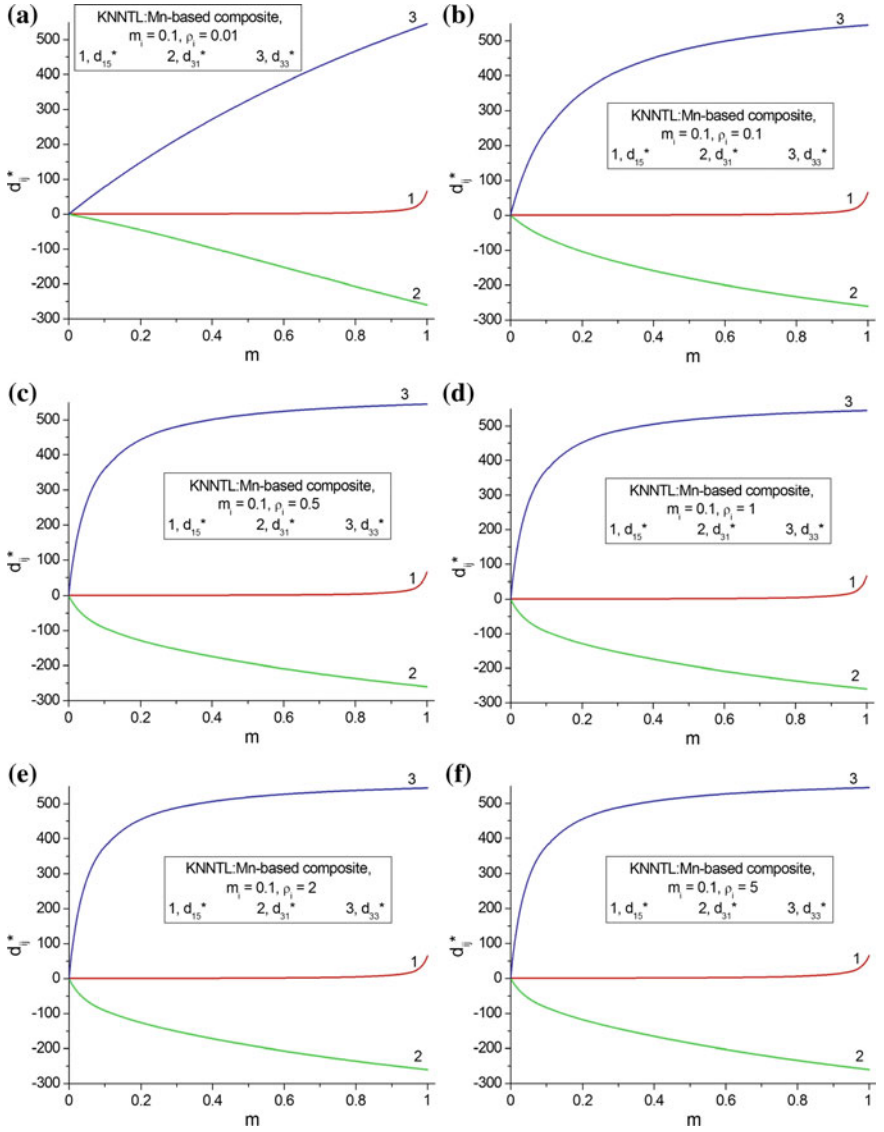

Fig. 2.23 Volume-fraction dependences of piezoelectric coefficients d_{ij}^* (in pC/N) of the 1–0–3 [001]-poled KNNTL:Mn SC/modified $PbTiO_3$ (I) FC/monolithic PE composite with square cross section rods at the volume fraction of FC $m_i = 0.1$. The schematic of the composite is shown in Fig. 2.21

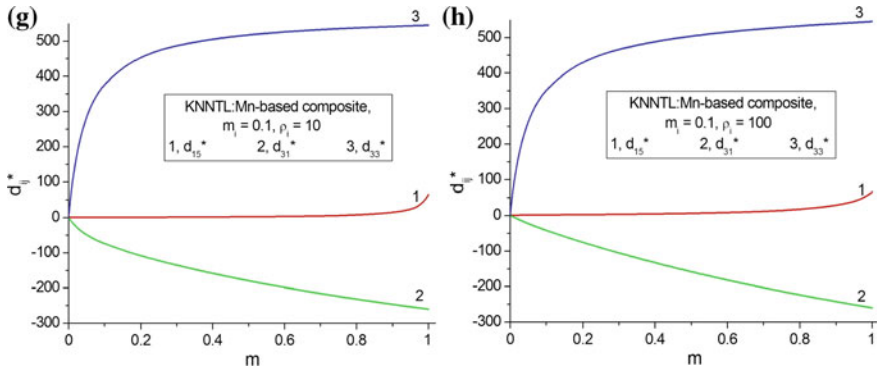

Fig. 2.23 (continued)

[001]-poled PMN–0.33PT SC, the [001]-poled KNNTL:Mn SC is characterised by a relatively small anisotropy of $d_{3j}^{(1)}$, see data in Table 1.2.

When predicting the piezoelectric properties of the KNNTL:Mn-based composite (Fig. 2.23), we also assume that the 0–3 matrix is unpoled. The highly oblate FC inclusions ($\rho_i \gg 1$) in the 0–3 matrix lead to a weakening of the transverse piezoelectric effect from to the SC rods in the composite (Fig. 2.21) and, therefore, lead to a decrease of $|d_{31}^*|$. The system of the SC rods oriented parallel to the poling axis OX_3 favours a strong longitudinal piezoelectric effect, and large values of d_{33}^* are achieved in the presence of FC inclusions at any aspect ratio ρ_I, see curve 3 in Figs. 2.22 and 2.23. This effect due to the 0–3 matrix plays an important role in forming the hydrostatic piezoelectric response of the 1–0–3 composite [46–48] and is to be taken into consideration for the prediction of the PS of related composite structures. The effect of the elastic anisotropy of the 0–3 matrix on the hydrostatic PS of a PZN–0.08PT-based composite leads to large values of its piezoelectric coefficient $d_h^* \sim 10^3$ pC/N [48] while the piezoelectric coefficient $d_h^{(1)}$ of the [001]-poled PZN–0.08PT SC is negative. According to data from Table 1.3, we obtain $d_h^{(1)} = -20$ pC/N.

It can be seen in graphs in Fig. 2.24 that changes in the piezoelectric coefficients d_{ij}^* of the 1–0–3 composite at $\rho_i = 100$ remain small when we vary the volume fraction of FC m_i. This behaviour correlates with minor changes in the ratios of the elastic compliances $s_{11}^{(0-3)}/s_{uv}^{(0-3)}$ of the 0–3 matrix, see data in Table 2.4. On increasing the volume fraction m_i, we observe a decrease of both $|d_{31}^*|$ and d_{33}^*, see Fig. 2.24a, b. In the same case, the piezoelectric coefficient d_{15}^* increases (Fig. 2.24c), but within a restricted range.

Thus, the 1–0–3 SC/FC/polymer composite represents an example of a material wherein three components with contrasting properties influence the PS, and the piezoelectric anisotropy of the composite depends on properties of the 0–3 FC/polymer matrix. The performance of the studied composite is to be taken into account in sensor, actuator and hydroacoustic applications.

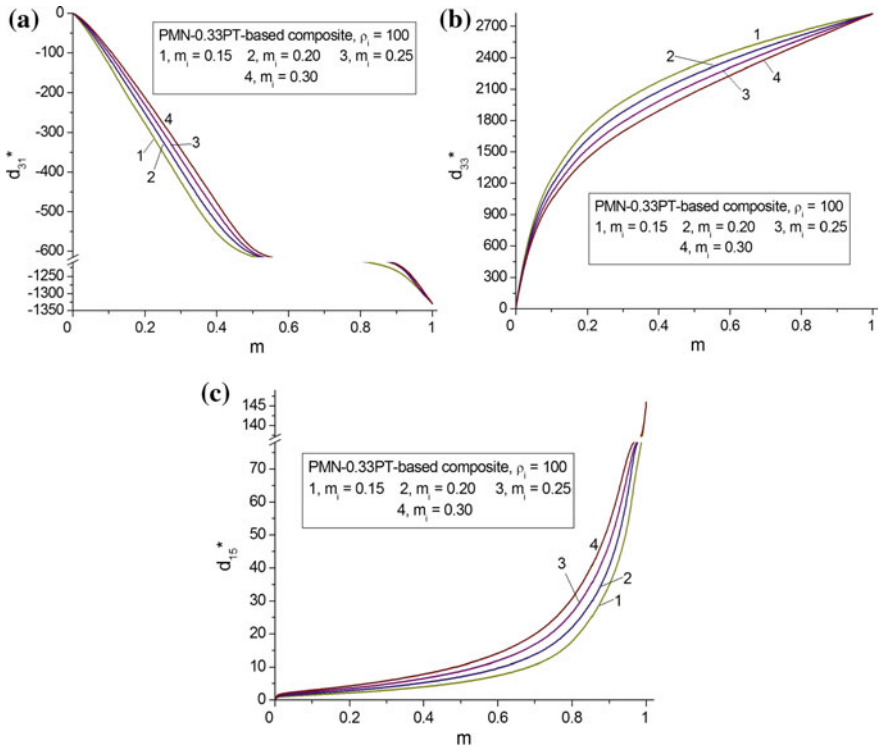

Fig. 2.24 Volume-fraction dependences of piezoelectric coefficients d_{ij}^* (in pC/N) of the 1–0–3 [001]-poled PMN–0.33PT SC/modified $PbTiO_3$ (I) FC/monolithic PE composite with square cross section rods at $\rho_i = 100$. The schematic of the composite is shown in Fig. 2.21

2.3 1–1-Type Composites

A 1–1 connectivity pattern means that each component of a two-component composite is distributed continuously in one direction. Despite the relatively simple microgeometry of the 1–1 composite (Fig. 2.25a) that resembles the well-known 1–3 composite shown in Fig. 2.11, electromechanical properties and related parameters of the 1–1 composite were studied only for some FC/polymer combinations [57, 58]. In Sect. 2.3 we consider examples of the volume-fraction behaviour of the piezoelectric coefficients d_{ij}^* and PS of the 1–1-type FC-based composites.

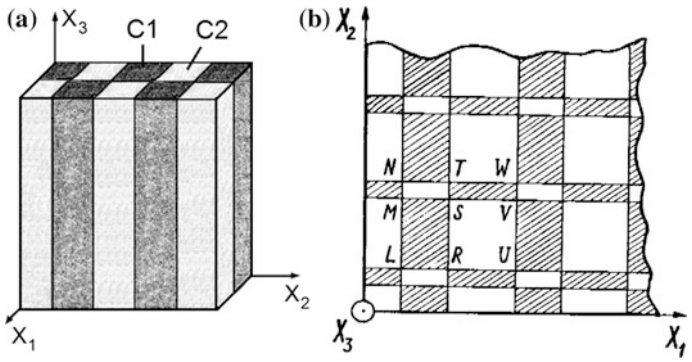

Fig. 2.25 Schematic of the 1–1 composite (**a**) and cross section of the 1–1 composite by the (X_1OX_2) plane (**b**). m and $1 - m$ are volume fractions of components C1 (dashed in **b**) and C2, respectively. ($X_1X_2X_3$) is the rectangular co-ordinate system (**b** reprinted from paper by Glushanin and Topolov [57], with permission from IOP Publishing)

2.3.1 1–1 Ceramic/Polymer Composites

It is assumed that the 1–1 composite contains rectangular FC and polymer parallelepipeds which are alternating in the OX_1 and OX_2 directions (Fig. 2.25). The height of each parallelepiped equals h (that measured along the poling axis OX_3), and conditions $h \gg |LN|$ and $h \gg |LU|$ are valid over the whole composite sample (Fig. 2.25) where the regular distribution of the FC and polymer components is observed. Effective electromechanical properties of the 1–1 composite are determined by means of the matrix method [57] and represented as functions of two parameters, $t = |MS|/|MV|$ and $n = |RS|/|RT|$. The volume faction of FC as a main piezoelectric component in this composite (see C1 in Fig. 2.25a) is given by

$$m = nt + (1-n)(1-t) \tag{2.23}$$

As follows from (2.23), $m = 1$ (limiting case) is achieved at either $n = t = 1$ or $n = t = 0$. If $n = 0$ or 1 and $0 < t < 1$, then we obtain the 2–2 parallel-connected FC/polymer composite (see Sect. 2.1.1). The similar 2–2 composite can be also considered at $t = 0$ or 1 and $0 < n < 1$.

The 1–1 FC/polymer composite poled along OX_3 (Fig. 2.25a) is described by *mm*2 symmetry and characterised by a following peculiarity [57, 58]. The effective electromechanical properties evaluated for a pair of parameters (t, n) remain unchanged for parameters ($1 - t$, $1 - n$). For instance, the piezoelectric coefficients d_{ij}^* obey the condition

$$d_{ij}^*(t,n) = d_{ij}^*(1-t, 1-n) \tag{2.24}$$

Equation (2.24) suggests that the analysis of the PS of the composite can be carried out, for example, at $0 < t \leq 0.5$ and $0 < n < 1$. Hereafter we consider the piezoelectric coefficients d_{3j}^* ($j = 1$, 2 and 3) and their anisotropy. As in the 1–3-type composites, the piezoelectric coefficient d_{15}^* in the 1–1-type composites remains relatively small in the wide volume-fraction (m) range. Such a feature is common in the 1–3, 1–1 and related composite structures because of the system of long piezoelectric rods (see C1 in Figs. 2.11 and 2.25a) distributed continuously along one poling axis.

Examples of the $d_{3j}^*(t, n)$ dependence (Fig. 2.26) show that the piezo-passive polymer component plays the important role in forming the PS of the composite and influences the piezoelectric anisotropy. For the araldite-containing composite, a similar monotonic behaviour of $d_{31}^*(t, n)$ and $d_{32}^*(t, n)$ is observed; see Fig. 2.26a, b. In the composite that contains auxetic PE, we observe the sign-variable and non-monotonic behaviour of $d_{31}^*(t, n)$ and $d_{32}^*(t, n)$; see Fig. 2.26d, e. We note that the non-monotonic behaviour in the latter case is observed at $m \ll 1$, i.e., when the volume fraction of the auxetic polymer component is large and this component can influence the transverse PS of the composite to a large extent. It should be reminded that the change in sgn d_{31}^* and sgn d_{32}^* is observed in the presence of the PCR-7M FC that is characterised by the large transverse piezoelectric coefficient $d_{31}^{(1)}$ (see Table 1.5). At the same time, the $d_{33}^*(t, n)$ dependence is similar in both the composites; see Fig. 2.26c, f. This behaviour means that the polymer component plays a passive role in forming the longitudinal PS of the 1–1 composite.

2.3.2 1–1–0 Ceramic/Porous Polymer Composites

A modification of the 1–1 composite structure shown in Fig. 2.25a leads to changes in the PS. Now we assume that the polymer rods of the composite contain a system of spheroidal air pores that are described by (2.18) relative to the axes of the rectangular co-ordinate system ($X_1X_2X_3$). The schematic of the pore is shown in the inset in Fig. 2.19. As in the case of the 1–3–0 composite considered in Sect. 2.2.4, the pores are regularly distributed in the polymer medium and occupy the sites of a simple tetragonal lattice with unit-cell vectors parallel to the OX_k axes. The shape of each pore is characterised by the aspect ratio $\rho_p = a_{1,p}/a_{3,p}$, and this value is constant over the composite sample. The radius or the largest semi-axis of each pore remains considerably less than the length of the side of the square being the intersection of the FC rod by the (X_1OX_2) plane shown in Fig. 2.25a. The FC/porous polymer composite is characterised by 1–1–0 connectivity. The effective electromechanical properties of the 1–1–0 composite are evaluated in two stages [57, 58], and these stages are similar to those described in Sect. 2.2.4.

Graphs in Fig. 2.27 show that the porous polymer influences the piezoelectric coefficients d_{3j}^* ($j = 1$, 2 and 3) and their anisotropy, and this influence depends on the aspect ratio ρ_p. For instance, at $\rho_p = 0.1$ (prolate pores), we see the considerable

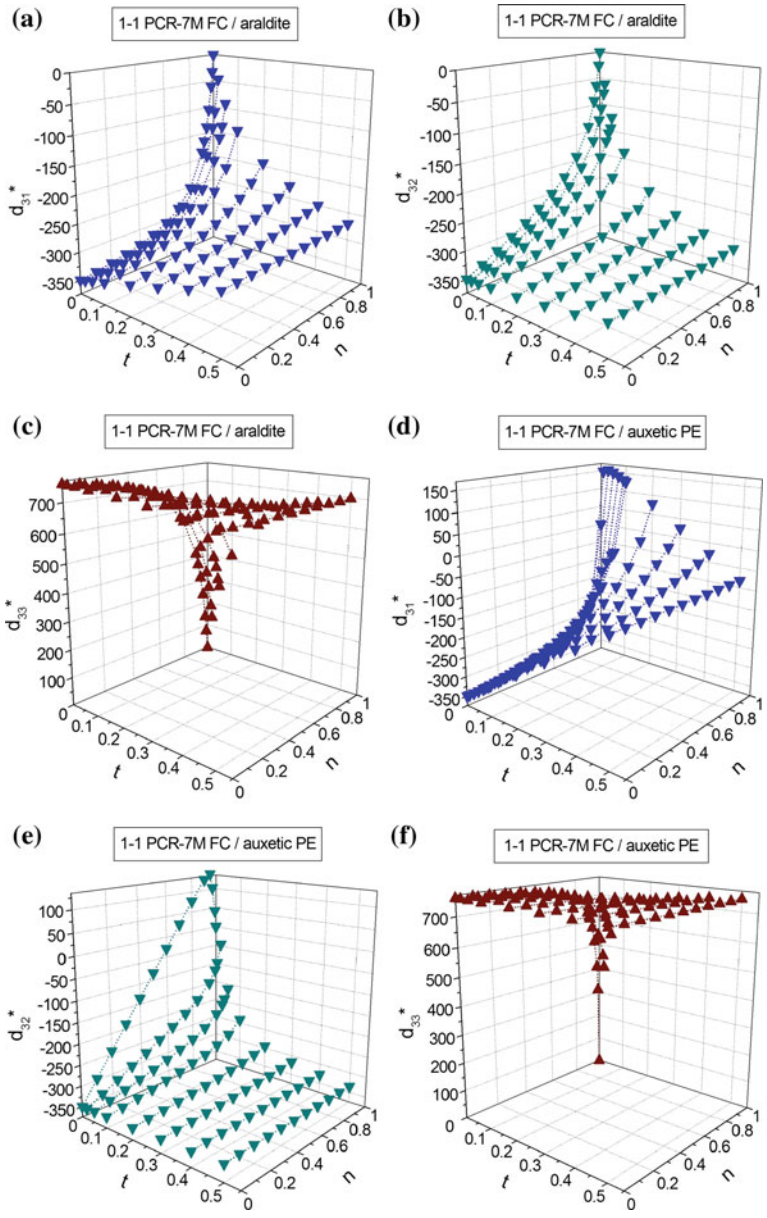

Fig. 2.26 Volume-fraction dependences of piezoelectric coefficients d_{ij}^* (in pC/N) of 1–1 PCR-7M FC/polymer composites. The schematic of the composite is shown in Fig. 2.25a

analogy between the d_{31}^* and d_{32}^* curves shown in Fig. 2.27a, b. At $\rho_p = 1$ (spherical pores), some distinctions between the d_{31}^* and d_{32}^* curves (Fig. 2.27d, e) are observed. At $\rho_p = 100$ (heavily oblate pores), the obvious distinctions between d_{31}^*

and d_{32}^* (Fig. 2.27g, h) are observed. Such an 'evolution' of the curves is concerned with considerable changes in the elastic anisotropy of the porous polymer that influences the transverse PS to a large extent. As for the d_{33}^* curves, they undergo less considerable changes when the aspect ratio ρ_p increases from 0.1 to 100; see Fig. 2.27c, f, i. This is due to the weaker influence of the porous polymer on the longitudinal PS in the studied 1–1–0 composite.

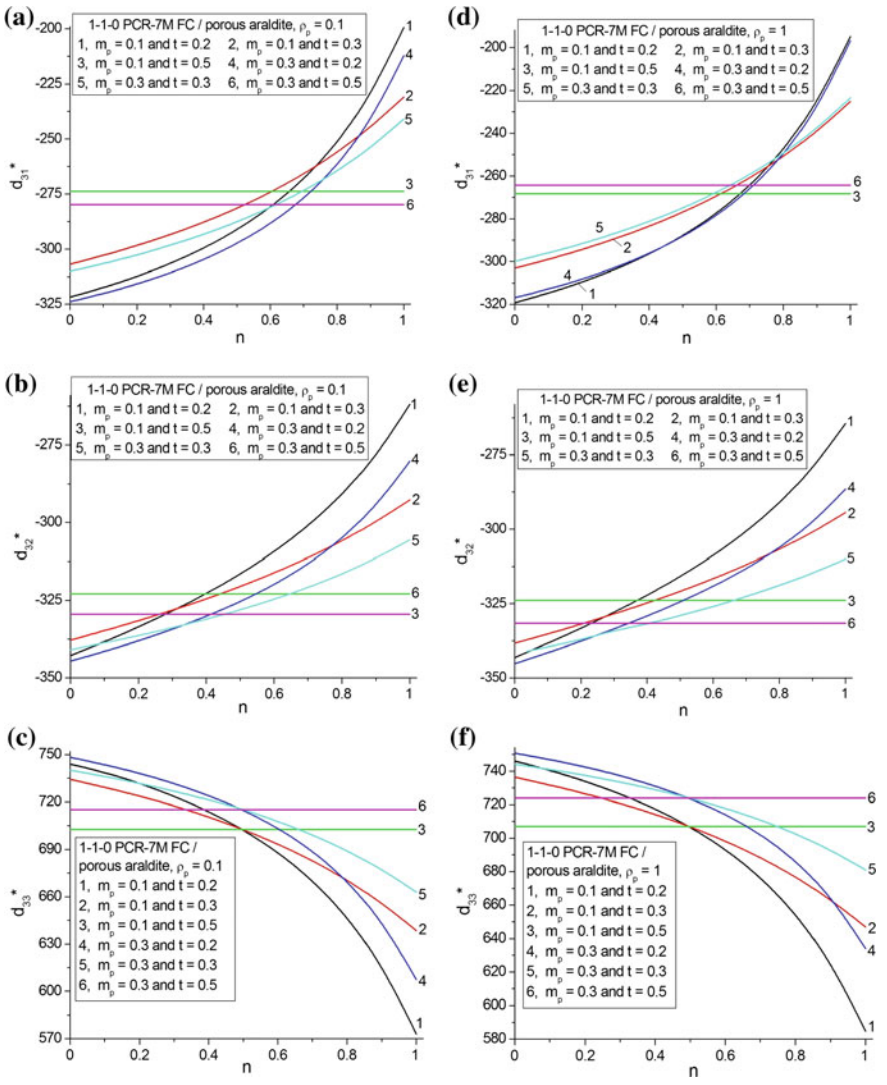

Fig. 2.27 Volume-fraction dependences of piezoelectric coefficients d_{ij}^* (in pC/N) of the 1–1–0 PCR-7M FC/porous araldite composites at ρ_p = 0.1 (**a**–**c**), ρ_p = 1 (**d**–**f**), and ρ_p = 100 (**g**–**i**). The arrangement of the FC rods in the composite is shown in Fig. 2.25a, see C1

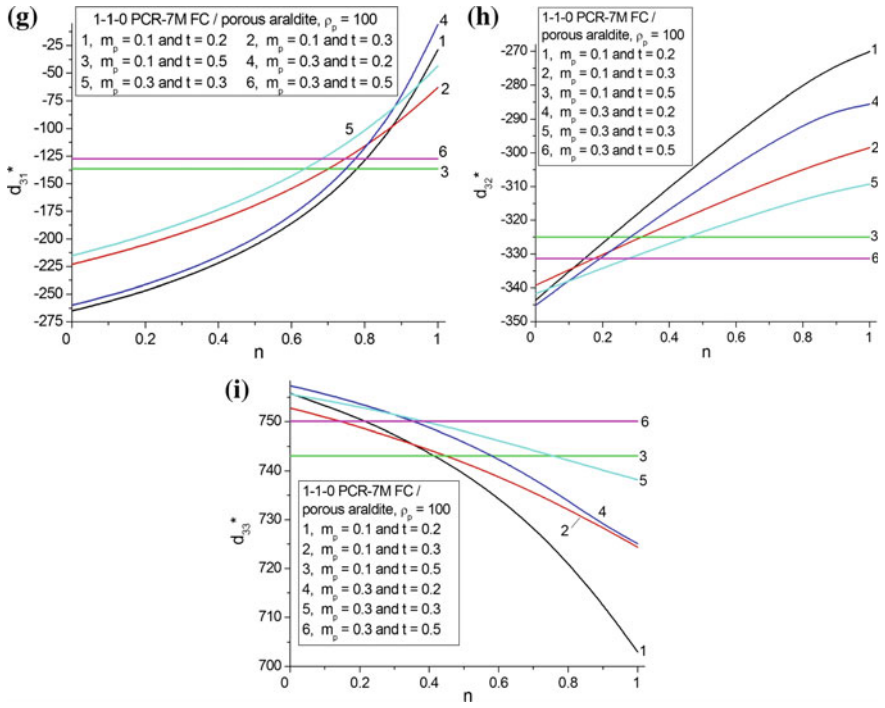

Fig. 2.27 (continued)

Thus, we see an analogy between the PS of the 1–1-type and 1–3-type composites. However the 1–1 composite structure (Fig. 2.25a) opens up additional opportunities to vary the transverse PS and anisotropy of the piezoelectric coefficients d_{3j}^*. This feature of the 1–1-type composites is to be taken into account at a selection of potential materials for piezoelectric transducer, actuator and related applications.

2.4 0–3-Type Composites

The 0–3 composite system is one of the most common piezo-composite types studied earlier (see, for instance, [8, 10–12, 16–18, 59]). The 0–3 composite shown in Fig. 2.28 consists of the three-dimensionally connected matrix reinforced by a system of isolated inclusions. The widespread type of the 0–3 composites is the FC/polymer composite wherein the polymer matrix can be either piezo-passive or piezo-active, and the main piezoelectric component is poled FC [10–12]. Effective electromechanical properties and related parameters of the 0–3 composites are highly dependent on their microstructure, properties and volume fractions of the

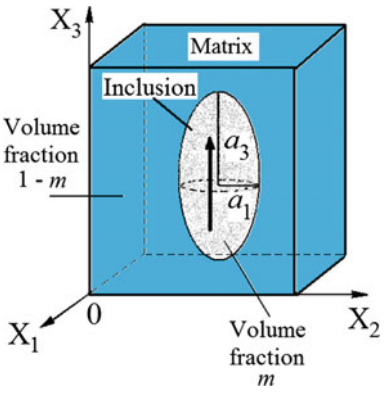

Fig. 2.28 Schematic of the 0–3 composite. The poling direction is denoted by an arrow. a_1 and a_3 are semi-axes of the spheroidal inclusion, m and $1 - m$ are volume fractions of components (reprinted from Topolov et al. [59], with permission from Taylor and Francis)

components, poling conditions, technological factors, etc. [10–14. 59]. In Sect. 2.4 we discuss examples of the PS of various 0–3 composites.

The first example is concerned with a 0–3 ZTS-19 FC/clay composite that was first considered in work [60]. Clay is regarded as a piezo-passive isotropic component with elastic moduli $c_{11} = 4.48 \times 10^8$ Pa and $c_{12} = 1.73 \times 10^8$ Pa and dielectric permittivity $\varepsilon_{pp}/\varepsilon_0 = 8.0$ [61, 62]. ZTS-19 is the typical FC material based on Pb(Zr, Ti)O_3 [10–12], and the full set of electromechanical constants of this FC is given in Table 1.5. It is assumed that the FC inclusions are spheroidal and regularly distributed in the large clay matrix, and the poling axis of each inclusion and the composite sample as a whole is OX_3 (Fig. 2.28). The shape of each FC inclusion is described by (2.13) in the axes of the rectangular co-ordinate system ($X_1X_2X_3$), and the aspect ratio of each inclusion is $\rho = a_1/a_3$. The FC inclusions occupy the sites of a simple tetragonal lattice with unit-cell vectors parallel to the OX_k axes shown in Fig. 2.28. Results of the FEM modelling of the piezoelectric properties of the 0–3 composite are graphically represented in Fig. 2.29. It is seen that even at the ideal poling of the ZTS-19 inclusions aligned in the clay matrix, the piezoelectric coefficients d_{ij}^* of the composite obey the condition

$$d_{ij}^*/d_{ij}^{(1)} \ll 1 \tag{2.25}$$

in the wide volume-fraction (m) range. In Fig. 2.29 we show the volume-fraction dependence of d_{ij}^* in the presence of the non-oblate FC inclusions, i.e., $0 < \rho \leq 1$. The isolated FC (piezoelectric) inclusions surrounded by the piezo-passive matrix promote a lower PS of the 0–3 composite in comparison to the 1–3, 2–2 and 1–1 composites where the piezoelectric component is distributed continuously along the poling axis. For the composite with the oblate FC inclusions ($\rho > 1$), the $d_{ij}^*/d_{ij}^{(1)}$ ratio from (2.25) becomes smaller in comparison to that at $0 < \rho \leq 1$.

In the second example a relatively low PS and validity of (2.25) are predicted for a 0–3 [001]-poled PMN–0.33PT SC/araldite composite (Fig. 2.30). Calculations of d_{ij}^* were performed by means of the FEM. We observe the rapid decrease of $|d_{3j}^*|$

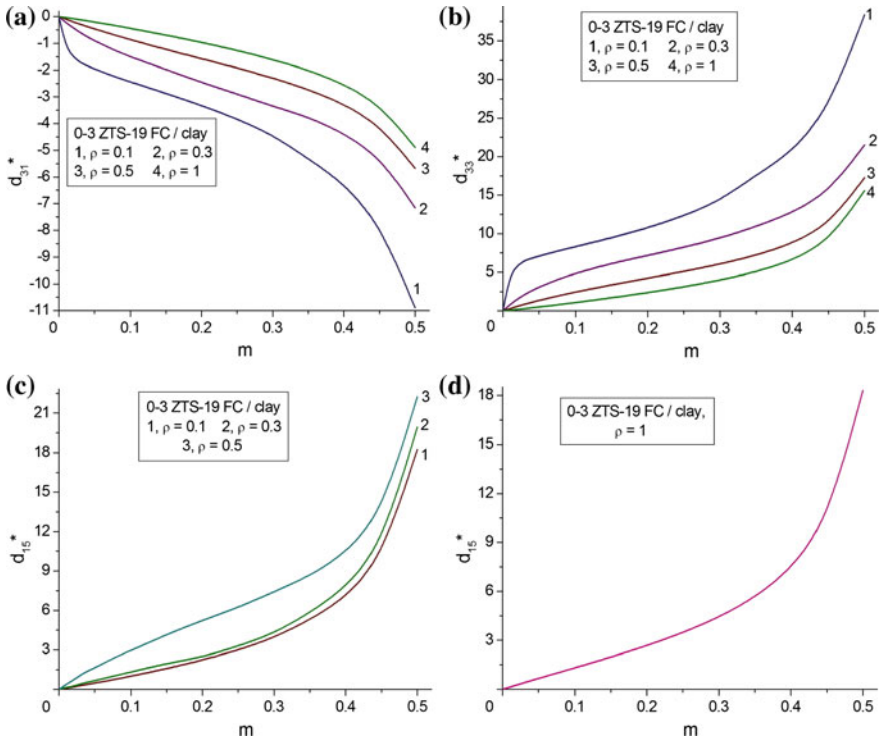

Fig. 2.29 Volume-fraction dependences of piezoelectric coefficients d_{ij}^* (in pC/N) of the 0–3 ZTS-19 FC/clay composite. The schematic of the composite is shown in Fig. 2.28

(Fig. 2.30a, b) on increasing the aspect ratio ρ of the SC inclusions. The piezoelectric coefficient d_{15}^* becomes smaller than that in the 0–3 ZTS-19 FC/clay composite, see Figs. 2.29c, d and 2.30c. Such behaviour may be accounted for by a lesser difference between elastic constants of the SC and polymer components in comparison to the elastic properties of the ZTS-19 FC and clay in the first example. Moreover, the piezoelectric coefficient $d_{15}^{(1)}$ of the ZTS-19 FC is approximately three times larger than $d_{15}^{(1)}$ of the PMN–0.33PT SC; see data in Tables 1.3 and 1.5.

The third example is concerned with a 0–3 SC/FC composite. The piezoelectric performance of such composites was first studied in work [63]. It is assumed that the SC inclusions (volume fraction m) are regularly distributed in the large FC matrix (volume fraction $1 - m$), and both the components are poled along the OX_3 axis (Fig. 2.28). The shape of each SC inclusion is described by (2.13), the aspect ratio is $\rho_i = a_1/a_3$, and a_1, $a_2 = a_1$ and a_3 are semi-axes of the SC inclusion. The domain arrangement in each SC inclusion is shown in Fig. 1.2a, and the co-ordinate axes OX_j obey conditions $OX_1 \| [100]$, $OX_2 \| [010]$ and $OX_3 \| [001]$. Hereby we consider two modes of the arrangement of the SC inclusions, namely, the simple cubic and body-centered arrangements. Among the components of interest, we choose the

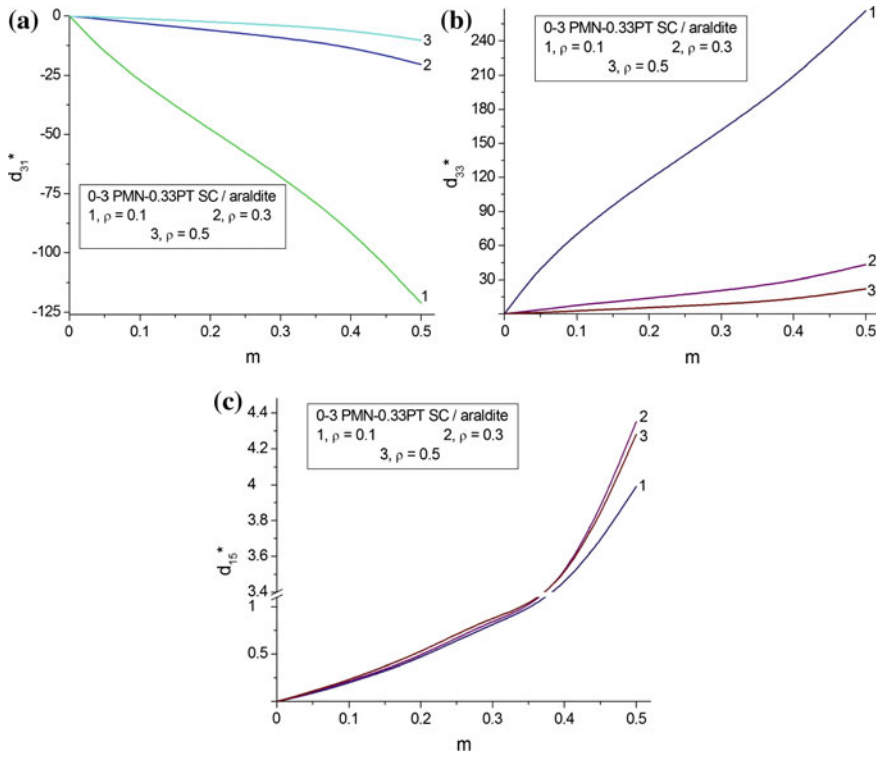

Fig. 2.30 Volume-fraction dependences of piezoelectric coefficients d_{ij}^* (in pC/N) of the 0–3 [001]-poled PMN–0.33PT SC/araldite composite. The schematic of the composite is shown in Fig. 2.28

PMN–0.33PT SC with the high piezoelectric activity (see data in Table 1.3) and the modified $PbTiO_3$ FC with the large piezoelectric anisotropy and moderate piezoelectric activity (see data in Table 1.5). As follows from Table 2.5, changes in the aspect ratio ρ lead to changes in the piezoelectric coefficients d_{ij}^* and piezoelectric anisotropy. At ρ = const and m = const, we observe minor changes in d_{ij}^* when the arrangement of the SC inclusions in the FC matrix changes. We add that the $d_{ij}^*/d_{ij}^{(1)}$ ratio undergoes major changes, however the condition (2.25) holds for the three piezoelectric coefficients of the composite (i.e., for ij = 31, 33 and 15 simultaneously) in restricted ranges of ρ and m.

In the fourth example we assume that the spheroidal SC inclusions are surrounded by the porous polymer medium (see the inset in Fig. 2.19). The polymer matrix contains a system of spheroidal pores with the aspect ratio ρ_p, see also (2.18). As in the case of the 1–3–0 composite, the pores are regularly distributed in the polymer medium and occupy the sites of a simple tetragonal lattice with unit-cell vectors parallel to the OX_k axes (see Sect. 2.2.4). The composite that

Table 2.5 Piezoelectric coefficients d_{ij}^* (in pC/N) and the anisotropy factor $d_{33}^*/|d_{31}^*|$ of the 0–3 [001]-poled PMN–0.33PT SC/modified $PbTiO_3$ FC (I) composite at different modes of the arrangement of SC inclusions, FEM calculations

m	d_{31}^*	d_{33}^*	d_{15}^*	$d_{33}^*/\|d_{31}^*\|$	d_{31}^*	d_{33}^*	d_{15}^*	$d_{33}^*/\| d_{31}^*\|$
	ρ = 0.1, simple cubic arrangement				ρ = 0.1, body-centered arrangement			
0.05	−10.2	64.8	69.4	6.35	−10.3	63.8	69.4	6.39
0.10	−14.2	74.6	70.9	5.25	−14.2	72.8	71.0	5.31
0.20	−23.8	97.5	74.5	4.10	−23.9	93.8	74.6	4.13
0.30	−36.3	126	79.0	3.47	−36.5	120	79.1	3.48
0.50	−75.8	212	92.4	2.80	−77.0	201	92.7	2.80
	ρ = 0.3, simple cubic arrangement				ρ = 0.3, body-centered arrangement			
0.05	−9.99	63.8	69.4	6.39	−10.2	64.2	70.5	6.29
0.10	−13.7	72.8	71.0	5.31	−14.0	73.5	72.9	5.25
0.20	−22.7	93.8	74.6	4.13	−23.4	95.8	77.8	4.09
0.30	−34.5	120	79.1	3.48	−35.8	124	82.6	3.46
0.50	−71.9	201	92.7	2.80	−75.8	212	93.6	2.80
	ρ = 0.5, simple cubic arrangement				ρ = 0.5, body-centered arrangement			
0.05	−9.71	62.9	69.5	6.48	−10.1	63.6	70.6	6.30
0.10	−13.1	70.7	71.0	5.40	−13.8	72.5	72.8	5.25
0.20	−21.3	89.2	74.7	4.19	−22.8	93.5	77.6	4.10
0.30	−31.9	113	79.2	3.54	−34.8	121	82.4	3.48
0.50	−67.6	190	93.1	2.81	−73.9	206	92.5	2.79

consists of the system of the aligned SC inclusions and the porous polymer matrix is described by 0–3–0 connectivity. In the 0–3–0 composite m is the volume fraction of the SC component, and m_p is porosity of the matrix therein. The volume-fraction (m) dependence of the piezoelectric coefficients d_{ij}^* of the 0–3–0 composite with spherical pores (ρ_p = 1) is represented in Fig. 2.31. It is seen that at the aspect ratio of the SC inclusion $\rho > 0.1$, the piezoelectric coefficients $|d_{3j}^*|$ become small, and changes in porosity m_p of the matrix do not lead to appreciable changes in d_{ij}^* of the composite. The piezo-passive polymer matrix and the isolated piezoelectric inclusions promote a weakening of the PS even at the relatively large elastic compliances of the inclusions and matrix in the composite.

2.5 3–β Composites

In the last decades, FC/polymer composites with 3–β connectivity are of interest [10, 16–19, 64] due to their considerable PS and large hydrostatic parameters. The first index 3 means that the first component (FC) is distributed continuously in the composite sample along three co-ordinate axes, and the second index is β = 0, 1, 2, or 3, i.e., the number of the axes, along which the second component (polymer) is

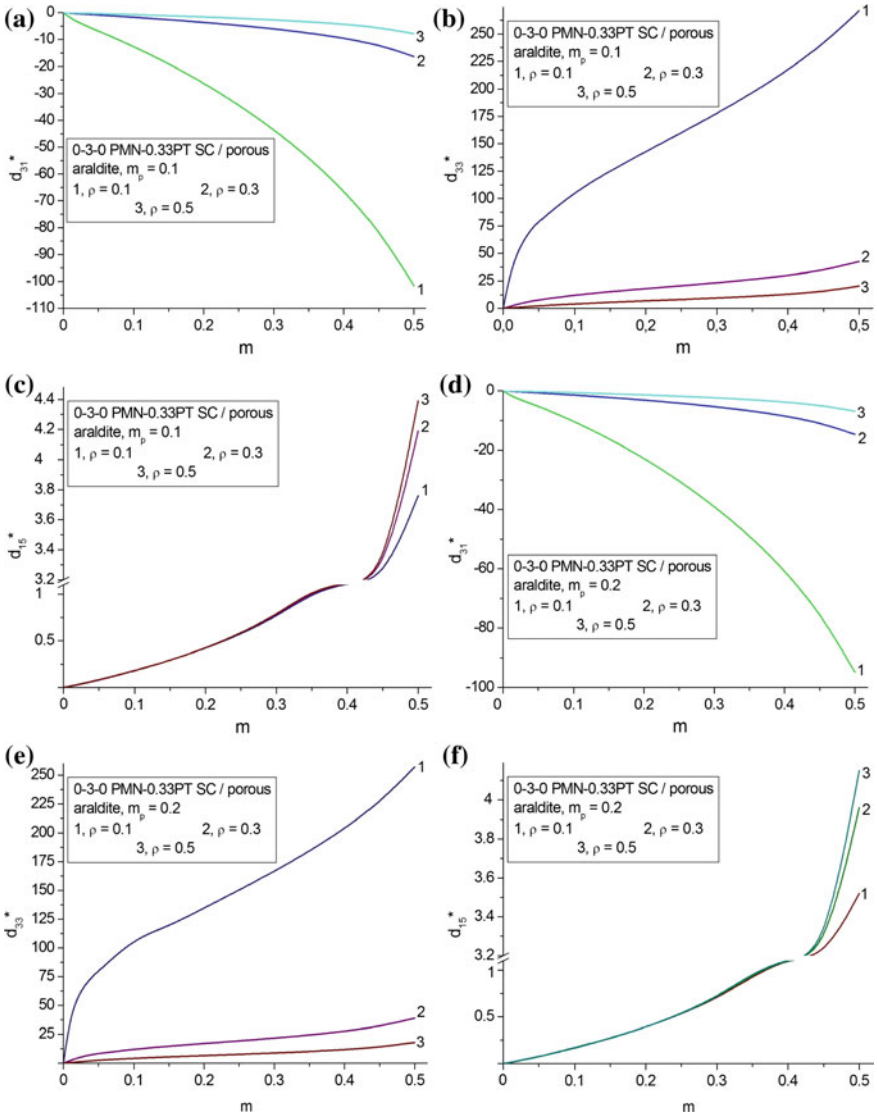

Fig. 2.31 Volume-fraction dependences of piezoelectric coefficients d_{ij}^* (in pC/N) of the 0–3–0 [001]-poled PMN–0.33PT SC/porous araldite composite at porosity of the polymer matrix $m_p = 0.1$ (**a**–**c**) and $m_p = 0.2$ (**d**–**f**). Each pore in the polymer matrix is characterised by the aspect ratio $\rho_p = 1$

distributed, varies from zero to three. To the date, no paper is known where the four connectivity patterns at $\beta = 0$, 1, 2, and 3 are compared and the effective parameters of the 3–β composites are analysed in detail. In Sect. 2.5 we show examples of the piezoelectric properties and their anisotropy in some 3–β composites based on FCs.

Piezoelectric properties of ZTS-19 FC/clay composites with connectivity patterns 3–0 and 3–1 are characterised by similar volume-fraction dependences (Fig. 2.32), and quantitative differences stem from the specifics of the shape of the clay inclusions. The structure of the 3–0 composite is similar to that shown in Fig. 2.28. In the 3–0 composite, the FC matrix contains spheroidal clay inclusions that are distributed over the sample. The shape of each clay inclusion is described by (2.13) in the axes of the rectangular co-ordinate system ($X_1X_2X_3$), and the aspect ratio of each inclusion is $\rho = a_1/a_3$. The clay inclusions occupy the sites of a simple tetragonal lattice with unit-cell vectors parallel to the OX_k axes shown in Fig. 2.28. In the studied 3–0 composite, m_{cl} is the volume fraction of clay, and $1 - m_{cl}$ is the volume fraction of FC. The poling direction of the FC component and composite as a whole is OX_3. The 3–1 composite is regarded as a limiting case of the 3–0 composite at $\rho = 0$. In the 3–1 composite, the regular arrangement of clay circular rods is also assumed.

Graphs in Fig. 2.32 were built by taking into account FEM calculations. It is seen that the transverse piezoelectric effect becomes stronger (Fig. 2.32a) on increasing the aspect ratio ρ, i.e., at the transition from the prolate to spherical shape

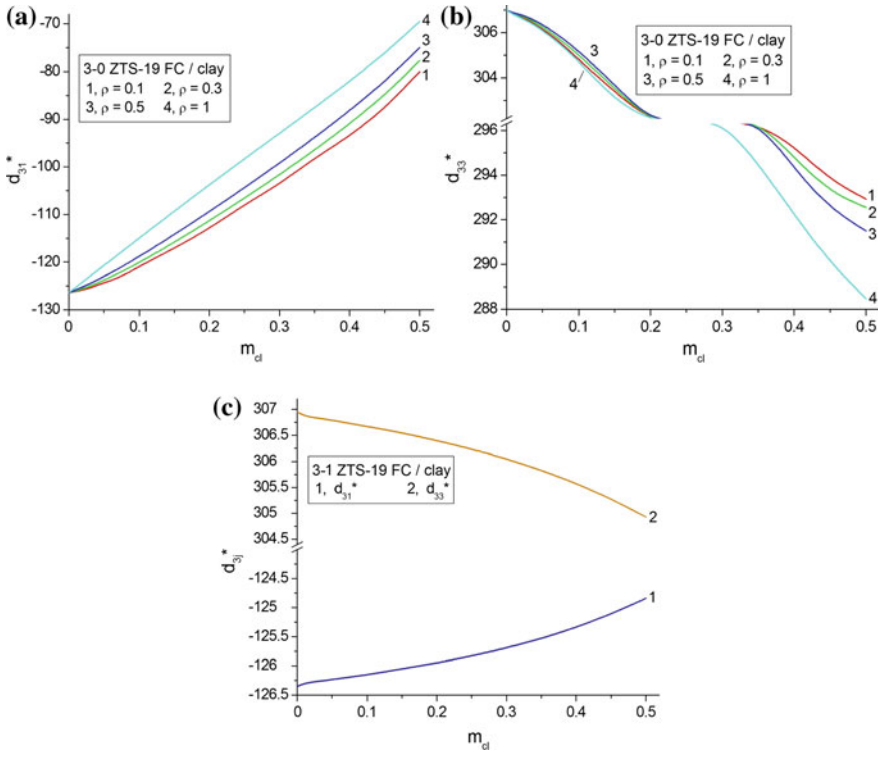

Fig. 2.32 Volume-fraction dependences of piezoelectric coefficients d_{3j}^* (in pC/N) of 3–0 (**a**–**b**) and 3–1 (**c**) ZTS-19 FC/clay composites

of the clay inclusion. The weakening of the longitudinal piezoelectric effect on increasing the aspect ratio ρ (Fig. 2.32b) is caused by the shape of the same clay inclusions.

For instance, the larger piezoelectric coefficient d_{33}^* at m_{cl} = const is expected in the presence of the clay inclusions with a smaller aspect ratio ρ. Minor changes in the d_{33}^* curves at $0 < \rho \leq 1$ (Fig. 2.32b) are accounted for by the strong influence of the poled FC matrix on the PS of the composite. Figure 2.32c shows that changes in d_{3j}^* of the 3–1 composite are observed in the narrower ranges in comparison to the 3–0 composite. Such a feature is concerned with the presence of the clay inclusions that are continuously distributed along the poling axis OX_3 and make no serious obstacles at the poling of the composite sample at the electric field $\boldsymbol{E} \| OX_3$. It should be added that the results on the FEM modelling of the electromechanical properties of the 3–0 composite were used in work [60] where the ZTS-19 FC/clay composite was first manufactured and characterised as a piezo-active composite with a few connectivity patterns.

Examples of the volume-fraction behaviour of the piezoelectric coefficient d_{33}^* of composites based on the PZT-5H FC are shown in Fig. 2.33, where m is the volume fraction of the FC component. The related 3–β composites with the regular arrangement of their components were manufactured and studied in work [19]. The largest values of d_{33}^* at m = const are achieved in the 3–1 composite (Fig. 2.33a) where the polymer rods are distributed continuously along the poling axis OX_3. A decrease of d_{33}^* at m = const in the 3–2 and 3–3 composites (Fig. 2.33b, c) in comparison to d_{33}^* of the 3–1 composite is caused by technological factors, non-dense contacts between the FC and polymer components in samples, incomplete poling of some fragments of the samples, etc.

Our analysis of the $d_{33}^*(m)$ dependences in Fig. 2.33 enables us to conclude that these dependences can be approximated by

$$d_{33}^*(m) = a_0 + a_1 m + a_2 m^2 + a_3 m^3. \tag{2.26}$$

In (2.26) a_i are coefficients that do not depend on m. We add for a comparison that a volume-fraction dependence $d_{33}^*(m_{pl})$ in a ZTS-19 FC/polymer composite from work [65] is represented as

$$d_{33}^*\left(m_{pl}\right) = a_0^* + a_1^* m_{pl} + a_2^* {m_{pl}}^2 + a_3^* {m_{pl}}^3 + a_4^* {m_{pl}}^4 \tag{2.27}$$

In (2.27) a_i* are coefficients that do not depend on m_{pl}, and m_{pl} is the volume fraction of the polymer component. A difference between the polynomials (2.26) and (2.27) can be accounted for by specifics of the composite mcirogeometry, poling conditions and other factors.

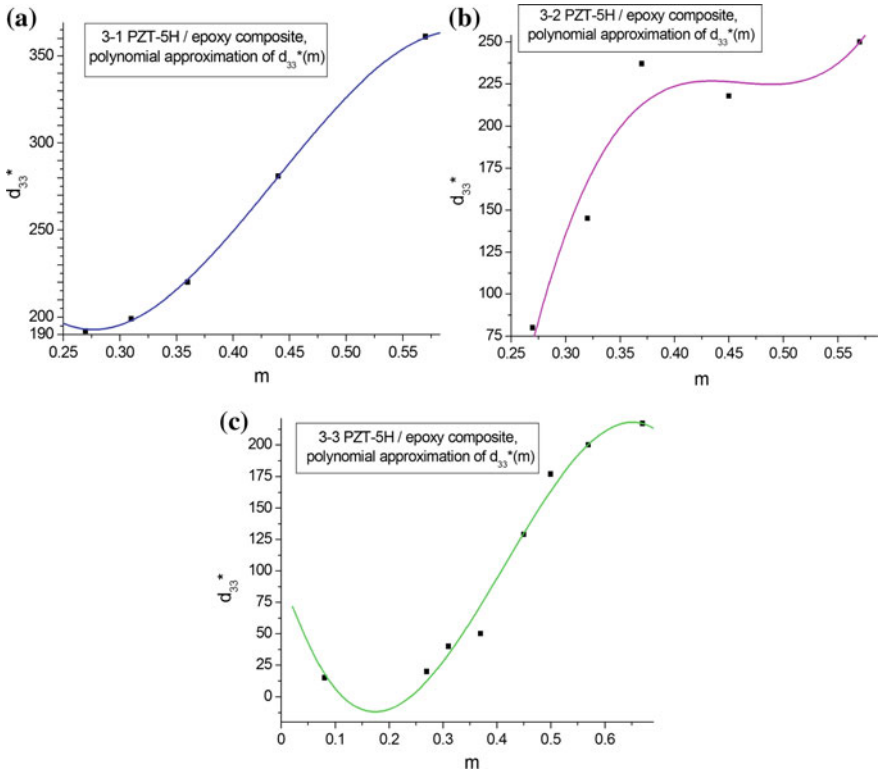

Fig. 2.33 Volume-fraction dependences of the piezoelectric coefficient d_{33}^* (in pC/N) of 3–β PZT-5H FC/epoxy composites and examples of the polynomial approximation of $d_{33}^*(m)$ at $\beta = 1$ (**a**), $\beta = 2$ (**b**) and $\beta = 3$ (**c**). Experimental points (black squares in graphs) are adapted from work [19])

2.6 Electromechanical Coupling Factors and Their Relations to d_{ij}^*

Based on (1.16)–(1.18), we analyse ECFs related to the 1–3 SC/polymer composite. Figure 2.34a shows links between the piezoelectric coefficient d_{31}^* and ECFs k_{31}^* and k_p^* which are concerned with the transverse piezoelectric effect. In Fig. 2.34b links between the piezoelectric coefficient d_{33}^* and ECFs k_{33}^* and k_t^* are observed, and these parameters are concerned with the longitudinal piezoelectric effect. The effective parameters of the 1–3 PMN-0.33PT-based composite were evaluated by means of the matrix method, see Sect. 2.2.2. A correlation between $d_{3j}^*(m)$ and $k_{3j}^*(m)$ (see curves 1 and 2 in Fig. 2.34) is accounted for by a restricted influence of the dielectric and elastic properties of the 1–3 composite on its electromechanical coupling and by the proportionality $k_{3j}^* \sim d_{3j}^*$ in accordance with (1.16). A small

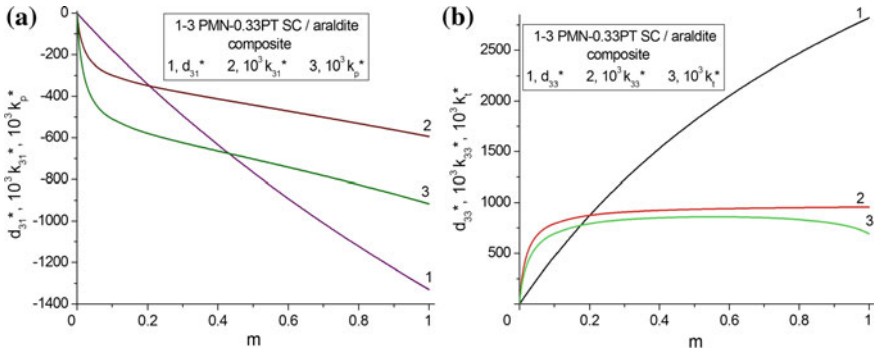

Fig. 2.34 Volume-fraction (m) dependence of piezoelectric coefficients d_{3j}^* (in pC/N) and ECFs k_{3j}^*, k_p^* and k_t^* in the 1–3 [001]-poled PMN–0.33PT SC/araldite composite. The schematic of the composite is shown in Fig. 2.11

difference between the ECFs k_{33}^* and k_t^* (see curves 2 and 3 in Fig. 2.34b) in the wide m range is typical of the 1–3 composite poled along the OX_3 axis [12, 42, 44].

A considerable anisotropy of the ECFs can be observed in the 1–3-type composite wherein the matrix is characterised by a specific elastic anisotropy [55]. This elastic anisotropy is caused by auxetic polymers, pores or FC inclusions in the polymer medium [8, 46–48, 52, 54, 55]. Examples of the large anisotropy of the piezoelectric coefficients d_{3j}^* and ECFs related to the longitudinal and transverse piezoelectric effects in the 1–3–0 composite with the porous polymer matrix are shown in Table 2.6. The highly oblate pores promote the larger anisotropy of d_{3j}^* on increasing porosity m_p in the polymer matrix. The similar conditions for the large anisotropy of the ECFs are valid in narrower volume-fraction ranges $[m_1, m_2]$ in comparison to the anisotropy of d_{3j}^*, see 3rd, 4th and 5th columns in Table 2.6. On increasing porosity m_p in the matrix, the volume-fraction range corresponding to the

Table 2.6 Volume-fraction ranges $[m_1, m_2]$ wherein conditions for the large anisotropy of piezoelectric coefficients d_{3j}^* and ECFs hold for the 1–3–0 [001]-poled PMN–0.33PT SC/porous araldite composite[a]

ρ_p	m_p	Validity of the condition $d_{33}^*/\lvert d_{31}^*\rvert \geq 5$	Validity of the condition $k_{33}^*/\lvert k_{31}^*\rvert \geq 5$	Validity of the condition $k_t^*/\lvert k_p^*\rvert \geq 5$
10	0.2	[0.001, 0.048]	–	–
10	0.3	[0.001, 0.111]	–	–
100	0.1	[0.001, 0.273]	[0.001, 0.196]	–
100	0.2	[0.001, 0.300]	[0.001, 0.245]	[0.001, 0.093]
100	0.3	[0.001, 0.309]	[0.001, 0.275]	[0.001, 0.130]

The schematic of the composite is shown in Fig. 2.19

[a]The volume fraction of SC m is varied from 0.001 to 0.999

large anisotropy of d_{3j}^* becomes wider, see 3rd column in Table 2.6 at ρ_p = 100. This effect is concerned with the influence of elastic properties of the porous polymer matrix on the ECFs of the composite [12, 55], and such an influence strongly depends on the oscillation mode and volume fraction of SC. It should be reminded that the PMN–0.33PT SC, the only piezoelectric component in the studied 1–3–0 composite, does not exhibit the remarkable anisotropy of the piezoelectric coefficients $d_{3j}^{(1)}$, see data in Table 1.3.

2.7 Hydrostatic Piezoelectric Response and Its Relation to d_{ij}^*

As is known from Sect. 1.3, the hydrostatic piezoelectric coefficient d_h is directly used as a measure of PS at the transmitter function of the hydrophone. The effective hydrostatic piezoelectric coefficient d_h^* from (2.1) is related to a composite sample with electrodes applied perpendicular to the OX_3 axis, and this axis is often regarded as a poling axis of the composite [4, 10, 12, 17]. The piezoelectric coefficient d_h^* from (2.21) has important links to the hydrostatic squared figure of merit (2.2) and hydrostatic ECF

$$k_h^* = d_h^* / \left(\varepsilon_{33}^{*\sigma} s_h^{*E}\right)^{1/2} \tag{2.28}$$

In (2.28) $\varepsilon_{33}^{*\sigma}$ is the dielectric permittivity of the composite at σ = const, and

$$s_h^{*E} = \sum_{a=1}^{3} \sum_{b=1}^{3} s_{ab}^{*E} \tag{2.29}$$

is the hydrostatic elastic compliance of the composite at E = const.

An example of interrelations between the hydrostatic parameters from (2.1), (2.2) and (2.28) is shown in Fig. 2.35. Calculations were performed by means of the matrix method. The maximum of each parameter shown in Fig. 2.35 is caused by the behaviour of the piezoelectric coefficients d_{3j}^* shown in Fig. 2.16a, see curves 2 and 3. Maxima of $(Q_h^*)^2$ from (2.2) and k_h^* from (2.28) are observed at smaller volume fractions m (curves 2 and 3 in Fig. 2.35) in comparison to max d_h^* (curve 1 in Fig. 2.35). This is accounted for by the influence of dielectric properties of the composite on $(Q_h^*)^2$ and k_h^*. The diffuse min k_h^* at $m \approx 0.9$ (curve 2 in Fig. 2.35) is caused by the non-monotonic volume-fraction behaviour of elastic compliances s_{ab}^{*E} that determine s_h^{*E} from (2.29).

In the related 1–3–0 composite, maxima of the hydrostatic parameters from (2.1), (2.2) and (2.28) depend on the aspect ratio of the air pore ρ_p and porosity m_p which are characteristics of the matrix, see Fig. 2.19. Table 2.7 suggests that increasing maxima of the parameters correlates with increasing the aspect ratio ρ_p at

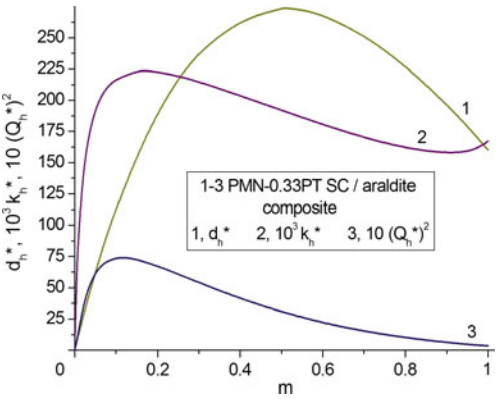

Fig. 2.35 Volume fraction dependence of the hydrostatic piezoelectric coefficient d_h^* (in pC/N), squared figure of merit $(Q_h^*)^2$ (in 10^{-12} Pa^{-1}) and ECF k_h^* of the 1–3 [001]-poled PMN–0.33PT SC/araldite composite. The schematic of the composite is shown in Fig. 2.11

Table 2.7 Maximum values of the hydrostatic piezoelectric coefficient d_h^* (in pC/N), squared figure of merit $(Q_h^*)^2$ (in 10^{-12} Pa^{-1}) and ECF k_h^* of the 1–3–0 [001]-poled PMN–0.33PT SC/porous araldite composite

ρ_p	Max d_h^*	Max $[(Q_h^*)^2]$	Max k_h^*
Composite at $m_p = 0.1$			
0.1	282 ($m = 0.486$)[a]	8.32 ($m = 0.105$)	0.196 ($m = 0.150$)
0.5	294 ($m = 0.478$)	9.19 ($m = 0.109$)	0.219 ($m = 0.145$)
1	313 ($m = 0.464$)	10.8 ($m = 0.099$)	0.240 ($m = 0.138$)
10	609 ($m = 0.356$)	56.8 ($m = 0.066$)	0.448 ($m = 0.096$)
100	1390 ($m = 0.194$)	684 ($m = 0.020$)	0.760 ($m = 0.046$)
Composite at $m_p = 0.2$			
0.1	291 ($m = 0.463$)	9.43 ($m = 0.096$)	0.177 ($m = 0.134$)
0.5	316 ($m = 0.448$)	11.4 ($m = 0.091$)	0.214 ($m = 0.125$)
1	353 ($m = 0.425$)	15.1 ($m = 0.084$)	0.254 ($m = 0.114$)
10	829 ($m = 0.294$)	133 ($m = 0.045$)	0.549 ($m = 0.070$)
100	1640 ($m = 0.146$)	1520 ($m = 0.011$)	0.816 ($m = 0.032$)
Composite at $m_p = 0.3$			
0.1	303 ($m = 0.438$)	10.9 ($m = 0.086$)	0.162 ($m = 0.117$)
0.5	340 ($m = 0.418$)	14.2 ($m = 0.079$)	0.211 ($m = 0.106$)
1	394 ($m = 0.390$)	20.8 ($m = 0.071$)	0.265 ($m = 0.094$)
10	998 ($m = 0.252$)	236 ($m = 0.032$)	0.609 ($m = 0.054$)
100	1780 ($m = 0.120$)	2550 ($m = 0.007$)	0.840 ($m = 0.024$)

The schematic of the composite is shown in Fig. 2.19

[a]The volume fraction of SC which is related to the maximum of the hydrostatic parameter is given in parentheses

m_p = const. This is consistent with data in Table 2.6 and with the statement that the elastic anisotropy of the porous polymer matrix strongly influences the hydrostatic parameters of the 1–3–0 composite.

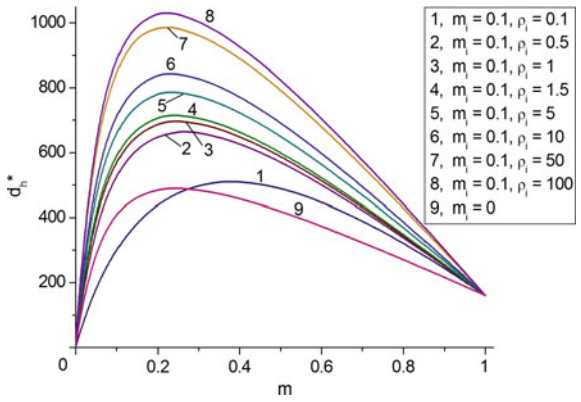

Fig. 2.36 Volume-fraction dependence of the hydrostatic piezoelectric coefficient d_h^* (in pC/N) of the 2–0–2 [001]-poled PMN–0.33PT SC/modified $PbTiO_3$ FC (I)/PE composite. Curve 9 is related to the 2–2 [001]-poled PMN–0.33PT SC/PE composite (reprinted from paper by Topolov et al. [39], with permission from Taylor and Francis)

The similar behaviour of the hydrostatic parameters from (2.1), (2.2) and (2.28) is observed in the 2–0–2 SC/FC/polymer composite described in Sect. 2.1.3. Changes in the aspect ratio of the FC inclusions ρ_i in the 0–3 FC/polymer layer lead to changes in the piezoelectric properties and their anisotropy (Fig. 2.9). As a result, the larger hydrostatic piezoelectric coefficient d_h^* of the 2–0–2 composite is achieved at the larger aspect ratio ρ_i (Fig. 2.36). We note that the max d_h^* value at ρ_i = 100 (curve 8 in Fig. 2.36) is approximately two times larger than the max d_h^* value related to the 2–2 composite (curve 9 in Fig. 2.36) that does not contain the FC inclusions. Such a large difference is achieved even at the relatively small volume fraction of FC m_i = 0.1. The reason for the large difference is concerned [39] with the large elastic anisotropy of the 0–3 FC/polymer layer at $\rho_i \gg 1$, and this effect is to be taken into account at predicting the effective properties and hydrostatic parameters of advanced piezo-active composites.

2.8 Conclusion

This chapter has been devoted to the piezoelectric coefficients d_{ij}^*, their anisotropy and links between microgeometric characteristics of piezo-active composites and their d_{ij}^*. The piezoelectric coefficients d_{ij}^* play the important role at the analysis of the PS and ways for improving the performance and PS of the composites. The main results of this chapter are formulated as follows.

(i) Examples of the PS of the composites are considered for the following connectivity patterns: 0–3, 0–3–0, 1–1, 1–1–0, 1–3, 1–2–2, 1–0–3, 1–3–0, 2–2, 2–0–2, 3–0, 3–1, 3–2, and 3–3. The studied composites are based on either FCs or domain-engineered SCs. Changes in the volume fraction of the piezoelectric component and microgeometry of the composite enable us to vary d_{ij}^* and their anisotropy in wide ranges. As follows from the analysis

of the volume-fraction dependences of d_{ij}^*, the main emphasis at the study of the microgeometry–PS relations is to be placed on the longitudinal and transverse piezoelectric coefficients d_{ij}^* and ways to control the PS for the specific connectivity pattern.

(ii) The system of the aligned FC (or SC) rods in the large polymer matrix promotes the large piezoelectric coefficient d_{33}^* and related ECFs.

(iii) The auxetic polymer matrix strongly influences the elastic and piezoelectric anisotropy of the composite and the anisotropy of its ECFs due to the negative Poisson's ratio of the polymer. Volume fractions that correspond to $d_{31}^* = 0$ depend on the elastic properties of the FC (or SC) and polymer components.

(iv) The system of oblate spheroidal air pores in the polymer matrix promotes the considerable anisotropy of the piezoelectric coefficients d_{ij}^* and ECFs, and this trend is often observed in the 1–3-type and 2–2-type composites. The elastic anisotropy of the composite plays the important role in the formation of the large anisotropy of the ECFs. The large hydrostatic parameters are achieved in the same composites with the porous polymer matrix.

(v) In the 2–0–2 composite with contrasting properties of the components, the SC component strongly influences the PS. The 0–3 FC/polymer layer exhibits a considerable level of elastic anisotropy and plays the important role in forming the large piezoelectric anisotropy and pronounced hydrostatic piezoelectric response of the 2–0–2 composite.

(vi) Links between the PS, ECFs and hydrostatic parameters of the 1–3-type composites are important at the prediction of their performance and at the selection of materials for piezotechnical applications. In the 1–0–3 SC/FC/polymer composite with contrasting properties of components, the 0–3 matrix influences the piezoelectric anisotropy of the composite.

(vii) In the 0–3 composite the PS and piezoelectric anisotropy can be varied in restricted ranges because of the isolated piezoelectric inclusions. The porous matrix with 3–0 connectivity can influence the piezoelectric anisotropy of the 0–3–0 composite to some extent.

(viii) The $d_{33}^*(m)$ dependence (2.26) related to the 3–β FC/polymer composites (β = 1, 2 and 3) suggests that their longitudinal PS is mainly caused by the continuous distribution of the FC component along three co-ordinate axes and depends on the connectivity index β to a small degree.

Data from this chapter can be taken into account to predict the PS, electromechanical coupling and hydrostatic piezoelectric response of various two- and three-component composites. These materials can be of interest in modern piezotechnical applications including transducers, sensors, actuators, hydrophones, and energy-harvesting systems where the piezoelectric coefficients d_{ij}^* and related parameters are exploited.

References

1. Ikeda T (1990) Fundamentals of piezoelectricity. Oxford University Press, Oxford, New York, Toronto
2. Zheludev IS (1971) Physics of crystalline dielectrics. Vol 2: Electrical properties. Plenum, New York
3. Jaffe B, Cook WR, Jaffe H (1971) Piezoelectric ceramics. Academic Press, London, New York
4. Sherman CH, Butler JL (2007) Transducers and arrays for underwater sound. Springer, New York
5. Tichý J, Erhart J, Kittinger E, Přívratská J (2010) Fundamentals of piezoelectric sensorics. Mechanical, dielectric, and thermodynamical properties of piezoelectric materials. Springer, Berlin
6. Uchino K (2008) Piezoelectric motors and transformers. In: Heywang W, Lubitz K, Wersing W (eds) Piezoelectricity, evolution and future of a technology. Springer, Berlin, pp 257–277
7. Haertling G (1999) Ferroelectric ceramics: history and technology. J Am Ceram Soc 82:797–818
8. Bowen CR, Topolov VYu, Kim HA (2016) Modern piezoelectric energy-harvesting materials. Springer International Publishing, Switzerland
9. Shvarstman VV, Kholkin AL (2011) Nanoscale investigation of polycrystalline ferroelectric materials via piezoresponse force microscopy. In: Pardo L, Ricote J (eds) Multifunctional polycrystalline ferroelectric materials. Processing and properties. Springer, Dordrecht, pp 409–468
10. Topolov VYu, Bowen CR (2009) Electromechanical properties in composites based on ferroelectrics. Springer, London
11. Khoroshun LP, Maslov BP, Leshchenko PV (1989) Prediction of effective properties of piezo-active composite materials. Naukova Dumka, Kiev (in Russian)
12. Topolov VYu, Bisegna P, Bowen CR (2014) Piezo-active composites. Orientation effects and anisotropy factors. Springer, Berlin, Heidelberg
13. Chan HLW, Ng PKL, Choy CL (1999) Effect of poling procedure on the properties of lead zirconate titanate/vinylidene fluoride-trifluoroethylene composites. Appl Phys Lett 74:3029–3031
14. Nan CW, Weng GJ (2000) Influence of polarization orientation on the effective properties of piezoelectric composites. J Appl Phys 88:416–423
15. Newnham RE, Skinner DP, Cross LE (1978) Connectivity and piezoelectric-pyroelectric composites. Mater Res Bull 13:525–536
16. Gururaja TR, Safari A, Newnham RE, Cross LE (1988) Piezoelectric ceramic-polymer composites for transducer applications. In: Levinson LM (ed) Electronic ceramics: properties, devices, and applications. Marcel Dekker, New York, pp 92–128
17. Akdogan EK, Allahverdi M, Safari A (2005) Piezoelectric composites for sensor and actuator applications. IEEE Trans Ultrason Ferroelectr Freq Control 52:746–775
18. Safari A, Akdogan EK (2006) Rapid prototyping of novel piezoelectric composites. Ferroelectrics 331:153–179
19. Smay JE, Tuttle B, Cesarano J III (2008) Robocasting of three-dimensional piezoelectric structures. In: Safari A, Akdoğan EK (eds) Piezoelectric and acoustic materials for transducer applications. Springer, New York, pp 305–318
20. Topolov VYu, Turik AV (2000) Non-monotonic concentration dependence of electromechanical properties of piezo-active 2–2 composites. J Phys D Appl Phys 33:725–737
21. Grekov AA, Kramarov SO, Kuprienko AA (1987) Anomalous behavior of the two-phase lamellar piezoelectric texture. Ferroelectrics 76:43–48
22. Levassort F, Lethiecq M, Millar C, Pourcelot L (1998) Modeling of highly loaded 0–3 piezoelectric composites using a matrix method. IEEE Trans Ultrason Ferroelectr Freq Control 45:1497–1505
23. Gibiansky LV, Torquato S (1997) On the use of homogenization theory to design optimal piezocomposites for hydrophone applications. J Mech Phys Solids 45:689–708

24. Grekov AA, Kramarov SO, Kuprienko AA (1989) Effective properties of a transversely isotropic piezoelectric composite with cylindrical inclusions. Mech Compos Mater 25:54–61
25. Evans KE, Alderson KL (1992) The static and dynamic moduli of auxetic microporous polyethylene. J Mater Sci Lett 11:1721–1724
26. Ren K, Liu Y, Geng X, Hofmann HF, Zhang QM (2006) Single crystal PMN–PT/epoxy 1–3 composite for energy-harvesting application. IEEE Trans Ultrason Ferroelectr Freq Control 53:631–638
27. Wang F, He C, Tang Y (2007) Single crystal $0.7Pb(Mg_{1/3}Nb_{2/3})O_3$–$0.3PbTiO_3$/epoxy 1–3 piezoelectric composites prepared by the lamination technique. Mater Chem Phys 105:273–277
28. Topolov VYu, Krivoruchko AV (2009) Polarization orientation effect and combination of electromechanical properties in advanced $0.67Pb(Mg_{1/3}Nb_{2/3})O_3$–$0.33PbTiO_3$ single crystal/polymer composites with 2–2 connectivity. Smart Mater Struct 18:011–065
29. Zhang R, Jiang B, Cao W (2001) Elastic, piezoelectric, and dielectric properties of multidomain $0.67Pb(Mg_{1/3}Nb_{2/3})O_3$–$0.33PbTiO_3$ single crystals. J Appl Phys 90:3471–3475
30. Zhang R, Jiang B, Cao W (2003) Single-domain properties of $0.67Pb(Mg_{1/3}Nb_{2/3})O_3$–$0.33PbTiO_3$ single crystals under electric field bias. Appl Phys Lett 82:787–789
31. Peng J, Luo H, He T, Xu H, Lin D (2005) Elastic, dielectric, and piezoelectric characterization of $0.70Pb(Mg_{1/3}Nb_{2/3})O_3$–$0.30PbTiO_3$ single crystal. Mater Lett 59:640–643
32. Liu G, Jiang W, Zhu J, Cao W (2011) Electromechanical properties and anisotropy of single- and multi-domain $0.72Pb(Mg_{1/3}Nb_{2/3})O_3$–$0.28PbTiO_3$ single crystals. Appl Phys Lett 99:162901
33. Sun E, Cao W, Jiang W, Han P (2011) Complete set of material properties of single domain $0.24Pb(In_{1/2}Nb_{1/2})O_3$–$0.49Pb(Mg_{1/3}Nb_{2/3})O_3$-$0.27PbTiO_3$ single crystal and the orientation effects. Appl Phys Lett 99:032901
34. Yin J, Jiang B, Cao W (2000) Elastic, piezoelectric, and dielectric properties of $0.955Pb(Zn_{1/3}Nb_{2/3})O_3$–$0.045PbTiO_3$ single crystals. IEEE Trans Ultrason Ferroelectr Freq Control 47:285–291
35. Zhang R, Jiang B, Cao W, Amin A (2002) Complete set of material constants of $0.93Pb(Zn_{1/3}Nb_{2/3})O_3$–$0.07PbTiO_3$ domain engineered single crystal. J Mater Sci Lett 21:1877–1879
36. Zhang S, Li F, Jiang X, Kim J, Luo J, Geng X (2015) Advantages and challenges of relaxor-$PbTiO_3$ ferroelectric crystals for electroacoustic transducers—a review. Prog Mater Sci 68:1–66
37. Turik AV, Topolov VYu (1997) Ferroelectric ceramics with a large piezoelectric anisotropy. J Phys D Appl Phys 30:1541–1549
38. Dongyu X, Xin C, Shifeng H (2015) Investigation of inorganic fillers on properties of 2–2 connectivity cement/polymer based piezoelectric composites. Constr Build Mater 94:678–683
39. Topolov VYu, Bowen CR, Ermakov IA (2016) Remarkable hydrostatic piezoelectric response of novel 2–0–2 composites. Ferroelectr Lett Sect 42:90–95
40. Topolov VYu, Ermakov IA (2016) Piezoelectric properties and hydrostatic parameters of the novel 2–0–2 composite based on a relaxor-ferroelectric single crystal. Nano- i Mikrosistemnaya Tekhnika 18:696–699
41. Huang JH, Kuo W-S (1996) Micromechanics determination of the effective properties of piezoelectric composites containing spatially oriented short fibers. Acta Mater 44:4889–4898
42. Chan HLW, Unsworth J (1989) Simple model for piezoelectric ceramic/polymer 1–3 composites used in ultrasonic transducer applications. IEEE Trans Ultrason Ferroelectr Freq Control 36:434–441
43. Topolov VYu, Bisegna P (2010) Anisotropic piezoelectric properties of 1–3 ceramic/polymer composites comprising rods with elliptic cross section. J Electroceram 25:26–37
44. Bezus SV, Topolov VYu, Bowen CR (2006) High-performance 1–3-type composites based on $(1 - x)$ $Pb(A_{1/3}Nb_{2/3})O_3 - xPbTiO_3$ single crystals (A = Mg, Zn). J Phys D Appl Phys 39:1919–1925

45. Topolov VYu, Krivoruchko AV, Bisegna P, Bowen CR (2008) Orientation effects in 1–3 composites based on $0.93Pb(Zn_{1/3}Nb_{2/3})O_3$–$0.07PbTiO_3$ single crystals. Ferroelectrics 376:140–152
46. Topolov VYu, Bowen CR, Bisegna P, Krivoruchko AV (2015) New orientation effect in piezo-active 1–3-type composites. Mater Chem Phys 151:187–195
47. Topolov VYu, Bowen CR, Bisegna P (2015) New aspect-ratio effect in three-component composites for piezoelectric sensor, hydrophone and energy-harvesting applications. Sens Actuators A – Phys 229:94–103
48. Topolov VYu, Bowen CR, Bisegna P, Panich AE (2015) Effect of the matrix subsystem on hydrostatic parameters of a novel 1–3-type piezo-composite. Funct Mater Lett 8:1550049
49. COMSOL, Inc. (2007) COMSOL Multiphysics™ User's Guide (version 3.4). http://www.comsol.com/
50. Bowen CR, Topolov VYu, Isaeva AN, Bisegna P (2016) Advanced composites based on relaxor-ferroelectric single crystals: from electromechanical coupling to energy-harvesting applications. Cryst Eng Comm 18:5986–6001
51. Topolov VYu, Turik AV (2001) On increasing the hydrostatic sensitivity of three-component piezocomposites. Tech Phys Lett 27:81–83
52. Topolov VYu, Turik AV (2001) Porous piezoelectric composites with extremely high reception parameters. Tech Phys 46:1093–1100
53. Panich AE, Topolov VYu, Glushanin SV (2006) High-performance 1–3-type relaxor-ferroelectric-based composites. In: Vibroengineering, 6th international conference proceedings, October 12–14, 2006. Kaunas University of Technology, Lithuania. Technologija, Kaunas, pp 226–230
54. Topolov VYu, Panich AE (2009) Problem of piezoelectric sensitivity of 1–3-type composites based on ferroelectric ceramics. Ferroelectrics 392:107–119
55. Topolov VYu, Krivoruchko AV, Bisegna P (2011) Electromechanical coupling and its anisotropy in a novel 1–3–0 composite based on single-domain $0.58Pb(Mg_{1/3}Nb_{2/3})O_3$–$0.42PbTiO_3$ crystal. Compos Sci Technol 71:1082–1088
56. Dunn ML, Taya M (1993) Electromechanical properties of porous piezoelectric ceramics. J Am Ceram Soc 76:1697–1706
57. Glushanin SV, Topolov VYu (2001) Features of electromechanical properties of piezoelectric composites with elements of connectivity 1–1. J Phys D Appl Phys 34:2518–2529
58. Glushanin SV, Topolov VYu (2001) Anisotropy of the electromechanical properties and a high piezoelectric sensitivity of the 1–1 type ferroelectric piezocomposites. Tech Phys Lett 27:626–628
59. Topolov VYu, Bisegna P, Bowen CR (2011) Analysis of the piezoelectric performance of modern 0–3-type composites based on relaxor-ferroelectric single crystals. Ferroelectrics 413:176–191
60. Filippov SE, Vorontsov AA, Topolov VYu, Brill OE, Bisegna P, Panich AE (2014) Features of the piezoelectric effect in a novel PZT-type ceramic/clay composite. Ferroelectr Lett Sect 41:82–88
61. Bowles JE (1996) Foundation analysis and design. McGraw-Hill, New York
62. Balkevich VL (1996) Technical ceramics. Stroyizdat, Moscow (in Russian)
63. Glushanin SV, Topolov VYu (2005) Features of the electromechanical properties of 0–3 composites of the $Pb(Zr, Ti)O_3$-based ferroelectric ceramics – polymer type. Tech Phys Lett 31:346–348
64. Bowen CR, Topolov VYu (2003) Piezoelectric sensitivity of $PbTiO_3$-based ceramic/polymer composites with 0–3 and 3–3 connectivity. Acta Mater 51:4965–4976
65. Borzov PA, Vorontsov AA, Topolov VYu, Brill OE (2016) Piezoelectric performance and features of microgeometry of novel composites based on ferroelectric ZTS-19 ceramics. In: Parinov IA, Chang S-H, Topolov VYu (eds) Proceedings of the 2015 International Conference on "Physics, Mechanics of New Materials and Their Applications", Devoted to the 100th Anniversary of the Southern Federal University. Nova Science Publishers, New York, pp 115–122

Chapter 3
Microgeometry of Composites and Their Piezoelectric Coefficients g_{ij}^*

Abstract Piezoelectric coefficients g_{ij} represent a link between an external mechanical stress applied to a sample and an electric field formed by polarisation charges of the sample as a result of the direct piezoelectric effect. The piezoelectric coefficients g_{ij} also characterise a link between a strain and electric displacement at the converse piezoelectric effect. The piezoelectric sensitivity associated with g_{ij} is of importance for sensor, energy-harvesting, acoustic, and hydroacoustic applications, for piezo-ignition systems, etc. Examples of the effective piezoelectric coefficients g_{ij}^*, $\max g_{33}^*$ and their links to the piezoelectric coefficients d_{ij}^* are discussed for piezo-active composites with various connectivity patterns (2–2-type, 1–3-type, 1–1-type, 0–3-type, and 3–β composites). The important role of the microgeometric factor and polymer component at achieving the large values of g_{ij}^* of the composite is shown.

As follows from (1.9), the piezoelectric coefficients g_{ij} represent a link between an external mechanical stress σ_j applied to a sample and an electric field E_i formed by polarisation charges of the sample as a result of the direct piezoelectric effect. In accordance with (1.8), the piezoelectric coefficients g_{ij} are used to describe the link between a strain ξ_j and electric displacement D_i at the converse piezoelectric effect [1]. The aforementioned link of the direct piezoelectric effect means that an output voltage (or electric field, or electric signal) is generated by the applied stress field (or a load). The PS associated with this generation is of importance for sensor, energy-harvesting, acoustic, and hydroacoustic applications, for piezo-ignition systems, for measuring and for quality control during production [1–6], etc. Equations (1.20) and (1.22) suggest that the piezoelectric coefficients d_{ij} studied in Chap. 2 and the piezoelectric coefficients g_{ij} to be analysed in this chapter are linked by dielectric properties that are described by a second-order rank tensor. We remind the reader that the piezoelectric properties are described by a third-rank tensor, and therefore, a link between g_{ij} and d_{ij} seems to be relatively simple due to the lower rank of the tensor of the dielectric properties.

In this chapter we discuss the PS of some modern two- and three-component composites in the context of their effective piezoelectric coefficients g_{ij}^* and relations

V. Y. Topolov et al., *Piezo-Active Composites*, Springer Series in Materials Science 271, https://doi.org/10.1007/978-3-319-93928-5_3

between d_{ij}^* and g_{ij}^*. Hereby we consider examples of the connectivity patterns, that were introduced in Chap. 2, to show the role of the microgeometric factors leading to large values of $|g_{ij}^*|$ in the composites.

3.1 2–2-Type Composites

The simplicity of the 2–2 composite structure shown in Figs. 2.1 and 2.2 and various possibilities of varying the electromechanical properties and related parameters of the piezo-active composites in wide ranges [7–11] make the 2–2 connectivity attractive to analyse its PS in the context of the piezoelectric coefficients g_{ij}^*. In Sect. 3.1 we consider examples of the PS of parallel-connected composites based on SCs poled along specific crystallographic directions.

As is known from various literature data [8, 10–13], the high-performance 2–2-type composites are often based on relaxor-ferroelectric SCs such as PMN–*x*PT or PZN–*x*PT. However these SCs are characterised by small values of the piezoelectric coefficient g_{33} in comparison to some ferroelectric materials. For example, in the [001]-poled SC from the 4*mm* symmetry class, g_{33} is linked with the piezoelectric coefficient d_{33} in accordance with (1.20) by the relation $g_{33} = d_{33}/\varepsilon_{33}^{\sigma}$, where $\varepsilon_{33}^{\sigma}$ is the dielectric permittivity of the stress-free sample. Based on experimental data from Table 1.3, we obtain for the PMN–0.33PT SC g_{33} = 38.9 mV m/N. Using experimental data from Table 1.2, we obtain for the KNNTL:Mn SC g_{33} = 94.7 mV m/N. Such a large g_{33} value is achieved in the SC sample where d_{33} is about 5.2 times smaller than d_{33} of the PMN–0.33PT SC, and $\varepsilon_{33}^{\sigma}$ is about 12.6 times smaller than $\varepsilon_{33}^{\sigma}$ of the PMN–0.33PT SC. Moreover, the KNNTL:Mn SC is a lead-free ferroelectric material that can be of interest due to its remarkable electromechanical properties.

To predict the volume-fraction behaviour of the effective properties of the 2–2-type composite, we apply the matrix method [7, 8, 11]. We show examples of the volume-fraction dependence of the piezoelectric coefficients g_{ij}^* (Fig. 3.1) in the parallel-connected 2–2-type composites. These composites are from the *mm*2 symmetry class, and relations between their piezoelectric coefficients g_{ij}^* and d_{ij}^* are represented in accordance with (1.20) as follows:

$$g_{3j}^* = d_{3j}^*/\varepsilon_{33}^{*\sigma},\ g_{24}^* = d_{24}^*/\varepsilon_{22}^{*\sigma} \text{ and } g_{15}^* = d_{15}^*/\varepsilon_{11}^{*\sigma}, \tag{3.1}$$

where j = 1, 2 and 3. As for the piezoelectric coefficient d_{15}^* in the 2–2 composites analysed in Sect. 2.1 (see Figs. 2.3–2.7), the g_{15}^* is concerned with the 'sleeping PS' of the composite. The relatively small g_{15}^* value in a wide volume-fraction range (curve 1 in Fig. 3.1) is due to the small d_{15}^* values and the slow increase of the dielectric permittivity $\varepsilon_{11}^{*\sigma}$, see (3.1). The composite structure shown in Fig. 2.2 suggests that the OX_1 direction is unfavourable to develop a high PS because there is a system of planar interfaces x_1 = const in the 2–2 composite. In contrast to g_{15}^*,

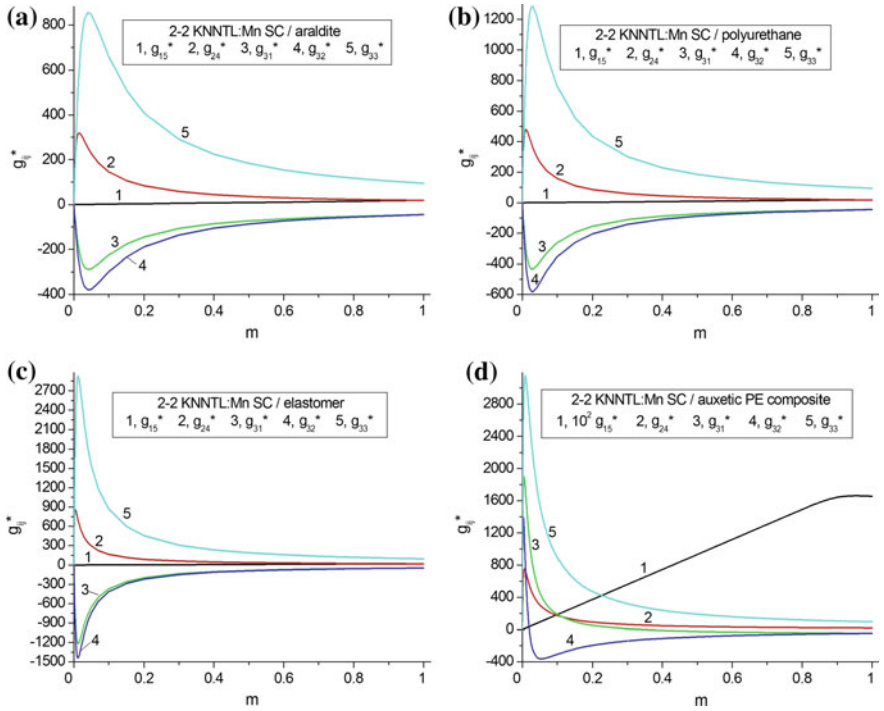

Fig. 3.1 Volume-fraction dependences of piezoelectric coefficients g_{ij}^* (in mV m/N) of 2–2 [001]-poled KNNTL:Mn SC/polymer composites. The schematic of the composite is shown in Fig. 2.2

values of the piezoelectric coefficients g_{24}^* and g_{3j}^* can be varied in wide ranges (see Fig. 3.1) mainly due to changes in the piezoelectric coefficients d_{24}^* and d_{3j}^* from (3.1). The dielectric permittivities $\varepsilon_{22}^{*\sigma}$ and $\varepsilon_{33}^{*\sigma}$ from (3.1) strongly influence g_{24}^* and g_{3j}^* at volume fractions of SC $m < 0.05$, i.e., in a volume-fraction range where the $\varepsilon_{pp}^{*\sigma}$ values are comparable to the dielectric permittivity of the polymer component. Maxima and minima of g_{ij}^* (see curves 2–5 in Fig. 3.1) are observed at $m \ll 1$, where $|d_{ij}^*|$ increase rapidly, and the dielectric permittivities $\varepsilon_{pp}^{*\sigma}$ exhibit a slow monotonic increase. A further increase of $|d_{ij}^*|$ at $m > 0.1$ becomes slow and cannot strongly influence the piezoelectric coefficients g_{ij}^*. The decrease in absolute values of g_{ij}^* becomes considerable at $m > 0.1$, when the dielectric permittivities $\varepsilon_{pp}^{*\sigma}$ of the composite become large in comparison to ε_{pp} of the polymer component. We add that the similar volume-fraction behaviour of the piezoelectric coefficients g_{ij}^* is observed in 2–2 parallel-connected FC/polymer composites [7, 8, 14].

Of specific interest is the KNNTL:Mn SC/auxetic PE composite for which high PS and large values of $|g_{ij}^*|$ are predicted in Fig. 3.1d. At $m < 0.1$, we observe non-monotonic $g_{ij}^*(m)$ dependences that differ from those in the related composites (cf., for instance, Fig. 3.1c, d). This is accounted for by the active influence of the

elastic properties of the auxetic polymer component on the piezoelectric response of the composite, especially at large volume fractions of the polymer component. Such a trend was also observed and analysed in a case of the polarisation orientation effect in the 2–2-type composites [11].

Modifications of the 2–2 composite structure shown in Fig. 2.2 enable us to improve specific parameters of the studied composites. These modifications are concerned with the presence of inclusions in the polymer layers. For instance, a 2–2–0 composite with porous polymer layers is of interest due to increasing its hydrostatic parameters [12] in comparison to those of the related 2–2 composite. A 2–0–2 SC/FC/polymer composite studied in recent work [13] is also characterised by large hydrostatic parameters. Our next example is concerned with the PS of a 2–0–2 lead-free composite with two SC components.

It is assumed that the 2–0–2 composite consists of a system of parallel-connected layers of two types (*Type I* and *Type II* layers) with interfaces that are parallel to the (X_2OX_3) plane. The similar composite structure is shown in Fig. 2.8. The composite layers are regularly arranged along the coordinate OX_1 axis. The Type I layer is a domain-engineered SC and is characterised by a spontaneous polarisation $\boldsymbol{P}_s^{(1)}$ and volume fraction m, and the main crystallographic axes of this SC are oriented as follows: X $\|[001]\|$ OX_1, Y $\|[010]\|$ OX_2 and Z $\|[001]\|$ OX_3. Here the $[hkl]$ direction is given in the perovskite unit-cell axes. The Type II layer is a piezoelectric SC/polymer medium with 0–3 connectivity, and the volume fraction of the Type II layers is $1 - m$. The shape of each inclusion is shown in the inset of Fig. 2.8 and obeys (2.13) in the co-ordinate OX_f axes. Hereby $\rho_i = a_1/a_3$ is the aspect ratio of the SC inclusion, and m_i is the volume fraction of the SC inclusions in the Type II layer. The linear sizes of each SC inclusion in the Type II layer are much smaller than the thickness of each layer of the composite sample. The SC inclusions in the Type II layer occupy sites of a simple tetragonal lattice with unit-cell vectors parallel to the OX_f axes. The orientation of the crystallographic axes X, Y and Z of each SC inclusion in the Type II layer is given by X$\|OX_1$, Y$\|OX_2$ and Z$\|OX_3$.

The effective electromechanical properties of the aforementioned 2–0–2 composite are evaluated in two stages as described in Sect. 2.1.3. Among the lead-free components of interest, we consider the [001]-poled KNNTL:Mn SC in the Type I layer, a piezoelectric $Li_2B_4O_7$ (LBO) SC as an inclusion material in the Type II layer, and monolithic PE and polyurethane as matrix materials in the Type II layer. The full set of electromechanical constants of the LBO SC is shown in Table 3.1. We note that the LBO SC is a highly original component to use in a composite for the following reasons. For instance, the symmetry of the LBO SC in the Type II layer coincides with the macroscopic symmetry of the [001]-poled KNNTL:Mn SC in the Type I layer. The signs of the piezoelectric coefficients e_{ij} of the LBO SC (see Table 3.1) coincide with the signs of e_{ij} of the highly anisotropic $PbTiO_3$-type FCs [16, 17], however the piezoelectric effect in the LBO SC is weaker than that in the poled $PbTiO_3$-type FCs. The LBO SC is characterised by a considerable elastic anisotropy (Table 3.1), and the large ratio $c_{13}^E/c_{12}^E \approx 9.4$ has no analogies with other FCs and SCs.

Table 3.1 Room-temperature elastic moduli c_{ab} (in 10^{10} Pa), piezoelectric coefficients e_{ij} (in C/m^2) and dielectric permittivity ε_{pp}^{ξ} of the LBO SC, 4*mm* symmetry [15]

c_{11}^E	c_{12}^E	c_{13}^E	c_{33}^E	c_{44}^E	c_{66}^E	e_{31}	e_{33}	e_{15}	$\varepsilon_{11}^{\xi}/\varepsilon_0$	$\varepsilon_{33}^{\xi}/\varepsilon_0$
13.5	0.357	3.35	5.68	5.85	4.67	0.290	0.928	0.472	8.90	8.07

In the presence of the two SC components, that belong to the 4*mm* symmetry class, and an isotropic polymer component, the 2–0–2 composite is described by *mm*2 symmetry. Examples of the dependence of the piezoelectric coefficients g_{3j}^* of the 2–2–0 SC/SC/polymer composite on the volume fractions m and m_i and aspect ratio ρ_i are shown in Fig. 3.2.

As follows from Fig. 3.2a–c, the effect of the aspect ratio ρ_i of the SC inclusions on the PS is appreciable, even at relatively small volume fractions of the KNNTL:Mn SC ($m \leq 0.2$) and LBO SC ($m_i = 0.1$). The small values of the volume fractions m and m_i enable the composite to achieve large absolute values of g_{3j}^*, see Fig. 3.2a–c. A non-monotonic dependence of g_{3j}^* on ρ_i is observed in Fig. 3.2a–c at $0 < \rho_i < 3$, i.e., in the region where the elastic compliances of the Type II layer undergo large changes. Differences between $\min g_{31}^*$ (Fig. 3.2a) and $\min g_{32}^*$ (Fig. 3.2b) are accounted for by the role of the composite interfaces $x_1 = \text{const}$ (see Fig. 2.8). The interfaces influence the piezoelectric effect concerned with g_{31}^* to a larger extent in comparison to the piezoelectric effect concerned with g_{32}^*. As a consequence, the depth of $\min g_{31}^*$ is larger than that of $\min g_{32}^*$ (cf. Fig. 3.2a, b), however values of $|g_{31}^*|$ near $\min g_{31}^*$ are smaller than values of $|g_{32}^*|$ near $\min g_{32}^*$. The sequence of curves 1–4 in Fig. 3.2a–c is related to the strong influence of the SC component in the Type I layer (main piezoelectric component) on the PS. On increasing the volume fraction m, $|g_{3j}^*|$ and PS decrease at $\rho_i = \text{const}$ and $m_i = \text{const}$. This occurs mainly because of the large dielectric permittivity $\varepsilon_{33}^{(1),\sigma}$ of the Type I layer in comparison to $\varepsilon_{33}^{(2),\sigma}$ of the Type II layer.

The LBO SC can influence an anisotropy of the piezoelectric coefficients g_{3j}^*, especially at $\rho_i \gg 1$. This is due to the influence of the elastic anisotropy of the Type II layer on the piezoelectric properties of the composite, and the similar effect was discussed in Sect. 2.1.3. On comparing the graphs in Fig. 3.2d, e, we conclude that the piezoelectric coefficient g_{33}^* is smaller at $m = \text{const}$ and $m_i = \text{const}$ for the polyurethane-containing composite. The polymer matrix with the smaller elastic compliances s_{ab} (i.e., PE in comparison to polyurethane, see data in Table 2.1) leads to a stiffer Type II layer which leads to a decrease in the PS of the composite as a whole.

The studied 2–0–2 KNNTL:Mn SC/LBO SC/PE composite has obvious advantages over various FCs and piezo-active composites. For instance, a nanostructured Mn-modified $(K_{0.5}Na_{0.5})NbO_3$ polycrystalline FC is characterised [18] by the piezoelectric coefficient $g_{33} = 220$ mV m/N. The piezoelectric coefficient $d_{33} = 340$ pC/N of the Mn-modified $(K_{0.5}Na_{0.5})NbO_3$ FC is comparable to d_{33}^* of the 2–0–2 composite, however the piezoelectric coefficient g_{33}^* of the

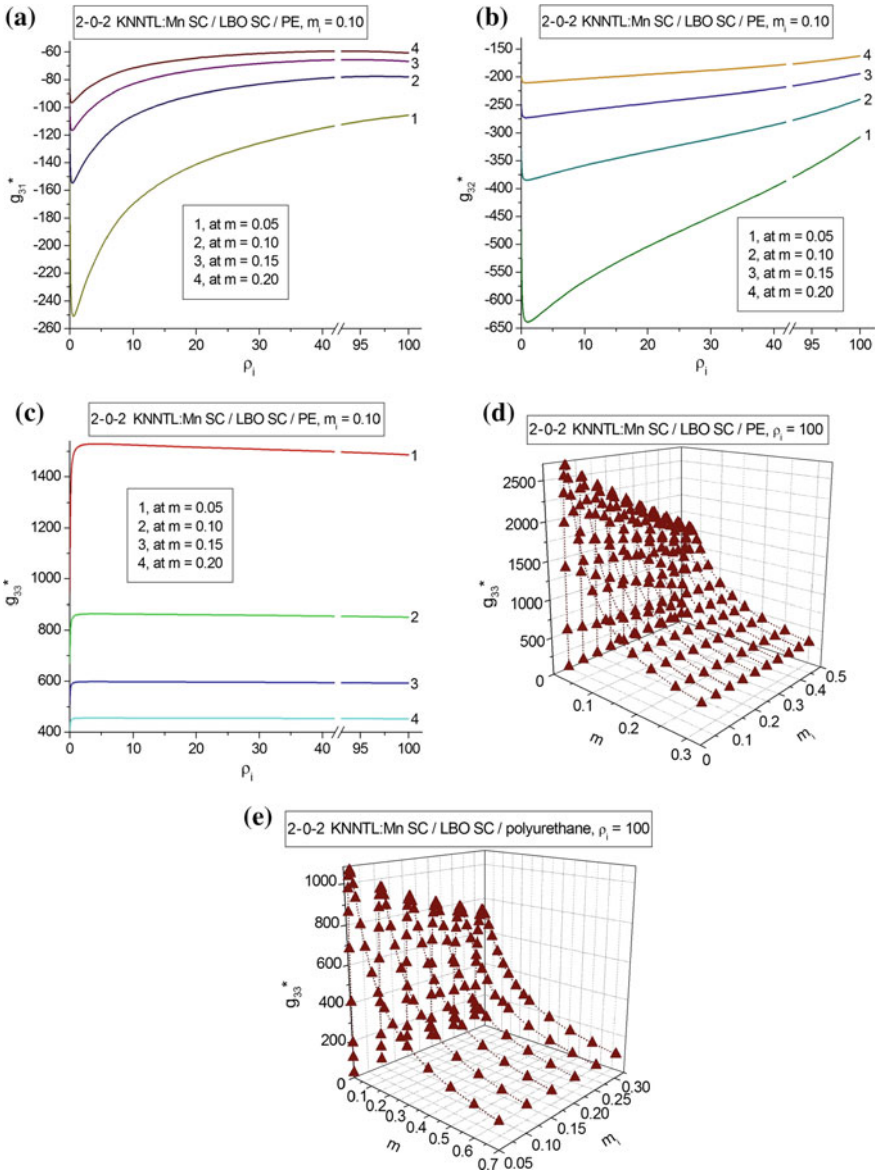

Fig. 3.2 Aspect-ratio (ρ_i) and volume-fraction (m and m_i) dependences of piezoelectric coefficients g_{ij}^* (in mV m/N) of the 2–0–2 [001]-poled KNNTL:Mn SC/LBO SC/PE composite (**a**–**d**) and 2–0–2 [001]-poled KNNTL:Mn SC/LBO SC/polyurethane composite (**e**)

aforementioned FC is smaller than g_{33}^* of the composite (see Fig. 3.2c, d). A novel grain-oriented and highly textured modified $PbTiO_3$ material was manufactured recently [19], and its piezoelectric coefficient g_{33} = 115 mV m/N is also smaller

than g_{33}^* of the studied 2–0–2 composite. In a 2–2 [111]-poled PMN–0.33PT SC/PVDF composite [20], the value of $\max g_{33}^* = 539$ mV m/N is comparable to $\max g_{33}^* = 605$ mV m/N related to a 2–2 [001]-poled PMN–0.33PT SC/PVDF composite.

Our further comparison of the PS and piezoelectric coefficients g_{ij}^* is concerned with composites based on the domain-engineered PMN–xPT SCs. In Table 3.2 we show data on g_{ij}^* of some composites whereby the SC component is poled along either the [001] or [011] direction in the perovskite unit cell. These results obtained within the framework of the matrix method suggest that the PS of the PMN–0.33PT-based composite is higher than the PS of the related PMN–0.28PT-based

Table 3.2 Piezoelectric coefficients g_{ij}^* (in mV m/N) of 2–2 parallel-connected composites based on PMN–xPT SCs

Polymer	m	g_{31}^*	g_{32}^*	g_{33}^*	g_{15}^*	g_{24}^*
[001]-poled PMN–0.33PT SC/polymer						
Elastomer	0.05	−314	−339	722	0.516	190
	0.10	−163	−177	376	1.03	99.1
	0.15	−111	−119	254	1.55	67.0
	0.20	−84.0	−90.2	191	2.06	50.6
Auxetic PE	0.05	242	−31.5	660	0.516	176
	0.10	87.1	−81.4	355	1.03	95.6
	0.15	42.4	−75.0	244	1.55	65.5
	0.20	22.1	−65.3	186	2.06	49.8
[001]-poled PMN–0.28PT SC/polymer						
Elastomer	0.05	−196	−225	463	0.412	152
	0.10	−102	−115	238	0.824	79.2
	0.15	−68.9	−77.3	160	1.24	53.6
	0.20	−52.3	−58.2	121	1.65	40.5
Auxetic PE	0.05	153	−47.7	450	0.412	140
	0.10	52.8	−63.4	234	0.824	76.0
	0.15	25.1	−53.9	158	1.24	52.2
	0.20	12.7	−45.3	120	1.65	39.7
[011]-poled PMN–0.28PT SC/polymer						
Elastomer	0.05	116	−600	465	2.88	300
	0.10	68.2	−318	242	5.77	159
	0.15	49.1	−216	164	8.65	108
	0.20	39.0	−164	124	11.5	81.7
Auxetic PE	0.05	−25.1	−470	390	2.88	284
	0.10	−19.5	−281	221	5.77	154
	0.15	−5.86	−200	154	8.65	106
	0.20	−1.14	−155	119	11.5	80.7

composite, and in both composite systems the SC component is [001]-poled. The larger $|g_{ij}^*|$ values are attained due to the larger $|d_{ij}|$ values of the SC component; see Tables 1.3 and 1.4. For example, the inequality $|g_{32}^*| > g_{33}^*$ holds in the composites based on the [011]-poled PMN–0.28PT SC. As follows from Table 1.4, the piezoelectric coefficients d_{3j} of this SC obey the condition $|d_{32}| > d_{33}$.

On increasing m, the considerable decrease of the $|g_{ij}^*|$ values of the composites listed in Table 3.2 is a result of the monotonic increase of the dielectric permittivities $\varepsilon_{pp}^{*\sigma}$ and the slow increase of $|d_{ij}^*|$ at $m > 0.05$. We remind the reader that the piezoelectric coefficients g_{ij}^* of the 2–2-type composites listed in Table 3.2 obey (3.1). The use of an auxetic polymer component influences $\mathrm{sgn}g_{31}^*$, irrespective of the SC component. A change in $\mathrm{sgn}g_{31}^*$ is also accounted for by a change in the poling direction of the SC component, which is seen in Table 3.2 for composites based on the [001]- and [011]-poled PMN–0.28PT SCs. It should be added that the g_{33}^* values shown in Table 3.2 are comparable to those of the 2–2 KNNTL:Mn SC/araldite composite (see curve 5 in Fig. 3.1a). As can be seen from Table 2.1, araldite has the lowest elastic compliances $|s_{ab}|$ among the polymer components and cannot achieve a high PS for the composite. However such shortcomings can be compensated by use of a KNNTL:Mn SC with large $|g_{3j}|$ values, and we see a number of examples of a high PS of the KNNTL:Mn-based composites in Fig. 3.1.

3.2 1–3-Type Composites

The 1–3 composite structure has been widely studied for PS and exhibits relations between the piezoelectric performance of the composite and its components [7–9, 21–29]. In the 1–3 composite shown in Fig. 2.11, C1 is a component with a high piezoelectric activity, and this component is self-connected in one dimension, often along the poling axis of the composite sample. C2 a component with a low piezoelectric activity or a piezo-passive component, and it is self-connected in three dimensions. A further modification of the composite structure is concerned with a formation of a porous polymer matrix, heterogeneous FC/polymer or SC/polymer matrix, laminar polymer matrix, etc. [23, 24, 28, 29]. In these cases we consider the 1–3-type composite keeping in mind that the system of long parallel rods represent the main piezoelectric component therein; see C1 in Fig. 2.11. In Sect. 3.2 we discuss examples of the behaviour of the piezoelectric coefficients g_{ij}^* of some 1–3-type composites on the assumption that a regular distribution of components over a composite sample is observed.

The graphs in Fig. 3.3 show that maxima or minima of g_{3j}^* are observed at volume fractions of SC $m \ll 1$. Moreover, values of $\max g_{33}^*$ related to composites with a non-auxetic polymer components are approximately equal to the $\max g_{33}^*$ values of the related 2–2 composites. This can be seen by comparing curve 3 in Fig. 3.3a–c and curve 5 in Fig. 3.1a–c. Minor differences between the $\max g_{33}^*$ values are a result of the analogous conditions for the longitudinal piezoelectric

response in the 2–2 parallel-connected (Fig. 2.2) and 1–3 (Fig. 2.11) composites. The auxetic polymer component strongly influences the piezoelectric response of these composites, especially at $0 < m < 0.02$, and we do not pay attention to these details here because of the very small volume fractions of SC m. It is also seen from Fig. 3.3 that $\max g_{33}^*$ and $\min g_{31}^*$ are observed at similar volume fractions and the difference is very small, as a rule, less than 0.01. This feature is due to the columnar structure of the 1–3 composite (Fig. 2.11) and due to the similar influence of the dielectric permittivity $\varepsilon_{pp}^{*\sigma}$ on g_{31}^* and g_{33}^* in accordance with (3.1). As with 2–2 composites, the 1–3 composites are characterised by relatively small values of g_{15}^* in a wide volume-fraction range, see curve 1 in Fig. 3.3. The interfaces that separate the C1 and C2 components in the 1–3 composite shown in Fig. 2.11 impede the shear piezoelectric response and lead to the 'sleeping PS', i.e., the piezoelectric coefficient g_{15}^* remains relatively small in comparison to $|g_{3j}^*|$ in the wide volume-fraction range. A similar situation concerning the small piezoelectric coefficient d_{15}^* was discussed in Sect. 2.2 on the 1–3-type composites, see also curves 1 in Figs. 2.12 and 2.16. Softening the polymer component in the 1–3 composite leads to the larger values of $|g_{3j}^*|$ for m = const, especially at $m \ll 1$,

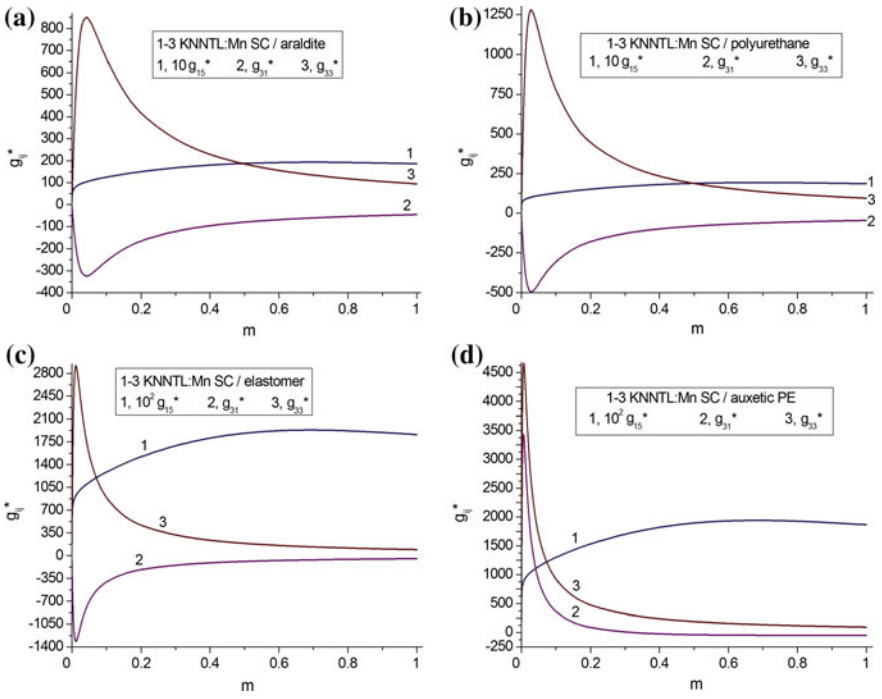

Fig. 3.3 Volume-fraction dependences of piezoelectric coefficients g_{ij}^* (in mV m/N) of 1–3 [001]-poled KNNTL:Mn SC/polymer composites. The schematic of the composite is shown in Fig. 2.11

however the extremum points of $g_{3j}^{*}(m)$ shift towards smaller volume fractions m (Fig. 3.3).

The next important example of large values of $|g_{3j}^{*}|$ is concerned with a 1–0–3 SC/FC/composite (see the schematic in Fig. 2.21) that was considered in Sect. 2.2.5. As in Sect. 2.2.5, we neglect the piezoelectric activity of the 0–3 FC/polymer matrix in comparison to the piezoelectric activity of the SC rods and consider the FC inclusions to be in an unpoled state. Elastic and dielectric properties of the 0–3 matrix influence the piezoelectric coefficients g_{ij}^{*} of the composite (Table 3.3) in a wide aspect-ratio (ρ_i) range even at relatively small volume fractions of FC m_i. Changes in g_{3j}^{*} are concerned with the large changes in the $s_{11}^{(0-3)}/s_{uv}^{(0-3)}$ ratios (Table 2.4) during a transition from a prolate ($0 < \rho_i < 1$) to an oblate ($\rho_i > 1$) shape of the FC inclusion in the 0–3 matrix. Moreover, its dielectric permittivity $\varepsilon_{33}^{(0-3)}$ decreases on increasing ρ_i at $m_i = \text{const}$, and this decrease becomes a stimulus to increase g_{33}^{*}, especially at $m \ll 1$.

In contrast to g_{3j}^{*}, the piezoelectric coefficient g_{15}^{*} remains small and almost independent of the aspect ratio at ρ_i at $m_i = \text{const}$ (see Table 3.3), i.e., we observe a shear 'sleeping PS' by analogy with the case of 1–3 composites. We remember that the similar conditions (2.17) were formulated for the piezoelectric coefficients d_{ij}^{*} of the 1–3 composite. The shear 'sleeping PS' of the 1–0–3 composite is a result of its microgeometry (Fig. 2.11), namely, the system of interfaces $x_1 = \text{const}$ and $x_2 = \text{const}$ which separate the SC rod and surrounding 0–3 matrix and, therefore, impede the shear piezoelectric response to a certain extent.

As seen from Table 3.3, the piezoelectric coefficients g_{3f}^{*} at $\rho_i \geq 5$ and relatively small volume fractions m obey the condition

$$g_{33}^{*}/|g_{3f}^{*}| \geq 5 \tag{3.2}$$

that characterises the large piezoelectric anisotropy of the studied 1–0–3 composite, where $f = 1$ and 2. The condition (3.2) is to be taken into account at the prediction of the hydrostatic piezoelectric response, figures of merit, transducer characteristics [7, 8, 28–31], etc.

In the case of a 1–3–0 composite with a porous 3–0 matrix (Fig. 2.19), we also achieve large values of g_{3j}^{*} and small values of g_{15}^{*} (Table 3.4). The highly oblate shape of the air pores in the polymer matrix (i.e., $\rho_p \gg 1$) is more preferable to achieve a high longitudinal PS, or large values of g_{33}^{*}, at the valid condition (3.2) for the large anisotropy of g_{3j}^{*}. The system of highly oblate pores in the polymer matrix of the composite shown in Fig. 2.19 leads to a considerable elastic anisotropy of the matrix [29, 32], and this anisotropy promotes a certain weakening of the transverse PS and validity of the condition (3.2) across a wider m range in comparison to the aforementioned 1–0–3 composite. Due to the large piezoelectric coefficient d_{33} of the PMN–0.33PT SC (see Table 1.3), the values of $d_{33}^{*} \sim 10^3$ pC/N are typical for the studied 1–3–0 composite at $m > 0.05$, and we attain a good combination of

Table 3.3 Piezoelectric coefficients g_{ij}^* (in mV m/N) of the 1–0–3 [001]-poled KNNTL:Mn SC/modified $PbTiO_3$ (I) FC/monolithic PE composite with square cross section rods at $m_i = 0.1$

ρ_i	m	g_{31}^*	g_{33}^*	g_{15}^*
0.1	0.05	−214	864	11.4
	0.10	−179	677	13.0
	0.15	−145	519	14.3
	0.20	−123	415	15.4
0.5	0.05	−342	1430	11.4
	0.10	−216	840	13.0
	0.15	−161	588	14.3
	0.20	−131	451	15.4
1	0.05	−349	1490	11.4
	0.10	−216	856	13.0
	0.15	−160	594	14.3
	0.20	−130	454	15.3
2	0.05	−339	1520	11.4
	0.10	−209	862	13.0
	0.15	−155	597	14.2
	0.20	−126	45	15.3
5	0.05	−305	1530	11.3
	0.10	−191	864	12.9
	0.15	−144	598	14.2
	0.20	−118	456	15.3
10	0.05	−265	1530	11.1
	0.10	−170	864	12.8
	0.15	−131	598	14.1
	0.20	−109	456	15.2
100	0.05	−131	1510	10.1
	0.10	−102	858	11.9
	0.15	−88.4	594	13.3
	0.20	−79.9	454	14.5

large d_{33}^* and g_{33}^* values, i.e., the high level of the longitudinal PS is achieved. As follows from Table 3.4, changes in the porosity m_p of the matrix lead to minor changes in g_{ij}^* of the composite, and the latter changes are mainly due to a small decrease of the dielectric permittivity $\varepsilon_{33}^{(3-0)}$ of the porous matrix on increasing m_p at ρ_p = const. The set of g_{3j}^* from Table 3.4 is to be taken into account at the analysis of the hydrostatic PS, figures of merit and ECFs.

Table 3.4 Piezoelectric coefficients g_{ij}^{*} (in mV m/N) of the 1–3–0 [001]-poled PMN–0.33PT SC/porous polyurethane composite with square cross section rods

ρ_p	m_p	m	g_{31}^{*}	g_{33}^{*}	g_{15}^{*}
0.1	0.1	0.05	−201	528	6.34
		0.10	−124	320	7.23
		0.15	−89.7	229	7.94
		0.20	−70.7	178	8.54
	0.2	0.05	−209	549	638
		0.10	−127	327	7.25
		0.15	−91.1	232	7.96
		0.20	−71.5	180	8.56
	0.3	0.05	−218	572	6.41
		0.10	−128	331	7.27
		0.15	−92.4	235	7.97
		0.20	−72.3	181	8.57
1	0.1	0.05	−201	543	6,34
		0.10	−122	325	7.23
		0.15	−88.4	231	7.94
		0.20	−69.6	179	8.54
	0.2	0.05	−212	585	6.37
		0.10	−124	335	7.25
		0.15	−88.5	236	7.95
		0.20	−69.4	182	8.55
	0.3	0.05	−245	689	6.41
		0.10	−125	344	7.27
		0.15	−88.6	240	7.97
		0.20	−69.2	184	8.57
100	0.1	0.05	−67.3	719	6.35
		0.10	−45.2	374	7.23
		0.15	−36.9	253	7.94
		0.20	−32.5	191	8.54
	0.2	0.05	−54.0	743	6.39
		0.10	−38.6	380	7.26
		0.15	−32.7	255	7.96
		0.20	−29.6	192	8.56
	0.3	0.05	−49.2	753	6.43
		0.10	−36.3	382	7.29
		0.15	−31.3	256	7.98
		0.20	−28.5	193	8.58

3.3 1–1-Type Composites

As is known from Sect. 2.3, the 1–1 FC/polymer composite (Fig. 2.25a) with the poling axis OX_3 and regular arrangement of components is characterised by $mm2$ symmetry. By analogy with (2.24), the piezoelectric coefficients g_{ij}^* of the 1–1 composite shown in Fig. 2.25a obey the condition

$$g_{ij}^*(t,n) = g_{ij}^*(1-t,1-n) \tag{3.3}$$

Equations (3.1) are also valid for g_{ij}^* of the 1–1 FC/polymer composite poled along OX_3. As with the 1–3 composite, the 1–1 composite is characterised by relatively small values of g_{15}^* because of the system of interfaces x_1 = const and x_2 = const (see Fig. 2.25a). The microgeometric analogy between the 1–3 and 1–1 composite structures (cf. Figs. 2.11 and 2.25a) suggests that large values of $|g_{3j}^*|$ are to be attained at volume fractions of FC $m \ll 1$: in this case the dielectric permittivity of the composite $\varepsilon_{33}^{*\sigma}$ obeys the condition $\varepsilon_{33}^{*\sigma} \ll \varepsilon_{33}^{(1),\sigma}$ where $\varepsilon_{33}^{(1),\sigma}$ is related to the FC component. The system of the long parallel FC rods poled along the OX_3 axis and the large volume fraction of the adjacent polymer rods in the 1–1 composite shown in Fig. 2.25a promote the large $|g_{3j}^*|$ values and high level of the PS.

The graphs in Fig. 3.4 show that the piezoelectric coefficients g_{3j}^* can be varied in a wide range, however these changes can be observed in a narrow range of the parameters t and n from (2.23). In fact, this can be considered a specific kind of the 'sleeping PS' in a composite structure with a complicated system of interfaces (Fig. 2.25a). In the case of an auxetic polymer matrix, changes in $\mathrm{sgn}g_{31}^*$ and $\mathrm{sgn}g_{32}^*$ are observed; see Fig. 3.4d, e. The sign-variable behaviour of g_{31}^* and g_{32}^* promote a validity of the condition (3.2), and the n and t ranges, wherein the condition (3.2) holds, depend on the elastic properties of the FC and polymer components. The considerable increase of $|g_{3j}^*|$ at $n \to 1$ and $t \to 0$ (Fig. 3.4) indicates that the condition $\varepsilon_{33}^{*\sigma} \ll \varepsilon_{33}^{(1),\sigma}$ holds, and the piezoelectric coefficients $|d_{3j}^*|$ show a large increase, see, e.g. Figure 2.26. A similar increase of $|g_{3j}^*|$ is achieved in the presence of the porous polymer matrix [33, 34] that surrounds the FC rods of the 1–1-type composite. Thus, the PS concerned with the piezoelectric coefficients g_{3j}^* of the 1–1-type composite depends on the elastic and dielectric properties of the polymer component to a large extent.

3.4 0–3-Type Composites

The 0–3 FC/polymer composite system is one of the most common composite types used for piezoelectric sensor applications [7, 9]. The 0–3 composite is schematically represented in Fig. 2.28. It is assumed that this composite consists of a

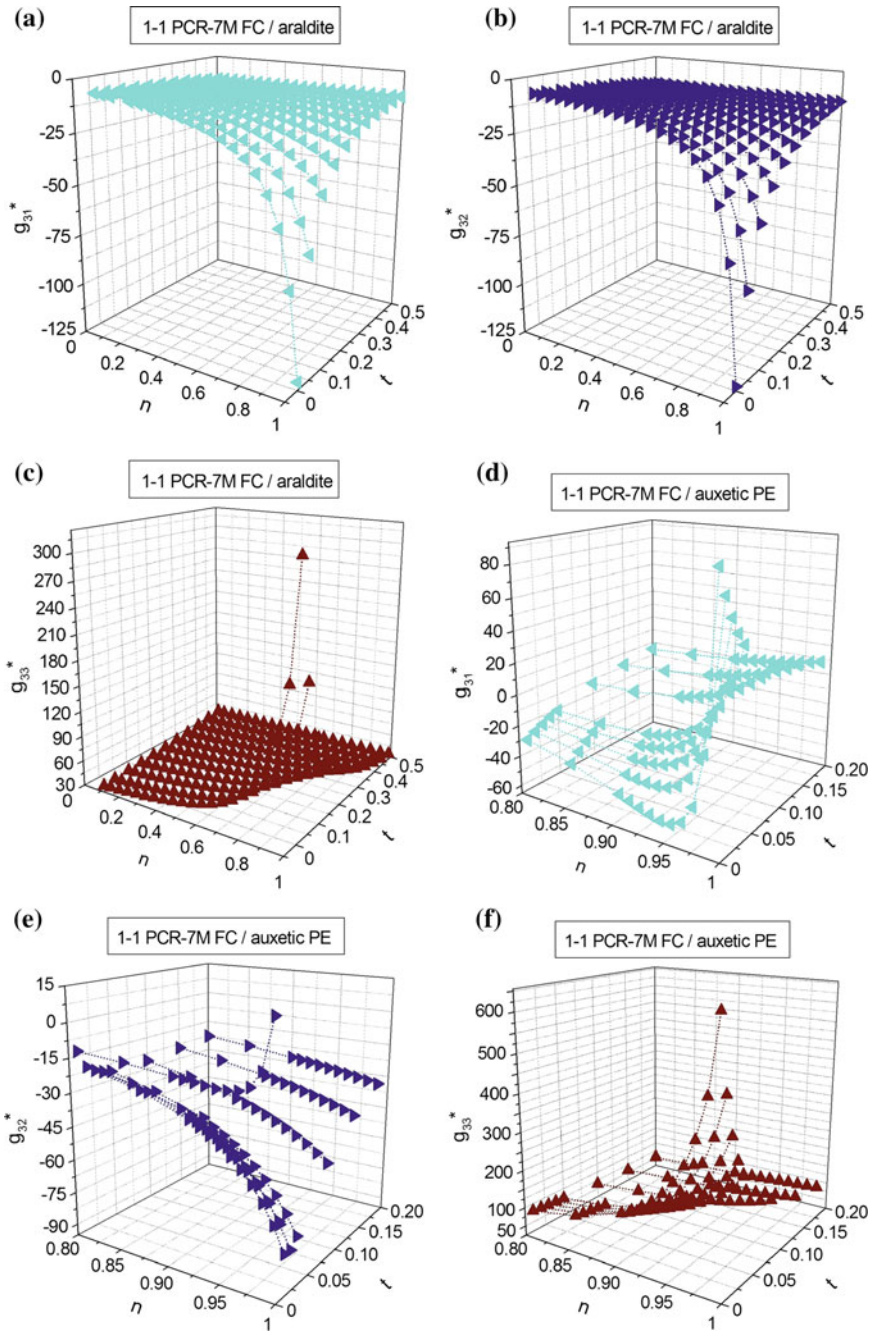

Fig. 3.4 Volume-fraction dependences of piezoelectric coefficients g_{ij}^* (in mV m/N) of 1–1 FC/polymer composites. The schematic of the composite is shown in Fig. 2.25a

three-dimensionally connected polymer matrix which is reinforced by a system of discrete FC inclusions, and the poling axis of the composite is OX_3. The inclusions of the 0–3 composite are piezoelectric and distributed regularly throughout the sample. The shape of each inclusion is spheroidal and obeys (2.13). The centres of symmetry of the inclusions are located in apices of rectangular parallelepipeds and form a simple lattice. The matrix polymer component can be either piezo-active or piezo-passive. The next important kind of the 0–3 composite is the ferroelectric SC/polymer composite [7, 8].

As the effective parameters of the 0–3 composites are highly dependent [7, 9, 35–40] on their microstructure, properties and volume fractions of the components and poling conditions, the interrelations between the microgeometry and effective piezoelectric properties become complicated and require a careful and consistent physical interpretation. In Sect. 3.4 we discuss a number of examples of the PS and behaviour of the piezoelectric coefficients g_{ij}^* in 0–3-type composites that are based on either FCs or SCs.

Poled $(Pb_{1-x}Ca_x)TiO_3$ FCs are of interest (Table 3.5) due to their non-monotonic behaviour of both the piezoelectric anisotropy factors ($e_{33}/e_{31} > 0$ and $d_{33}/d_{31} < 0$) at molar concentrations $0.10 \leq x \leq 0.30$. Opposite signs of the piezoelectric coefficients e_{31} and d_{31} and minor changes in the piezoelectric coefficient g_{33} at changes in x (see Table 3.5) make these FCs unique and attractive components in the 0–3 composite, whose schematic structure is shown in Fig. 2.28.

The effective properties of the 0–3 $(Pb_{1-x}Ca_x)TiO_3$ FC/polymer composite are calculated in specific ranges of volume fractions m and aspect ratios ρ by means of FEM [8]. The calculated volume-fraction dependences of the piezoelectric coefficients g_{ij}^* are shown in Table 3.6. These dependences are similar to those determined by means of EFM [40] for the 0–3 $(Pb_{1-x}Ca_x)TiO_3$-based composites with prolate FC inclusions, i.e., at $0 < \rho < 1$. As follows from Table 3.6, the piezoelectric coefficient g_{33}^* of the 0–3 composite can be over two times larger than the g_{33} value of the FC component, and minor differences between the $\max g_{33}^*$ values take place at $0.15 \leq x \leq 0.30$. The largest $\max g_{33}^*$ value is achieved at the volume fraction near $m = 0.10$ (see data for $x = 0.15$ in Table 3.6) that avoids potential technological problems when manufacturing the composite samples at a specific volume-fraction range. It is important that the piezoelectric coefficients g_{3j}^* of the composite obey the condition (3.2) for the large piezoelectric anisotropy because of the strong influence of the highly anisotropic FC component. We see from Table 3.6 that the piezoelectric coefficient g_{15}^* undergoes large changes on increasing the volume fraction of FC m, however the longitudinal PS remains higher than the shear PS in the whole m range. This is due to the highly prolate shape of the FC inclusion (i.e., the aspect ratio $\rho \gg 1$) and for the anisotropy of its piezoelectric properties (see the d_{33}/d_{31} ratios in Table 3.5).

The g_{33}^* values from Table 3.6 are smaller than the g_{33} value of a 0–3 $PbTiO_3$ FC/70/30 mol% copolymer of vinylidene fluoride and trifluoroethylene composite [43] and comparable to the g_{33}^* values of 0–3 composites [44–47] based on PZT-type FCs. The larger g_{33}^* values of the 0–3 composite from work [43, 44] may

Table 3.5 Calculated values of c_{ab}^{E} (in 10^{10} Pa), piezoelectric coefficients e_{ij} (in C/m^2), relative dielectric permittivities $\varepsilon_{pp}^{\xi}/e_0$, piezoelectric coefficient g_{33} (in mV m/N), and piezoelectric anisotropy factor d_{33}/d_{31} of the $(Pb_{1-x}Ca_x)TiO_3$ FC[a] at room temperature (reprinted from Glushanin et al. [40], with permission from Elsevier)

x	c_{11}^{E}	c_{12}^{E}	c_{13}^{E}	c_{33}^{E}	c_{44}^{E}	e_{31}
0.10	19.1	5.22	5.15	18.6	6.85	0.676
0.15	18.8	5.09	5.01	18.3	6.76	0.751
0.20	18.5	4.76	4.68	18.0	6.79	0.844
0.23	18.7	5.03	4.93	18.2	6.76	1.06
0.24	18.4	4.72	4.61	17.9	6.76	1.07
0.25	18.9	5.19	5.06	18.3	6.76	1.33
0.26	18.9	5.14	5.02	18.3	6.77	1.36
0.30	18.6	4.89	4.80	18.1	6.77	1.08
x	e_{33}	e_{15}	$\varepsilon_{11}^{\xi}/\varepsilon_0$	$\varepsilon_{33}^{\xi}/\varepsilon_0$	g_{33}	d_{33}/d_{31}
0.10	3.90	1.62	111	109	21.1	−11.7
0.15	4.15	1.73	118	115	21.4	−13.0
0.20	4.31	1.77	126	123	20.6	−18.7
0.23	4.55	1.80	137	133	19.7	−30.3
0.24	4.69	1.87	145	141	19.4	−39.8
0.25	5.09	1.95	152	147	19.5	−71.9
0.26	5.30	2.03	161	156	19.1	−65.2
0.30	5.48	2.27	202	197	20.2	−17.6

[a]The full sets of electromechanical constants of poled FCs (∞mm symmetry) have been calculated by the effective medium method [41, 42]. It is assumed that spherical grains of the FC sample are split into 90° lamellar domains of two types with equal volume fractions, and these domains are separated by planar 90° domain walls. The 90° domain walls are assumed to be practically motionless so that a contribution from their displacements under external electric or mechanical fields into the electromechanical constants of the poled FC medium approaches zero [41, 42]. The electromechanical constants of the single-domain SC have been evaluated by the method put forward in work [41] on the basis of experimental room-temperature data on the ferroelectric $(Pb_{1-x}Ca_x)TiO_3$ solid solutions

be concerned with the presence of a ferroelectric polymer component and with a modification of the $PbTiO_3$-type FC composition for improving the piezoelectric performance. At the same time, experimental g_{33}^{*} values related to a 0–3 PZT FC/PVDF composite manufactured by hot-pressing are approximately two–three times smaller [37] than g_{33}^{*} from Table 3.6. We remind the reader that according to data from Table 1.6, the PZT-type FCs are characterised by a piezoelectric coefficient g_{33} within the range from 14.3 to 49.0 mV m/N. As follows from Table 3.5 for various $(Pb_{1-x}Ca_x)TiO_3$ FCs, $g_{33} \approx 20$ mV m/N with the piezoelectric coefficient d_{33} being a few times smaller than the d_{33} of the PZT-type FCs listed in Table 1.5.

Thus, the longitudinal PS associated with the piezoelectric coefficient g_{33}^{*} of the 0–3 FC-based composites can be strongly dependent on the electromechanical properties of components and technological conditions for manufacturing. These

circumstances are to be taken into account along with the microgeometric features of the 0–3 composite structure.

An important example of the PS is concerned with a 0–3 lead-free SC/polymer composite that was highlighted in Sect. 2.4. In this lead-free composite we consider the prolate spheroidal SC inclusions poled along the OX_3 axis (Fig. 2.28) and compare the piezoelectric coefficients g_{3j}^* of such a composite to g_{3j}^* of the related 1–3 composite. It is assumed that in the 1–3 composite, the system of circular cylindrical SC rods are regularly distributed in the polymer matrix. Both the 0–3 and 1–3 composites based on SCs are characterised by a uniform orientation of the main crystallographic axes X, Y and Z in all of the SC inclusions (rods) as follows: $X \| OX_1$, $Y \| OX_2$ and $Z \| OX_3$. The graphs in Fig. 3.5 suggest that the transition from a 1–3 connectivity pattern to the 0–3 pattern leads to a drastic decrease of $|g_{3j}^*|$ in the whole volume-fraction range (cf., for instance, curves 1 and 2 in Fig. 3.5). Increasing the aspect ratio ρ in the range of $0 < \rho < 1$ leads to a considerable decrease of $\max g_{33}^*$ and $|\min g_{31}^*|$ and, therefore, to the weakening of the PS of the 0–3 composite. The main reason for such a decrease is due to a decrease of the piezoelectric coefficients $|d_{3j}^*|$ on increasing ρ at m = const. The use of less prolate piezoelectric inclusions with a larger ρ value in the 0–3 composite structure (Fig. 2.28) would lead to smaller values of $|d_{3j}^*|$ due to the strong influence of the depolarisation and elastic fields. However, despite the weakening of the PS due to the decrease of $|d_{3j}^*|$, the values of $|g_{3j}^*|$ of the KNNTL:Mn SC/polyurethane composite at m = const (Fig. 3.5) remain larger than $|g_{3j}^*|$ of the 0–3 $(Pb_{1-x}Ca_x)TiO_3$ FC/araldite composite at $\rho = 0.1$ (Table 3.6). The large values of $|g_{3j}^*|$ of the 0–3 composite are due to the KNNTL:Mn SC component with large $|g_{3j}|$ values [48] and by the larger elastic compliances $|s_{ab}|$ of polyurethane in comparison to $|s_{ab}|$ of araldite (see Table 2.1).

Taking into account experimental data on PVDF (Table 3.7), we analysed the PS of the 0–3 and 1–3 KNNTL:Mn SC/PVDF composites at two different orientations

Table 3.6 Piezoelectric coefficients g_{ij}^* (in mV m/N)[a] of the 0–3 $(Pb_{1-x}Ca_x)TiO_3$ FC/araldite composite at $\rho = 0.1$, FEM data

m	g_{31}^*	g_{33}^*	g_{15}^*	g_{31}^*	g_{33}^*	g_{15}^*	g_{31}^*	g_{33}^*	g_{15}^*	g_{31}^*	g_{33}^*	g_{15}^*
	At x = 0.15			At x = 0.20			At x = 0.25			At x = 0.30		
0.05	−15.7	47.2	4.18	−15.8	46.2	4.00	−14.3	44.7	3.69	−12.9	39.2	3.25
0.10	−15.0	47.5	7.69	−14.3	46.4	7.35	−13.2	44.3	6.78	−11.9	38.5	5.96
0.15	−13.6	45.8	10.7	−12.9	44.6	10.2	−11.6	42.4	9.42	−10.6	36.6	8.28
0.20	−12.2	44.0	13.3	−11.5	42.8	12.7	−10.2	40.6	11.7	−9.41	34.9	10.3
0.30	−9.76	40.9	17.7	−9.06	39.8	16.9	−7.82	37.7	15.6	−7.39	32.3	13.7
0.40	−7.70	38.6	21.8	−7.02	37.5	20.9	−5.82	35.5	19.3	−5.71	30.3	16.9
0.50	−5.77	37.4	28.3	−5.11	36.4	27.2	−3.96	34.5	25.2	−4.16	29.4	22.3

[a]The values of g_{ij}^* have been calculated by using the full set of electromechanical constants (FEM data on s_{ab}^{*E}, e_{ij}^* and $\varepsilon_{pp}^{*\xi}$) of the 0–3 composite, see the schematic in Fig. 2.28

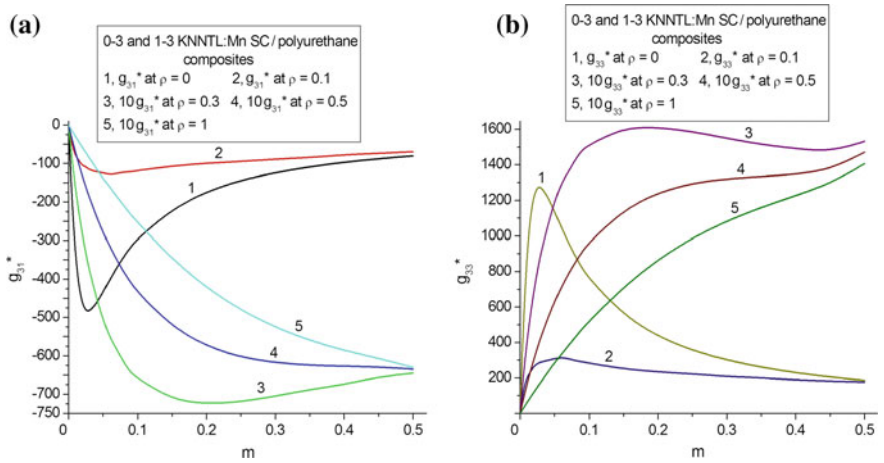

Fig. 3.5 Volume-fraction dependences of piezoelectric coefficients g_{3j}^* (in mV m/N) of 0–3 ($\rho > 0$) and 1–3 ($\rho = 0$) [001]-poled KNNTL:Mn SC/polyurethane composites, FEM data. The schematic of the 0–3 composite is shown in Fig. 2.28

of the remanent polarisation vector of PVDF (Table 3.8). The small piezoelectric coefficients e_{15} and e_{31} in comparison to $|e_{33}|$ of PVDF (see Table 3.7) and opportunities to pole the composite components in different directions [8, 35, 36, 49] make PVDF attractive as a ferroelectric polymer component. We remind the reader that the coercive field E_c of PVDF [50] is much larger than E_c of the KNNTL:Mn, PMN–xPT, PZN–xPT, and other important ferroelectric solid solutions [10, 48] in the SC state. As seen from Table 3.8, the PVDF matrix strongly influences the PS of the composites and enables us to observe a sign-variable behaviour of the piezoelectric coefficients g_{3j}^* at the relatively small volume fractions of SC m. This means that the conditions

$$g_{31}^* = 0 \text{ at } g_{33}^* \neq 0 \text{ or } g_{33}^* = 0 \text{ at } g_{31}^* \neq 0 \tag{3.4}$$

hold in specific ρ and m ranges which depend on the electromechanical properties and poling directions of the components. On varying ρ at m = const, we observe a unique 'aspect-ratio effect': both g_{31}^* and g_{33}^* demonstrate the non-monotonic

Table 3.7 Room-temperature elastic moduli c_{ab}^E (in 10^{10} Pa), piezoelectric coefficients e_{ij} (in C/m^2) and relative dielectric permittivity $\varepsilon_{pp}^{\xi}/\varepsilon_0$ of poled PVDF [49] at the remanemt polarisation $\boldsymbol{P}_r^{(2)} \uparrow\uparrow OX_3$

c_{11}^E	c_{12}^E	c_{13}^E	c_{13}^E	c_{44}^E	c_{66}^E
0.4840	0.2720	0.2220	0.4630	5.26×10^{-3}	0.1060
e_{15}	e_{31}	e_{33}	$\varepsilon_{11}^{\xi}/\varepsilon_0$	$\varepsilon_{33}^{\xi}/\varepsilon_0$	
1.999×10^{-3}	4.344×10^{-3}	−0.1099	7.504	8.003	

Table 3.8 Piezoelectric coefficients g^*_{3j} (in mV m/N)[a] of 0–3 ($\rho > 0$) and 1–3 ($\rho = 0$) [001]-poled KNNTL:Mn SC/PVDF composites[b]

ρ	g^*_{31}	g^*_{33}	g^*_{31}	g^*_{33}	g^*_{31}	g^*_{33}
	At $m = 0.05$		At $m = 0.10$		At $m = 0.15$	
PVDF matrix with the remanent polarisation $\boldsymbol{P}_r^{(2)} \uparrow\uparrow OX_3$						
0	−279	714	−210	657	−171	519
0.1	42.0	−183	2.89	−79.2	−183	−24.1
0.3	78.2	−292	41.4	−197	15.4	−130
0.5	94.8	−339	58.2	−245	31.0	−175
1	112	−387	80.1	−306	53.0	237
PVDF matrix with the remanent polarisation $\boldsymbol{P}_r^{(2)} \uparrow\downarrow OX_3$						
0	−253	812	−202	628	−163	490
0.1	−132	408	−119	363	−108	327
0.3	−126	395	−113	352	−104	320
0.5	−129	410	−116	366	−106	332
1	−134	431	−122	391	−112	358

[a]The values of g^*_{3j} have been calculated by using the full set of electromechanical constants (FEM data on s^{*E}_{ab}, e^*_{ij} and $\varepsilon^{*\xi}_{pp}$) of the composite

[b]The schematic of the 0–3 composite is shown in Fig. 2.28

behaviour (see Table 3.8), and this behaviour is due to the elastic and dielectric properties of the composite in the presence of the PVDF matrix with the dominating longitudinal piezoelectric effect.

Relations between the piezoelectric coefficients g^*_{3j} and d^*_{3j} of the 0–3 KNNTL:Mn SC SC/PVDF composite are shown in Fig. 3.6. As described previously, the piezoelectric coefficients g^*_{3j} and d^*_{3j} are linked by (3.1). A change in the aspect ratio ρ of the SC inclusion leads to a change in the anisotropy of g^*_{3j} and d^*_{3j}. On taking into account data from Figs. 3.5 and 3.6 and Table 3.8, we state that the larger changes in the piezoelectric coefficients g^*_{3j} are observed in the PVDF-containing composites. Moreover, the values of $|g^*_{3j}|$ in specific ranges of m and ρ are a few times larger than $|g^*_{3j}|$ of the 0–3 FC-based composites, see Table 3.6 and work [37, 40, 43–47].

The next example of the PS is related to the 0–3-type composite [51] with the porous polymer matrix. According to work [51], the system of spheroidal SC inclusions is surrounded by the porous polymer matrix, and the shape of each pore is spheroidal with the aspect ratio ρ_p. A regular arrangement of the inclusions and pores takes place over the whole composite sample. The polymer matrix with isolated pores is characterised by 3–0 connectivity while the composite as a whole is characterised by 0–3–0 connectivity. The effective electromechanical properties of the studied composite are evaluated in two stages. At the first stage, the properties of the 3–0 matrix are determined using (2.19). At the second stage, FEM is applied to attain the full set of electromechanical constants of the 0–3–0 composite. The highly oblate air pore strongly influences the elastic anisotropy of the matrix and the anisotropy of the piezoelectric coefficients g^*_{3j} of the composite. Figure 3.7

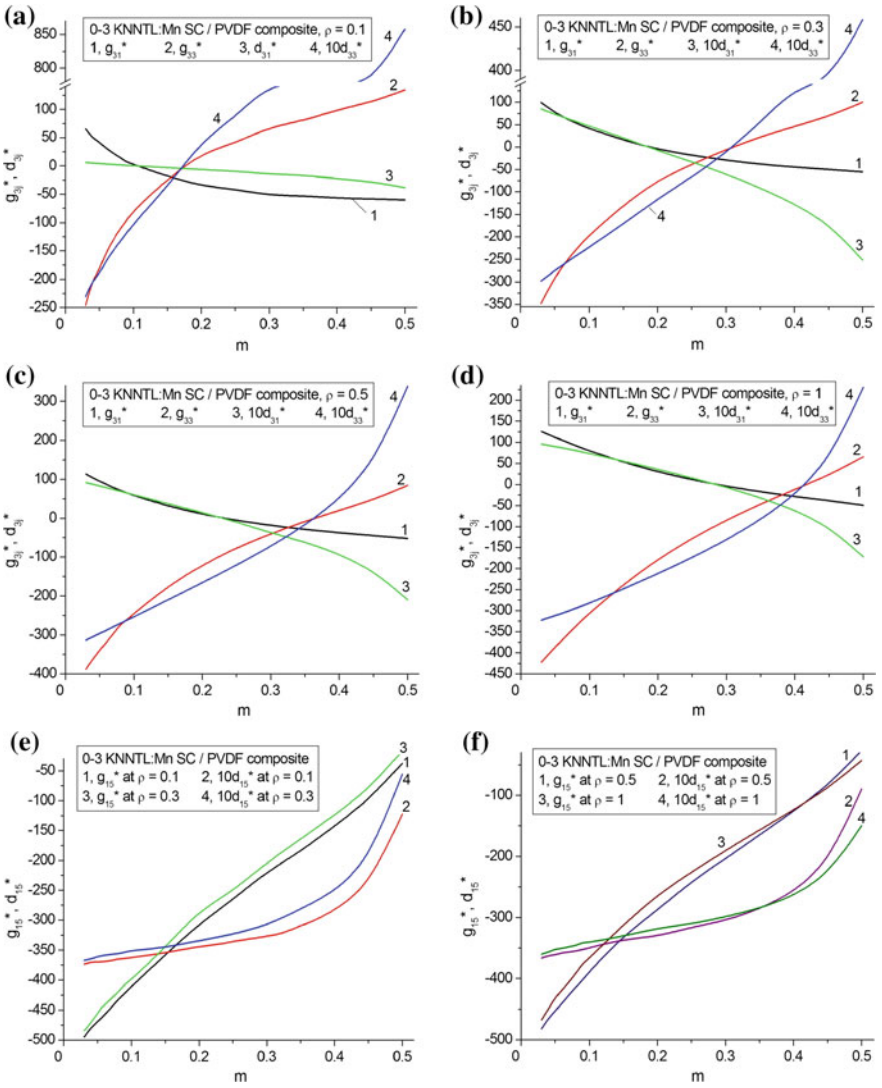

Fig. 3.6 Volume-fraction dependences of piezoelectric coefficients g_{ij}^* (in mV m/N) and d_{ij}^* (in pC/N) of the 0–3 [001]-poled KNNTL:Mn SC/PVDF composite with the remanent polarisation of the PVDF matrix $\boldsymbol{P}_r^{(2)} \uparrow\uparrow OX_3$, FEM data. The schematic of the 0–3 composite is shown in Fig. 2.28

shows that even at relatively small porosity levels of the matrix ($m_p = 0.1$), large changes in g_{3j}^* are observed, and these changes are caused by changes in the volume fraction m and aspect ratio ρ of the SC inclusions. It is also seen from Fig. 3.7 that the piezoelectric coefficients g_{3j}^* obey (3.2) for a large anisotropy. The volume-fraction (m) range wherein the condition (3.2) is valid strongly depends on

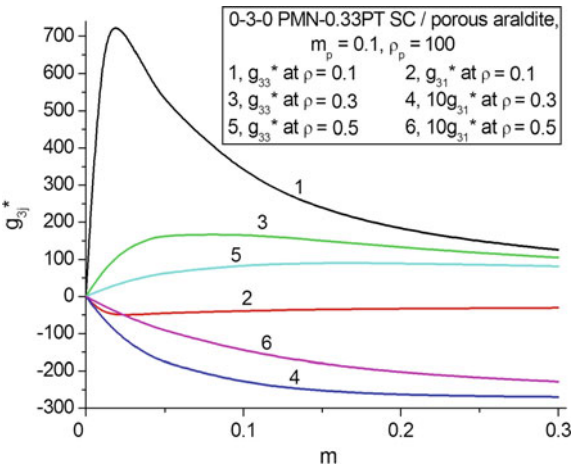

Fig. 3.7 Volume-fraction dependences of piezoelectric coefficients g_{3j}^* (in mV m/N) of the 0–3–0 [001]-poled PMN–0.33PT SC/porous araldite composite (reprinted from paper by Topolov et al. [51], with permission from Taylor and Francis)

the aspect ratios ρ and ρ_p of the SC inclusion and pore, respectively, and on the porosity of the matrix m_p. The values of g_{3j}^* shown in Fig. 3.7 are comparable to those related to the 0–3 KNNTL:Mn SC/PVDF, see Table 3.8 and Fig. 3.6a–d.

In the next example of the PS we consider a SC-based composite wherein the matrix surrounding the SC inclusions is either monolithic FC or porous FC with 3–0 connectivity, and both components are poled along the OX_3 axis [52]. Table 3.9 shows the piezoelectric performance of the 0–3 and 0–3–0 composites with two relaxor-ferroelectric components. Hereby changes in the piezoelectric coefficients g_{ij}^* take place in relatively narrow ranges when the volume fraction of SC m is varied from 0.05 to 0.50. Both the SC and FC components are characterised by a similar anisotropy of the piezoelectric coefficients d_{3j}: according to data from Tables 1.3 and 1.5, $d_{33}/d_{31} = -2.12$ and -2.03 for the [001]-poled PMN–0.33PT SC and PMN–0.35PT FC, respectively. This feature does not promote a considerable anisotropy of g_{3j}^* in the composites, see Table 3.9. An increase of the aspect ratio ρ in both the 0–3 and 0–3–0 composites does not lead to appreciable changes in g_{ij}^* at m = const, and such a stability can be accounted for by the considerable elastic stiffness of the FC matrix. The formation of air pores in the FC matrix promotes an increase of $|g_{ij}^*|$ in comparison to the case of the 0–3 composite, see Table 3.9. This is due to a decrease of the dielectric permittivity of the porous FC matrix in comparison to the monolithic FC matrix. We add that the g_{33}^* values related to the 0–3 SC/FC composite (Table 3.9) are approximately equal to $\max g_{33}^* = 20$ mV m/N found for a 0–3 PMN FC/sulphoaluminate cement composite [53] wherein only the FC component exhibits the piezoelectric properties.

The numerous results on the PS of the 0–3-type composites make these materials attractive in sensor and related piezotechnical applications [2, 4, 9, 44], where flexible piezoelectric elements are required and the shape of the element can conform with the device configuration.

Table 3.9 Piezoelectric coefficients g_{ij}^* (in mV m/N) of 0–3 SC/FC and 0–3–0 SC/porous FC composites based on the [001]-poled PMN–0.33PT SC, FEM data

m	g_{31}^*	g_{33}^*	g_{15}^*	g_{31}^*	g_{33}^*	g_{15}^*	g_{31}^*	g_{33}^*	g_{15}^*
	At $\rho = 0.1$			At $\rho = 0.3$			At $\rho = 0.5$		
0–3 PMN–0.33PT SC/PMN–0.35 FC[a]									
0.05	−5.83	12.7	21.5	−5.86	12.8	21.5	−5.88	12.9	21.6
0.10	−6.14	13.4	20.8	−6.19	13.5	20.8	−6.24	13.6	20.8
0.15	−6.47	14.1	20.1	−6.54	14.2	20.1	−6.61	14.4	20.1
0.20	−6.83	14.8	19.3	−6.91	15.0	19.3	−7.00	15.2	19.4
0.30	−7.63	16.5	17.9	−7.75	16.8	18.0	−7.87	17.0	18.0
0.40	−8.58	18.5	16.6	−8.72	18.8	16.6	−8.85	19.1	16.7
0.50	−9.69	20.8	15.4	−9.83	21.1	15.4	−9.96	21.4	15.4
0–3–0 PMN–0.33PT SC/porous PMN–0.35 FC at $m_p = 0.3$ and $\rho_p = 1$[b]									
0.05	−8.74	21.4	31.9	−8.76	21.4	31.9	−8.79	21.2	31.9
0.10	−9.27	22.5	30.2	−9.31	22.5	30.2	−9.35	22.6	30.1
0.15	−9.82	23.6	28.5	−9.87	23.6	28.5	−9.93	23.7	28.4
0.20	−10.4	24.6	26.8	−10.4	24.7	26.8	−10.5	24.7	26.8
0.30	−11.5	26.8	23.8	−11.6	26.9	23.8	−11.7	26.9	23.8
0.40	−12.7	29.0	21.1	−12.8	29.1	21.1	−12.8	29.1	21.0
0.50	−13.9	31.2	18.6	−13.9	31.1	18.6	−13.9	31.1	18.5

[a]The schematic of the 0–3 composite is shown in Fig. 2.28
[b]The full set of electromechanical constants of the poled porous PMN–0.35PT FC has been found in work [52]

3.5 3–β Composites

In a composite with 3–β connectivity, the first component (main piezoelectric component) is distributed continuously along three co-ordinate axes, and the second component is distributed along β co-ordinate axes, where $\beta = 0$, 1, 2, or 3. Traditionally such composites contain FC and polymer components that are often distributed regularly [54, 55]. To the best of our knowledge, there are fairly restricted experimental data on the PS of the 3–β FC/polymer composites [44, 54, 55] and no papers where the four types of the piezoelectric coefficients, d_{ij}^*, e_{ij}^*, g_{ij}^*, and h_{ij}^*, were analysed.

In the first example, we consider the longitudinal PS that is described by the piezoelectric coefficient g_{33}^*. Its volume-fraction dependence (Fig. 3.8) was found based on experimental data on the piezoelectric coefficient d_{33}^* and dielectric permittivity $\varepsilon_{33}^{*\sigma}$, see (3.1). As follows from Fig. 3.8, $\max g_{33}^*$ is achieved at a relatively large volume fraction of FC (i.e., $0.4 < m < 0.5$). To a large extent, the location of $\max g_{33}^*$ depends on dielectric and elastic properties of the components. The value of $\max g_{33}^*$ (Fig. 3.8) is comparable to experimental values of g_{33}^* related to some 0–3 PZT-type FC/polymer composites, see e.g. [45–47].

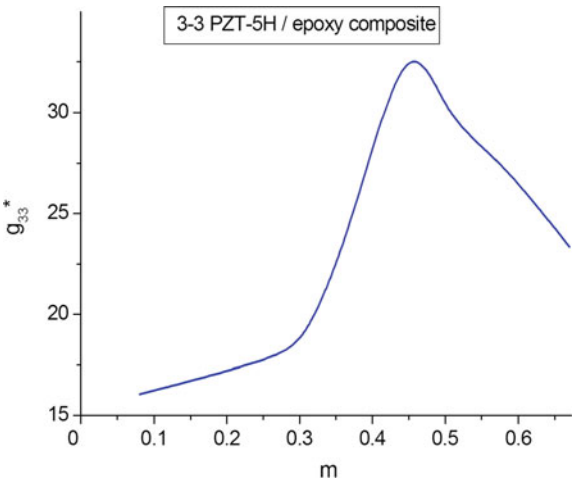

Fig. 3.8 Volume-fraction dependence of the piezoelectric coefficient g_{33}^* (in mV m/N) of the 3–3 PZT-5H FC/epoxy composite (evaluated from experimental data [54])

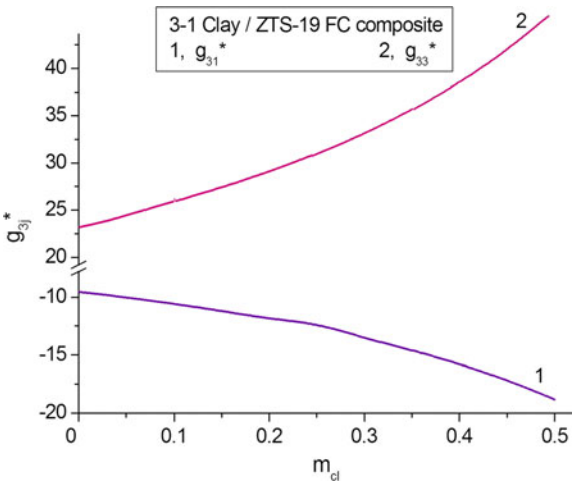

Fig. 3.9 Volume-fraction dependence of the piezoelectric coefficients g_{3j}^* (in mV m/N) of the 3–1 ZTS-19 FC/clay composite, FEM data

The second example is concerned with a 3–1 FC/clay composite wherein the system of circular cylinders (clay rods) are aligned parallel to the poling axis OX_3, and centres of symmetry of bases of the cylinders form a square lattice on the (X_1OX_2) plane. It is assumed that the volume fractions of clay m_{cl} and FC m are linked by the equation $m_{cl} = 1 - m$. On increasing the volume fraction of clay m_{cl}, we observe a monotonic increase of $|g_{3j}^*|$, see Fig. 3.9. This increase is mainly due to the influence of the small dielectric permittivity ε_{pp} of clay on the effective properties of the composite. As for the elastic properties of clay, their influence on the piezoelectric coefficients g_{3j}^* of the composite is restricted because of the stiff FC matrix surrounding each clay rod in the 3–1 composite.

As with g_{33}^* of the 3–3 FC/polymer composite in Fig. 3.8, at equal volume fractions of components, the g_{33}^* value of the 3–1 FC/clay composite is approximately two times larger than g_{33} of the FC component (see data at $m_{cl} = 0$ and $m_{cl} = 0.5$ in Fig. 3.9). Such a similarity is observed in the presence of different FC components, PZT-5H and ZTS-19, however differences between their electromechanical properties (Table 1.5) are not very large. It should be added that the effective properties of the 3–1 composite were used for the interpretation of the piezoelectric performance of a ZTS-19 FC/clay composite [56].

3.6 Piezoelectric Sensitivity, Figures of Merit and Anisotropy

The relationships between the PS and squared figures of merit from (1.41) and (1.42) have been discussed in papers on piezo-active composites; see, for instance [9, 24, 26, 56, 57]. In Sect. 3.6 we show a few examples of the behaviour of the squared figures of merit related to the longitudinal and transverse PS of the composites. The squared figures of merit $(Q_{3j}^*)^2$ of the composite can be represented as

$$(Q_{3j}^*)^2 = d_{3j}^* g_{3j}^* = (g_{3j}^*)^2 \varepsilon_{33}^{*\sigma} \tag{3.5}$$

in the case where the piezoelectric coefficients d_{3j}^* and g_{3j}^* are linked by the relation $d_{3j}^* = \varepsilon_{33}^{*\sigma} g_{3j}^*$ [see (1.20)], where $j = 1$, 2 and 3. Formula (3.5) suggests that large values of $(Q_{33}^*)^2$ can be achieved from large piezoelectric coefficient g_{33}^*. However, large g_{33}^* values are often related to relatively small volume fractions of the main piezoelectric component, and this is typical of various composites considered in this chapter; see, for instance, Figs. 3.1, 3.2, 3.3 and 3.4. At the small volume fractions of the main piezoelectric component, the dielectric permittivity $\varepsilon_{33}^{*\sigma}$ of the composite remains small in comparison to that of the main piezoelectric component. Thus, there is a need to find a 'compromise' between the relatively large g_{33}^* values and moderate $\varepsilon_{33}^{*\sigma}$ values in the composite. The squared figures of merit $(Q_{31}^*)^2$ and $(Q_{32}^*)^2$, which are concerned with the transverse piezoelectric effect, can be small [8, 58] in comparison to $(Q_{33}^*)^2$ to satisfy conditions for effective energy harvesting and transformation, or to achieve a considerable hydrostatic piezoelectric response, etc. As follows from (3.5), the condition

$$(Q_{33}^*)^2 \gg (Q_{3f}^*)^2 (f = 1 \text{ and } 2) \tag{3.6}$$

is linked with validity of (3.2), i.e., with the large piezoelectric anisotropy of the composite.

The first example of validity of (3.2) and (3.6) is concerned with the 1–3–0 SC/porous polymer composite whose structure is shown schematically in Fig. 2.19. As

in Sect. 2.2.4, a regular distribution of SC rods and air pores over the composite sample is assumed. The graphs in Fig. 3.10 have been built for volume fractions of SC $0.001 \leq m \leq 0.30$, since in this volume-fraction range there are extreme points of $(Q^*_{3j})^2$ and appreciable changes in the anisotropy of g^*_{3j}, where $j = 1, 2$ and 3. Even at relatively small porosity levels for the polymer matrix ($m_p = 0.1$), the anisotropy of g^*_{3j} becomes higher on increasing the aspect ratio ρ_p of the air pores, see Fig. 3.10a. This highlights that the elastic anisotropy of the polymer matrix containing highly oblate pores (see the inset in Fig. 2.19) favours a validity of the condition (3.2), see curve 3 in Fig. 3.10. Differences between $(Q^*_{3j})^2$ (see Fig. 3.10b, c) on variation of the volume fraction of SC m and the aspect ratio ρ_p of the air pores in the polymer matrix are mainly accounted for by the strong influence of the elastic anisotropy of the porous matrix on the PS of the composite.

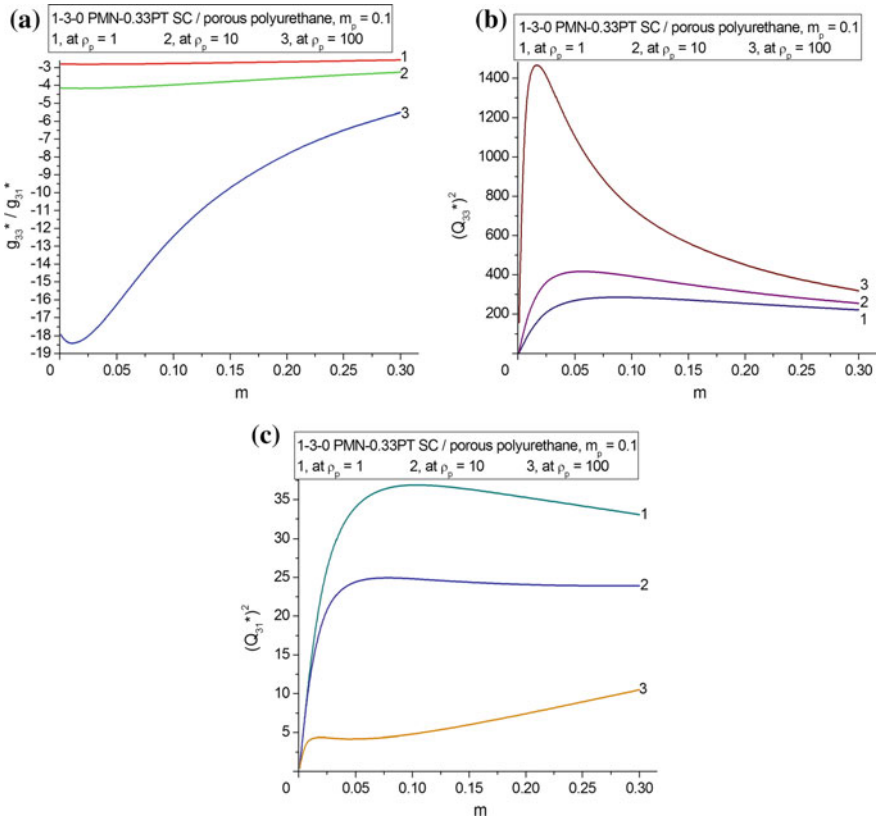

Fig. 3.10 Volume-fraction dependences of the anisotropy of piezoelectric coefficients g^*_{3j} (**a**) and squared figures of merit $(Q^*_{3j})^2$ (**b** and **c**, in 10^{-12} Pa^{-1}) of the 1–3–0 [001]-poled PMN–0.33PT SC/porous polyurethane composite. The schematic of the composite is shown in Fig. 2.19

Our comparison of curves 1–3 in Fig. 3.10b, c enables us to state that the composite at $\rho_p = 100$ provides large values of $(Q_{33}^*)^2$ at validity of the condition (3.6) in the large volume-fraction (m) range. Large values of $(Q_{33}^*)^2$ are also achieved due to the relatively small $\varepsilon_{33}^{*\sigma}$ values of the composite in comparison to $\varepsilon_{33}^{(1),\sigma}$ of its SC component, and the $\varepsilon_{33}^{*\sigma}$ values are influenced by the aspect ratio ρ_p of the pore to a large extent. It should be added that the $(Q_{33}^*)^2$ values from Fig. 3.10b are one–two orders-of-magnitude larger than a value of $(Q_{33}^*)^2 = 17 \times 10^{-12}$ Pa^{-1} for a perforated 1–3-type PZT FC/epoxy composite [57]. The advantage of the studied 1–3–0 PMN–0.33PT-based composite over the perforated 1–3-type PZT-based composite is primarily the large piezoelectric coefficient $d_{3j}^{(1)}$ of the [001]-poled PMN–0.33PT SC in comparison with $d_{3j}^{(1)}$ of poled PZT-type FCs, see Tables 1.3 and 1.5. The oblate shape of the air pores in the polymer matrix, see inset in Fig. 2.19, plays an important role in achieving a large piezoelectric anisotropy in the composite. For example, the condition (3.2) holds for the 1–3–0 PMN–0.33PT SC/porous polyurethane composite at an aspect ratio $\rho_p = 100$ in the following volume-fraction ranges of SC: $0 < m \leq 0.264$ (at $m_p = 0.1$), $0 < m \leq 0.294$ (at $m_p = 0.2$), and $0 < m \leq 0.304$ (at $m_p = 0.3$). This may be concerned with the active influence of the air pores on the dielectric and piezoelectric properties of the porous matrix and composite as a whole, and the use of a larger porosity level can promote a larger elastic anisotropy of the porous polymer matrix that strongly influences the PS of the composite.

In the second example we observe a large piezoelectric anisotropy in a 1–3-type composite (Table 3.10) whereby using an auxetic PE strongly influences the PS and leads to a change in $\text{sgn}g_{31}^*$ at a volume fraction of SC $0.30 < m < 0.35$. Hereby conditions (3.2) and (3.6) hold at large values of g_{33}^* and $(Q_{33}^*)^2$ in a relatively wide volume-fraction range, see data from the 5th and 7th columns in Table 3.10. The $(Q_{33}^*)^2$ value becomes smaller than $(Q_{33}^*)^2$ of the 1–3–0 PMN-0.33PT-based

Table 3.10 Piezoelectric coefficients d_{3j}^* (in pC/N) and g_{3j}^* (in mV m/N), and squared figures of merit $(Q_{3j}^*)^2$ (in 10^{-12} Pa^{-1}) of the 1–3-type [001]-poled PMN–0.28PT SC/auxetic PE composite[a] in the region of the large piezoelectric anisotropy

m	d_{31}^*	d_{33}^*	g_{31}^*	g_{33}^*	$(Q_{31}^*)^2$	$(Q_{33}^*)^2$
0.20	190	1080	21.1	120	4.01	130
0.25	90.8	1100	7.98	96.5	0.725	106
0.30	5.11	1110	0.371	80.5	1.90×10^{-3}	89.4
0.35	−69.4	1120	−4.28	69.1	0.297	77.4
0.40	−135	1130	−7.22	60.6	0.975	68.5
0.45	−192	1140	−9.11	53.9	1.75	61.4

[a]See the schematic of the composite in Fig. 2.11. Calculations have been performed by means of FEM

composite, see Fig. 3.10b. This is due to smaller piezoelectric coefficients $d_{3j}^{(1)}$ of the [001]-poled PMN–0.28PT SC in comparison with $d_{3j}^{(1)}$ of the [001]-poled PMN–0.33PT SC, see data in Table 1.3. For instance, the piezoelectric coefficient $d_{33}^{(1)}$ of the PMN–0.28PT SC is approximately 2.4 times smaller than $d_{33}^{(1)}$ of the PMN–0.33PT SC.

The third example is concerned with the 1–3-type FC-based composite wherein the sgng_{31}^{*} changes with a change in the aspect ratio η of the FC rod in the form of an elliptical cylinder. We remind the reader that a similar 1–3-type composite was analysed in Sect. 2.2.1. In our present example, the second component of the composite is the same auxetic PE, as mentioned earlier. As follows from Table 3.11, conditions (3.2) and (3.6) hold in a wide η range, however the $(Q_{33}^{*})^2$ value is smaller than that predicted for the PMN–0.28PT-based composite, see Table 3.10. This difference between the $(Q_{33}^{*})^2$ values of the related composites with auxetic PE is due to the large piezoelectric coefficients $d_{3j}^{(1)}$ of the [001]-poled PMN–0.28PT SC in comparison to $d_{3j}^{(1)}$ of the poled PCR-7M FC, cf. data in Tables 1.3 and 1.5. It should be added for comparison that the g_{33}^{*} values from Table 3.11 are almost equal to g_{33}^{*} = 53 mV m/N that is related to the aforementioned 1–3-type perforated PZT FC/epoxy composite [57]. The larger $(Q_{33}^{*})^2$ values from Table 3.11 in comparison to $(Q_{33}^{*})^2$ of 1–3-type perforated PZT FC/epoxy composite [57] are due to the higher piezoelectric activity of the poled PCR-7M FC (see Table 1.5). For instance, the piezoelectric coefficient $d_{33}^{(1)}$ of the PCR-7M FC is approximately two—five times larger than $d_{33}^{(1)}$ of various PZT FC compositions.

Table 3.11 Effective piezoelectric coefficients d_{3j}^{*} (in pC/N), g_{3j}^{*} (in mV m/N), and squared figures of merit $(Q_{3j}^{*})^2$ (in 10^{-12} Pa^{-1}) of the 1–3-type PCR-7M FC/auxetic PE composite[a] at the volume fraction of FC m = 0.3

η	d_{31}^{*}	d_{32}^{*}	d_{33}^{*}	g_{31}^{*}	g_{32}^{*}	g_{33}^{*}	$(Q_{31}^{*})^2$	$(Q_{32}^{*})^2$	$(Q_{33}^{*})^2$
0.01	−64.6	47.0	726	−4.78	3.48	53.8	0.309	0.164	39.1
0.1	−44.9	50.9	727	−3.32	3.77	53.8	0.149	0.192	39.1
0.2	−28.7	52.1	728	−2.13	3.86	53.8	0.0611	0.201	39.2
0.4	−5.62	49.7	728	−0.420	3.68	53.8	2.36×10^{-3}	0.183	39.2
0.6	10.5	44.0	729	0.70	3.25	53.9	8.09×10^{-3}	0.143	39.3
0.8	22.0	37.1	729	1.62	2.74	53.9	0.0356	0.102	39.3
1	30.1	30.1	729	2.23	2.23	53.9	0.0671	0.0671	39.3

[a]A cross section of the 1–3-type composite is shown in Fig. 2.14. Calculations have been performed by means of FEM

3.7 Hydrostatic Piezoelectric Sensitivity and Figures of Merit

The hydrostatic piezoelectric response of a composite [3, 7] is related to its hydrostatic piezoelectric coefficients d_h^* and g_h^* and squared figure of merit $(Q_h^*)^2$ from (2.1) and (2.2). Important problems for the improvement of the hydrostatic piezoelectric response of poled FCs and piezo-active composites based on FCs were discussed in work [6–8]. The FC and composite materials are used as active elements of hydrophones [3] that are sensitive to hydrostatic pressure, acoustic waves in water etc. A hydrophone sensitivity [3] is associated with a voltage caused by stresses induced by the acoustic pressure, and the larger sensitivity means the larger voltage at the same pressure level. In Sect. 3.7 we consider relations between the piezoelectric coefficients g_{3j}^* and hydrostatic parameters of some SC-based composites.

In a 1–3 PZN–0.07PT SC/PVDF composite, $\max g_{33}^*$ and $\min g_{31}^*$ are observed in Table 3.12 at volume fractions of SC $m \approx 0.05$, i.e., in the volume-fraction region wherein the dielectric permittivity of the composite $\varepsilon_{33}^{*\sigma}$ is small in comparison with $\varepsilon_{33}^{(1),\sigma}$ of its SC component. The m values related to extreme points of g_{3j}^* are larger than those related to extreme points of g_{3j}^* in other piezo-active composites [7, 8, 11, 23, 24] based on either SCs or FCs. This is due to the presence of the second piezoelectric component, i.e., ferroelectric PVDF polymer that strongly influences the PS of the 1–3 composite [26], especially at $m \ll 1$. The value of $\max[(Q_h^*)^2]$ is approximately two–three times larger than $(Q_h^*)^2$ of conventional 1–3 FC/polymer composites [7, 9], and this high performance is achieved not only due to the piezoelectric polymer component but also due to the SC component with a large piezoelectric coefficient $d_{33}^{(1)}$, see Table 1.3.

The important example of the PS and figures of merit is related to the 2–0–2 SC/SC/polymer composite considered in Sect. 3.1. We assume that the Type I layer of the 2–0–2 composite is represented by a [001]-poled SC, and in the Type II layer, spheroidal SC inclusions are regularly distributed in a polymer medium. Hereafter the Type II layer is regarded as a 0–3 SC/polymer composite. A volume-fraction behaviour of the effective parameters of the 2–0–2 composite based on the [001]-poled KNNTL:Mn SC is shown in Fig. 3.11. We remind that some characteristics of this composite were also highlighted in Fig. 3.2. In the presence of the Type II layer with the system of the aligned highly oblate SC inclusions ($\rho_i \gg 1$), we achieve the considerable hydrostatic PS and figure of merit. The graphs in Fig. 3.11a–c suggest that on increasing the volume fraction m_i of the SC inclusions in the Type II layer, the piezoelectric coefficients $|g_{3j}^*|$ decrease at $m = \text{const}$. However the decrease of the piezoelectric coefficient g_{33}^* is less pronounced (Fig. 3.11c) in comparison to $|g_{31}^*|$ (Fig. 3.11a) and $|g_{32}^*|$ (Fig. 3.11b), i.e., the transverse PS of the composite decreases more rapidly than its longitudinal PS. Such a feature of the piezoelectric performance of the studied 2–0–2 composite

Table 3.12 Effective piezoelectric coefficients d_{3j}^* (in pC/N), g_{3j}^* (in mV m/N), and squared figures of merit $(Q_{33}^*)^2$ and $(Q_h^*)^2$ (in 10^{-12} Pa^{-1}) which have been calculated for the 1–3 [001]-poled PZN–0.07PT SC/PVDF composite[a] by using the FEM and matrix method[b]

m	$-d_{31}^*$	d_{33}^*	$-g_{31}^*$	g_{33}^*	$(Q_{33}^*)^2$	$(Q_h^*)^2$
0.01	5.02 (5.08)	18.4 (18.3)	34.6 (35.3)	127 (127)	2.34 (2.32)	0.482 (0.460)
0.03	35.8 (36.0)	119 (119)	106 (107)	353 (353)	42.0 (42.0)	6.68 (6.53)
0.05	66.1 (66.5)	216 (215)	110 (111)	361 (360)	78.0 (77.4)	11.8 (11.3)
0.07	96.1 (96.6)	308 (307)	105 (105)	335 (334)	103 (103)	14.5 (14.1)
0.09	126 (126)	396 (396)	96.7 (96.7)	304 (304)	120 (120)	15.9 (15.9)
0.12	170 (170)	522 (522)	86.0 (86.0)	264 (264)	138 (138)	16.7 (16.7)
0.20	283 (283)	823 (823)	65.7 (65.7)	191 (191)	157 (157)	15.3 (15.3)
0.30	418 (418)	1140 (1140)	51.7 (51.7)	141 (141)	161 (161)	11.4 (11.4)
0.40	546 (545)	1410 (1410)	43.0 (43.3)	111 (112)	157 (158)	8.12 (8.28)
0.50	668 (667)	1650 (1650)	37.3 (37.2)	92.1 (92.1)	152 (152)	5.36 (5.49)
0.60	785 (784)	1850 (1850)	33.3 (33.2)	78.4 (78.4)	145 (145)	3.31 (3.40)
0.70	896 (895)	2030 (2030)	30.1 (30.1)	68.3 (68.3)	139 (139)	1.86 (1.91)
0.80	1000 (1000)	2190 (2190)	27.6 (27.6)	60.5 (60.5)	132 (132)	0.901 (0.914)
0.90	1110 (1110)	2330 (2330)	25.9 (25.9)	54.3 (54.3)	127 (127)	0.320 (0.322)
0.99	1200 (1200)	2440 (2440)	24.4 (24.4)	49.7 (49.7)	121 (121)	0.0600 (0.0599)

[a]See the schematic of the composite in Fig. 2.11. The spontaneous polarisation of the SC component is $\boldsymbol{P}_s^{(1)} \uparrow\uparrow OX_3$, and the remanent polarisation of the polymer component is $\boldsymbol{P}_r^{(2)} \uparrow\uparrow OX_3$
[b]Values of the effective parameters calculated using the matrix method are given in parentheses

leads to large values of $(Q_h^*)^2$ (Fig. 3.11b) in wide ranges of volume fractions m and m_i. The non-monotonic behaviour of $(Q_h^*)^2$ at m = const (Fig. 3.11d) is caused by the elastic anisotropy of the Type II layer to a large extent. We underline that, despite the smaller piezoelectric coefficient $d_{33}^{(1)}$ of the KNNTL:Mn SC [48] in comparison with $d_{33}^{(1)}$ of the PZN–0.07PT SC, the value of $\max[(Q_h^*)^2]$ shown in Fig. 3.11d is about two times larger than that related to the PZN–0.07PT-based

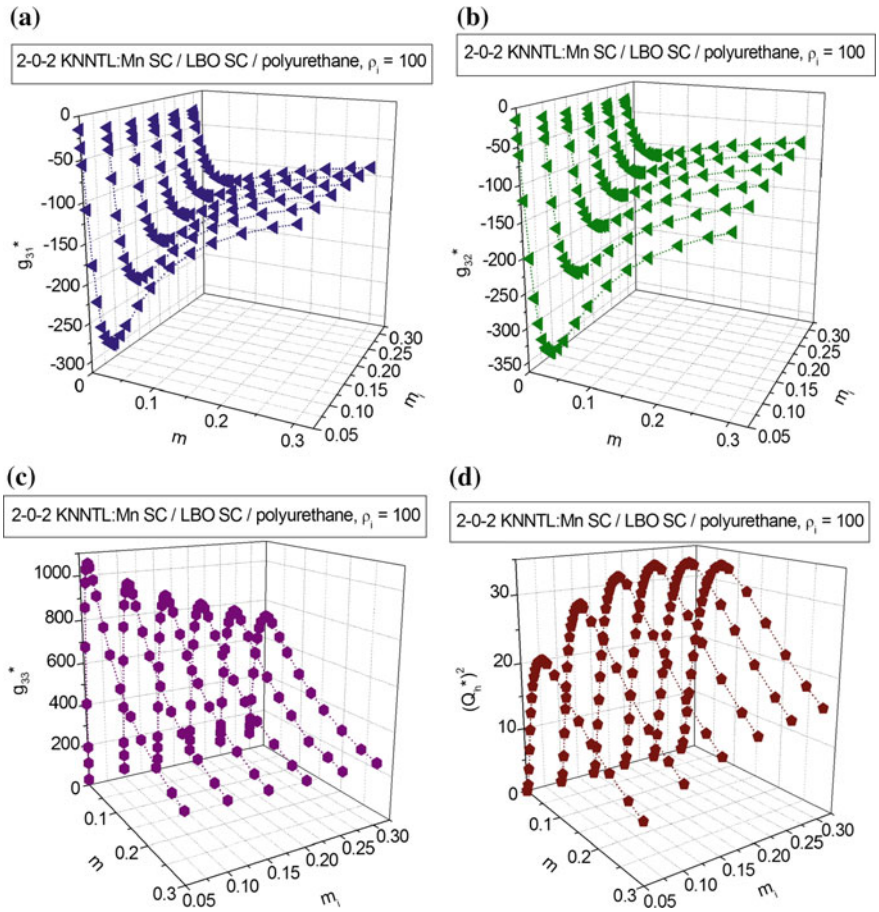

Fig. 3.11 Volume-fraction dependences of piezoelectric coefficients g_{3j}^{*} (**a**–**c**, in mV m/N) and hydrostatic squared figure of merit $(Q_h^{*})^2$ (**d**, in 10^{-12} Pa^{-1}) of the 2–0–2 [001]-poled KNNTL:Mn SC/LBO SC/polyurethane composite

composite, see Table 3.12. This is mainly achieved due to the large piezoelectric coefficient $g_{33}^{(1)}$ = 94.7 mV m/N of the KNNTL:Mn SC [48].

In Table 3.13 we show changes in the PS and squared figures of merit of the same 2–0–2 composite based on the KNNTL:Mn SC at variations of the microgeometric characteristics of the Type II layer and the volume fraction m of SC in the Type I layer. Changes in the aspect ratio ρ_i and volume fraction m_i of the SC inclusions in the Type II layer are to be taken into account at the prediction of the longitudinal PS and hydrostatic response: these changes strongly influence the elastic anisotropy of the Type II layer and, therefore, weaken the transverse PS of the composite as a whole. Due to this weakening at $\rho_i \gg 1$, we observe large $(Q_h^{*})^2$ values (Table 3.13) that undergo minor changes at volume fraction m = const

Table 3.13 Effective piezoelectric coefficients g_{33}^* and g_h^* (in mV m/N), and squared figures of merit $(Q_{33}^*)^2$ and $(Q_h^*)^2$ (in 10^{-12} Pa^{-1}) of the 2–0–2 [001]-poled KNNTL:Mn SC/LBO SC/polyurethane composite[a]

ρ_i	m_i	m	g_{33}^*	g_h^*	$(Q_{33}^*)^2$	$(Q_h^*)^2$
0.01	0.10	0.05	745	162	59.1	2.78
		0.10	594	121	81.0	3.34
		0.15	470	90.8	87.3	3.26
		0.20	385	70.9	87.9	2.98
		0.25	324	56.9	86.4	2.66
		0.30	280	46.7	83.9	2.33
1	0.10	0.05	1000	214	121	5.55
		0.10	715	141	146	5.69
		0.15	534	99.3	141	4.89
		0.20	422	74.3	131	4.07
		0.25	348	58.1	121	3.37
		0.30	296	46.7	112	2.80
100	0.10	0.05	931	98	94.2	26.9
		0.10	688	335	119	28.1
		0.15	521	231	119	23.3
		0.20	415	168	113	18.5
		0.25	344	127	106	14.5
		0.30	293	99.2	99.6	11.4
0.01	0.20	0.05	569	135	33.6	1.89
		0.10	491	105	48.9	2.26
		0.15	409	82.8	56.4	2.31
		0.20	346	66.5	60.1	2.22
		0.25	299	54.6	61.9	2.06
		0.30	262	45.4	62.7	1.88
1	0.20	0.05	876	197	89.2	4.51
		0.10	666	135	117	4.78
		0.15	511	96.2	119	4.21
		0.20	409	72.4	114	3.58
		0.25	340	56.8	108	3.01
		0.30	291	45.8	102	2.52
100	0.20	0.05	829	529	71.8	29.3
		0.10	646	380	96.5	33.4
		0.15	500	270	99.5	29.0
		0.20	403	199	96.7	23.6
		0.25	336	152	92.4	18.8
		0.30	288	118	87.8	14.8

[a]The EFM and matrix method were applied to evaluate the electromechanical properties of the 0–3 SC/polymer layer and 2–0–2 SC/SC/polymer composite, respectively

(Type I layer) and on increasing the volume fraction m_i of SC in the Type II layer. The dielectric properties of the Type II layer influence the PS, $(Q_{33}^*)^2$ and $(Q_h^*)^2$ of the composite to a restricted degree only. It should be added that the large g_{33}^* and $(Q_h^*)^2$ values of the studied lead-free 2–0–2 composite (see data in Fig. 3.11c, d and Table 3.13) are important in piezoelectric sensor, hydroacoustic and other applications.

3.8 Conclusion

This chapter has been devoted to the piezoelectric coefficients g_{ij}^*, their anisotropy and links between microgeometric characteristics of piezo-active composites and their PS. As follows from numerous papers, experimental and theoretical studies on the composites, their piezoelectric coefficients g_{ij}^* play an important role for the description of the PS, figures of merit and related characteristics. Specific trends in improving the PS of the composite and increasing its piezoelectric coefficients g_{ij}^* have been discussed for specific connectivity patterns. The main results of this chapter are formulated as follows.

(i) Examples of the PS concerned with the piezoelectric coefficients g_{ij}^* and related parameters of are discussed for the 0–3-type, 1–1-type, 1–3-type, 2–2-type, and 3–β composites. The studied composites are based on either FCs or domain-engineered SCs, and examples of the composite patterns with planar and non-planar interfaces are analysed.

(ii) Various volume-fraction dependences of the piezoelectric coefficients g_{ij}^* of the studied two- and three-component composites are characterised by relatively sharp extreme of g_{3j}^* at small volume fractions m of the main piezoelectric component that is represented by FC, ferroelectric SC etc. Along with the drastic changes in g_{3j}^*, examples of the 'sleeping PS' are observed. This feature of the studied piezo-active composites is caused by the strong influence of the dielectric properties and system of interfaces on g_{3j}^*. Elastic properties of the composite influence the PS of the composites to a lesser degree. An additional opportunity to change the piezoelectric coefficients g_{3j}^* is concerned with the elastic anisotropy that can be large in porous and heterogeneous polymer matrices or layers. In contrast to g_{3j}^*, the shear piezoelectric coefficients (e.g. g_{15}^* or g_{24}^*) undergo less considerable changes in the wide volume-fraction range, and such a behaviour is associated with some microgeometric features of the composites.

(iii) Because of the small volume fractions m at which extreme of the piezoelectric coefficients g_{3j}^* and g_h^* are achieved in the studied composites, values of $m < 0.1$ are to be chosen on manufacturing. In this case, one can keep the high PS and avoid a significant decrease of $\max|g_{3j}^*|$ and $\max g_h^*$.

(iv) The auxetic polymer component influences the PS and anisotropy of the piezoelectric coefficients g_{3j}^*, especially at volume fractions of the main piezoelectric component $m \ll 1$. A use of the auxetic polymer component enables one to reach a change in sign of some piezoelectric coefficients g_{3j}^* of the studied composites and becomes a good stimulus to form highly anisotropic composite structures.

(v) As follows from the performance of the lead-free composites based on the domain-engineered KNNTL:Mn SC, the high PS and large values of squared figures of merit of the composites are mainly achieved due to the large

piezoelectric coefficient $g_{33}^{(1)}$ of their SC component. The high PS of the studied lead-free composites can be regarded as their advantage over the conventional FC/polymer composites.

(vi) The present results show the potential of the studied composites that are suitable for piezoelectric sensor, transducer, energy-harvesting, and hydroacoustic applications.

References

1. Zheludev IS (1971) Physics of crystalline dielectrics. Vol 2: Electrical properties. Plenum, New York
2. Steinem C, Janshoff A (eds) (2007) Piezoelectric sensors. Springer, Berlin
3. Sherman CH, Butler JL (2007) Transducers and arrays for underwater sound. Springer, New York
4. Fraden J (2010) Handbook of modern sensors. Physics, designs, and applications. Springer, New York
5. Sharapov V (2011) Piezoceramic sensors. Springer, Heidelberg
6. Lupeiko TG, Lopatin SS (2004) Old and new problems in piezoelectric materials research and materials with high hydrostatic sensitivity. Inorg Mater 40 (Suppl. 1):S19–S32
7. Topolov VYu, Bowen CR (2009) Electromechanical properties in composites based on ferroelectrics. Springer, London
8. Topolov VYu, Bisegna P, Bowen CR (2014) Piezo-active composites. Orientation effects and anisotropy factors. Springer, Berlin
9. Akdogan EK, Allahverdi M, Safari A (2005) Piezoelectric composites for sensor and actuator applications. IEEE Trans Ultrason Ferroelectr Freq Control 52:746–775
10. Zhang S, Li F (2012) High performance ferroelectric relaxor-$PbTiO_3$ single crystals: status and perspective. J Appl Phys 111:031301
11. Topolov VYu, Krivoruchko AV, Bowen CR (2012) Anisotropy of electromechanical properties and hydrostatic response of advanced 2–2-type composites. Physica Status Solidi A 209:1334–1342
12. Topolov VYu, Glushanin SV (2009) Features of the hydrostatic piezoelectric response of a novel 2–2–0 composite based on single-domain $0.67Pb(Mg_{1/3}Nb_{2/3})O_3$–$0.33PbTiO_3$ crystal. Compos Sci Technol 69:2532–2537
13. Topolov VYu, Bowen CR, Ermakov IA (2016) Remarkable hydrostatic piezoelectric response of novel 2–0–2 composites. Ferroelectr Lett Sect 43:90–95
14. Grekov AA, Kramarov SO, Kuprienko AA (1987) Anomalous behavior of the two-phase lamellar piezoelectric texture. Ferroelectrics 76:43–48
15. Adachi M, Shiosaki T, Kobayashi H, Ohnishi O, Kawabata A (1985) Temperature compensated piezoelectric lithium tetraborate crystal for high frequency surface acoustic wave and bulk wave device applications. In: Proceedings of 1985 IEEE Ultrasonics Symposium, IEEE, New York, pp 228–232
16. Ikegami S, Ueda I, Nagata T (1971) Electromechanical properties of $PbTiO_3$ ceramics containing La and Mn. J Acoust Soc Am 50:1060–1066
17. Nagatsuma K, Ito Y, Jyomura S, Takeuchi H, Ashida S (1985) Elastic properties of modified $PbTiO_3$ ceramics with zero temperature coefficients. In: Taylor GW (ed) Ferroelectricity and related phenomena. Piezoelectricity, vol 4. Gordon and Breach Science Publishers, New York, pp 167–176

18. Gusakova LG, Poguibko VM, Spiridonov NA, Ishchuk VM, Kisel NK (2012) Lead-free nanostructured piezoceramic material based on (K, Na)NbO_3. Nanosyst Nanomater Nanotechnol 10:303–312 (in Russian)
19. Yan Y, Zhou JE, Maurya D, Wang YU, Priya S (2016) Giant piezoelectric voltage coefficient in grain-oriented modified $PbTiO_3$ material. Nat Commun 7:13089
20. Topolov VYu, Krivoruchko AV (2009) Polarization orientation effect and combination of electromechanical properties in advanced $0.67Pb(Mg_{1/3}Nb_{2/3})O_3$–$0.33PbTiO_3$ single crystal/polymer composites with 2–2 connectivity. Smart Mater Struct 18:065011
21. Grekov AA, Kramarov SO, Kuprienko AA (1989) Effective properties of a transversely isotropic piezoelectric composite with cylindrical inclusions. Mech Compos Mater 25:54–61
22. Chan HLW, Unsworth J (1989) Simple model for piezoelectric ceramic/polymer 1–3 composites used in ultrasonic transducer applications. IEEE Trans Ultrason Ferroelectr Freq Control 36:434–441
23. Gibiansky LV, Torquato S (1997) On the use of homogenization theory to design optimal piezocomposites for hydrophone applications. J Mech Phys Solids 45:689–708
24. Bezus SV, Topolov VYu, Bowen CR (2006) High-performance 1–3-type composites based on $(1 - x)$ $Pb(A_{1/3}Nb_{2/3})O_3$–$xPbTiO_3$ single crystals (A = Mg, Zn). J Phys D Appl Phys 39:1919–1925
25. Wang F, He C, Tang Y (2007) Single crystal $0.7Pb(Mg_{1/3}Nb_{2/3})O_3$–$0.3PbTiO_3$/epoxy 1–3 piezoelectric composites prepared by the lamination technique. Mater Chem Phys 105:273–277
26. Topolov VYu, Krivoruchko AV, Bisegna P, Bowen CR (2008) Orientation effects in 1–3 composites based on 0.93Pb(Zn1/3Nb2/3)O3–0.07PbTiO3 single crystals. Ferroelectrics 376:140–152
27. Topolov VYu, Bisegna P (2010) Anisotropic piezoelectric properties of 1–3 ceramic/polymer composites comprising rods with elliptic cross section. J Electroceram 25:26–37
28. Topolov VYu, Bowen CR, Bisegna P, Krivoruchko AV (2015) New orientation effect in piezo-active 1–3-type composites. Mater Chem Phys 151:187–195
29. Bowen CR, Topolov VYu, Isaeva AN, Bisegna P (2016) Advanced composites based on relaxor-ferroelectric single crystals: from electromechanical coupling to energy-harvesting applications. CrystEngComm 18:5986–6001
30. Topolov VYu, Bowen CR, Bisegna P (2015) New aspect-ratio effect in three-component composites for piezoelectric sensor, hydrophone and energy-harvesting applications. Sens Actuators A – Phys 229:94–103
31. Topolov VYu, Bowen CR, Bisegna P, Panich AE (2015) Effect of the matrix subsystem on hydrostatic parameters of a novel 1–3-type piezo-composite. Funct Mater Lett 8:1550049
32. Topolov VYu, Krivoruchko AV, Bisegna P (2011) Electromechanical coupling and its anisotropy in a novel 1–3–0 composite based on single-domain $0.58Pb(Mg_{1/3}Nb_{2/3})O_3$–$0.42PbTiO_3$ crystal. Compos Sci Technol 71:1082–1088
33. Glushanin SV, Topolov VYu (2001) Features of electromechanical properties of piezoelectric composites with elements of connectivity 1–1. J Phys D Appl Phys 34:2518–2529
34. Glushanin SV, Topolov VYu (2001) Anisotropy of the electromechanical properties and a high piezoelectric sensitivity of the 1–1 type ferroelectric piezocomposites. Tech Phys Lett 27:626–628
35. Chan HLW, Ng PKL, Choy CL (1999) Effect of poling procedure on the properties of lead zirconate titanate/vinylidene fluoride-trifluoroethylene composites. Appl Phys Lett 74:3029–3031
36. Ng KL, Chan HLW, Choy CL (2000) Piezoelectric and pyroelectric properties of PZT/P(VDF-TrFE) composites with constituent phases poled in parallel or antiparallel directions. IEEE Trans Ultrason Ferroelectr Freq Control 47:1308–1315
37. Venkatragavaraj E, Satish B, Vinod PR, Vijaya MS (2001) Piezoelectric properties of ferroelectric PZT–polymer composites. J Phys D Appl Phys 34:487–492
38. Chiang CK, Popielarz R (2002) Polymer composites with high dielectric constant. Ferroelectrics 275:1–9

39. Wilson SA, Maistros GM, Whatmore RW (2005) Structure modification of 0–3 piezoelectric ceramic/polymer composites through dielectrophoresis. J Phys D Appl Phys 38:175–182
40. Glushanin SV, Topolov VYu, Krivoruchko AV (2006) Features of piezoelectric properties of 0–3 $PbTiO_3$-type ceramic/polymer composites. Mater Chem Phys 97:357–364
41. Topolov VYu, Turik AV, Chernobabov AI (1994) On the mechanism of high piezoelectric anisotropy in lead titanate-based ferroelectrics. Crystallogr Rep 39:805–809
42. Topolov VYu, Turik AV, Chernobabov AI (1994) On the piezoelectric anisotropy in modified $PbTiO_3$ ceramics. Ferroelectrics 154:271–276
43. Ngoma JB, Cavaille JY, Paletto J, Perez J (1990) Dielectric and piezoelectric properties of copolymer-ferroelectric composite. Ferroelectrics 109:205–210
44. Gururaja TR, Safari A, Newnham RE, Cross LE (1988) Piezoelectric ceramic-polymer composites for transducer applications. In: Levinson M (ed) Electronic ceramics: properties, devices, and applications. Marcel Dekker, New York, pp 92–128
45. Lushcheykin GA (1987) Polymer and composition piezoelectrics. Izvestiya Akademii Nauk SSSR Seriya Fizicheskaya 51:2273–2276 (in Russian)
46. Pardo L, Mendiola J, Alemany C (1988) Theoretical treatment of ferroelectric composites using Monte Carlo calculations. J Appl Phys 64:5092–5097
47. Babu I, van den Ende DA, de With G (2010) Processing and characterization of piezoelectric 0–3 PZT/LCT/PA composites. J Phys D Appl Phys 43:425402
48. Huo X, Zhang R, Zheng L, Zhang S, Wang R, Wang J, Sang S, Yang B, Cao W (2015) (K, Na, Li)(Nb, Ta)O_3:Mn lead-free single crystal with high piezoelectric properties. J Am Ceram Soc 98:1829–1835
49. Kar-Gupta R, Venkatesh TA (2007) Electromechanical response of 1–3 piezoelectric composites: an analytical model. Acta Mater 55:1093–1108
50. Sessler GM (1981) Piezoelectricity in polyvinylidenefluoride. J Acoust Soc Am 70:1596–1608
51. Topolov VYu, Bisegna P, Glushanin SV, Panich AA (2011) Interrelations between microstructure and piezoelectric sensitivity in novel 0–3–0 composites based on 0.67Pb$(Mg_{1/3}Nb_{2/3})O_3$–0.33$PbTiO_3$ single crystal. Ferroelectrics 413:11–28
52. Topolov VYu, Bisegna P, Bowen CR (2011) Analysis of the piezoelectric performance of modern 0–3-type composites based on relaxor-ferroelectric single crystals. Ferroelectrics 413:176–191
53. Cheng X, Huang S, Chang J, Lu L, Liu F, Ye Z, Wang S (2005) Dielectric and piezoelectric properties of piezoelectric ceramic–sulphoaluminate cement composites. Smart Mater Struct 14:N59–N63
54. Smay JE, Tuttle B, Cesarano J III (2008) Robocasting of three-dimensional piezoelectric structures. In: Safari A, Akdoğan EK (eds) Piezoelectric and acoustic materials for transducer applications. Springer, New York, pp 305–318
55. Smay JE, Cesarano J III, Tuttle BA, Lewis JA (2002) Piezoelectric properties of 3–*X* periodic $Pb(Zr_xTi_{1-x})O_3$–polymer composites. J Appl Phys 92:6119–6127
56. Filippov SE, Vorontsov AA, Topolov VYu, Brill OE, Bisegna P, Panich AE (2014) Features of the piezoelectric effect in a novel PZT-type ceramic/clay composite. Ferroelectr Lett Sect 41:82–88
57. Mendiola J, Jimenez B (1984) Review of recent work on piezoelectric composite systems. Ferroelectrics 53:159–166
58. Bowen CR, Topolov VYu, Kim HA (2016) Modern piezoelectric energy-harvesting materials. Springer International Publishing, Switzerland

Chapter 4
Piezoelectric Coefficients e_{ij}^* and d_{ij}^*: Combination of Properties at Specific Microgeometry

Abstract Piezoelectric coefficients e_{ij} are used to describe a link between an external mechanical strain and a piezoelectric polarisation caused by the direct piezoelectric effect. The piezoelectric coefficients e_{ij} are of importance to analyse a link between a mechanical stress and an external electric field at the converse piezoelectric effect. Examples of the piezoelectric sensitivity of composites with various connectivity patterns are discussed in terms of the effective piezoelectric coefficients e_{ij}^* and relations between the piezoelectric coefficients e_{ij}^* and d_{ij}^*. Of specific interest are a non-monotonic behaviour of e_{ij}^*, large values of $|e_{ij}^*|$ and considerable anisotropy of e_{3j}^* as well as their links to the microgeometry and properties of components.

The piezoelectric coefficients e_{ij} are used to describe the link between an external mechanical strain ξ_j that is applied to a sample and its polarisation P_i by the direct piezoelectric effect in accordance with (1.5). The piezoelectric coefficients e_{ij} enable us to analyse the link between a mechanical stress σ_j and an electric field E_i applied to the sample. This is a case of the converse piezoelectric effect, and the relevant relation between σ_j and E_i is given by (1.4). The PS concerned with the piezoelectric coefficients e_{ij} is often associated with polarisation charges at surfaces of the deformed (or mechanically loaded) sample [1–3], and this is important for piezoelectric sensor applications, measuring the quality control of a production, surfaces of machine parts etc. [4, 5]. As follows from (1.20) and (1.21), the piezoelectric coefficients d_{ij} studied in Chap. 2 and the piezoelectric coefficients e_{ij} to be analysed in this chapter are linked by elastic properties that are described by a fourth-order rank tensor, and this link is more complicated than that between the piezoelectric coefficients g_{ij} and d_{ij} (see Chap. 3). The piezoelectric coefficient e_{33} related to the longitudinal piezoelectric effect in poled FCs influences the thickness ECF k_t in accordance with (1.17). It should be mentioned that the piezoelectric coefficients e_{ij} of poled FCs and domain-engineered SCs (see [2, 6–8] and Tables 1.6 and 3.5) are varied in a relatively narrow range, namely, from approximately 1 to 30 C/m^2. Moreover, the widespread perovskite-type FCs are divided into two groups, see Table 1.6. In the first group, there are the FCs with $e_{31} < 0$ and $e_{33} > 0$. The second

V. Y. Topolov et al., *Piezo-Active Composites*, Springer Series in Materials Science 271, https://doi.org/10.1007/978-3-319-93928-5_4

group contains the FCs with $e_{31} > 0$ and $e_{33} > 0$. In contrast to e_{ij}, the piezoelectric coefficients d_{ij} of poled FCs and domain-engineered SCs are found in a wide range. As follows from Tables 1.1–1.5 and [2, 6, 7], the order-of-magnitude of d_{ij} is (10^0–10^3) pC/N.

In this chapter we discuss the PS of some composites in terms of their effective piezoelectric coefficients e_{ij}^* and relations between e_{ij}^* and d_{ij}^*. We also consider examples of the non-monotonic behaviour of e_{ij}^*, large values of $|e_{ij}^*|$ and considerable anisotropy of e_{ij}^* which can be due to the specific piezoelectric components and microgeometric features of the composites.

4.1 2–2-Type Composites

The 2–2 composite structure shown in Figs. 2.1 and 2.2 represents a system of alternating layers of two components, and at least one of them is piezoelectric, e.g. poled FC or SC. We assume that the OX_3 axis shown in Figs. 2.1 and 2.2 is the poling axis of the composite. In Sect. 4.1 we discuss volume-fraction dependences of the piezoelectric coefficients e_{ij}^* in both series- and parallel-connected 2–2-type composites.

The literature has reported that some of the effective parameters of the 2–2 series-connected PZT-type FC/polymer composites are characterised by non-monotonic volume-fraction dependences. Among such parameters, one can mention the thickness ECF k_t^* [7, 8], piezoelectric coefficient e_{31}^*, dielectric permittivity $\varepsilon_{11}^{*\sigma}$ [9], etc. In the 2–2 parallel-connected PZT-type FC/polymer composites a non-monotonic volume-fraction behaviour of the piezoelectric coefficients e_{33}^*, g_{3j}^* and h_{33}^* [6] is observed. In the 2–2 parallel-connected PZN–0.07PT SC/polymer composite a non-monotonic behaviour of e_{33}^* is observed [10] at rotations of the main crystallographic axes of the [011]-poled SC component.

Hereafter in Sect. 4.1 we apply the matrix method to find the full set of electromechanical constants of the 2–2-type composite (see the description of the matrix method in Sect. 2.1.1).

In the first example of the PS, we consider a 2–2 series-connected composite based on the PCR-7M FC. Due to the poled FC layers and interfaces oriented perpendicular to the poling axis OX_3 (Fig. 2.1), the composite as a whole is described by ∞mm symmetry. As is known from Table 1.6, the poled PCR-7M FC is characterised by large values of the piezoelectric coefficients e_{33} and e_{15}. We remind the reader that in accordance with (1.21), the piezoelectric coefficients e_{ij}^* of the composite from the ∞mm symmetry group are represented as follows:

$$\begin{aligned} &e_{31}^* = e_{32}^* = d_{31}^*\left(c_{11}^{*E} + c_{12}^{*E}\right) + d_{33}^* c_{13}^{*E}, e_{33}^* = 2d_{31}^* c_{13}^{*E} + d_{33}^* c_{33}^{*E} \text{ and} \\ &e_{15}^* = e_{24}^* = d_{15}^* c_{55}^{*E} = d_{15}^* c_{44}^{*E} = d_{24}^* c_{44}^{*E} \end{aligned} \tag{4.1}$$

Equations (4.1) mean a combination of the elastic (c_{ab}^{*E}) and piezoelectric (d_{ij}^{*}) properties, and this combination influences a behaviour of the piezoelectric coefficients e_{ij}^{*} of the composite in the wide volume-fraction range. As in Chaps. 2 and 3, the volume fraction of the main piezoelectric component of the composite equals m.

The piezoelectric coefficients $e_{ij}^{*}(m)$ of the 2–2 series-connected composites demonstrate a monotonic behaviour, however the $|e_{3j}^{*}(m)|$ values remain relatively small in comparison to the $|e_{3j}|$ values of the FC even at volume fractions $0.90 \leq m \leq 0.95$ (Table 4.1). Moreover, the $|d_{3j}^{*}(m)|$ values are also small in the same volume-fraction region, see Table 4.1. This is due to the poor orientation of the piezoelectric (poled FC) layers (see C1 in Fig. 2.1) with respect to the poling direction OX_3. In the external electric field $\boldsymbol{E} \| OX_3$, a considerable depolarisation field appears in the FC layers, and these layers provide a small contribution to the piezoelectric response of the composite with respect to OX_3 [6]. The shear PS concerned with $e_{15}^{*}(m)$ and $d_{15}^{*}(m)$ is affected by the orientation of the layers of the composite (Fig. 2.1) to a lesser degree. As follows from Table 4.1, conditions

$$e_{15}^{*} \gg |e_{3j}^{*}| \text{ and } d_{15}^{*} \gg |d_{3j}^{*}| \tag{4.2}$$

hold for the composites based on the PCR-7M FC, where $j = 1$ and 3. On increasing the elastic compliance s_{11} of the polymer component, the piezoelectric coefficient $e_{33}^{*}(m)$ of the composite decreases at m = const. The auxetic polymer component has only a small influence on the piezoelectric coefficients $e_{ij}^{*}(m)$ of the composite, and such an influence is accounted for by the large volume fractions of the FC component.

The second example of the PS is concerned with the 2–2 series-connected composite based on the modified $PbTiO_3$ FC. For this composite, as follows from Table 4.1, conditions (4.1) are not valid, and $e_{31}^{*}(m) < 0$ despite $e_{31} > 0$ of the FC component (see Table 1.6). Such a performance is observed in the presence of the FC that is characterised by the large piezoelectric and elastic anisotropy (see Table 1.5) and, therefore, can influence the PS of the 2–2 composite in a different way than in the first example. We add that the condition $e_{31}^{*}(m_e) = 0$ holds at a volume fraction from the range $0.96 < m_e < 1$.

The third example of the PS of the 2–2 series-connected composite is represented in Table 4.2. The piezoelectric component is a domain-engineered KNNTL:Mn SC with an unusual combination of the piezoelectric coefficients e_{ij}. According to experimental data [11], the piezoelectric coefficients e_{ij} of the [001]-poled KNNTL:Mn SC (4*mm* symmetry) obey the condition $e_{33} < e_{15} < |e_{31}|$. As a result, the PS related to e_{31}^{*} of the composite plays a dominating role, and the condition

$$e_{33}^{*} < e_{15}^{*} < \left|e_{31}^{*}\right| \tag{4.3}$$

is valid at large volume fractions m. To a large extent, the volume-fraction behaviour of the piezoelectric coefficients $e_{ij}^{*}(m)$ is due to the orientation of the

Table 4.1 Volume-fraction dependences of piezoelectric coefficients e_{ij}^* (in C/m^2) and d_{ij}^* (in pC/N) of 2–2 FC/polymer series-connected composites[a] at large volume fractions of FC m

Polymers	m	e_{31}^*	e_{33}^*	e_{15}^*	d_{31}^*	d_{33}^*	d_{15}^*
Composite based on the PCR-7M FC							
Araldite	0.80	–0.169	0.0492	7.14	–1.38	2.73	776
	0.90	–0.349	0.186	11.1	–2.80	5.80	831
	0.95	–0.644	0.590	14.5	–5.51	11.7	856
Elastomer	0.80	–0.233	0.0102	0.704	–1.74	3.59	782
	0.90	–0.510	0.0443	1.52	–3.47	7.34	833
	0.95	–1.03	0.173	2.96	–6.87	14.7	857
Auxetic PE	0.80	–0.109	0.00319	3.20	–0.803	1.25	780
	0.90	–0.242	0.0140	6.00	–1.60	2.99	833
	0.95	–0.495	0.0564	9.49	–3.19	6.44	857
Composite based on the modified $PbTiO_3$ (III) FC							
Araldite	0.80	–0.0350	0.138	0.572	–0.505	4.44	47.8
	0.90	–0.0452	0.465	1.04	–0.922	8.94	51.1
	0.95	–0.0228	1.21	1.58	–1.56	15.8	52.6
Elastomer	0.80	–0.0750	0.0285	0.0440	–0.625	5.50	48.0
	0.90	–0.141	0.110	0.0973	–1.11	10.8	51.1
	0.95	–0.217	0.354	0.198	–1.82	18.5	52.6
Auxetic PE	0.80	–0.0402	0.00938	0.219	–0.304	2.52	47.9
	0.90	–0.0821	0.0389	0.451	–0.573	5.42	51.1
	0.95	–0.141	0.141	0.815	–1.03	10.3	52.6

[a]See the schematic of the 2–2 series-connected composite in Fig. 2.1

composite layers (Fig. 2.1) with respect to the poling axis OX_3. As in the PCR-7M-based composite, the piezoelectric coefficient $e_{33}^*(m)$ of the KNNTL: Mn-based composite decreases at m = const on increasing the elastic compliance s_{11} of polymer.

The fourth example of the PS is concerned with the performance of the 2–2 parallel-connected composite based on the PCR-7M FC (Fig. 4.1). Due to the orientation of the interfaces parallel to the poling axis OX_3 (Fig. 2.2) such a composite is characterised by $mm2$ symmetry. The orientation of the composite layers shown in Fig. 2.2 is favourable to pole the parallel-connected composite in the electric field $\boldsymbol{E}\|OX_3$, and this microgeometric feature leads to large values of the piezoelectric coefficient $e_{33}^*(m)$, see curve 5 in Fig. 4.1. The large piezoelectric coefficient $e_{24}^*(m)$ in curve 2 of Fig. 4.1 is caused by the weak influence of the composite interfaces (Fig. 2.2) on the shear piezoelectric response related to the (X_2OX_3) plane. According to (1.21), the link between the piezoelectric coefficients e_{ij}^* and d_{ij}^* for materials with $mm2$ symmetry is given by

Table 4.2 Volume-fraction dependences of piezoelectric coefficients e_{ij}^* (in C/m^2) of the 2–2 [001]-poled KNNTL: Mn SC/polymer series-connected composite[a] at large volume fractions of FC m

Polymer	m	e_{31}^*	e_{33}^*	e_{15}^*
Araldite	0.80	–1.90	0.201	0.751
	0.90	–3.23	0.606	1.43
	0.95	–4.44	1.36	2.31
Polyurethane	0.80	–1.75	0.109	0.431
	0.90	–3.09	0.357	0.877
	0.95	–4.46	0.904	1.56
Elastomer	0.80	–2.37	0.0398	0.0545
	0.90	–4.06	0.133	0.121
	0.95	–5.71	0.361	0.249
Auxetic PE	0.80	–1.26	0.0142	0.276
	0.90	–2.43	0.0540	0.581
	0.95	–3.97	0.172	1.09

[a]See the schematic of the 2–2 series-connected composite in Fig. 2.1

$$e_{3j}^* = d_{31}^* c_{1j}^{*E} + d_{32}^* c_{2j}^{*E} + d_{33}^* c_{3j}^{*E}, e_{15}^* = d_{15}^* c_{55}^{*E} \text{ and } e_{24}^* = d_{24}^* c_{44}^{*E}, \tag{4.4}$$

where j = 1, 2 and 3. It should be noted that the piezoelectric coefficients e_{ij}^* from (4.4) are caused by a combination of the elastic (c_{ab}^{*E}) and piezoelectric (d_{ij}^*) properties, and this combination differs from that in (4.1).

Changes in $e_{ij}^*(m)$ correlate with the $d_{ij}^*(m)$ dependences of the same composite to a considerable degree, see Figs. 4.1 and 2.3. However there is an important peculiarity related to $e_{33}^*(m)$ at large volume fractions m: Fig. 4.1e shows the presence of max $e_{33}^*(m)$ at large volume fractions m and depends on elastic properties of the polymer component. On increasing the elastic compliance s_{11} of the polymer component, max $e_{33}^*(m)$ increases, i.e., the longitudinal PS of the composite becomes more pronounced in the presence of the softer polymer even at its small volume fractions. We observe only a limited influence of the auxetic polymer component on the $e_{ij}^*(m)$ dependence, cf. Figs. 2.3d and 4.1d. This is due to the anisotropic elastic properties of the 2–2 parallel-connected composite. The non-monotonic behaviour of $e_{33}^*(m)$ is mainly caused [6] by a competition of the items from (4.4): at j = 3 and large volume fractions m, we have

$$d_{33}^* c_{33}^{*E} > 0,\ d_{31}^* c_{13}^{*E} < 0 \text{ and } d_{32}^* c_{23}^{*E} < 0 \tag{4.5}$$

For the studied PCR-7M-based composites, conditions $d_{33}^* > 0$, $d_{32}^* < 0$ and $d_{31}^* < 0$ hold at $0 < m < 1$. A very slow increase of d_{33}^* at $m \to 1$ irrespective of the polymer component [6, 12] can lead to a less pronounced influence of the positive item $d_{33}^* c_{33}^{*E}$ from (4.5) on the piezoelectric coefficient e_{33}^* in comparison to the remaining negative items from (4.5).

The fifth example of the PS enables us to underline the important role of the arrangement of the composite layers (Fig. 2.2) in forming the piezoelectric

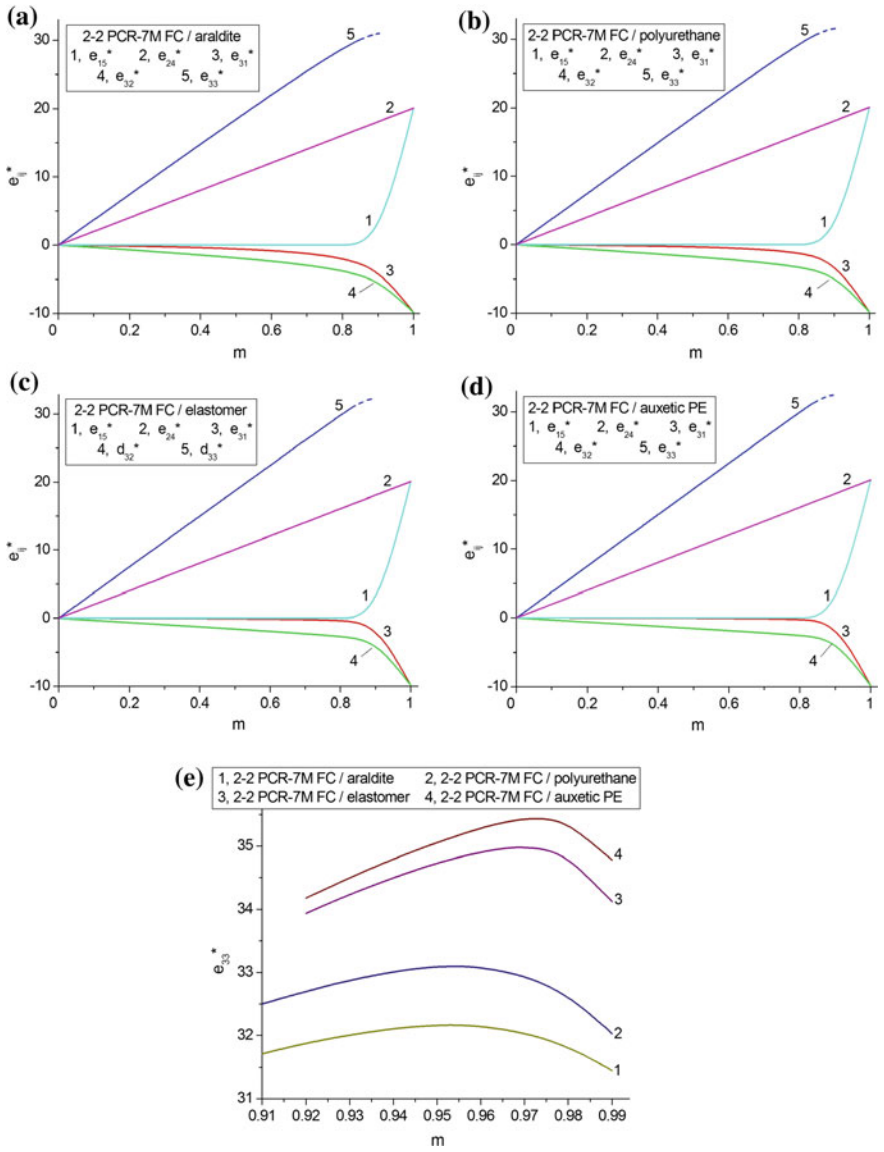

Fig. 4.1 Volume-fraction dependences of piezoelectric coefficients e_{ij}^* (in C/m^2) of 2–2 PCR-7M FC/polymer parallel-connected composites (**a**–**d**) and behaviour of the piezoelectric coefficient e_{33}^* (in C/m^2) near its maximum in the 2–2 composites based on the PCR-7M FC (**e**). The schematic of the 2–2 parallel-connected composite is shown in Fig. 2.2

coefficients $e_{ij}^*(m)$. Comparison of Fig. 4.2a to any graph of Fig. 4.1a–d testifies to the similar character of the $e_{ij}^*(m)$ dependences in the 2–2 PCR-7M- and KNNTL: Mn-based composites, and this similarity is observed despite considerable

differences between the piezoelectric coefficients e_{ij} of these piezoelectric coefficients.

In Fig. 4.2 we do not show examples of the $e_{ij}^*(m)$ dependences for different KNNTL:Mn-based composites because of the similarity of the graphs, such as those shown in Fig. 4.1a–d. The graph in Fig. 4.2b suggests that max $e_{33}^*(m)$ depends on the polymer component. As in the fourth example of the PS, the larger max e_{33}^* value is achieved by the presence of a polymer with a larger elastic compliance s_{11}. We note that Fig. 4.2a represents the case of the considerable increase of $e_{33}^*(m)$, i.e., by approximately 1.8 times in comparison to the e_{33} value of the KNNTL:Mn SC [11].

By comparing the piezoelectric coefficients $e_{ij}^*(m)$ and $d_{ij}^*(m)$, we underline the key role of the effect of the combination of properties, and such an effect was discussed in a series of papers, see, for instance [6, 12–14]. In the case of the 2–2 composites represented in Sect. 4.1, we should consider important combinations of the piezoelectric and elastic properties in anisotropic materials, see, for instance, (4.1) and (4.4). As is known from earlier studies [6, 12, 13], these combinations are implemented in different ways in the presence of the piezoelectric components from different symmetry groups and at different microgeometric features of the composite samples.

It should be added that the piezoelectric coefficients $e_{ij}^*(m)$ and max $e_{33}^*(m)$ are taken into account by the analysis of the hydrostatic piezoelectric coefficient e_h^* of various 2–2 and 2–0–2 composites [12, 13, 15, 16] based on relaxor-ferroelectric SCs. In these composites, the rotation of the main crystallographic axes in the SC layers plays the key role in forming the large hydrostatic piezoelectric coefficients d_h^*, e_h^* and g_h^*. The combination of the large hydrostatic piezoelectric coefficients is important at the selection of the studied 2–2-type composites for hydroacoustic applications.

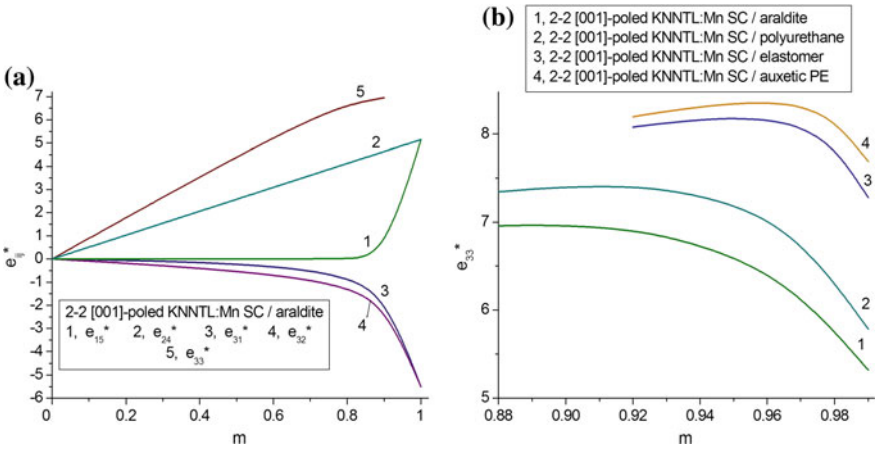

Fig. 4.2 Volume-fraction dependences of piezoelectric coefficients e_{ij}^* (in C/m^2) of the 2–2 [001]-poled KNNTL:Mn SC/araldite parallel-connected composite (**a**) and behaviour of the piezoelectric coefficient e_{33}^* (in C/m^2) near its maximum in the 2–2 composites based on the KNNTL:Mn SC (**b**). The schematic of the 2–2 parallel-connected composite is shown in Fig. 2.2

4.2 1–3-Type Composites

In the 1–3 composite shown in Fig. 2.11, C1 is a component with a higher piezoelectric activity, and C2 is a component with a lower piezoelectric activity or a piezo-passive component. The presence of the parallel piezoelectric rods (either FC or SC) in a large matrix leads to the strong influence of the rods on the piezoelectric properties and their anisotropy and favours a non-monotonic behaviour of many effective parameters of the 1–3 composite [6, 8, 12]. In Sect. 4.2 we consider the piezoelectric coefficients $e_{ij}^*(m)$ and compare them to the piezoelectric coefficients $d_{ij}^*(m)$.

The first example of relations between $e_{ij}^*(m)$ and $d_{ij}^*(m)$ is shown in Fig. 4.3, where m is the volume fraction of FC. The corresponding composite contains the system of long cylindrical FC rods poled along OX_3 and regularly distributed in a piezo-passive polymer matrix. The EFM is applied [6, 10, 12] to predict the effective electromechanical properties of the 1–3 composite. The link between its piezoelectric coefficients e_{ij}^* and d_{ij}^* is described in terms of (4.1). Due to the composite microgeometry, conditions

$$e_{33}^* \gg e_{15}^* \text{ and } e_{33}^* \gg \left|e_{31}^*\right| \tag{4.6}$$

hold in wide volume-fraction ranges. For both the longitudinal and transverse piezoelectric effects, we observe the monotonic $e_{3j}^*(m)$ and $d_{3j}^*(m)$ dependences, see curves 1 and 2 in Fig. 4.3. A 'deformation' of these curves at the transition from $d_{3j}^*(m)$ to $e_{3j}^*(m)$ is accounted for by the elastic properties of the composite while (1.20) and (1.21) hold.

In the second example we consider relations between $e_{3j}^*(m)$ and $d_{3j}^*(m)$ of the 1–3 $(Pb_{1-x}Ca_x)TiO_3$ FC/araldite composite with the cylindrical FC rods arranged regularly in the polymer matrix. The $e_{3j}^*(m)$ and $d_{3j}^*(m)$ dependences shown in Fig. 4.4 were calculated by means of the EFM. We remind the reader that the poled $(Pb_{1-x}Ca_x)TiO_3$ FCs [17], like high-anisotropic $PbTiO_3$-type FCs [6, 7], are of interest due to positive signs of their piezoelectric coefficients e_{3j}, see Table 3.5. The piezoelectric coefficient e_{31} of the $(Pb_{1-x}Ca_x)TiO_3$ FCs exhibits a non-monotonic behaviour on increasing the molar concentration x in the range $0.10 \le x \le 0.30$, and this influences the mutual arrangement of the e_{31}^* curves related to the composite (see curves 1–4 in Fig. 4.4a). The monotonic increase of e_{33} of the $(Pb_{1-x}Ca_x)TiO_3$ FCs at $0.10 \le x \le 0.30$ (see Table 3.5) causes a monotonic increase of e_{33}^* at m = const (see curves 5–8 in Fig. 4.4a). We observe the monotonic $e_{3j}^*(m)$ dependences in Fig. 4.4a at the non-monotonic $d_{31}^*(m)$ behaviour and the valid condition (1.44), see curves 1–4 in Fig. 4.4b. This is an important feature of the 1–3 composite based on the FC with the large anisotropy of the piezoelectric coefficients d_{3j} [6, 18]. Due to relatively small contributions from $d_{31}^* c_{1j}^{*E}$ into e_{3j}^* from (4.1), we assume that $e_{3j}^* \approx d_{33}^* c_{3j}^{*E} > 0$, where j = 1 and 3. In

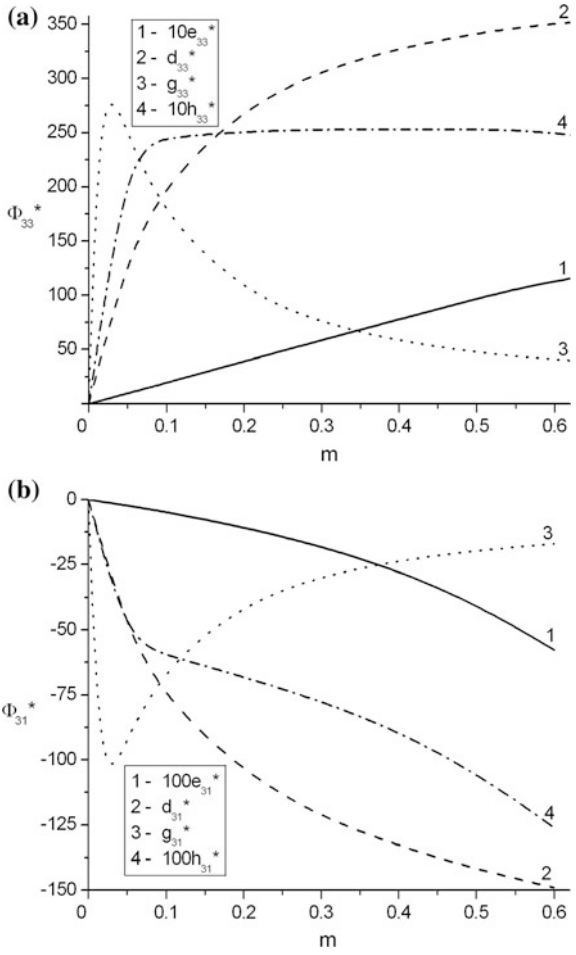

Fig. 4.3 Volume-fraction dependences of piezoelectric coefficients e^*_{3j} (in C/m^2), d^*_{3j} (in pC/N), g^*_{3j} (in mV m/N), and h^*_{3j} (in 10^8 V/m) of the 1–3 PZT-5 FC/araldite composite: **a** $j = 3$ and **b** $j = 1$ (reprinted from monograph by Topolov and Bowen [6], with permission from Springer)

this case the differences between curves 1–4 and 5–8 in Fig. 4.4a are mainly associated with the difference between the elastic moduli c^{*E}_{13} and c^{*E}_{33}.

The third example of the PS is concerned with the $e^*_{ij}(m)$ dependence in the 1–3 composite based on the KNNTL:Mn SC (Fig. 4.5). For a square arrangement of the SC rods with the square cross section, this composite is characterised by 4*mm* symmetry. The full set of electromechanical constants of the composite shown in Fig. 2.11 are calculated by means of the matrix method [6, 12] that is applied to each vertical face of the SC rod. Despite the condition $e_{33} < e_{15} < |e_{31}|$ that is valid for this SC poled along [001], the piezoelectric coefficients e^*_{ij} of the related 1–3 composite obey the conditions (4.6) in a wide volume-fraction range, see Fig. 4.5. The presence of max $e^*_{33}(m)$ is caused by a competition of the items from (4.4), see also Sect. 4.1. We can observe a deep analogy between Figs. 4.2b and 4.6 and state that a difference between the max $e^*_{33}(m)$ values of the related 1–3 and 2–2

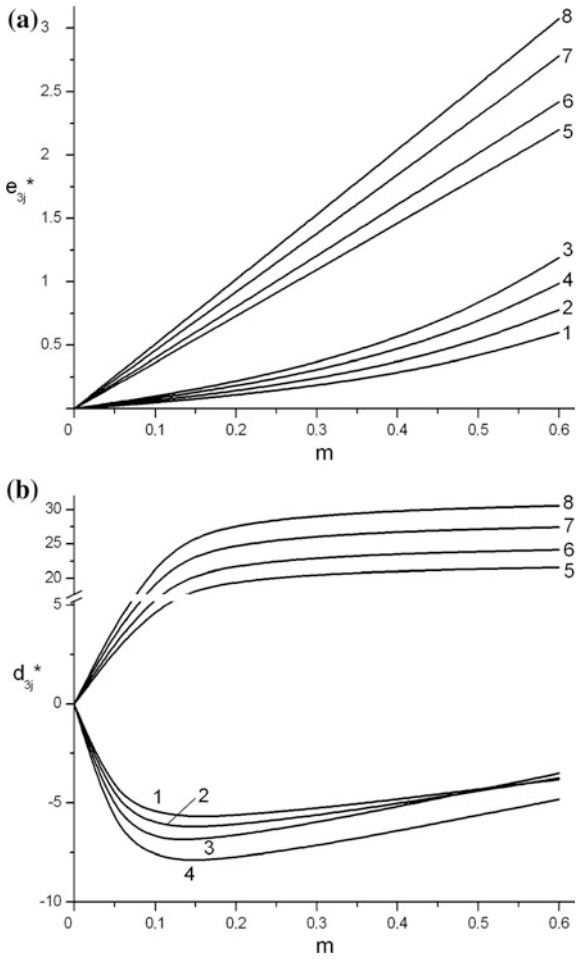

Fig. 4.4 Volume-fraction dependences of piezoelectric coefficients e_{3j}^* (**a**, in C/m^2) and d_{3j}^* (**b**, in pC/N) of the 1–3 $(Pb_{1-x}Ca_x)TiO_3$ FC/araldite composite. In each graph curves 1–4 correspond to $j = 1$, and curves 5–8 correspond to $j = 3$. Curves 1 and 5 are related to the composite with $x = 0.10$, curves 2 and 6 are related to the composite with $x = 0.20$, curves 3 and 7 are related to the composite with $x = 0.25$, and curves 4 and 8 are related to the composite with $x = 0.30$ (reprinted from paper by Topolov et al. [18], with permission from IOP Publishing)

composites is small. This is due to the continuous distribution of the SC rods (1–3 connectivity, Fig. 2.11) and SC layers (2–2 connectivity, Fig. 2.2) along the poling axis OX_3. The volume fraction of the SC component in both the 2–2 parallel-connected and 1–3 composites is determined by the specific area occupied by this component in the (X_2OX_3) plane in comparison to the whole composite sample. In both the aforementioned composites, a strain ξ_3 applied along OX_3 will generate a piezoelectric polarisation P_3 in similar way. Thus, the microgeometric feature again becomes the important factor that influences the PS and behaviour of the piezoelectric coefficients e_{ij}^* in the wide volume-fraction range.

In the fourth example, we consider a performance of the 1–3-type composite shown in Fig. 2.18a. It is assumed that the piezoelectric parallelepiped-shaped SC rods are parallel to the poling axis OX_3 and regularly distributed in the laminar matrix (2–2 connectivity), and the polymer layers of this matrix are regularly

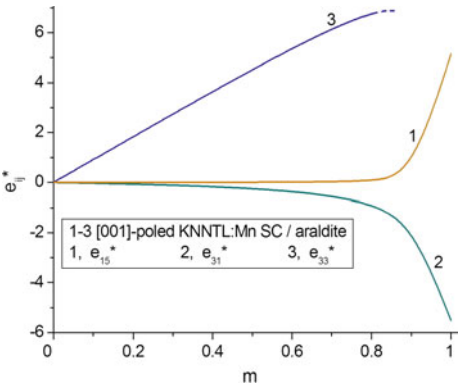

Fig. 4.5 Volume-fraction dependences of piezoelectric coefficients e^*_{ij} (in C/m^2) of the 1–3 [001]-poled KNNTL:Mn SC/araldite composite. The schematic of the 1–3 composite is shown in Fig. 2.11

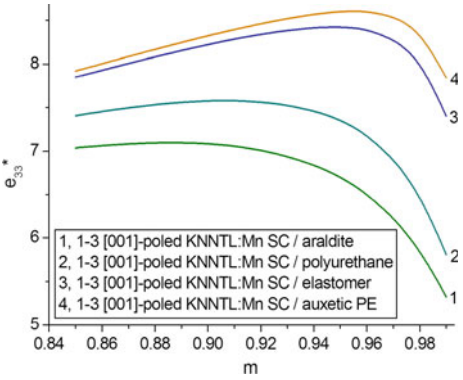

Fig. 4.6 Volume-fraction behaviour of the piezoelectric coefficient e^*_{33} (in C/m^2) near its maximum in the 1–3 composites based on the KNNTL:Mn SC. The schematic of the 1–3 composite is shown in Fig. 2.11

distributed along the poling axis OX_3. Such a composite is described by 1–2–2 connectivity, and its piezoelectric coefficients d^*_{3j} were discussed in work [19] and Sect. 2.2.3. In Table 4.3 we show relations between e^*_{3j} and d^*_{3j} at the volume fraction of araldite m_{ar} = const in the laminar matrix and the volume fraction of SC m = const. The full set of electromechanical constants of the composite was evaluated by means of FEM [19]. Due to the system of the piezoelectric SC rods (Fig. 2.18a) oriented parallel to OX_3, conditions (4.6) hold in the wide m_{ar} and m ranges. The piezoelectric coefficients e^*_{33} and d^*_{33} undergo minor changes at variations of m_{ar} and m = const (see columns 4 and 6 in Table 4.3) because the elastic compliances of the laminar matrix $|s^{(m)}_{ab}|$ and $|s^E_{ab}|$ of the SC rod obey the condition $|s^{(m)}_{ab}| \gg |s^E_{ab}|$. Changes in the elastic compliances $s^{(m)}_{ab}$ and their anisotropy at changes in the volume fractions m_{ar} and m lead to changes in the transverse piezoelectric effect, see columns 3 and 5 in Table 4.3. In general, one can state a correlation between the piezoelectric coefficients e^*_{3j} and d^*_{3j} of the 1–2–2 composite at m_{ar} = const due to a combination of elastic and piezoelectric properties. It should be added that max e^*_{33} of this composite is located in the range $0.9 < m < 1$, and the

volume fraction m related to the maximum point undergoes minor changes at variations of m_{ar}. The reason for max e_{33}^* is similar to that in the 2–2 parallel-connected (see Sect. 4.1) and 1–3 composites.

The fifth example is concerned with max e_{33}^* of the 1–3-type composites based on the [001]-poled relaxor-ferroelectric SCs. Data in Table 4.4 show that the largest value of max e_{33}^* is achieved in the PMN–0.28PT-based composite. The volume fraction m related to max e_{33}^* is smaller than in the remaining composites listed in Table 4.4. It should be mentioned that the PMN–0.28PT composition is located in the stability region of the ferroelectric rhombohedral ($3m$ symmetry) phase, and a 'distance' between this composition and the morphotropic phase boundary at the phase diagram of PMN–xPT at room temperature is approximately 5% [20, 21]. The largest max e_{33}^* value (Table 4.4) is achieved in the presence of the SC component with the unusual anisotropy of the piezoelectric coefficients e_{3j}, see the 4th column of Table 4.4. We remind for comparison that for the [001]-poled KNNTL:Mn SC promoting the large max e_{33}^*/e_{33} ratio in the related composites (see Fig. 4.6), the anisotropy of e_{3j} is characterised by the ratio [11] $e_{33}/e_{31} = -0.824$ that differs from e_{33}/e_{31} of the [001]-poled PMN–0.28PT SC by 4.4%.

In the sixth example of the PS, we show changes in max e_{33}^* of the 1–3–0 composite (Table 4.5). The composite microgeometry and procedure of evaluation of the effective properties are described in Sect. 2.2.4. In the porous 3–0 matrix of this composite we vary the aspect ratio of the air pore ρ_p and porosity m_p. We observe increasing the max e_{33}^* value on increasing m_p at ρ_p = const. The relatively

Table 4.3 Volume-fraction dependences of piezoelectric coefficients e_{ij}^* (in C/m^2) and d_{3j}^* (in pC/N) of the 1–2–2 [001]-poled PMN–0.33PT SC/araldite/polyurethane composite[a]

m_{ar}	m	e_{31}^*	e_{33}^*	d_{31}^*	d_{33}^*
0.05	0.5	−0.0347	11.8	−914	2580
	0.7	−0.0784	16.4	−1100	2710
	0.9	−0.276	21.0	−1260	2790
0.10	0.5	−0.0427	11.8	−885	2560
	0.7	−0.0962	16.4	−1080	2700
	0.9	−0.333	20.9	−1250	2790
0.20	0.5	−0.0586	11.7	−849	2520
	0.7	−0.131	16.4	−1060	2680
	0.9	−0.440	20.8	−1250	2790
0.30	0.5	−0.0745	11.7	−827	2490
	0.7	−0.166	16.4	−1050	2660
	0.9	−0.539	20.7	−1240	2780
0.40	0.5	−0.0905	11.7	−811	2450
	0.7	−0.200	16.3	−1040	2640
	0.9	−0.632	20.7	−1240	2770
0.50	0.5	−0.107	11.7	−799	2400
	0.7	−0.234	16.3	−1030	2620
	0.9	−0.720	20.7	−1240	2770

[a]See the schematic of the 1–2–2 composite in Fig. 2.18a

Table 4.4 Maximum values of the piezoelectric coefficient e_{ij}^* (in C/m^2) of 1–3-type [001]-poled PMN–xPT SC/auxetic PE and [001]-poled PZN–yPT SC/auxetic PE composites,[a] the piezoelectric coefficient e_{33} (in C/m^2) and anisotropy factor e_{33}/e_{31} of SC

SC	max e_{33}^*	e_{33}	e_{33}/e_{31}
PMN–0.33PT	22.3 (m = 0.937)[b]	21.0	−7.58
PMN–0.30PT	28.1 (m = 0.984)	27.0	−11.2
PMN–0.28PT	30.9 (m = 0.949)	17.7	−0.860
PZN–0.045PT	17.1 (m = 0.963)	14.0	−2.92
PZN–0.07PT	16.4 (m = 0.976)	15.0	−6.43
PZN–0.08PT	19.1 (m = 0.968)	15.9	−3.46

[a]See the schematic of the 1–3-type composite in Fig. 2.11
[b]Volume fraction at which max e_{33}^* is achieved in the composite

Table 4.5 Maximum values of the piezoelectric coefficient e_{ij}^* (in C/m^2) of the 1–3–0 [001]-poled PMN–0.28PT SC/porous araldite composite[a]

ρ_p	m_p	max e_{33}^*
0.01	0.1	26.1 (m = 0.891)[b]
	0.2	27.1 (m = 0.902)
	0.3	27.9 (m = 0.912)
1	0.1	25.5 (m = 0.884)
	0.2	26.1 (m = 0.891)
	0.3	26.8 (m = 0.899)
100	0.1	26.6 (m = 0.892)
	0.2	27.0 (m = 0.897)
	0.3	27.4 (m = 0.903)

[a]See the schematic of the 1–3–0 composite in Fig. 2.19
[b]Volume fraction at which max e_{33}^* is achieved in the composite

small differences between the max e_{33}^* values at m_p = const (see Table 4.5) are accounted for by a restricted influence of elastic properties of the porous matrix on the piezoelectric performance of the composite at large volume fractions m. As seen from Table 4.5, irrespective of ρ_p and porosity m_p, max e_{33}^* of the composite is achieved at $m \approx 0.9$, i.e., at the obvious prevalence of SC over porous polymer. The max e_{33}^* values listed in Table 4.5 are smaller than max e_{33}^* of the related PMN–0.28PT-based composite from Table 4.4. This is due to the larger elastic stiffness of the porous araldite in comparison to auxetic PE.

4.3 0–3-Type Composites

In the case of the 0–3 composite configuration (Fig. 2.28), there are restricted opportunities to vary its PS because of the isolated piezoelectric inclusions. The 0–3 composite shown in Fig. 2.28 consists of the three-dimensionally connected matrix

reinforced by a system of the spheroidal inclusions (either FC or SC), and the poling axis is OX_3. The shape of each inclusion is described by (2.13) in the axes of the rectangular co-ordinate system ($X_1X_2X_3$), semi-axes of the inclusion are a_1, $a_2 = a_1$ and a_3, and its aspect ratio is $\rho = a_1/a_3$. As in Sect. 2.4, we consider the composite with the regular distribution of the inclusions in the large matrix, and ρ = const is assumed for each inclusion.

In Table 4.6 we show the piezoelectric coefficients e_{3j}^* and d_{3j}^* of the 0–3 SC/polymer and SC/FC composites wherein the main piezoelectric component is a domain-engineered PMN–0.33PT SC. The piezoelectric coefficients e_{3j}^* and d_{3j}^* were calculated by means of FEM, see details in monograph [12]. The aspect ratio ρ from the range of $0.1 \leq \rho \leq 0.5$ is related to the prolate inclusion aligned along the OX_3 axis, and such a shape and arrangement of the SC inclusions would facilitate poling of the 0–3 composite sample (Fig. 2.28) in the electric field $\boldsymbol{E} \| OX_3$. However even in this case we observe the considerable decrease of the piezoelectric coefficients $|d_{ij}^*|$ of the composite (see columns 7–9 in Table 4.6) in comparison to the piezoelectric coefficients $|d_{ij}|$ of its SC component (see columns 8–10 in Table 1.3). An increase of the piezoelectric coefficients $|d_{3j}^*|$ takes place when replacing the araldite matrix with the poled FC matrix, i.e., in the presence of two piezoelectric components. The larger $|d_{3j}^*|$ and $|e_{3j}^*|$ values at m = const and ρ = const are expected in the composite with the PMN–0.35PT FC matrix as compared to the composite with the modified $PbTiO_3$ (I) FC matrix, see Table 4.6. This is due to the larger piezoelectric coefficients $|d_{ij}|$ of the PMN–0.35PT FC (see Table 1.5). The matrix in the 0–3 PMN–0.33PT SC/PMN–0.35PT FC composite actively promotes its PS and large $|e_{3j}^*|$ values at relatively small differences between elastic properties of the SC and FC components. We also note minor changes in e_{ij}^* and d_{ij}^* of the 0–3 PMN–0.33PT SC/PMN–0.35PT FC composite at changes of the aspect ratio ρ, see Table 4.6.

A modification of the FC matrix leads to some changes in the PS of the composite. Now we assume that the FC matrix contains spherical air pores that are distributed regularly. The shape of each air pore is described by (2.18) at the condition $a_{1,p} = a_{2,p} = a_{3,p}$. The SC/porous FC composite is described by 0–3–0 connectivity, and an example of the PS of such a composite is shown in Table 4.7. Decreasing $|e_{ij}^*|$ in comparison to the related 0–3 composite (see Table 4.6) is caused by the porous FC matrix whose elastic compliances are larger than those of the monolithic FC matrix. However, on the same reason, the larger $|d_{ij}^*|$ values in comparison to the 0–3 SC/FC composite are achieved. The minor changes in the piezoelectric coefficients e_{ij}^* and d_{ij}^* at changes of the aspect ratio ρ (see Table 4.7) are observed because of the piezoelectric components with the comparable piezoelectric coefficients e_{ij}.

Table 4.6 Aspect-ratio (ρ) and volume-fraction (m) dependences of piezoelectric coefficients e_{ij}^* (in C/m^2) and d_{ij}^* (in pC/N) of 0–3 SC/polymer composites[a] based on the [001]-poled PMN–0.33PT SC

Matrix components	ρ	m	e_{31}^*	e_{33}^*	e_{15}^*	d_{31}^*	d_{33}^*	d_{15}^*
Araldite	0.1	0.1	−0.0246	0.631	4.20×10^{-4}	−27.2	70.1	0.200
		0.3	−0.140	2.73	2.96×10^{-3}	−67.5	161	0.820
		0.5	−0.475	5.84	3.20×10^{-2}	−121	26.7	3.99
	0.3	0.1	-6.88×10^{-3}	0.0467	4.20×10^{-4}	−3.04	7.25	0.210
		0.3	-5.04×10^{-2}	0.255	3.14×10^{-3}	−9.12	20.4	0.860
		0.5	−0.242	1.02	3.46×10^{-2}	−20.5	43.1	4.35
	0.5	0.1	-3.54×10^{-3}	1.44×10^{-2}	5.10×10^{-4}	−1.19	2.68	0.230
		0.3	-2.60×10^{-2}	8.37×10^{-2}	3.34×10^{-3}	−3.99	8.57	0.900
		0.5	−0.138	0.458	3.43×10^{-2}	−10.3	22.0	4.28
Modified $PbTiO_3$ (I) FC	0.1	0.1	−0.121	8.36	3.84	−14.2	74.6	70.9
		0.3	−0.897	11.2	4.54	−36.3	126	79.0
		0.5	−1.71	13.9	5.63	−75.8	212	92.4
	0.3	0.1	-8.69×10^{-2}	8.19	3.85	−13.7	72.8	71.0
		0.3	−0.814	10.8	4.55	−34.5	120	79.0
		0.5	−1.60	13.4	5.64	−71.9	201	92.7
	0.5	0.1	-3.84×10^{-2}	8.01	3.84	−13.1	70.7	71.0
		0.3	−0.679	10.3	4.55	−31.9	113	79.2
		0.5	−1.47	13.0	5.67	−67.6	190	93.1
PMN–0.35PT FC	0.1	0.1	−4.89	27.2	13.9	−232	505	422
		0.3	−4.66	25.7	13.1	−275	595	329
		0.5	−4.44	24.2	12.3	−346	742	259
	0.3	0.1	−4.89	27.2	13.9	−233	509	422
		0.3	−4.66	25.7	13.1	−280	606	330
		0.5	−4.44	24.1	12.3	−353	757	259
	0.5	0.1	−4.89	27.2	13.9	−235	513	423
		0.3	−4.66	25.7	13.2	−284	615	331
		0.5	−4.44	24.1	12.3	−358	769	260

[a]See the schematic of the 0–3 composite in Fig. 2.28

Table 4.7 Aspect-ratio (ρ) and volume-fraction (m) dependences of piezoelectric coefficients e_{ij}^* (in C/m^2) and d_{ij}^* (in pC/N) of the 0–3–0 [001]-poled PMN–0.33PT SC/porous PMN–0.35PT FC[a] composite

ρ	m	e_{31}^*	e_{33}^*	e_{15}^*	d_{31}^*	d_{33}^*	d_{15}^*
0.1	0.1	−1.72	16.5	8.80	−206	500	396
	0.3	−2.13	17.4	9.24	−279	651	313
	0.5	−2.58	18.3	9.54	−391	880	246
0.3	0.1	−1.78	16.5	8.89	−208	504	396
	0.3	−2.27	17.5	9.22	−284	659	312
	0.5	−2.73	18.4	9.52	−397	889	245
0.5	0.1	−1.84	16.5	8.87	−210	507	395
	0.3	−2.42	17.5	9.19	−288	665	312
	0.5	−2.87	18.4	9.48	−401	896	244

[a]The matrix is a poled FC medium with spherical air pores at porosity $m_p = 0.3$. The SC component is represented by a system of aligned spheroidal inclusions that are distributed in the porous FC matrix

4.4 Conclusion

This chapter has been devoted to the piezoelectric coefficients e_{ij}^*, PS and their links to the piezoelectric coefficients d_{ij}^* in various composites. Changes in the piezoelectric coefficients e_{ij}^* enable us to show ways for improving the PS of the studied composites. The main results of this chapter are formulated in the following form.

(i) Examples of the composites based on either FCs or domain-engineered SCs are considered, and the following connectivity patterns are of interest to reach large values of the piezoelectric coefficients e_{ij}^*: 1–3, 1–2–2, 1–3–0, and 2–2. Changes in the volume fraction of the piezoelectric component and microgeometry of the composite enable us to vary e_{ij}^* and their anisotropy, however these variations are less appreciable in comparison to those considered in Chaps. 2 and 3. The main reason consists in the relatively narrow range wherein the piezoelectric coefficients e_{ij} of various materials are found.

(ii) The system of the piezoelectric rods or layers which are oriented parallel to the poling axis OX_3 (see Figs. 2.2, 2.11, 2.18a, and 2.19) promotes the large piezoelectric coefficient e_{33}^* and influences the anisotropy of e_{3j}^* in the composite. Examples of validity of conditions (4.2), (4.3) and (4.6) are considered for a few composites, and features of the volume-fraction behaviour of e_{ij}^* are interpreted by taking into account microgeometric characteristics of the composites.

(iii) Relations between the piezoelectric coefficients e_{ij}^* and d_{ij}^* are analysed for various composites, and the effect of combination of the anisotropic elastic and piezoelectric properties is highlighted. The role of the elastic properties in forming max e_{33}^* and validity of conditions (4.5) for the 1–3-type

composites are discussed. The large max e_{33}^* value in comparison to e_{33} of the piezoelectric component is achieved in the 1–3-type composites that are based on either the [001]-poled KNNTL:Mn SC (Fig. 4.6) or PMN–0.28PT SC (Table 4.4). In both these SCs, the unusual anisotropy of the piezoelectric coefficients e_{3j} strongly influences the longitudinal piezoelectric effect in the composites and e_{33}^* related to this effect. The large piezoelectric coefficients d_{3j} of the SC (or FC) component cannot serve as a pledge to achieve large e_{33}^* values in the composite based on this component.

(iv) In the 0–3 and 0–3–0 composites the piezoelectric coefficients e_{3j}^* undergo changes in restricted ranges due to the isolated piezoelectric inclusions. These changes are caused by changes of the aspect ratio of the inclusions or porosity of the matrix in the 0–3-type composites.

The PS associated with the piezoelectric coefficients e_{ij}^* is to be taken into account in sensor applications where surface charges can be detected on a deformed sample or where a mechanical stress field is caused by an electric field applied to a sample.

References

1. Zheludev IS (1971) Physics of crystalline dielectrics. Vol 2: Electrical properties. Plenum, New York
2. Jaffe B, Cook WR, Jaffe H (1971) Piezoelectric ceramics. Academic Press, London
3. Ikeda T (1990) Fundamentals of piezoelectricity. Oxford University Press, New York
4. Steinem C, Janshoff A (eds) (2007) Piezoelectric sensors. Springer, Berlin
5. Sharapov V (2011) Piezoceramic sensors. Springer, Heidelberg
6. Topolov VYu, Bowen CR (2009) Electromechanical properties in composites based on ferroelectrics. Springer, London
7. Ikegami S, Ueda I, Nagata T (1971) Electromechanical properties of $PbTiO_3$ ceramics containing La and Mn. J Acoust Soc Am 50:1060–1066
8. Khoroshun LP, Maslov BP, Leshchenko PV (1989) Prediction of effective properties of piezo-active composite materials. Naukova Dumka, Kiev (in Russian)
9. Huebner W, Reidmeyer MR, Stevenson JW, Busse L (1995) Fabrication of 2–2 connectivity PZT/thermoplastic composites for high efficiency linear arrays. In: Pandey RK, Liu M, Safari A (eds) ISAF'94: Proceedings of the ninth IEEE international symposium on applications of ferroelectrics. University Park, Pennsylvania, USA, 7–10 August 1994. IEEE, Piscataway, pp 206–209
10. Krivoruchko AV, Topolov VYu (2007) On the remarkable performance of novel 2–2-type composites based on [011] poled $0.93Pb(Zn_{1/3}Nb_{2/3})O_3$–$0.07PbTiO_3$ single crystals. J Phys D Appl Phys 40:7113–7120
11. Huo X, Zhang R, Zheng L, Zhang S, Wang R, Wang J, Sang S, Yang B, Cao W (2015) (K, Na, Li)(Nb, Ta)O_3:Mn lead-free single crystal with high piezoelectric properties. J Am Ceram Soc 98:1829–1835
12. Topolov VYu, Bisegna P, Bowen CR (2014) Piezo-active composites. Orientation effects and anisotropy factors. Springer, Berlin, Heidelberg

13. Topolov VYu, Krivoruchko AV (2009) Polarization orientation effect and combination of electromechanical properties in advanced $0.67Pb(Mg_{1/3}Nb_{2/3})O_3$–$0.33PbTiO_3$ single crystal/polymer composites with 2–2 connectivity. Smart Mater Struct 18:065011
14. Newnham RE, Skinner DP, Cross LE (1978) Connectivity and piezoelectric-pyroelectric composites. Mater Res Bull 13:525–536
15. Topolov VYu, Bowen CR, Ermakov IA (2016) Remarkable hydrostatic piezoelectric response of novel 2–0–2 composites. Ferroelectr Lett Sect 43:90–95
16. Topolov VYu, Bowen CR, Krivoruchko AV (2017) Piezoelectric performance and hydrostatic parameters of novel 2–2-type composites. IEEE Trans Ultrason Ferroelectr Freq Control 64:1599–1607
17. Glushanin SV, Topolov VYu, Krivoruchko AV (2006) Features of piezoelectric properties of 0–3 $PbTiO_3$-type ceramic/polymer composites. Mater Chem Phys 97:357–364
18. Topolov VYu, Bisegna P, Krivoruchko AV (2008) Features of electromechanical properties of 1–3 composites based on $PbTiO_3$-type ceramics. J Phys D Appl Phys 41:035406
19. Bowen CR, Topolov VYu, Isaeva AN, Bisegna P (2016) Advanced composites based on relaxor-ferroelectric single crystals: from electromechanical coupling to energy-harvesting applications. CrystEngComm 18:5986–6001
20. Shuvaeva VA, Glazer AM, Zekria D (2005) The macroscopic symmetry of $Pb(Mg_{1/3}Nb_{2/3})_{1-x}Ti_xO_3$ in the morphotropic phase boundary region (x = 0.25–0.5). J Phys: Condens Matter 17:5709–5723
21. Singh AK, Pandey D, Zakharko O (2006) Powder neutron diffraction study of phase transitions in and a phase diagram of $(1-x)[Pb(Mg_{1/3}Nb_{2/3})O_3]$–$xPbTiO_3$. Physical Review B 74:024101

Chapter 5
Piezoelectric Coefficients h_{ij}^*: New Opportunities to Improve Sensitivity

Abstract Piezoelectric coefficients h_{ij} characterise a link between an external mechanical strain applied to a sample and an electric field caused by the direct piezoelectric effect. At the converse piezoelectric effect, the piezoelectric coefficients h_{ij} characterise the link between a mechanical stress in the sample and electric displacement. Examples of the volume-fraction behaviour of the effective piezoelectric coefficients h_{ij}^* and the piezoelectric sensitivity associated with h_{ij}^* are analysed for the 2–2-type, 1–3-type and 0–3-type composites based on ferroelectrics. Relations between the piezoelectric coefficients h_{ij}^* and e_{ij}^* and some cases of the large anisotropy of h_{3j}^* are discussed for some composites.

In comparison to the piezoelectric coefficients d_{ij} and g_{ij}, the piezoelectric coefficients h_{ij} are considered and analysed in the literature on piezoelectric materials and applications to a small degree; see, for instance, monographs [1–3]. As is known from (1.11), the piezoelectric coefficients h_{ij} characterise the link between an external mechanical strain ξ_j that is applied to a sample and an electric field E_i caused by the direct piezoelectric effect. At the the converse piezoelectric effect, the piezoelectric coefficients h_{ij} are introduced to describe the link between a mechanical stress σ_j and an electric displacement D_i as shown in (1.10). In both the aforementioned links, the piezoelectric coefficients h_{ij} are accompanied by the minus sign, and it is an important feature of the piezoelectric effect [1, 3] described in terms of (1.10) and (1.11). The PS concerned with h_{ij} can be associated with a voltage between surfaces of the deformed sample, and this is important for piezoelectric sensor applications and monitoring the quality control of a production, surfaces of machine parts etc. [4, 5]. Equations (1.21) and (1.22) show that the piezoelectric coefficients d_{ij} and h_{ij} are linked by elastic and dielectric properties. The elastic properties are described by a fourth-rank tensor, and the dielectric properties are described by a second-rank tensor. Such an intricate character of the link between d_{ij} and h_{ij} in an anisotropic piezoelectric medium makes the problem of the microgeometry—PS relations more complicated and cannot lead to simple solutions concerning the effective properties of piezo-active composites. As follows from (1.21) and (1.23), the piezoelectric coefficients h_{ij} and e_{ij} are linked by the

V. Y. Topolov et al., *Piezo-Active Composites*, Springer Series
in Materials Science 271, https://doi.org/10.1007/978-3-319-93928-5_5

dielectric properties that are described by a second-rank tensor. This facilitates an analysis of the PS in terms of h_{ij} and by taking into account features of the behaviour of the piezoelectric coefficients e_{ij} (see Chap. 4). Like e_{ij}, the piezoelectric coefficients h_{ij} of the perovskite-type FCs [6] are divided into two groups. The first group contains materials with $h_{31} < 0$ and $h_{33} > 0$, and the second group contains materials with $h_{31} > 0$ and $h_{33} > 0$. For both these groups, the condition $h_{15} > 0$ holds. We remind that for poled FCs, the relation $\mathrm{sgn}e_{3j} = \mathrm{sgn}h_{3j}$ holds because of validity of (1.21) and (1.23).

In this chapter we describe examples of the PS of composites in terms of their effective piezoelectric coefficients h^*_{ij} and relations between h^*_{ij} and e^*_{ij}. Of specific interest are examples of the non-monotonic volume-fraction behaviour of h^*_{ij}, large values of $|h^*_{ij}|$ and large anisotropy of h^*_{ij} of some composites. We add that the main piezoelectric component of the studied composites is either the poled FC or domain-engineered SC.

5.1 2–2-Type Composites

The 2–2 composite structure shown in Figs. 2.1 and 2.2 is characterised by a system of alternating layers of two components, and at least one of them is piezoelectric, e.g. poled FC or SC. We assume that the OX_3 axis shown in Figs. 2.1 and 2.2 is the poling axis of the composite sample as a whole. In this section we discuss volume-fraction dependences of the piezoelectric coefficients h^*_{ij} in both series- and parallel-connected 2–2-type composites. Hereby we apply the matrix method [6] to determine the effective electromechanical properties of the 2–2-type composite (see details in Sect. 2.1.1).

The first example of the PS is concerned with a 2–2 series-connected composite based on FC. We remind that due to the poled FC layers and interfaces oriented perpendicular to the poling axis OX_3 (Fig. 2.1), the series-connected FC/polymer composite is described by ∞mm symmetry. In accordance with (1.21), the link between the piezoelectric coefficients e^*_{ij} and h^*_{ij} of such a composite is given by the following relations:

$$e^*_{31} = e^*_{32} = h^*_{31}\varepsilon^{*\xi}_{33},\ e^*_{33} = h^*_{33}\varepsilon^{*\xi}_{33} \text{ and } e^*_{15} = e^*_{24} = h^*_{15}\varepsilon^{*\xi}_{11}. \tag{5.1}$$

Relations between the piezoelectric coefficients e^*_{ij} and h^*_{ij} of the composite based on the PCR-7 M FC at large volume fractions of FC m are shown in Table 5.1. It is an original case of the composite for which conditions

$$\left|h^*_{31}\right| \gg h^*_{33} \text{ and } \left|h^*_{31}\right| \gg h^*_{15} \tag{5.2}$$

Table 5.1 Volume-fraction dependences of piezoelectric coefficients h_{ij}^* (in 10^8 V/m) and e_{ij}^* (in C/m^2) of 2–2 FC/polymer series-connected composites[a] at large volume fractions of FC m

Polymer	m	h_{31}^*	h_{33}^*	h_{15}^*	e_{31}^*	e_{33}^*	e_{15}^*
Composite based on the PCR-7 M FC							
Araldite	0.80	−9.63	2.80	3.18	−0.169	0.0492	7.14
	0.90	−10.0[a]	5.33	4.98	−0.349	0.186	11.1
	0.95	−9.40	8.63	6.93	−0.644	0.590	14.5
Elastomer	0.80	−10.6	0.466	0.256	−0.233	0.0102	0.704
	0.90	−11.7	1.02	0.501	−0.510	0.0443	1.52
	0.95	−12.0[b]	2.03	0.960	−1.03	0.173	2.96
Auxetic PE	0.80	−10.8	0.315	1.25	−0.109	0.00319	3.20
	0.90	−12.0	0.694	2.26	−0.242	0.0140	6.00
	0.95	−12.4[c]	1.41	3.77	−0.495	0.0564	9.49
Composite based on the modified $PbTiO_3$ (III) FC							
Araldite	0.80	−2.16	8.50	3.59	−0.0350	0.138	0.572
	0.90	−1.56	16.0	5.88	−0.0452	0.465	1.04
	0.95	−0.477	25.4	8.63	−0.0228	1.21	1.58
Elastomer	0.80	−3.77	1.44	0.272	−0.0750	0.0285	0.0440
	0.90	−4.01	3.13	0.536	−0.141	0.110	0.0973
	0.95	−3.80	6.20	1.04	−0.217	0.354	0.198
Auxetic PE	0.80	−4.15	0.970	1.36	−0.0402	0.00938	0.219
	0.90	−4.51	2.13	2.51	−0.0821	0.0389	0.451
	0.95	−4.43	4.32	4.35	−0.141	0.141	0.815

[a]See the schematic of the 2–2 series-connected composite in Fig. 2.1
[b]Diffuse min $h_{31}^* \approx -10.0 \times 10^8$ V/m is observed at m = 0.87–0.90
[c]Diffuse min $h_{31}^* \approx -12.0 \times 10^8$ V/m is observed at m = 0.93–0.96
[d]Diffuse min $h_{31}^* \approx -12.4 \times 10^8$ V/m is observed at m = 0.94–0.97

hold in specific ranges of m. This is accounted for by the orientation of the FC layers (see C1 in Fig. 2.1) with respect to the poling axis OX_3. At such an orientation, dielectric properties of the composite play the active role in the combination effect in accordance with (5.1), and the transverse PS concerned with h_{31}^* becomes dominating. However in a composite based on the modified $PbTiO_3$ FC, the piezoelectric coefficient h_{33}^* undergoes considerable changes (see Table 5.1), and conditions (5.2) become invalid. Such a performance is achieved due to positive signs of h_{3j} and a large anisotropy of h_{3j} of the FC component, see data in Table 1.6. In both the aforementioned 2–2 series-connected composites, changes in the piezoelectric coefficient h_{15}^* are appreciable in the relatively narrow volume-fraction range (m = 0.80–0.95, see Table 5.1) and depend on elastic properties of the polymer component.

The next important example of the PS is related to a 2–2 parallel-connected composite based on the [001]-poled KNNTL:Mn SC. This SC is of value as a piezoelectric material with large values of $|h_{3j}|$ at $|h_{31}| > h_{33}$: in accordance with

experimental data by Huo et al. [7], $h_{31} = -1.29 \times 10^{10}$ V/m and $h_{33} = 1.06 \times 10^{10}$ V/m. These values are about two orders-of-magnitude larger than h_{3j} of the perovskite FCs listed in Table 1.6. Figure 5.1 shows that the piezoelectric coefficients h_{ij}^* of the parallel-connected composite obey conditions

$$h_{33}^* \gg \left|h_{31}^*\right|,\ h_{33}^* \gg \left|h_{32}^*\right|,\ h_{33}^* \gg h_{15}^*, \quad \text{and} \quad h_{33}^* \gg h_{24}^* \tag{5.3}$$

in specific volume-fraction ranges, including a region near diffuse max h_{33}^* (see curve 5 in Fig. 5.1). The system of the interfaces $x_1 = \text{const}$ in the parallel-connected composite shown in Fig. 2.2 becomes an important factor that leads to the dominating longitudinal PS and validity of conditions (5.2). An even increase of the dielectric permittivity $\varepsilon_{33}^{*\xi}$ in the wide m range and the non-monotonic behaviour of the piezoelectric coefficient e_{33}^* (see curve 5 in Fig. 4.2 a) promote the large value of max h_{33}^* in accordance with (5.1). We note that the mutual arrangement of curves in Fig. 5.1 differs from the arrangement in Fig. 4.2a where the volume-fraction dependences of e_{ij}^* are represented for the same 2–2 composite. Such a difference is accounted for by the strong influence of dielectric properties of the composite on their piezoelectric coefficients h_{ij}^*.

5.2 1–3-Type Composites

In this section we discuss examples of the piezoelectric coefficients h_{ij}^* the 1–3 and related composites. In Fig. 2.11 where the typical 1–3 composite is shown, C1 is a component with a higher piezoelectric activity (e.g. poled FC or domain-engineered SC), and C2 is a component with a lower piezoelectric activity or a piezo-passive component.

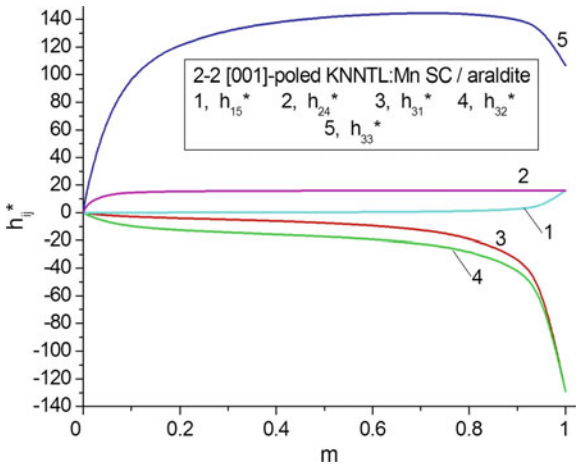

Fig. 5.1 Volume-fraction dependences of piezoelectric coefficients h_{ij}^* (in 10^8 V/m) of the 2–2 [001]-poled KNNTL: Mn SC/araldite parallel-connected composite. The schematic of the 2–2 parallel-connected composite is shown in Fig. 2.2

The first example is concerned with the 1–3 PZT-5 FC/araldite composite whose piezoelectric coefficients d_{3j}^*, e_{3j}^*, g_{3j}^*, and h_{3j}^* are shown in Fig. 4.3. To a large extent, changes in h_{3j}^* correlate with changes in d_{3j}^* and e_{3j}^* in the studied volume-fraction range. The longitudinal piezoelectric coefficient h_{33}^* of the 1–3 composite obeys conditions

$$h_{33}^* \gg \left|h_{31}^*\right| \text{ and } h_{33}^* \gg h_{15}^* \tag{5.4}$$

in the wide volume-fraction (m) range. Thus, the system of the aligned FC rods poled along the OX_3 axis (Fig. 2.11) would promote the considerable PS concerned with h_{33}^* of the 1–3 composite.

In the second example we show Fig. 5.2 where the piezoelectric coefficients h_{ij}^* of composites based on the KNNTL:Mn SC are represented at $0 < m < 1$. Changes in the polymer component lead to minor changes in the $h_{ij}^*(m)$ dependence. This dependence is formed at the active influence of the piezoelectric coefficients e_{ij}^* and dielectric permittivities $\varepsilon_{pp}^{*\xi}$ in accordance with (5.1). However these properties

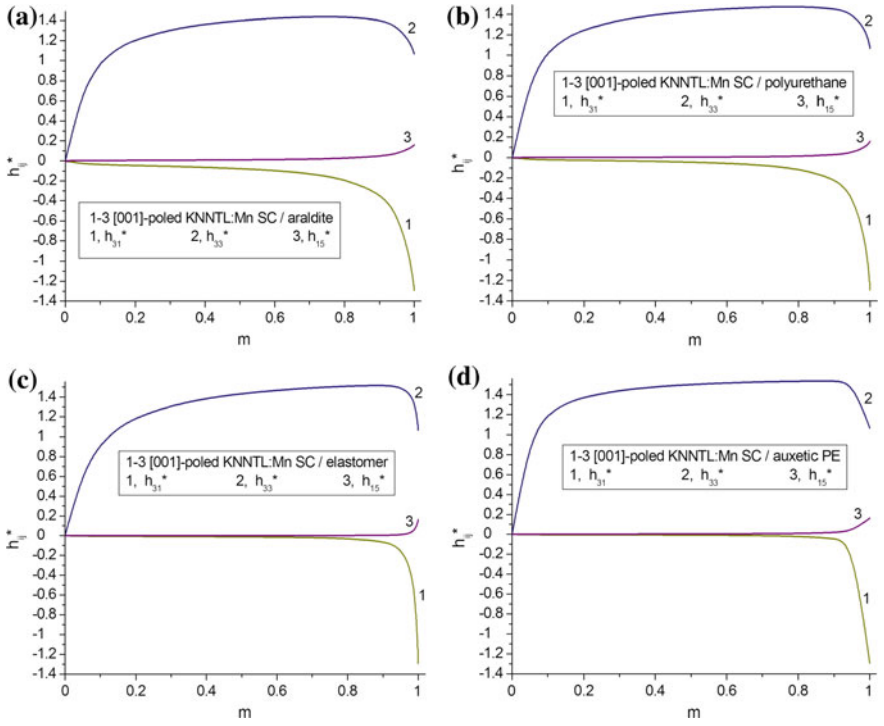

Fig. 5.2 Volume-fraction dependences of piezoelectric coefficients h_{ij}^* (in 10^{10} V/m) of 1–3 [001]-poled KNNTL:Mn SC/polymer composites. The schematic of the 1–3 composite is shown in Fig. 2.11

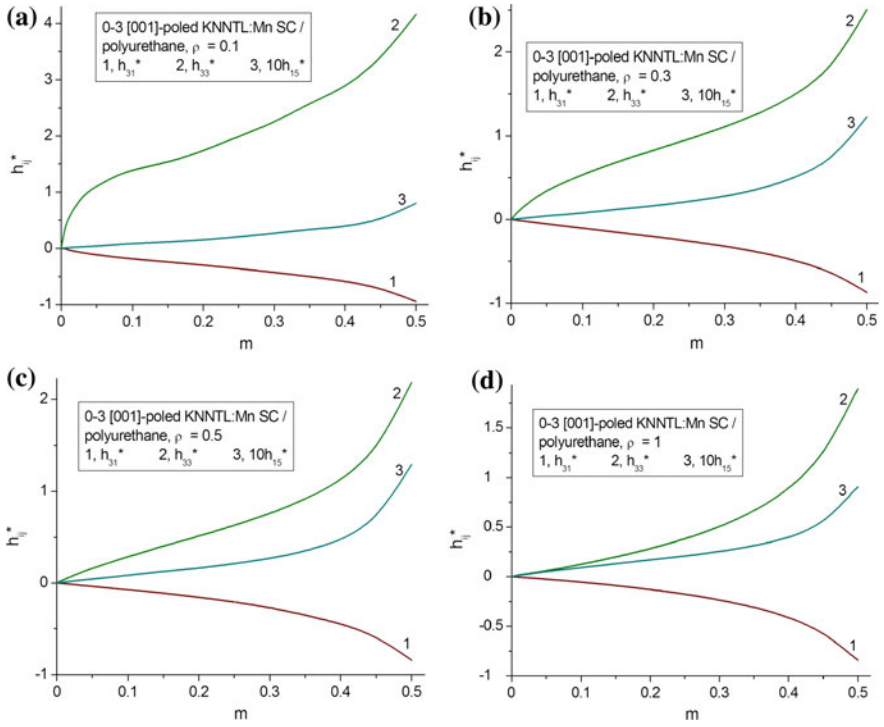

Fig. 5.3 Volume-fraction dependences of piezoelectric coefficients h^*_{ij} (in 10^9 V/m) of the 0–3 [001]-poled KNNTL:Mn SC/polyurethane composite at ρ = const. The schematic of the 0–3 composite is shown in Fig. 2.28

undergo minor changes when replacing the polymer matrix in the 1–3 composite from Fig. 2.11. Changes in the polymer component do not lead to considerable changes of the value of max h^*_{33} (see curve 2 in Fig. 5.3) that is achieved at large volume fractions m. We add that this value is comparable to that found for the related 2–2 parallel-connected composite, see curve 5 in Fig. 2.2.

In the third example we consider relations between max e^*_{33} and max h^*_{33} which are found for a 1–3–0 composite with a porous polymer matrix. Such a composite is described in Sect. 2.2.4, see the schematic in Fig. 2.19. As follows from Table 5.2, changes in the porous polymer matrix would lead to tiny changes in max h^*_{33}, both in its value and location. The large values of the volume fractions m related to max h^*_{33} suggest that the elastic properties of the porous matrix would play a secondary role in forming the large piezoelectric coefficient h^*_{33}. It is also seen from Table 5.2 that max e^*_{33} is achieved at large (but smaller in comparison to max h^*_{33}) values of m. As a consequence, changes in max e^*_{33} at changes in the porous matrix become not very considerable. Like the 1–3 composites considered in the previous examples, the 1–3–0 composite based on the PMN–0.28PT SC is characterised by the large anisotropy of h^*_{3j}, and conditions (5.4) are valid in the wide m range.

Table 5.2 Maxima of piezoelectric coefficients h^*_{33} (in 10^{10} V/m) and e^*_{33} (in C/m^2) of the 1–3–0 [001]-poled PMN–0.28PT SC/porous araldite composite[a]

Porosity m_p in the matrix	Aspect ratio $\rho_p = 0.01$		Aspect ratio $\rho_p = 1$		Aspect ratio $\rho_p = 100$	
	max h^*_{33}	max e^*_{33}	max h^*_{33}	max e^*_{33}	max h^*_{33}	max e^*_{33}
0.1	0.431 (0.992)[b]	26.1 (0.891)	–[c]	25.5 (0.884)	0.434 (0.938)	26.6 (0.892)
0.2	0.432 (0.967)	27.1 (0.902)	0.431 (0.988)	26.1 (0.891)	0.435 (0.938)	27.0 (0.897)
0.3	0.433 (0.959)	27.9 (0.912)	0.432 (0.971)	26.8 (0.899)	0.435 (0.939)	27.4 (0.903)

[a]See the schematic of the composite in Fig. 2.19
[b]The volume fraction of SC m that is related to the maximum value is given in parentheses
[c]Monotonic $h^*_{33}(m)$ dependence

5.3 0–3-Type Composites

The 0–3 composite shown in Fig. 2.28 consists of the large matrix reinforced by the spheroidal inclusions (either FC or SC), and the poling axis of the composite as a whole is OX_3. We assume that the shape of each inclusion is described by (2.13) in the axes of the rectangular co-ordinate system ($X_1X_2X_3$), semi-axes of each inclusion are a_1, $a_2 = a_1$ and a_3, and its aspect ratio is defined as $\rho = a_1/a_3$. As in Sect. 2.4, we assume that the composite is characterised by the regular distribution of the spheroidal inclusions in the matrix. In this section we consider the PS of some 0–3-type composites whose electromechanical properties are evaluated by means of the FEM.

Graphs in Fig. 5.3 suggest that in a case of prolate SC inclusions poled along [001] $\parallel OX_3$, the piezoelectric coefficient h^*_{33} obeys conditions (5.4), i.e., the longitudinal PS is dominating. However for the [001]-poled KNNTL:Mn SC, $h_{33} = 1.06 \times 10^{10}$ V/m [7] that is a few times larger than h^*_{33} predicted for the 0–3

Table 5.3 Aspect-ratio (ρ) and volume-fraction (m) dependences of piezoelectric coefficients h^*_{ij} (in 10^9 V/m) and e^*_{ij} (in C/m^2) of the 0–3–0 [001]-poled PMN–0.33PT SC/porous PMN–0.35PT FC[a] composite

ρ	m	h^*_{31}	h^*_{33}	h^*_{15}	e^*_{31}	e^*_{33}	e^*_{15}
0.1	0.1	−0.129	1.24	0.922	−1.72	16.5	8.80
	0.3	−0.180	1.49	0.899	−2.13	17.4	9.24
	0.5	−0.251	1.82	0.875	−2.58	18.3	9.54
0.3	0.1	−0.132	1.24	0.922	−1.78	16.5	8.89
	0.3	−0.187	1.50	0.897	−2.27	17.5	9.22
	0.5	−0.262	1.83	0.872	−2.73	18.4	9.52
0.5	0.1	−0.135	1.24	0.920	−1.84	16.5	8.87
	0.3	−0.197	1.50	0.894	−2.42	17.5	9.19
	0.5	−0.277	1.84	0.868	−2.87	18.4	9.48

[a]The matrix is a poled FC medium with spherical air pores at porosity $m_p = 0.3$. The SC component is represented by a system of aligned spheroidal inclusions that are distributed in the porous FC matrix

composite, see curve 2 in Fig. 5.3. On increasing the aspect ratio ρ of the SC inclusion, the piezoelectric coefficient h^*_{33} becomes smaller at m = const. The similar decrease is also typical of the piezoelectric coefficient e^*_{33} as seen, for instance, from Table 4.6. It should be added that increasing the aspect ratio ρ does not lead to considerable changes in h^*_{31} and h^*_{15} of the composite, see curves 1 and 3 in Fig. 5.3. Thus, the isolated aligned piezoelectric inclusions in the 0–3 composite can influence its piezoelectric coefficients h^*_{ij} to a restricted degree.

The final example of the PS is concerned with a 0–3–0 composite wherein spheroidal SC inclusions are surrounded by a porous FC matrix. The performance of such a composite was discussed briefly in Sect. 4.3. We assume that each pore in the matrix of the 0–3–0 composite has the spherical form and radius being much smaller than the semi-axes of the inclusion a_1 and a_3. The composite sample as a whole is poled along the OX_3 axis. Data in Table 5.3 show that the correlation between the piezoelectric coefficients h^*_{3j} and e^*_{3j} is observed: we see the increase of $|h^*_{3j}|$ and $|e^*_{3j}|$ on increasing the volume fraction of SC m. Like e^*_{33}, the piezoelectric coefficient h^*_{33} takes almost equal values at m = const and various aspect ratios ρ, see the 4th column of Table 5.3. We observe validity of the inequality

$$h^*_{33} \gg \left|h^*_{31}\right| \tag{5.5}$$

in wide m ranges, and the value of the piezoelectric coefficient h^*_{15} remains comparable to the h^*_{33} value. Such a performance of the 0–3–0 composite can be concerned with specifics of an electromechanical interaction of its piezoelectric components. In contrast to h^*_{3j}, the piezoelectric coefficient h^*_{15} decreases on increasing m and e^*_{15}, see the 5th and 8th columns of Table 5.3. As follows from (5.1), the piezoelectric coefficients h^*_{15} and e^*_{15} are linked by the dielectric permittivity $\varepsilon^{*\zeta}_{11}$, and its influence on h^*_{15} increases on increasing the volume fraction m.

5.4 Conclusion

This chapter has been devoted to the analysis of the piezoelectric coefficients h^*_{ij} and related PS of some two- and three-component composites. The following connectivity patterns can be of interest when studying h^*_{ij} and ways to improve the PS: 1–3, 1–3–0, 2–2, 0–3, and 0–3–0. Changes in the volume fraction of the piezoelectric component and microgeometry of the composite lead to changes in h^*_{ij} and their anisotropy, however these changes are different for different connectivity patterns and depend on the main piezoelectric component of the composite. Examples of validity of conditions (5.2)–(5.5) are discussed for a few composites, and features of the volume-fraction and aspect-ratio behaviour of the piezoelectric coefficients h^*_{ij} are interpreted by taking into account microgeometry and properties of components. Of specific interest is the PS of the 2–2 and 1–3 composites based on the KNNTL:

Mn SC: in these composites values of $h_{33}^{*} \sim 10^{10}$ V/m are achieved in wide volume-fraction ranges due to the large piezoelectric coefficient h_{33} of the SC component. In composites based on relaxor-ferroelectric SCs values of $h_{33}^{*} \sim (10^{8}–10^{9})$ V/m are achieved.

The PS associated with the piezoelectric coefficients h_{ij}^{*} can be taken into account in sensor applications, especially at the direct piezoelectric effect, when the electric field is caused by the mechanical strain of the sample.

References

1. Zheludev IS (1971) Physics of crystalline dielectrics. Vol 2: Electrical properties. Plenum, New York
2. Jaffe B, Cook WR, Jaffe H (1971) Piezoelectric ceramics. Academic Press, London
3. Ikeda T (1990) Fundamentals of piezoelectricity. Oxford University Press, Oxford, New York, Toronto
4. Steinem C, Janshoff A (eds) (2007) Piezoelectric sensors. Springer, Berlin, Heidelberg
5. Sharapov V (2011) Piezoceramic sensors. Springer, Heidelberg, Dordrecht, London, New York
6. Topolov VYu, Bowen CR (2009) Electromechanical properties in composites based on ferroelectrics. Springer, London
7. Huo X, Zhang R, Zheng L, Zhang S, Wang R, Wang J, Sang S, Yang B, Cao W (2015) (K, Na, Li) (Nb, Ta)O_3: Mn lead-free single crystal with high piezoelectric properties. J Am Ceram Soc 98:1829–1835

Chapter 6
Improving Piezoelectric Sensitivity

After the game, the king and the pawn go into the same box.
United we stand, divided we fall.

Proverbs

Abstract The piezoelectric sensitivity of the composite is described in terms of four types of the piezoelectric coefficients, d_{ij}^*, e_{ij}^*, g_{ij}^*, and h_{ij}^*. The role of each type of the piezoelectric coefficients and its merit in determining the PS in composites with various microgeometric features are discussed. Diagrams that link electric and mechanical fields and contain the four types of the piezoelectric coefficients are represented for the direct and converse piezoelectric effects. Examples of orders-of-magnitude of the aforementioned piezoelectric coefficients are given for modern composites based on single crystals. Some ways for improving the piezoelectric sensitivity of the composites are discussed.

6.1 Piezoelectric Coefficients and Ways to Improve Piezoelectric Sensitivity of Modern Composites

The monograph has described the role of the microgeometry and electromechanical properties of composites in forming their PS. As follows from (1.4) to (1.11) and results from Chaps. 2 to 5, the PS of a composite can be described in terms of four types of the piezoelectric coefficients, d_{ij}^*, e_{ij}^*, g_{ij}^*, and h_{ij}^*. The links between the variables from (1.4) to (1.11) by the direct and converse piezoelectric effect are shown in Figs. 6.1 and 6.2, respectively. Hereby we highlight the role of each type of the piezoelectric coefficients and its merit in determining the PS in composites with various microgeometric features. The schematics shown in Figs. 6.1 and 6.2 are mnemonic and suggest the sign that precedes the piezoelectric coefficient from (1.4) to (1.11). If we go from the left side to right side along the upper (or ascending) line, the piezoelectric coefficient is to be taken with a plus. In contrast, in a case of the

V. Y. Topolov et al., *Piezo-Active Composites*, Springer Series
in Materials Science 271, https://doi.org/10.1007/978-3-319-93928-5_6

bottom (or descending) line, the piezoelectric coefficient is to be taken with a minus. For instance, the electric displacement D_k as a result of an external mechanical strain ξ_l at the direct piezoelectric effect is determined in (1.5), and the piezoelectric coefficient e_{kl} that links D_k and ξ_l is taken with a plus (see also the line that links ξ and D in Fig. 6.1). The second item in the right part of (1.5) shows the link between the electric field E_r and electric displacement D_k, and at $E_r = 0$ we have the piezoelectric effect that is described by the first item in the right part of (1.5), and the PS is characterised by e_{kl}. The electric field E_k produced due to a mechanical stress σ_l is described in terms of (1.9), and the piezoelectric coefficient g_{kl} in this case is taken with a minus (see also the line that links σ and E in Fig. 6.1). The minus sign in (1.9) originates from experimental results on polarisation charges [1] at surfaces of a piezoelectric sample: these charges generate the electric field $\boldsymbol{E}$ in the direction that is opposite to the piezoelectric polarisation $\boldsymbol{P}$ of the sample. Alternatively, we deal with the electric field $\boldsymbol{E}$ of a large dipole whose orientation is caused by the stress field at the direct piezoelectric effect. The minus sign in (1.4) is concerned with the converse piezoelectric effect at constant mechanical strain, i.e., in the deformed sample. In this case, the piezoelectric coefficient e_{fp} from (1.4) enables us to find a mechanical stress σ that leads to a non-deformed state of the sample ($\xi = 0$) in the external electric field $\boldsymbol{E}$. This $\boldsymbol{E}$ field differs from that generated by the polarisation charges at the direct piezoelectric effect in the previous case. It is obvious that the PS associated with the piezoelectric coefficient e_{kl} differs from the PS described in terms of d_{kl} or g_{kl}.

Figure 6.2 suggests that a similar link between E and ξ is described in terms of the piezoelectric coefficient d at the converse piezoelectric effect. The different signs of the piezoelectric coefficients for mechanical strain ξ and stress σ (see the right part of Fig. 6.2) can be concerned with elastic properties of an anisotropic piezoelectric medium. For example, the strain ξ_p at the converse piezoelectric effect is described by one of the items, d_{fp} E_f from (1.6) or g_{fp} D_f from (1.9), and the link between E_f and D_f is described by the dielectric permittivity, see (1.5). The

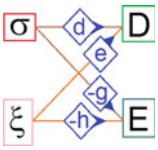

Fig. 6.1 Inter-relations between mechanical (left side) and electric (right side) variables at the direct piezoelectric effect. E, electric filed; D, electric displacement; ξ, mechanical strain; σ, mechanical stress

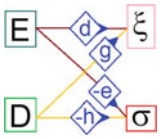

Fig. 6.2 Inter-relations between electric (left side) and mechanical (right side) variables at the converse piezoelectric effect. E, electric filed; D, electric displacement; ξ, mechanical strain; σ, mechanical stress

remaining items in the right parts of (1.6) and (1.8) are the strains $s_{pq}^{E}\sigma_q$ and $s_{pq}^{D}\sigma_q$ which depend on the elastic properties. The similar character of the strains $s_{pq}^{E}\sigma_q$ and $s_{pq}^{D}\sigma_q$ is consistent with the similar character of the piezoelectric strains d_{fp} E_f and g_{fp} D_f. The mechanical stress σ_p caused by the converse piezoelectric effect is associated with the items $(-e_{fp}E_f)$ and $(-h_{fp}D_f)$ from (1.4) to (1.10), respectively. In this case, the link between E_f and D_f is described in terms of (1.9). The contributions $c_{pq}^{E}\xi_q$ and $c_{pq}^{D}\xi_q$ to σ_p from (1.4) to (1.10), respectively, are similar because of the similar anisotropy of elastic moduli c_{pq}^{E} and c_{pq}^{D} of the piezoelectric medium. This is consistent with the similar anisotropy of the piezoelectric coefficients e_{fp} and h_{fp}.

The PS caused by the piezoelectric coefficient e_{kl} differs from the PS described in terms of the piezoelectric coefficient h_{kl}. In fact, the PS of each piezoelectric can be described in terms of four types of the piezoelectric coefficients shown in (1.4)–(1.11) and Figs. 6.1 and 6.2. As is known from studies on effective piezoelectric properties of composites (see, for instance, work [2]), the piezoelectric coefficients d_{kl} are widely used in averaging procedures applied to various connectivity patterns. The piezoelectric coefficients e_{kl} are also involved in averaging procedures [3] to find the effective properties of composites, however the number of such procedures described in the literature is relatively small. As follows from the literature, the piezoelectric coefficients g_{kl} and h_{kl} are seldom involved in similar averaging procedures. One of the reasons is concerned with the full sets of electromechanical constants that contain g_{kl} and h_{kl}, see (1.8)–(1.11). In these sets, the elastic properties are represented by the elastic compliances s_{pq}^{D} and elastic moduli c_{pq}^{D}, see (1.8) and (1.10), respectively. However the elastic compliances s_{pq}^{E} or elastic moduli c_{pq}^{E} are often found by means of experimental methods because conditions for measurements of s_{pq}^{D} and c_{pq}^{D} in piezoelectric media [1, 4, 5] are complicated in comparison to conditions for measurements of s_{pq}^{E} and c_{pq}^{E}.

Our present study enables us to state that the piezoelectric coefficients d_{ij}^* and g_{ij}^* are widely used to describe the PS of composites, and improving its PS is of value for many sensor, actuator, transducer, and other piezotechnical applications. The piezoelectric coefficients g_{ij}^* are of importance mainly at the direct piezoelectric effect. The piezoelectric coefficients e_{ij}^* and h_{ij}^* are less often desired for piezotechnical applications [4–6]. This is accounted for by changes in the mechanical strain ξ_{ik} and electric displacement D_f [1] which can be detected in experiments on piezoelectrics [4, 5] with a lesser accuracy than changes in the mechanical stress σ_{ik} or electric field E_f.

Factors that promote an improvement of the PS of the studied composites can be divided into the following groups:

(i) physical (concerned with electromechanical properties of components and with boundary conditions and distributions of internal electric and mechanical fields in composite materials),
(ii) microgeometric (the arrangement of the main piezoelectric component in the form of long rods, layers or inclusions along the poling direction to facilitate the poling of the composite, and formation of composite structures in the matrix component to achieve a large piezoelectric anisotropy), and
(iii) technological (providing favourable poling conditions, perfect bonding at interfaces, use of piezoelectric layers, rods, inclusions, etc. with almost equal properties, and formation of uniform porous structures in matrices of composite samples).

The methods to improve the PS of the composite with the appointed connectivity pattern and components are inseparably linked to the items (i)–(iii) and some, but not all, piezoelectric coefficients of the main component of the composite. The microgeometric factors from item (ii) are to be taken into account at forming the specific piezoelectric coefficient of the composite (d_{ij}^*, e_{ij}^*, g_{ij}^*, or h_{ij}^*). Since the maxima of the piezoelectric coefficients are found in various volume-fraction ranges even for a composite with a constant connectivity (see results in Chaps. 2–5), we should carefully consider both the microgeometry and properties of components. To the best of our knowledge, it is impossible to improve all the four types of the piezoelectric coefficients simultaneously because of features of the electromechanical coupling, microgeometry, piezoelectric anisotropy [2, 3, 6, 7], and other characteristics of the piezo-active composites.

Our results show that the modern composites based on the high-performance domain-engineered SCs are promising due to an improvement of piezoelectric coefficients, for instance, d_{3j}^* and g_{3j}^* or d_{3j}^* and e_{3j}^*. In Table 6.1 we show typical orders-of-magnitude of the piezoelectric coefficients of composites based on the [001]-poled domain-engineered SCs. There are examples of the high PS of the lead-free composites that are to be developed in the nearest future. Undoubtedly, an important stimulus to improve the PS of the composite is linked to applications [4–6] that are based on the effective properties and related parameters.

Table 6.1 Examples of improved PS of composites based on [001]-poled domain-engineered SCs

Connectivity	Main SC component	Remaining components	Piezoelectric coefficients, orders-of-magnitude	Section
2–2	PMN–0.33PT	Araldite	$d_{3j}^* \sim 10^3$ pC/N	2.1.2
		Elastomer	$g_{3j}^* \sim 10^3$ mV m/N	3.1
		Auxetic PE	$d_{33}^* \sim 10^3$ pC/N at $d_{31}^* \to 0$ or $d_{33}^* \sim 10^3$ pC/N at $d_{32}^* \to 0$	2.1.2
	PMN–0.28PT	Araldite	$d_{33}^* \sim 10^3$ pC/N, $d_{31}^* \sim 10^2$ pC/N and $d_{32}^* \sim 10^2$ pC/N	2.1.2
		Elastomer	$g_{3j}^* \sim 10^3$ mV m/N	3.1
		Auxetic PE	$d_{33}^* \sim 10^3$ pC/N at $d_{31}^* \to 0$ or $d_{33}^* \sim 10^2$ pC/N at $d_{32}^* \to 0$	2.1.2
	KNNTL:Mn	Araldite, polyurethane or elastomer	$g_{33}^* \sim 10^3$ mV m/N, $g_{31}^* \sim (10^2$–$10^3)$ mV m/N and $g_{32}^* \sim (10^2$–$10^3)$ mV m/N	3.1
		Araldite	$h_{33}^* \sim 10^{10}$ V/m, $h_{31}^* \sim 10^9$ V/m and $h_{32}^* \sim 10^9$ V/m	5.1
		Auxetic PE	$g_{33}^* \sim 10^3$ mV m/N at $g_{32}^* \to 0$ or $g_{33}^* \sim 10^2$ mV m/N at $g_{31}^* \to 0$	3.1
2–0–2	PMN–0.33PT	Modified $PbTiO_3$ FC and PE	$d_{33}^* \sim 10^3$ pC/N, $d_{31}^* \sim 10^2$ pC/N and $d_{32}^* \sim 10^3$ pC/N $d_h^* \sim (10^2$–$10^3)$ pC/N	2.7
	KNNTL:Mn	LBO SC and PE	$g_{33}^* \sim 10^3$ mV m/N, $g_{31}^* \sim 10^2$ mV m/N and $g_{32}^* \sim 10^2$ mV m/N	3.1
1–3	PMN–0.33PT	Araldite, polyurethane or elastomer	$d_{3j}^* \sim 10^3$ pC/N	2.2.2
		Auxetic PE	$d_{33}^* \sim 10^3$ pC/N at $d_{31}^* \to 0$	2.2.2
	KNNTL:Mn	Araldite, polyurethane or elastomer	$d_{3j}^* \sim 10^2$ pC/N	2.2.2
			$g_{33}^* \sim 10^3$ mV m/N and $g_{31}^* \sim (10^2$ –$10^3)$ mV m/N	3.2
			$h_{33}^* \sim 10^{10}$ V/m and $h_{31}^* \sim 10^8$ V/m	5.2
		Auxetic PE	$d_{33}^* \sim 10^2$ pC/N at $d_{31}^* \to 0$	2.2.2
			$g_{33}^* \sim 10^2$ mV m/N at $g_{31}^* \to 0$	3.2
			$h_{33}^* \sim 10^{10}$ V/m and $h_{31}^* \sim 10^8$ V/m	5.2

(continued)

Table 6.1 (continued)

Connectivity	Main SC component	Remaining components	Piezoelectric coefficients, orders-of-magnitude	Section
1–2–2	PMN–0.33PT	Araldite and PE	$d_{33}^* \sim 10^3$ pC/N and $d_{31}^* \sim 10^2$ pC/N	2.2.3
		Araldite and polyurethane	$e_{33}^* \sim 10^1$ C/m^2 and $e_{31}^* \sim (10^{-2}$–$10^{-1})$ C/m^2	4.2
1–3–0	PMN–0.33PT	Porous polyurethane	$d_{33}^* \sim 10^3$ pC/N and $d_{31}^* \sim (10^1$–$10^3)$ pC/N	2.2.4
		Porous araldite	$d_h^* \sim (10^2$–$10^3)$ pC/N	2.7
	PMN–0.28PT	Porous araldite	$e_{33}^* \sim 10^1$ C/m^2	4.2
1–0–3	PMN–0.33PT	Modified $PbTiO_3$ FC and PE	$d_{33}^* \sim 10^3$ pC/N and $d_{31}^* \sim (10^1$–$10^3)$ pC/N	2.2.5
	KNNTL:Mn	Modified $PbTiO_3$ FC and PE	$d_{33}^* \sim 10^2$ pC/N and $d_{31}^* \sim (10^1$–$10^2)$ pC/N	2.2.5
			$g_{33}^* \sim (10^2$ –$10^3)$ mV m/N and $g_{31}^* \sim (10^2$ –$10^3)$ mV m/N	3.2
0–3	KNNTL:Mn	PVDF	$g_{33}^* \sim 10^2$ mV m/N, $g_{31}^* \sim (10^1$–$10^2)$ mV m/N	3.4
	PMN–0.33PT	Modified $PbTiO_3$ FC	$e_{33}^* \sim 10^1$ C/m^2 and $e_{31}^* \sim (10^{-2}$–$10^0)$ C/m^2	4.3
		PMN–0.35PT FC	$e_{33}^* \sim 10^1$ C/m^2 and $e_{31}^* \sim 10^0$ C/m^2	4.3
0–3–0	PMN–0.33PT	Porous araldite	$g_{33}^* \sim 10^2$ mV m/N and $g_{31}^* \sim (10^1$–$10^2)$ mV m/N	3.4

To finish the present monograph, we would like to quote work [8]: “As niche applications become more prevalent in the future, composites and displacement-amplifying techniques and materials will proliferate in a continuing effort to widen the force–displacement envelope of performance. These devices, too, will become smarter and smarter as the applications demand”.

References

1. Ikeda T (1990) Fundamentals of piezoelectricity. Oxford University Press, Oxford, New York, Toronto
2. Topolov VYu, Bowen CR (2009) Electromechanical properties in composites based on ferroelectrics. Springer, London
3. Khoroshun LP, Maslov BP, Leshchenko PV (1989) Prediction of effective properties of piezo-active composite materials. Naukova Dumka, Kiev (in Russian)
4. Uchino K (1997) Piezoelectric actuators and ultrasonic motors. Kluwer, Boston
5. Ruschmeyer K, Helke G, Koch J, Lubitz K, Möckl Petersen A, Riedel M, Schönecker A (1995) Piezokeramik. Grundlage, Werkstoffe, Applikationen. Expert-Verlag, Malmsheim
6. Akdogan EK, Allahverdi M, Safari A (2005) Piezoelectric composites for sensor and actuator applications. IEEE Trans Ultrason Ferroelectr Freq Control 52:746–775
7. Topolov VYu, Bisegna P, Bowen CR (2014) Piezo-active composites. Orientation effects and anisotropy factors. Springer, Berlin, Heidelberg
8. Haertling GH (1999) Ferroelectric ceramics: history and technology. J Am Ceram Soc 82:797–818

Appendix A
List of Abbreviations

ECF	Electromechanical coupling factor
EFM	Effective field method
FC	Ferroelectric ceramic
FEM	Finite element method
KNN-T	$(K_{0.562}Na_{0.438})(Nb_{0.768}Ta_{0.232})O_3$
KNN-TL	$[Li_x(K_{0.501}Na_{0.499})_{1-x}](Nb_{0.660}Ta_{0.340})O_3$
KNNTL:Mn,	$[Li_x(K_{1-y}Na_y)_{1-x}](Nb_{1-z}Ta_z)O_3$:Mn (see Table 1.2)
LBO	$Li_2B_4O_7$
NBT–*x*BT	$(1 - x)(Na_{0.5}Bi_{0.5})TiO_3 - xBaTiO_3$
PCR	Piezoelectric ceramic from Rostov-on-Don (Russia)
*x*PIN–*y*PMN–(1 – *x* − *y*)PT	$xPb(In_{1/2}Nb_{1/2})O_3 - yPb(Mg_{1/3}Nb_{2/3})O_3 - (1 - x - y)PbTiO_3$
PMN–*x*PT	$(1 - x)Pb(Mg_{1/3}Nb_{2/3})O_3 - xPbTiO_3$
PS	Piezoelectric sensitivity
PZN–*y*PT	$(1 - x)Pb(Zn_{1/3}Nb_{2/3})O_3 - xPbTiO_3$
PZT	Piezoelectric ceramic of the $Pb(Zr, Ti)O_3$ type
SC	Single crystal
ZTS	Piezoelectric ceramic of the $Pb(Zr, Ti)O_3$ type (Russia)

V. Y. Topolov et al., *Piezo-Active Composites*, Springer Series in Materials Science 271, https://doi.org/10.1007/978-3-319-93928-5

Appendix B
Electromechanical Constants of Components

To analyse the piezoelectric performance, effective properties and related parameters of composites, we use full sets of electromechanical constants of components. A systematisation of data on the components is given in Table B.1.

Table B.1 Room-temperature electromechanical constants of components

Component	Composition	Set of constants	Table number
SC	$BaTiO_3$[a]	s^E_{ab}, d_{ij} and ε^σ_{pp}	1.1
	KNN-T[b]	s^E_{ab}, d_{ij} and ε^σ_{pp}	1.2
	KNN-TL[b]	s^E_{ab}, d_{ij} and ε^σ_{pp}	1.2
	KNNTL:Mn[b]	s^E_{ab}, d_{ij} and ε^σ_{pp}	1.2
	PMN–0.33PT[b]	s^E_{ab}, d_{ij} and ε^σ_{pp}	1.3
	PMN–0.33PT[c]	s^E_{ab}, d_{ij} and ε^σ_{pp}	2.3
	PMN–0.30PT[b]	s^E_{ab}, d_{ij} and ε^σ_{pp}	1.3
	PMN–0.29PT[d]	s^E_{ab}, d_{ij} and ε^σ_{pp}	1.4
	PMN–0.28PT[b]	s^E_{ab}, d_{ij} and ε^σ_{pp}	1.3
	PMN–0.28PT[d]	s^E_{ab}, d_{ij} and ε^σ_{pp}	1.4

(continued)

V. Y. Topolov et al., *Piezo-Active Composites*, Springer Series in Materials Science 271, https://doi.org/10.1007/978-3-319-93928-5

Table B.1 (continued)

Component	Composition	Set of constants	Table number
	PMN–0.28PT[c]	s^E_{ab}, d_{ij} and ε^σ_{pp}	2.3
	PZN–0.09PT[d]	s^E_{ab}, d_{ij} and ε^σ_{pp}	1.4
	PZN–0.08PT[b]	s^E_{ab}, d_{ij} and ε^σ_{pp}	1.3
	PZN–0.07PT[b]	s^E_{ab}, d_{ij} and ε^σ_{pp}	1.3
	PZN–0.07PT[d]	s^E_{ab}, d_{ij} and ε^σ_{pp}	1.4
	PZN–0.045PT[b]	s^E_{ab}, d_{ij} and ε^σ_{pp}	1.3
	0.26PIN– 0.42PMN– 0.32PT:Mn[b]	s^E_{ab}, d_{ij} and ε^σ_{pp}	1.3
	0.26PIN– 0.42PMN– 0.32PT:Mn[d]	s^E_{ab}, d_{ij} and ε^σ_{pp}	1.4
	0.27PIN– 0.40PMN– 0.33PT[b]	s^E_{ab}, d_{ij} and ε^σ_{pp}	1.3
	NBT–0.05BT[b]	s^E_{ab}, d_{ij} and ε^σ_{pp}	1.3
	LBO[e]	c^E_{ab}, e_{ij} and ε^ξ_{pp}	3.1
FC[f]	Compositions with perovskite-type structure ($BaTiO_3$, PZT, PCR, ZTS, modified $PbTiO_3$, etc.)	s^E_{ab}, d_{ij} and ε^σ_{pp}	1.5
	Compositions with perovskite-type structure ($BaTiO_3$, PZT, PCR, ZTS, modified $PbTiO_3$, etc.)	e_{ij}, g_{ij} and h_{ij}	1.6
	$(Pb_{1-x}Ca_x)TiO_3$[h]	c^E_{ab}, e_{ij} and ε^ξ_{pp}	3.5

(continued)

Table B.1 (continued)

Component	Composition	Set of constants	Table number
Polymer	Araldite[h]	s_{ab} and ε_{pp}	2.1
	Polyurethane[h]	s_{ab} and ε_{pp}	2.1
	Elastomer[h]	s_{ab} and ε_{pp}	2.1
	PE (monolithic)[h]	s_{ab} and ε_{pp}	2.1
	Auxetic PE[h]	s_{ab} and ε_{pp}	2.1
	PVDF[i]	s^E_{ab}, d_{ij} and ε^σ_{pp}	3.7

[a]Polydomain SC, *mm*2 symmetry, calculated electromechanical constants
[b]Domain-engineered [001]-poled SC, 4*mm* symmetry
[c]Single-domain [111]-poled SC, 3*m* symmetry
[d]Domain-engineered [011]-poled SC, *mm*2 symmetry
[e]Piezoelectric SC, 4*mm* symmetry
[f]Poled FC, ∞*mm* symmetry
[g]Calculated electromechanical constants
[h]Piezo-passive polymer, isotropic medium
[i]Poled ferroelectric polymer, ∞*mm* symmetry

Index

A
Anisotropy, 53, 78, 86, 93, 94, 113, 123, 130, 142, 145, 146, 150, 151, 165
  elastic, 22, 42, 53, 73, 75, 80, 90, 92–94, 102, 103, 108, 117, 123, 124, 127, 128, 130, 137
  electromechanical coupling, 2, 5, 6, 35, 44, 89, 94
    factors, 91, 113, 129, 166
  piezoelectric, 18, 68, 73, 75, 78, 84, 94, 113, 166
    large, 49, 57, 62, 90, 118
Anisotropy factor, 85, 147
Aspect ratio, 67, 71, 78, 82, 84, 87, 88, 91, 93, 102, 113, 115, 117–119, 123–125, 128, 146, 148, 159, 160
Aspect-ratio effect, 56, 116
Averaging procedure, 28, 165

B
Boundary conditions, 28, 38, 39, 57, 166

C
Ceramic. *See* ferroelectric ceramic
Coercive field, 3, 116
Combination of properties, 141
Composite
  α−β, 27
  0–3-type, 81, 130, 147, 159
  1–1-type, 76
  1–3-type, 56, 62, 64, 66, 73, 90, 144, 146, 156
    cross section, 56, 57, 59, 60, 62
  2–2-type, 50
  3−β, 120
  classification, 27
  component, 116
  connectivity, 27, 29, 35, 50, 65, 66, 78, 85, 87, 94, 100, 117, 144 *See also* connectivity pattern
  microgeometry, 27, 36, 40, 53, 56, 57, 76, 93, 108, 111, 113, 138, 142, 144, 146, 150, 160, 166
  schematic, 10, 15, 37, 51, 55, 63, 65, 67, 71, 77, 78, 82, 113, 140, 158 *See also* microgeometry
  piezo-active, 56, 62
Crystallographic axes
  main, 14, 44, 65, 66, 102, 115, 136, 141

D
Dielectric permittivity, 3, 12, 15, 16, 19–22, 28, 44, 82, 106–109, 111, 114, 116, 126, 156, 157
Domain, 14, 15, 18

E
Effective Field Method (EFM), 28, 51, 70, 113, 142
Elastic compliance, 5, 15, 20, 40, 44, 47, 63, 68, 103, 106, 115, 145, 165
  hydrostatic, 7, 91
  ratio, 91, 104
Elastic modulus, 3, 5, 28, 37, 82, 103, 114, 116, 165
Electric displacement, 3, 4, 8, 11, 39, 164

V. Y. Topolov et al., *Piezo-Active Composites*, Springer Series in Materials Science 271, https://doi.org/10.1007/978-3-319-93928-5

Electric field, 2–4, 10, 11, 15, 17, 39, 42, 88, 164
Electromechanical constants
full set, 5, 8, 14, 16, 18, 21, 28, 39, 43, 57, 62, 82, 102, 117, 136, 143, 145, 173
Electromechanical Coupling Factor (ECF), 5, 6, 37, 89, 91, 94
Electromechanical properties. *See* electromechanical constants
Energy, 6, 12
conversion, 5, 6 *See also* electromechanical coupling factor
harvesting, 122
Eshelby tensor, 51, 67, 71

F
Ferroelectric ceramic, 2, 6, 18, 20, 21
perovskite-type, 13, 16, 17, 23, 135
properties, 1, 8
Finite-element method, 28, 60, 71, 82, 113

H
Hierarchy-of-properties chain, 27

I
Inclusion, 147
air. *See* pore
ceramic, 66, 70, 77, 94, 108, 113, 147, 159
clay, 121
single-crystal, 83–85, 102, 103, 115, 117–119, 126, 148, 159, 160

L
Layer
ferroelectric ceramic, 2, 20
polymer, 36, 41, 42, 49, 50, 58, 66
single-crystal, 70

M
Matrix of the composite, 160
Matrix method, 28, 38, 44, 71, 100
Matrix of piezoelectric coefficients. *See* piezoelectric coefficients
Mechanical strain, 4, 37, 39, 164
Mechanical stress, 39, 164
Morphotropic phase boundary, 16, 44

O
Orientation effect, 56, 102
Oscillation mode, 6, 13, 50
longitudinal, 6
planar, 7, 57, 130
shear, 6
thickness, 7
transverse, 6

P
Piezo-active composite, 6, 26, 27, 29, 35, 62, 88, 122, 126, 166
Piezoelectric anisotropy. *See* anisotropy
Piezoelectric coefficient, 3, 5, 7, 10, 15, 16, 19–21, 23, 25, 28, 44, 49, 56
d_{3j}, 6, 13, 18, 41, 48, 49, 54, 57, 58, 73, 75, 78, 83, 88, 89, 91–94, 100, 108, 120, 124–127, 164
e_{ij}, 22, 26, 37, 38, 135, 136, 138–142, 145, 147, 150, 156, 160, 164, 165
g_{3j}, 56, 103, 104, 108, 113, 114, 120–122, 126, 131, 164
h_{ij}, 7, 22, 157–161, 165
hydrostatic, 7, 13, 56, 91, 93, 108, 122, 126, 141
matrix representation
Piezoelectric effect, 1, 4
converse, 2
Curie groups, 9
direct, 2, 4, 9
symmetry classes, 8
Piezoelectric element, 5, 10, 12, 13
Piezoelectric properties. *See* piezoelectric coefficient and piezoelectric effect
Piezoelectric sensitivity, 2, 5 *See also* piezoelectric coefficient
'sleeping', 48, 49, 54, 57, 68, 100, 107, 108, 111, 130
Polarisation
piezoelectric, 78, 86, 93, 113, 123, 130, 142, 146, 151, 165
remanent, 6, 57, 60, 116
sponaneous, 15, 43, 50, 65–67, 71, 102, 127
Polymer, 27
auxetic, 40, 42, 44, 59, 106, 107, 139
ferroelectric, 36, 114, 116
piezo-passive, 39, 55, 78, 85
porous, 57, 62, 66, 67, 78, 80, 85, 91, 94, 111, 122, 147, 158
properties, 141, 145, 150
Pore, 68, 90
aspect ratio, 50–53, 55, 67, 70, 71, 73, 75, 78, 80, 82–85, 87, 88, 91, 93, 102, 113, 115, 117–119, 123–125, 128, 146, 148, 151, 159, 160
Property
dielectri. *See* dielectric permittivity
effective, 27, 28, 36, 38, 51, 57, 67, 81, 113, 129, 165 *See also* averaging procedure

elastic. *See* elastic compliance and elastic modulus
electromechanical. *See* electromechanical constants
single-crystal, 8, 14–20, 172, 173

R
Rod, 55, 121
ferroelectric ceramic, 56, 57, 60, 66, 108, 125
single-crystal, 65, 67, 70, 71, 84, 108, 115, 123, 143, 144

S
Sensitivity. *See* piezoelectric sensitivity and piezoelectric coefficient
Single crystal
lead-free ferroelectric, 100
piezoelectric, 140
relaxor-ferroelectric, 17, 18, 22, 27, 29, 43, 50, 56, 119, 161
Squared figure of merit, 12, 13, 127
hydrostatic, 13, 91, 128

U
Unit cell
perovskite, 16–18, 105
representative, 57, 60 *See also* finite element method